Transport in Periodically Driven Systems

DISSERTATION ZUR ERLANGUNG DES DOKTORGRADES DER NATURWISSENSCHAFTEN (DR. RER. NAT.) DER FAKULTÄT FÜR PHYSIK

der Universität Regensburg

vorgelegt von

Martin Wackerl

aus

Garmisch-Partenkirchen

im Jahr 2020

Promotionsgesuch eingereicht am: 15.07.2020
Die Arbeit wurde angeleitet von: Prof. Dr. John Schliemann

Prüfungsausschuss:
Vorsitzender: Prof. Dr. Dominique Bougeard
1. Gutachter: Prof. Dr. John Schliemann
2. Gutachter: Prof. Dr. Klaus Richter
weiterer Prüfer: Prof. Dr. Christoph Lehner

Datum Promotionskolloquium: 26.10.2020

Contents

Chapter 1

Floquet Conductivity

1.1 Introduction

The field of light-matter interaction is one of the fastest growing fields in physics. This multifaceted area has many subfields, such as nonlinear optics, the interaction of photons with semiconductors or, at the most fundamental level, quantum field theory. Light-matter interaction is even an inherent part of everday life. This, for instance, includes lasers that are used in many areas of daily life, solar cells for generating electricity, or plants using light for photosynthesis. In industry, much effort is used to improve solar cells and the use of lasers for medical purposes has become standard.

The main interest of physicists and engineers is to deepen the understanding of light-matter interaction and to make new technologies applicable in everday life. The description of light-matter interaction often requires a microscopic theory, since many phenomena are only properly explainable within a quantum theory. Hence, finding such descriptions is of ultimate interest.

Quantum phenomena are often observed in reduced dimensions due to spatial confinement. The light absorption rate in solar cells can be enhanced by using semiconductor heterostructures. These have an increased density of states at the band gap, due to the spatial confinement. This increases the number of particles that can take part in absorption processes which, as a consequence, enhance the efficiency of solar cells. The inverse mechanism is used in light emitting diodes, where the confinement is used to enhance spontaneous emission of light.

The manipulation of quantum systems can be realized in many ways, for example by applying biases or voltages. However, one of the most promising tools for quantum engineering is the use of light, especially laser light. This light, emitted by stimulated emission, can be generated in a very wide frequency and intensity range. This is what makes laser light so advantageous as the path from theory to experiment becomes simplified. Possible effects induced by an external driving are the enhancement of tunneling amplitudes, or tuning the conductivity of materials [1–4]. Another field is the physics of cold atoms, which are often manipulated by time-periodic external optical fields. These systems offer a great way of simulating condensed matter systems such as “effective ferromagnetic domains [..], realization of the topological Haldane model [..], and the creation of a roton-maxon dispersion for a Bose-Einstein condensate in a shaken optical lattice. [..]” [1].

The current response of a system to an electric field is the conductivity. The im-

portance of controlling the conductivity of materials is underlined by mentioning computer chips exemplarily. The central processing units of mobile phones, laptops, desktop PCs but and also modern fridges and washing machines are based on transistors. The functionality of these can be traced back to the ability of switching between a conducting and a non-conducting state.

Paul Drude published his theory of electric transport in metals as long ago as in 1900 [5, 6], which is known as Drude theory today. To the present day several approaches have been developed to deepen the understanding of the microscopic mechanisms occurring in charge transport, including scattering theory using Fermi's golden rule [7, 8] or quantum corrections to the Drude conductivity. The latter covers weak (anti-)localization [9, 10] in the form of geometry or spin dependent corrections [11–19]. In contrast to studies of static systems, the development of lasers and masers generated a rising activity on explicitly time-dependent Hamiltonians, where the external field cannot be considered a small perturbation [20]. In the most recent decade, owing to the possibility of changing the topology of a system by means of external driving, the investigation of transport in driven systems increased [4, 21–29]. This includes transport in driven systems [30, 31], either with or without disorder [32–34], or the photo-voltaic Hall effect [23]. Most works studying the renormalization of conductivity, due to an external driving, use a perturbative approach regarding the external driving [4, 25]. This work aims in the presentation of a new general formalism that allows the determination of the Drude conductivity in the presence of a non-perturbative external driving. Linear response theory and Floquet formalism are unified to account for the probe bias and an external driving, providing an alternative approach to the Keldysh formalism [22]. Using a new type of four-times Green's function formalism, a Floquet-Dyson series is derived in a rigorous manner, providing new Feynman rules for the driven case compared to the static system. To prove the consistency, a generalized Floquet Fermi's golden rule is derived, yielding the same scattering time as the Dyson series, a link that was missing so far. Even more important, the theory properly describes not only impurity mediated intra- but also inter-Floquet-replica scattering, which has been completely neglected in literature thus far. Finally, a closed analytical form for the Floquet-Drude conductivity is presented and applied to a parabolic approximation of the 2DEG and the corresponding tight-binding model both with circularly polarized external driving. Regarding the 2DEG, the analysis shows that previous results overestimate the effect of the driving on the conductivity. The driven tight-binding model shows an entirely different driving dependency even in the low energy limit. This observation is mainly caused by the different eigenstates rather than the similar spectra. This observation has two important consequences. Both the parabolic dispersion and the square lattice are rather simple models for a realistic material. Nevertheless, even the results from these simplified models strongly deviate from each other, which underlines the importance of starting with a realistic model. The findings for the square lattice and parabolic dispersion might also be true for other materials, e.g. graphene [35]. As a consequence, previous works using effective models should be revised. (Reprinted text with permission from [36]. Copyright (2020) by the American Physical Society.)

1.2 Floquet Theory - Mathematical foundation

In physics, symmetries are often used to derive general statements about physical systems or to simplify calculations. In solid state theory, one famous example is the Bloch theorem. Felix Bloch used the spatial periodicity of a crystal to derive a general form of the wave function of electrons in a periodic potential [37]. The counterpart to translational invariance in time rather than in space [1] was investigated by the French mathematician M. G. Floquet in Ref. [38] as early as 1883. This section does not aim to give an introduction to Floquet theory with full mathematical rigor [38, 39]. It is rather a summary of the most important results and relations of the Floquet framework that are used in this work. Floquet theory is intended to treat time periodic Hamiltonians

$$H(t) = H(t+T) \tag{1.1}$$

with driving period $T = 2\pi/\Omega$. There are also extensions of Floquet theory to non-periodic drivings, e.g. Ref. [20], but those are not considered in this work. It can be shown by properties of the time evolution operator [1] that the solutions of the time-dependent Schrödinger equation

$$i\hbar\frac{\partial}{\partial t}\left|\psi_\alpha(t)\right\rangle = H(t)\left|\psi_\alpha(t)\right\rangle \tag{1.2}$$

are Floquet states

$$\left|\psi_\alpha(t)\right\rangle = e^{-\frac{i}{\hbar}\varepsilon_\alpha t}\left|u_\alpha(t)\right\rangle \ . \tag{1.3}$$

The index α labels a discrete set of quantum numbers. The exponential function contains the quasienergy [40] ε_α and $u_\alpha(t)$ is called the Floquet function. Since the solutions of Eq. (1.2) form an orthonormal and complete set at any fixed time, and the unitary time evolution conserves the scalar product [41, 42], they fulfill

$$\langle\psi_\alpha(t)|\psi_\beta(t)\rangle = \delta_{\alpha\beta} \quad , \quad \sum_\alpha |\psi_\alpha(t)\rangle\langle\psi_\alpha(t)| = \mathbb{1} \tag{1.4}$$

and equivalently for the Floquet functions

$$\langle u_\alpha(t)|u_\beta(t)\rangle = \delta_{\alpha\beta} \quad , \quad \sum_\alpha |u_\alpha(t)\rangle\langle u_\alpha(t)| = \mathbb{1}\,. \tag{1.5}$$

The Floquet state (1.3) together with the time-dependent Schrödinger equation (1.2) lead to the Floquet equation

$$H_F(t)\left|u_\alpha(t)\right\rangle = \varepsilon_\alpha\left|u_\alpha(t)\right\rangle \quad \text{with} \quad H_F(t) = H(t) - i\hbar\frac{\partial}{\partial t} \tag{1.6}$$

with H_F being the Floquet Hamiltonian. Remarkably, the Floquet Hamiltonian has time-independent eigenenergies, i.e. the quasienergies. The Floquet functions have the same periodicity as the Hamiltonian, which allows both to expand into Fourier series

$$\left|u_\alpha(t)\right\rangle = \sum_{n=-\infty}^{\infty}\left|u_\alpha^n\right\rangle e^{-in\Omega t} \quad , \quad \left|u_\alpha^n\right\rangle = \frac{1}{T}\int_0^T dt\ \left|u_\alpha(t)\right\rangle e^{in\Omega t} \tag{1.7}$$

$$H(t) = \sum_{n=-\infty}^{\infty} H_n\, e^{-in\Omega t} \quad , \quad H_n = \frac{1}{T}\int_0^T dt\, H(t)e^{in\Omega t}\,. \tag{1.8}$$

The Fourier coefficients in Eq. (1.7) form a basis, which is evidently proven by integrating Eq. (1.5) over one driving cycle

$$\frac{1}{T}\int_0^T dt\,\langle u_\alpha(t)|u_\beta(t)\rangle = \sum_{n=-\infty}^{\infty}\langle u_\alpha^n|u_\beta^n\rangle = \delta_{\alpha\beta}\,, \tag{1.9}$$

$$\frac{1}{T}\int_0^T dt\,\sum_\alpha |u_\alpha(t)\rangle\langle u_\alpha(t)| = \sum_\alpha\sum_{n=-\infty}^{\infty}|u_\alpha^n\rangle\langle u_\alpha^n| = \mathbb{1}\,. \tag{1.10}$$

Solving Eq. (1.6) is often rather challenging, but Eq. (1.6) can be formulated as an infinite dimensional eigenvalue equation using the Fourier expansions of the Floquet function and of the Hamiltonian

$$\sum_{m=-\infty}^{\infty}\underbrace{\left(H_{n-m}-n\hbar\Omega\,\delta_{mn}\right)}_{\equiv(\mathbf{H}_F)_{nm}}|u_\alpha^m\rangle = \varepsilon_\alpha|u_\alpha^n\rangle\,. \tag{1.11}$$

Eq. (1.11) is the basis for numerous numerical studies, where the infinite dimensional matrix is truncated at a sufficiently large order. The matrix representation of the Floquet equation (1.11) is also the starting point for the formulation of various perturbation theories [3, 21, 43–45].

1.3 Kubo formula

Linear response theory is an elementary concept of modern theoretical physics [46, 47]. It provides a systematic scheme to calculate the first order correction of an expectation value of an observable quantity [48] to some perturbation. The perturbations can be of various forms, for example magnetic fields, electric fields, temperature gradients, or pressure fields [49]. This demonstrates the power of linear response theory since it is applicable to numerous physical setups. In the present work, the particular focus is on the electrical conductivity linearly relating the current to a perturbing electric field.

The focus of the study is on a system of non-interacting particles in a d-dimensional Volume V, $d \in \{2,3\}$. The system is subjected to two different fields. The first one is a weak electric field inducing the probe bias, which is treated perturbatively with linear response theory. The other field is a periodic external driving of frequency $\Omega = 2\pi/T$, as schematically depicted in Fig. 1.1. Consider a system described by the Hamiltonian [50]

$$H = H_0 + V(t) \tag{1.12}$$

with H_0 being the Hamiltonian for the system without the time-dependent perturbation $V(t)$. The expectation value of a not explicitly time-dependent observable $\hat{A}$ is without the perturbing potential $V(t)$ given by

$$\langle\hat{A}\rangle_0 = \mathrm{tr}[\rho_0\hat{A}] \tag{1.13}$$

together with the density matrix for the grand canonical ensemble $\mathcal{H}_0 = H_0 - \mu\hat{N}$

$$\rho_0 = \frac{\exp(-\beta\mathcal{H}_0)}{\mathrm{tr}[\exp(-\beta\mathcal{H}_0)]}\,. \tag{1.14}$$

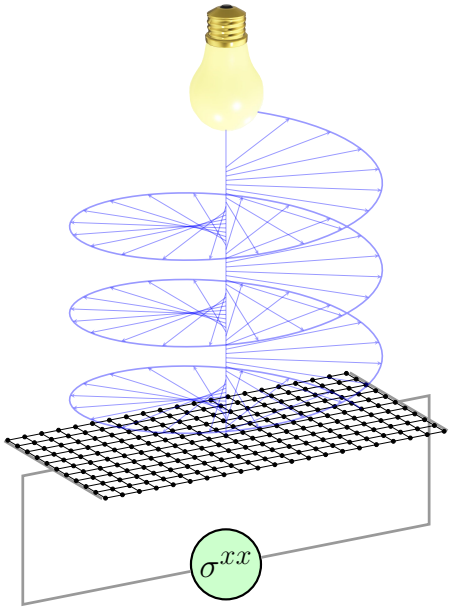

Figure 1.1: The figure shows a generic two dimensional system. The longitudinal conductivity is calculated using the Kubo formalism.

μ is the chemical potential and $\beta = 1/k_B T$ the inverse temperature. For a nonzero perturbation, the expectation value of an observable $\hat{A}$ is the trace over density matrix and observable operator

$$\langle \hat{A}(t) \rangle = \mathrm{tr}[\rho(t)\hat{A}(t)] \ . \tag{1.15}$$

The aim of the following is to find an expression for the density matrix $\rho(t)$. As in Ref. [50], the equation of motion for the density matrix is

$$i\hbar\dot{\rho}(t) = [\mathcal{H}_0, \rho(t)] + [V(t), \rho(t)] \ . \tag{1.16}$$

The perturbation is switched on at a certain time t_0, which leads to the recursive equation in the Dirac picture

$$\rho^D(t) = \rho_0 - \frac{i}{\hbar}\int_{-\infty}^{t} dt' \, [V^D(t'), \rho^D(t')] \ . \tag{1.17}$$

Keeping only terms up to linear order in the perturbation $V^D(t)$, one obtains

$$\Delta A(t) \equiv \langle \hat{A}(t) \rangle - \langle \hat{A} \rangle_0 = -\frac{i}{\hbar}\int_{-\infty}^{t} dt' \, \langle [\hat{A}^D(t), V^D(t')] \rangle \, , \tag{1.18}$$

which is known in literature as the "Kubo formula" [48–50]. Considering higher order corrections is straightforward and accounts for effects, such as the bulk photovoltaic effect [51, 52], which is a second order correction of the current caused by an electric field. In what follows, an equation for the linear response of the current operator to a probe bias is derived. The perturbation operator corresponding to the probe bias is the position integral over the current operator and the vector potential of the probe bias

$$V^D(t) = -\int_V d^d r \, \mathbf{J}(\mathbf{r}, t) \cdot \mathbf{A}(\mathbf{r}, t) \ . \tag{1.19}$$

The current operator in position representation for N particles is

$$\mathbf{J}(\mathbf{r},t) = -\frac{e}{2m}\sum_{i=1}^{N}\left(\mathbf{p}_i\delta(\mathbf{r}-\mathbf{r}_i)+\delta(\mathbf{r}-\mathbf{r}_i)\mathbf{p}_i\right) \tag{1.20}$$

$$= \frac{1}{V}\sum_{\mathbf{q}}\mathbf{J}(\mathbf{q},t)\,e^{i\mathbf{q}\cdot\mathbf{r}}\,, \tag{1.21}$$

where the time-dependence of the momentum operator $\mathbf{p}_i$ is suppressed and e is the electron charge and m the (effective) mass. The vector potential corresponding to the probe bias with frequency ω' is

$$\mathbf{A}^{\ell}(\mathbf{q},t') = \lim_{\eta'\to 0^+}\frac{1}{2\pi}\int_{-\infty}^{\infty}d\omega'\mathbf{A}^{\ell}(\mathbf{q},\omega')e^{-i(\omega'+i\eta')t'}\,, \tag{1.22}$$

whereby η' accounts for the adiabatic switch-on protocol of the bias which is assumed to be slow enough such that $\eta'\to 0$. The Kubo formula (1.18) for the linear current response to a probe bias is

$$\begin{aligned}\langle\mathbf{J}^{\ell}(\mathbf{q},\omega)\rangle = \sum_j \lim_{\eta_1\to 0^+}\frac{i}{\hbar V}\int_{-\infty}^{\infty}dt'\int_{-\infty}^{\infty}dt\;e^{i\omega t}\frac{i}{2\pi}\int_{-\infty}^{\infty}d\omega_1\Bigg[\frac{e^{-i\omega_1(t-t')}}{\omega_1+i\eta_1}\\ \times\left\langle[\mathbf{J}^{\ell}(\mathbf{q},t),\mathbf{J}^{j}(-\mathbf{q},t')]\right\rangle\mathbf{A}^{j}(\mathbf{q},t')\Bigg] - \frac{e^2n}{m}\mathbf{A}^{\ell}(\mathbf{q},\omega)\,,\end{aligned} \tag{1.23}$$

where the integral representation of the step function (1.436) was used. $\langle\cdot\rangle$ denotes the statistical average with respect to the system's state, which will in the presence of external driving not be in equilibrium. However, in what follows we shall assume the system to be in a stationary state so that occupation numbers of Floquet states are time-independent [22, 27, 53–57]. The expectation value of the particle density operator $\varrho(\mathbf{r}) = \sum_{i=1}^{N}\delta(\mathbf{r}-\mathbf{r}_i)$ is labeled as $n(\mathbf{r}) = \langle\varrho(\mathbf{r})\rangle$. The current operators $\mathbf{J}^{\ell,j}(\pm\mathbf{q},t^{(\prime)})$ are expanded with Floquet states (1.3) as basis

$$\mathbf{J}^{\ell}(\mathbf{q},t) = \sum_{\alpha\beta}\mathbf{J}^{\ell}_{\alpha\beta}(\mathbf{q},t)a^{\dagger}_{\alpha}(t_0=0)a_{\beta}(t_0=0)\;. \tag{1.24}$$

$a^{(\dagger)}_{\alpha,\beta}$ are creation and annihilation operators fulfilling [42, 58]

$$|\psi_{\alpha}(t)\rangle = a^{\dagger}_{\alpha}(t)|0\rangle \quad , \quad a_{\alpha}(t)|0\rangle = 0 \tag{1.25}$$

$$[a_{\alpha}(t),a^{\dagger}_{\beta}(t)]_{\pm} = \delta_{\alpha\beta} \quad , \quad [a_{\alpha}(t),a_{\beta}(t)]_{\pm} = [a^{\dagger}_{\alpha}(t),a^{\dagger}_{\beta}(t)]_{\pm} = 0\,, \tag{1.26}$$

where $|0\rangle$ is the vacuum state containing no particle, and the positive (negative) subscripts refer to fermionic anticommutators (bosonic commutators). The coefficients in Eq. (1.24) are

$$\mathbf{J}^{\ell}_{\alpha\beta}(\mathbf{q},t) = \langle\psi_{\alpha}(t)|\mathbf{J}^{\ell}(\mathbf{q})|\psi_{\beta}(t)\rangle \tag{1.27}$$

$$= \langle u_{\alpha}(t)|e^{\frac{i}{\hbar}\varepsilon_{\alpha}t}\mathbf{J}^{\ell}(\mathbf{q})e^{-\frac{i}{\hbar}\varepsilon_{\beta}t}|u_{\beta}(t)\rangle \tag{1.28}$$

$$= \sum_{n_1,n_2=-\infty}^{\infty} e^{i\left(\frac{1}{\hbar}(\varepsilon_{\alpha}-\varepsilon_{\beta})+(n_1-n_2)\Omega\right)t}\langle u^{n_1}_{\alpha}|\mathbf{J}^{\ell}(\mathbf{q})|u^{n_2}_{\beta}\rangle\,, \tag{1.29}$$

where Eq. (1.3) was used and $\mathbf{J}^\ell(\mathbf{q},0) \equiv \mathbf{J}^\ell(\mathbf{q})$. The fact that $\mathbf{J}^\ell(\mathbf{q})$ is time-independent is clarified later in Sec. 1.4.3. The commutator from Eq. (1.23) can be calculated using the last equation

$$[\mathbf{J}^\ell(\mathbf{q},t),\mathbf{J}^j(-\mathbf{q},t')] = \sum_{\alpha\beta\gamma\chi} \mathbf{J}^\ell_{\alpha\beta}(\mathbf{q},t)\mathbf{J}^j_{\gamma\chi}(-\mathbf{q},t')[a^\dagger_\alpha a_\beta, a^\dagger_\gamma a_\chi] \tag{1.30}$$

$$= \sum_{\alpha\beta\gamma\chi} \mathbf{J}^\ell_{\alpha\beta}(\mathbf{q},t)\mathbf{J}^j_{\gamma\chi}(-\mathbf{q},t')(a^\dagger_\alpha a_\chi \delta_{\beta\gamma} - a^\dagger_\gamma a_\beta \delta_{\alpha\chi}) \,. \tag{1.31}$$

The statistical average of this commutator is evaluated with respect to the aforementioned time-independent non-equilibrium density matrix. The distribution functions $\langle a^\dagger_{\alpha,\beta} a_{\alpha,\beta}\rangle = f_{\alpha,\beta}$ do not necessarily have to be equilibrium distribution functions, but it is assumed that these do not depend on time [22, 30, 53–57]. Hence, the statistical expectation value of the commutator using Eq. (1.29) becomes

$$\begin{aligned}\big\langle [\mathbf{J}^\ell(\mathbf{q},t),\mathbf{J}^j(-\mathbf{q},t')]\big\rangle = \sum_{\alpha\beta}\sum_{n_1..n_4=-\infty}^{\infty} e^{i\left(\frac{1}{\hbar}(\varepsilon_\alpha-\varepsilon_\beta)+(n_1-n_2)\Omega\right)t} \\ \times e^{i\left(\frac{1}{\hbar}(\varepsilon_\beta-\varepsilon_\alpha)+(n_3-n_4)\Omega\right)t'} \langle u^{n_1}_\alpha|\,\mathbf{j}^\ell(\mathbf{q})|u^{n_2}_\beta\rangle\langle u^{n_3}_\beta|\,\mathbf{j}^j(-\mathbf{q})|u^{n_4}_\alpha\rangle (f_\alpha - f_\beta) \,.\end{aligned} \tag{1.32}$$

The operators $\mathbf{j}(\mathbf{q})$ are the single-particle current operators

$$\mathbf{j}(\mathbf{q}) = \frac{-e}{2m}\big(\mathbf{p}\, e^{-i\mathbf{q}\cdot\mathbf{r}} + e^{-i\mathbf{q}\cdot\mathbf{r}}\mathbf{p}\big) \,. \tag{1.33}$$

Collecting the results from Eqs. (1.22),(1.23), and (1.32) yields

$$\begin{aligned}\langle \mathbf{J}^\ell(\mathbf{q},\omega)\rangle = \sum_j \lim_{\eta_1\to 0} -\frac{1}{\hbar V(2\pi)^2}\int_{-\infty}^{\infty}dt'\int_{-\infty}^{\infty}dt\int_{-\infty}^{\infty}d\omega_1\int_{-\infty}^{\infty}d\omega' \\ \times \sum_{\alpha\beta}\sum_{n_1..n_4=-\infty}^{\infty}\Bigg[e^{i\left(-\omega_1+\omega+\frac{1}{\hbar}(\varepsilon_\alpha-\varepsilon_\beta)+(n_1-n_2)\Omega\right)t} \\ \times\ e^{i\left(\omega_1-\omega'-i\eta'-\frac{1}{\hbar}(\varepsilon_\alpha-\varepsilon_\beta)+(n_3-n_4)\Omega\right)t'}\ \frac{f_\alpha - f_\beta}{\omega_1 + i\eta_1} \\ \times \langle u^{n_1}_\alpha|\,\mathbf{j}^\ell(\mathbf{q})|u^{n_2}_\beta\rangle\langle u^{n_3}_\beta|\,\mathbf{j}^j(-\mathbf{q})|u^{n_4}_\alpha\rangle\ \mathbf{A}^j(\mathbf{q},\omega')\Bigg] \\ - \frac{e^2 n}{m}\mathbf{A}^\ell(\mathbf{q},\omega) \,.\end{aligned} \tag{1.34}$$

Performing the time and the ω_1 integrals yields that the current is, as opposed to the undriven case, no longer a simple product of conductivity and electric field, since it is convoluted over the bias frequency ω'

$$\langle \mathbf{J}^\ell(\mathbf{q},\omega)\rangle = \sum_j \int_{-\infty}^{\infty} d\omega'\ \bar{\sigma}^{\ell j}(\mathbf{q},\omega,\omega')\mathbf{E}^j(\mathbf{q},\omega') \,. \tag{1.35}$$

The conductivity tensor depends on both the response frequency ω and the bias

frequency ω'

$$\begin{aligned}\bar{\sigma}^{\ell j}(\mathbf{q},\omega,\omega') = &\frac{i}{\hbar\omega V}\sum_{\alpha\beta}\sum_{n_1..n_4=-\infty}^{\infty}\frac{f_\alpha - f_\beta}{\omega+\frac{1}{\hbar}(\varepsilon_\alpha-\varepsilon_\beta)+(n_1-n_2)\Omega+i0^+}\\ &\times\langle u_\alpha^{n_1}|\,\mathbf{j}^\ell(\mathbf{q})|u_\beta^{n_2}\rangle\langle u_\beta^{n_3}|\,\mathbf{j}^j(-\mathbf{q})|u_\alpha^{n_4}\rangle\\ &\times\delta\big(\omega+(n_1-n_2+n_3-n_4)\Omega-\omega'\big)\\ &+i\frac{e^2 n}{m\omega}\delta_{\ell j}\delta(\omega-\omega')\;.\end{aligned} \tag{1.36}$$

The response and bias frequency ω and ω' are assumed to be in the central Floquet zone

$$|\omega|,|\omega'|<\frac{\Omega}{2}\quad\Rightarrow\quad\omega-\omega'<\Omega\;. \tag{1.37}$$

In other words, the Fourier decomposition of the vector potential for the electric field, see Eq. (1.22), contains only frequencies smaller than half of the driving frequency. Additionally, one should rather consider a current expectation value of the form $\langle J^\ell(\mathbf{q},\tilde{\omega}+p\Omega)\rangle$ together with Eq. (1.35) and $\omega=\tilde{\omega}+p\Omega$, such that the current expectation value is governed by

$$\langle\mathbf{J}^\ell(\mathbf{q},\tilde{\omega}+p\Omega)\rangle=\sum_j\int_{-\Omega/2}^{\Omega/2}d\omega'\;\bar{\sigma}^{\ell j}(\mathbf{q},\tilde{\omega}+p\Omega,\omega')\mathbf{E}^j(\mathbf{q},\omega')\;. \tag{1.38}$$

Anticipating that the focus is on the DC limit of the conductivity, only the case $p=0$ is considered in the present work, where $\omega=\tilde{\omega}$. In the DC limit, the argument of the delta distribution of the first term in Eq. (1.36) can, under condition (1.37), only be zero if

$$n_1-n_2+n_3-n_4=0\,. \tag{1.39}$$

This allows the extraction of the delta distribution

$$\bar{\sigma}^{\ell j}(\mathbf{q},\omega,\omega')=\sigma^{\ell j}(\mathbf{q},\omega)\delta(\omega-\omega') \tag{1.40}$$

together with

$$\begin{aligned}\sigma^{\ell j}(\mathbf{q},\omega)=&\frac{i}{\hbar\omega V}\sum_{\alpha\beta}\sum_{\substack{n_1..n_4=-\infty\\ \text{Eq. (1.39)}}}^{\infty}\Bigg[\frac{f_\alpha-f_\beta}{\omega+\frac{1}{\hbar}(\varepsilon_\alpha-\varepsilon_\beta)+(n_1-n_2)\Omega+i0^+}\\ &\times\langle u_\alpha^{n_1}|\,\mathbf{j}^\ell(\mathbf{q})|u_\beta^{n_2}\rangle\langle u_\beta^{n_3}|\,\mathbf{j}^j(-\mathbf{q})|u_\alpha^{n_4}\rangle\Bigg]+i\frac{e^2n}{m\omega}\delta_{\ell j}\;.\end{aligned} \tag{1.41}$$

Interestingly, introducing Wigner coordinates [27], a mean time $T=(t+t')/2$ and a relative time $\tau=t-t'$, in Eq. (1.32) and averaging the mean time over one driving cycle, whereas the relative time is Fourier transformed, lead to the same expression as Eq. (1.41). Under condition (1.39), the current is the product of conductivity and electric field

$$\langle\mathbf{J}^\ell(\mathbf{q},\omega)\rangle=\sum_j\int_{-\infty}^{\infty}d\omega'\;\sigma^{\ell j}(\mathbf{q},\omega)\delta(\omega-\omega')\mathbf{E}^j(\mathbf{q},\omega') \tag{1.42}$$

$$=\sum_j\sigma^{\ell j}(\mathbf{q},\omega)\mathbf{E}^j(\mathbf{q},\omega)\;. \tag{1.43}$$

Concentrating on the real part of the longitudinal conductivity $\ell = j = x$ and using the Dirac identity (1.433) lead to

$$\begin{aligned}\mathrm{Re}[\sigma^{xx}(0,\omega)] =& \frac{\pi}{V}\left(\frac{e}{m}\right)^2 \sum_{\alpha\beta} \sum_{\substack{n_1..n_4=-\infty \\ \text{Eq. (1.39)}}}^{\infty} \Bigg[\frac{f_\alpha - f_\beta}{\hbar\omega} \langle u_\alpha^{n_1}|p^x|u_\beta^{n_2}\rangle\langle u_\beta^{n_3}|p^x|u_\alpha^{n_4}\rangle \\ & \times \delta\big(\omega + \tfrac{1}{\hbar}(\varepsilon_\alpha - \varepsilon_\beta) + (n_1 - n_2)\Omega\big)\Bigg] .\end{aligned} \tag{1.44}$$

In the last step, it was assumed that the current is spatially homogeneous and that it is thus not a function of $\mathbf{r}$, see Eq. (1.33). Per construction $|\varepsilon_\alpha - \varepsilon_\beta| \leq \hbar\Omega$, the delta distribution in the last equation can thus only have support if

$$n_1 = n_2 \quad \overset{\text{Eq. (1.39)}}{\Rightarrow} \quad n_3 = n_4 \,. \tag{1.45}$$

This leads to the equation for the longitudinal conductivity

$$\begin{aligned}\mathrm{Re}\left[\sigma^{xx}(0,\omega)\right] =& \frac{\pi}{V}\left(\frac{e}{m}\right)^2 \sum_{n,n'=-\infty}^{\infty} \sum_{\alpha\beta} \Bigg[\frac{f_\alpha - f_\beta}{\hbar\omega} \langle u_\alpha^{n}|p^x|u_\beta^{n}\rangle\langle u_\beta^{n'}|p^x|u_\alpha^{n'}\rangle \\ & \times \delta\big(\omega + \tfrac{1}{\hbar}(\varepsilon_\alpha - \varepsilon_\beta)\big)\Bigg] .\end{aligned} \tag{1.46}$$

In the DC-limit, namely at zero response frequency $\omega \to 0$, the conductivity can be reformulated as an energy integral over the central Floquet zone

$$\lim_{\omega\to 0} \mathrm{Re}[\sigma^{xx}(0,\omega)] = \frac{\pi\hbar}{V}\left(\frac{e}{m}\right)^2 \int_{-\hbar\Omega/2}^{\hbar\Omega/2} d\varepsilon \left(-\frac{\partial f}{\partial \varepsilon}\right) \sigma(\varepsilon) \tag{1.47}$$

with

$$\sigma(\varepsilon) = \sum_{nn'} \sum_{\alpha\beta} \langle u_\alpha^n|\, p^x \,|u_\beta^n\rangle \,\langle u_\beta^{n'}|\, p^x \,|u_\alpha^{n'}\rangle \;\delta\big(\varepsilon - \varepsilon_\alpha\big)\delta\big(\varepsilon - \varepsilon_\beta\big) \,. \tag{1.48}$$

In Sec. 1.4.3 this quantity will be expressed with Green's functions. A similar result, Eqs. (1.47), (1.48), was already derived within the Keldysh framework in Ref. [22]. The derivation presented in this section circumvents an ansatz for the lesser Green's function, see Ref. [22]. The choice of the energy integration range in Eq. (1.47) is thus far arbitrary and must be chosen suitably for the model of interest. In derivating Eq. (1.46) the only requirement is

$$|\varepsilon_\alpha - \varepsilon_\beta| \leq \hbar\Omega \tag{1.49}$$

being a weaker restriction than claiming that the quasienergies fulfill $|\varepsilon_{\alpha,\beta}| \leq \hbar\Omega/2$ and allows even unbounded quasienergies. Eq. (1.49) can be fulfilled choosing a suitable λ, possibly momentum dependent, such that all quasienergies are within the range

$$\lambda - \frac{\hbar\Omega}{2} \leq \varepsilon_\alpha < \lambda + \frac{\hbar\Omega}{2} \,. \tag{1.50}$$

The choice of λ depends on the details of the system, e.g. for a parabolic dispersion or a square lattice, both without spin-orbit coupling, an appropriate choice would

be $\lambda = \varepsilon_\alpha$. For graphene, either with full band structure or in the Dirac-cone approximation, a better choice would be $\lambda = 0$. With the knowledge that the choice of the central Floquet is not unique, the DC-limit of the longitudinal conductivity in presence of an external driving is

$$\lim_{\omega\to 0} \mathrm{Re}[\sigma^{xx}(0,\omega)] = \frac{\pi\hbar}{V}\left(\frac{e}{m}\right)^2 \int_{\lambda-\hbar\Omega/2}^{\lambda+\hbar\Omega/2} d\varepsilon \left(-\frac{\partial f}{\partial \varepsilon}\right) \sigma(\varepsilon)\,, \tag{1.51}$$

being the main result of this section. The aim of the following section is to find a proper Green's function that allows for both formulating the result from the Kubo formula for the conductivity in terms of Green's functions and allowing for a successive scheme to include disorder potentials.

1.3.1 Time-dependent distribution function

A full description of a realistic driven system requires the treatment of very rich physics. This covers the population of Floquet bands [59]. General, the density matrix and, with that, also the distribution function of a periodically driven system are time-dependent [49]. Later, the regimes are discussed where the distribution can be assumed to be stationary.
Another important point is the investigation of time-scales. For instance, if the switch-on of the driving is not far in the past, the explicit switch-on protocol might be important for the physics in the temporal vicinity of the switch-on time [60]. There are works that investigate the time scale for forming a Floquet state, and it was found that several tens of driving cycles are sufficient for a Floquet state to be formed [61]. At intermediate time-scales there might already arise a change of the population dynamics [62]. The time scale of the intermediate regime is dominated by various physical processes causing heating of the system. This will be discussed in the following. If the heating is controlled by cooling processes, a prethermalized state might be achieved [59, 63]. The latter is approximately described by a time-independent non-equilibrium distribution function [64]. There are works that treat heating, and with that the absorption of energy from the driving field, semi-classically using the Boltzmann approach [30, 65]. However, a fully microscopic description of what is called "heating" is a rather challenging task due to the numerous processes that have to be considered. Absorption of photons by an electron might lead to interband transitions. A possible relaxation channel for these excited states is via phonons [66]. Thus, through electron-phonon interaction, lattice vibrations are induced, increasing the temperature of a system [59, 67]. Interactions are a different topic, as the interaction between electrons itself might be renormalized by the external driving, which is not discussed in this work and left as future work. The discussion of the long time behavior of a driven system is even more subtle. A closed quantum system will tend towards an infinite temperature state in the long time limit [68, 69]. The system must be cooled to avoid an infinite heating, where a possible realization is coupling to baths [59, 67]. The stronger the driving causes heating, the stronger the cooling by the bath must be, such that a balance of incoming and outflowing energy is achieved. To cool the system effectively, the coupling of the bath to the system might be strong, making a perturbative inclusion of the bath to the system rather challenging.

Since, in this work, the distribution is assumed to be time-independent, the actual conditions and requirements for this assumption must be further clarified. In a driven system, absorption of photons and with that energy consumption from the driving field is inherently present in an actual physical system. Hence, to control heating, absorption processes have to be controlled. Whereas the above aimed at the discussion of time scales, the focus is now on energy scales. Following Ref. [62] the photon energy $\hbar\Omega$, the band width of the spectrum W, the size of a gap in the spectrum Δ, and the interaction strength U are the most relevant energy scales. If the photon energy is considerably larger than the band width, $\hbar\Omega \gg W$, various perturbation theories are applicable [3, 21, 43]. The authors of Refs. [3, 21, 43] give in their works an overview of von Fleck, Floquet-Magnus, and the Brillouin-Wigner expansion. The latter is used to explain topological phase transitions in graphene caused by renormalization of effective hopping energies due to an external driving. Most importantly, the system becomes effectively time-independent in the high-frequency regime such that the external driving leads to a pure renormalization of the system's parameters [25, 70] rather than changing the population. Another promising regime, where a time-independent distribution is valid, can be realized in a gapped system, if the photon energy is reasonably smaller than the gap $\hbar\Omega \ll \Delta$. Exciting particles across the gap requires high-order photon processes, which are well known in literature to be strongly suppressed, as demonstrated in Refs. [71–73]. The last energy scale, the interaction strength U, requires an even deeper discussion than the others. It is well understood that in a static system, interactions can have a vast influence on the ground state of a system, especially if the interaction strength is the dominating energy scale. The situation is even more complicated if the ground state becomes time-dependent through an additional driving. Since the description of driven systems is still in its infancy, it is still not fully understood how to construct the time-dependent ground state. Nevertheless, if the interaction strength is smaller than both the bandwidth and the photon energy, it seems reasonable to treat the system as without interactions, thus validating a single particle picture. Collecting the above requirements on the different energy scales, the most promising regime for the realization of a non-equilibrium stationary state seems to be when interactions, band width, photon energy, and gap size form an increasing hierarchy $U \ll W \ll \hbar\Omega \ll \Delta$.

1.4 Green's functions

The Floquet solution of the time-dependent Schrödinger equation is $|\psi_\alpha(t)\rangle = e^{-\frac{i}{\hbar}\varepsilon_\alpha t}|u_\alpha(t)\rangle$, where the exponential function and the Floquet function $u_\alpha(t)$ depend on the same time t. An extension is the t-t'-Floquet state $|\psi_\alpha(t,t')\rangle = e^{-\frac{i}{\hbar}\varepsilon_\alpha t}|u_\alpha(t')\rangle$ where the wave function now depends on two times. The t-t'-formalism is intensely studied in Refs. [1, 20, 74]. A possible application of this formalism is the separation of time scales as, for example, done in Ref. [61] where Floquet theory for short laser pulses is investigated. In the following, a further extension to the t-t'-Floquet theory is presented. Within this formalism a new type of Green's functions is found. The properties of these, as well as relations to Green's functions used in other works, are analyzed. Finally the expression for the conductivity found in Sec. 1.3 is reformulated utilizing the new type of Green's functions.

1.4.1 The *t-t'*-formalism and -Green's functions

This subsection aims to introduce the *t-t'*-formalism. This includes basic definitions and relations used in this work. Furthermore, a proper Green's function that is suitable to express the result from the Kubo formula in terms of Green's functions is constructed. A deeper justification for the use of this formalism is given in Sec. 1.4.4, where it is shown that the straightforward approach using two time Green's functions fails to reproduce the expression obtained from the Kubo formula. Separating the periodic from the aperiodic time-dependence of a Floquet state yields the *t-t'*-Floquet state

$$|\psi_\alpha(t,t')\rangle = e^{-\frac{i}{\hbar}\varepsilon_\alpha t}|u_\alpha(t')\rangle\,, \tag{1.52}$$

recovering for $t = t'$ the Floquet state solution of the time-dependent Schrödinger equation and fulfilling the *t-t'*-Schrödinger equation

$$i\hbar\frac{\partial}{\partial t}|\psi_\alpha(t,t')\rangle = H_F(t')|\psi_\alpha(t,t')\rangle\ . \tag{1.53}$$

The time derivative on the left side of Eq. (1.53) depends on a different time than the Floquet Hamiltonian H_F on the right side. The advantage of discriminating the time dependence of the exponential from the periodic Floquet function lies in the fact that the evolution of the states is governed by the operator

$$U(t,t_0,t') = e^{-\frac{i}{\hbar}H_F(t')(t-t_0)}\,, \tag{1.54}$$

which avoids any time ordering [20, 75]. Following H. Sambe [76], we define, on the space of all states depending periodically with period T on a parameter t' having dimension of time, the scalar product

$$\langle\!\langle\varphi|\chi\rangle\!\rangle = \frac{1}{T}\int_0^T dt'\,\langle\varphi|t'\rangle\langle t'|\chi\rangle\,. \tag{1.55}$$

The notation $\langle t'|\psi\rangle \equiv |\psi(t')\rangle$ suggests to consider t' as a coordinate rather than a time parameter [36]. The corresponding operator $\hat{t}'$ can be defined to act multiplicatively on the above wave functions,

$$\hat{t}'|\psi(t')\rangle = \langle t'|\hat{t}'|\psi\rangle = t'|\psi(t')\rangle\,, \tag{1.56}$$

and the canonically conjugate operator is

$$\hat{w} \equiv -i\hbar\frac{\partial}{\partial t'} \quad \Rightarrow \quad [\hat{w},\hat{t}'] = -i\hbar \tag{1.57}$$

with a complete system of orthonormalized periodic eigenfunctions

$$\langle t'|\ell\rangle = e^{-i\Omega\ell t'} \quad , \quad \hat{w}|\ell\rangle = \ell\hbar\Omega|\ell\rangle \quad , \quad \langle\!\langle k|\ell\rangle\!\rangle = \delta_{k,\ell} \quad , \quad \text{with} \quad k,\ell\in\mathbb{Z}, \tag{1.58}$$

$$\sum_{\ell=-\infty}^{\infty}\langle t_1'|\ell\rangle\langle\ell|t_2'\rangle = T\sum_{s=-\infty}^{\infty}\delta(t_1'-t_2'+sT) = \langle t_1'|t_2'\rangle\,. \tag{1.59}$$

There is a *t-t'*-Floquet state for each Floquet zone. In general the *t-t'*-state for the ℓ-th Floquet zone is

$$|\psi_\alpha^\ell(t,t')\rangle = e^{i\ell\Omega(t'-t)}|\psi_\alpha(t,t')\rangle\,, \tag{1.60}$$

fulfilling the t-t'-Schrödinger equation, see Eq. (1.53). These states have the same time-evolution operator given in Eq. (1.54) as the t-t'-states of Eq. (1.52). Moreover, they have the properties

$$\langle\!\langle \psi_\alpha^\ell(t,t')|\psi_\beta^{\ell'}(t,t')\rangle\!\rangle = \delta_{\alpha\beta}\delta_{\ell\ell'}\,, \tag{1.61}$$

$$\sum_\alpha \sum_{\ell=-\infty}^{\infty} |\psi_\beta^\ell(t,t_1')\rangle\langle\psi_\alpha^\ell(t,t_2')| = \mathbb{1}T\sum_{s=-\infty}^{\infty}\delta(t_1'-t_2'+sT)\,. \tag{1.62}$$

Now, the notation $\langle t'|\psi_\alpha^\ell(t)\rangle \equiv |\psi_\alpha^\ell(t,t')\rangle$ for the t-t'-state of the ℓ-th Floquet zone is introduced. In second quantization this allows the definition of a system of creation and annihilation operators $b_{\alpha\ell}^\dagger(t)$, $b_{\alpha\ell}(t)$ with

$$|\psi_\alpha^\ell(t)\rangle = b_{\alpha\ell}^\dagger(t)|0\rangle \quad , \quad b_{\alpha\ell}(t)|0\rangle = 0 \tag{1.63}$$

with the (anti-)commutation relations

$$[b_{\alpha\ell}(t), b_{\beta\ell'}^\dagger(t)]_\pm = \delta_{\alpha\beta}\delta_{\ell\ell'} \quad , \quad [b_{\alpha\ell}(t), b_{\beta\ell'}(t)]_\pm = [b_{\alpha\ell}^\dagger(t), b_{\beta\ell'}^\dagger(t)]_\pm = 0\,. \tag{1.64}$$

Field operators can be constructed as

$$\Phi(t,t') = \sum_\alpha \sum_{\ell=-\infty}^{\infty} \psi_\alpha^\ell(t,t')b_{\alpha\ell}(t) \tag{1.65}$$

fulfilling

$$[\Phi(t,t_1'), \Phi^\dagger(t,t_2')]_\pm = T\sum_{s=-\infty}^{\infty}\delta(t_1'-t_2'+sT) \tag{1.66}$$

with again all other (anti-)commutators at equal times t being zero. The Floquet Hamiltonian H_F can be formulated as

$$H_F(t) = \sum_\alpha \sum_{\ell=-\infty}^{\infty} (\varepsilon_\alpha + r\hbar\Omega) b_{\alpha\ell}^\dagger(t) b_{\alpha\ell}(t)\,, \tag{1.67}$$

which is neither bounded from below nor from above. The time-evolution in the unprimed times of the t-t'-states from Eq. (1.60) is governed by the operator given in Eq. (1.54), hence the Heisenberg picture of the field operators is

$$\Phi_H(t,t') = U^\dagger(t,0,t')\Phi(t,t')U(t,0,t') = \sum_\alpha \sum_{\ell=-\infty}^{\infty} \psi_\alpha^\ell(t,t')b_{\alpha\ell}\,. \tag{1.68}$$

This quantity allows for the definition of a retarded/advanced Green's function

$$\mathcal{G}_0^{r,a}(t_1,t_2,t_1',t_2') = \mp i\Theta(\pm(t_1-t_2))\frac{1}{T}\big\langle\big[\Phi_H(t_1,t_1'), \Phi_H(t_2,t_2')\big]\big\rangle \tag{1.69}$$

$$= \mp i\Theta(\pm(t_1-t_2))\frac{1}{T}\sum_{\ell=-\infty}^{\infty}\sum_\alpha |\psi_\alpha^\ell(t_1,t_1')\rangle\,\langle\psi_\alpha^\ell(t_2,t_2')| \tag{1.70}$$

$$\begin{aligned} = \mp i\Theta(\pm(t_1-t_2))\frac{1}{T}\sum_{\ell=-\infty}^{\infty}\sum_\alpha & e^{-\frac{i}{\hbar}(\varepsilon_\alpha+\ell\hbar\Omega)(t_1-t_2)} \\ & \times |u_\alpha(t_1')\rangle\,\langle u_\alpha(t_2')|\, e^{i\ell\Omega(t_1'-t_2')} \end{aligned} \tag{1.71}$$

depending on four different times. The index "0" indicates that this Green's function is understood as Green's function for the bare system. This will become important later when the considerations include impurities in the physical system. $\Theta(\cdot)$ is the step function, being zero for negative arguments and one for positive arguments. A similar expression was already derived in Refs. [20, 77]. Moreover, with the spectral density

$$A(t_1,t_1',t_2,t_2') = \frac{1}{T}\big\langle\big[\Phi_H(t_1,t_1'),\Phi_H(t_2,t_2')\big]\big\rangle \tag{1.72}$$

$$= \frac{1}{T}\sum_{\ell=-\infty}^{\infty}\sum_{\alpha}\Big[e^{-\frac{i}{\hbar}(\varepsilon_\alpha+\ell\hbar\Omega)(t_1-t_2)}|u_\alpha(t_1')\rangle\langle u_\alpha(t_2')|e^{i\ell\Omega(t_1'-t_2')}\Big] \tag{1.73}$$

having Fourier components

$$A(\varepsilon,t_1',t_2') = \frac{\hbar}{T}\sum_{\ell=-\infty}^{\infty}\sum_{\alpha}\Big[\delta\big(\varepsilon-(\varepsilon_\alpha+\ell\hbar\Omega)\big)|u_\alpha(t_1')\rangle\langle u_\alpha(t_2')|e^{i\ell\Omega(t_1'-t_2')}\Big] \tag{1.74}$$

the familiar Lehmann representation of the Green's function is obtained

$$\mathcal{G}_0^{r,a}(\varepsilon,t_1',t_2') = \int_{-\infty}^{\infty}d\varepsilon'\,\frac{A(\varepsilon',t_1',t_2')}{\varepsilon-\varepsilon'\pm i0^+}\,. \tag{1.75}$$

The Green's function in Eq. (1.71) fulfills

$$\begin{aligned}\Big(i\partial_{t_1}-\tfrac{1}{\hbar}H_F(t_1')\Big)\mathcal{G}_0^{r,a}(t_1,t_2,t_1',t_2') &= \delta(t_1-t_2)\sum_{\alpha}|u_\alpha(t_1')\rangle\,\langle u_\alpha(t_2')| \\ &\quad\times\frac{1}{T}\sum_{\ell=-\infty}^{\infty}e^{i\ell\Omega(t_1'-t_2')}\end{aligned} \tag{1.76}$$

$$= \delta(t_1-t_2)\sum_{\ell=-\infty}^{\infty}\delta(t_1'-t_2'+\ell T)\mathbb{1} \tag{1.77}$$

where the Fourier expansion of the Dirac comb

$$\frac{1}{T}\sum_{\ell=-\infty}^{\infty}e^{i\ell\Omega t} = \sum_{\ell=-\infty}^{\infty}\delta(t+\ell T) \tag{1.78}$$

was used. The Green's function defined in Eq. (1.71) depends only on the difference of the unprimed times (t_1-t_2). This allows for the continuous Fourier transformation of the difference of times (t_1-t_2) on the energy ε. Eq. (1.71) is in energy space

$$\mathcal{G}_0^{r,a}(\varepsilon,t_1',t_2') = \frac{1}{T}\sum_{\ell=-\infty}^{\infty}\sum_{\alpha}\frac{|u_\alpha(t_1')\rangle\,\langle u_\alpha(t_2')|}{\frac{1}{\hbar}\varepsilon-\frac{1}{\hbar}\varepsilon_\alpha-\ell\Omega\pm i0^+}\,e^{i\ell\Omega(t_1'-t_2')} \tag{1.79}$$

$$= \frac{1}{T}\sum_{\ell=-\infty}^{\infty}\sum_{\alpha}\sum_{n,n'=-\infty}^{\infty}\frac{|u_\alpha^{n+\ell}\rangle\,\langle u_\alpha^{n'+\ell}|}{\frac{1}{\hbar}\varepsilon-\frac{1}{\hbar}\varepsilon_\alpha-\ell\Omega\pm i0^+}\,e^{-in\Omega t_1'}e^{in'\Omega t_2'}\,. \tag{1.80}$$

The last equation is a double Fourier series of the Green's function

$$\mathcal{G}_0^{r,a}(\varepsilon,t_1',t_2') = \frac{1}{T}\sum_{n,n'=-\infty}^{\infty}\mathcal{G}_0^{r,a}(\varepsilon,n,n')\;e^{-in\Omega t_1'}e^{in'\Omega t_2'} \tag{1.81}$$

together with the Fourier coefficients [78, 79]

$$\mathcal{G}_0^{r,a}(\varepsilon, n, n') = \sum_{\ell=-\infty}^{\infty} \sum_{\alpha} \frac{|u_\alpha^{n+\ell}\rangle \langle u_\alpha^{n'+\ell}|}{\frac{1}{\hbar}\varepsilon - \frac{1}{\hbar}\varepsilon_\alpha - \ell\Omega \pm i0^+} \,. \tag{1.82}$$

From now on, the quantities defined in the Eqs. (1.71), (1.79), and (1.82) will be referred to as "Green's functions". $\mathcal{G}_0^{r,a}(\varepsilon, n, n')$ can be related to the Floquet Hamiltonian in matrix form (1.11), as shown in the next section.

1.4.2 Properties of the *t-t'*-Green's function

Before proceeding with the calculations regarding the conductivity of a driven system, some elementary properties of the four time Green's function are summarized. This analysis involves the diagonalization of the Green's function, as well as a comparison of techniques and Green's functions used in other works. The Green's function defined in Eq. (1.71) is periodic in both the primed and unprimed times:

$$\mathcal{G}_0^{r,a}(t_1, t_2, t_1', t_2') = \mathcal{G}_0^{r,a}(t_1 + T, t_2 + T, t_1', t_2') \tag{1.83}$$

$$= \mathcal{G}_0^{r,a}(t_1, t_2, t_1' + T, t_2' + T) \,. \tag{1.84}$$

Performing a Fourier transformation in the relative time $(t_1 - t_2)$, as suggested in the foregoing section or using the shifted Fourier transform as in Refs. [30, 32, 33, 80–85]

$$\mathcal{G}_0^{r,a}(t_1, \varepsilon, t_1', t_2') = \int_{-\infty}^{\infty} dt_2 \; e^{\frac{i}{\hbar}\varepsilon(t_1 - t_2)} \mathcal{G}_0^{r,a}(t_1, t_2, t_1', t_2') \tag{1.85}$$

leads in both cases to Eq. (1.79), since the Green's function in Eq. (1.71) depends only on the relative time $(t_1 - t_2)$. The transformed object on the right side of Eq. (1.85) is, in case of the Green's function (1.71) independent of t_1, and consequently a Fourier series to expand the t_1-dependency as in Refs. [30, 32, 33, 80–85] is not needed. Making use of the definition in Eq. (1.81) and with the inverse Fourier transformation, it is shown that the four time Green's function is

$$\begin{aligned} \mathcal{G}_0^{r,a}(t_1, t_2, t_1', t_2') = & \frac{1}{2\pi\hbar T} \int_{-\infty}^{\infty} d\varepsilon \Bigg[e^{-\frac{i}{\hbar}\varepsilon(t_1 - t_2)} \\ & \times \sum_{n,n'=-\infty}^{\infty} \mathcal{G}_0^{r,a}(\varepsilon, n, n') e^{-in\Omega t_1'} \, e^{in'\Omega t_2'} \Bigg] \,. \end{aligned} \tag{1.86}$$

Using the Fourier representation of the delta distribution and the Dirac comb, see Eq. (1.78), it holds that

$$\begin{aligned} \delta(t_1 - t_2) \sum_{\ell=-\infty}^{\infty} \delta(t_1' - t_2' + \ell T) = & \frac{1}{2\pi\hbar T} \int_{-\infty}^{\infty} d\varepsilon \Bigg[e^{-\frac{i}{\hbar}\varepsilon(t_1 - t_2)} \\ & \times \sum_{n,n'=-\infty}^{\infty} e^{-in\Omega t_1'} \, e^{in'\Omega t_2'} \delta_{nn'} \Bigg] \,. \end{aligned} \tag{1.87}$$

Inserting Eqs. (1.86),(1.87) in (1.77) and using the Fourier expansion of the Hamiltonian, see Eqs. (1.1) and (1.8) and the matrix form of the Floquet equation (1.11), it follows from a comparison of the coefficients that

$$\varepsilon\,\mathcal{G}_0^{r,a}(\varepsilon,n,n') - \sum_{m=-\infty}^{\infty} \underbrace{\left(H_{n-m} - n\hbar\Omega\,\delta_{mn}\right)}_{\equiv(\mathbf{H}_F)_{nm}} \mathcal{G}_0^{r,a}(\varepsilon,m,n') = \hbar\delta_{n,n'}\ . \tag{1.88}$$

Comparing this with Eq. (1.82) leads to

$$\mathcal{G}_0^{r,a}(\varepsilon,n,n') = \sum_{\ell=-\infty}^{\infty}\sum_{\alpha}\frac{|u_\alpha^{n+\ell}\rangle\,\langle u_\alpha^{n'+\ell}|}{\frac{1}{\hbar}\varepsilon - \frac{1}{\hbar}\varepsilon_\alpha - \ell\Omega \pm i0^+} = \left(\frac{1}{\frac{1}{\hbar}\varepsilon - \frac{1}{\hbar}\mathbf{H}_F \pm i0^+}\right)_{nn'}\ . \tag{1.89}$$

The Green's function is equal to the inverse of the Floquet Hamiltonian, where the Floquet Hamiltonian $\mathbf{H}_F$ is here understood in matrix representation. Before a transformation diagonalizing the above Green's function is constructed, the relation of the four time Green's function given in Eq. (1.71), with the two time Green's functions used in other works, is demonstrated, e.g. Refs. [30, 32, 33, 80–85]. This involves an analysis of the Floquet and Wigner representation of the Green's functions [83]. The defining equation for the two time Green's function of the Schrödinger equation is

$$\left(i\partial_{t_1} - \tfrac{1}{\hbar}H(t_1)\right)G_0^{r,a}(t_1,t_2) = \delta(t_1-t_2)\,. \tag{1.90}$$

In contrast to Eq. (1.77), the partial derivative with respect to time and the Hamiltonian depend on the same time. The second difference is that on the right side of the above equation there is only a single delta distribution, compared to Eq. (1.77) where on the right side there is a delta distribution depending on the difference of the unprimed times and a Dirac comb. The solution of Eq. (1.90) is

$$G_0^{r,a}(t_1,t_2) = \mp i\Theta(\pm(t_1-t_2))\sum_{\alpha}|\psi_\alpha(t_1)\rangle\langle\psi_\alpha(t_2)|\,. \tag{1.91}$$

Introducing Wigner-coordinates [86], a relative time t and a mean time T,

$$t = t_1 - t_2 \quad , \quad T = \frac{t_1+t_2}{2} \tag{1.92}$$

and Fourier transforming the relative time onto an energy, whereas the mean time dependence is kept within a discrete Fourier series, the two time Green's function becomes

$$G_0^{r,a}(\varepsilon,T) = \sum_{N=-\infty}^{\infty} G_0^{r,a}(\varepsilon,N)e^{-iN\Omega T} \tag{1.93}$$

together with the Fourier coefficients

$$G_0^{r,a}(\varepsilon,N) = \sum_{\ell=-\infty}^{\infty}\sum_{\alpha}\frac{|u_\alpha^{\ell}\rangle\langle u_\alpha^{\ell-N}|}{\frac{1}{\hbar}\varepsilon + \frac{1}{2}N\Omega - \frac{1}{\hbar}\varepsilon_\alpha - \ell\Omega \pm i0^+}\ . \tag{1.94}$$

Following the nomenclature of the authors of Ref. [83] the Green's function in Eq. (1.93) is called to be in "Wigner representation" whereas the form in Eq. (1.94)

is called "Floquet representation". The relation between the latter Green's function and the ones in Eq. (1.89) was already established in Refs. [83, 87] and follows the steps:

$$\sum_{\ell=-\infty}^{\infty}\sum_{\alpha}\frac{|u_\alpha^\ell\rangle\langle u_\alpha^{\ell-N}|}{\frac{1}{\hbar}\varepsilon+\frac{1}{2}N\Omega-\frac{1}{\hbar}\varepsilon_\alpha-\ell\Omega\pm i0^+} \tag{1.95}$$

$$\overset{N\to m-n}{\longrightarrow}\sum_{\ell=-\infty}^{\infty}\sum_{\alpha}\frac{|u_\alpha^\ell\rangle\langle u_\alpha^{\ell-m+n}|}{\frac{1}{\hbar}\varepsilon+\frac{m-n}{2}\Omega-\frac{1}{\hbar}\varepsilon_\alpha-\ell\Omega\pm i0^+} \tag{1.96}$$

$$=\sum_{\ell=-\infty}^{\infty}\sum_{\alpha}\frac{|u_\alpha^{\ell+m}\rangle\langle u_\alpha^{\ell+n}|}{\frac{1}{\hbar}\varepsilon-\frac{m+n}{2}\Omega-\frac{1}{\hbar}\varepsilon_\alpha-\ell\Omega\pm i0^+} \tag{1.97}$$

$$\overset{\varepsilon\to\varepsilon+\frac{m+n}{2}}{\longrightarrow}\sum_{\ell=-\infty}^{\infty}\sum_{\alpha}\frac{|u_\alpha^{\ell+m}\rangle\langle u_\alpha^{\ell+n}|}{\frac{1}{\hbar}\varepsilon-\frac{1}{\hbar}\varepsilon_\alpha-\ell\Omega\pm i0^+}\,. \tag{1.98}$$

Despite this remarkable connection, the use of the four time Green's function is clearly superior than the use of the two time Green's function for the calculation of the conductivity in a driven system, as clarified later in Sec. 1.4.4.
It is of ultimate interest to find a transformation diagonalizing the Green's function spanned by the Fourier coefficients given in Eq. (1.82). Such a transformation is successively constructed in the following. From the matrix representation of the Floquet equation given in Eq. (1.11), it follows that a shifted eigenstate $|u_\alpha^n\rangle \to |u_\alpha^{n-m'}\rangle$ corresponds to a shifted quasienergy $\varepsilon_\alpha \to \varepsilon_\alpha - m'\hbar\Omega$

$$\sum_{n=-\infty}^{\infty}\left(H_{m-n}-n\hbar\Omega\delta_{m,n}\right)|u_\alpha^{m-m'}\rangle=(\varepsilon_\alpha-m'\hbar\Omega)\,|u_\alpha^{n-m'}\rangle\ . \tag{1.99}$$

Furthermore, the normalized eigenvectors of the Floquet matrix form an orthonormal basis with respect to the Floquet index ℓ and in the space of discrete quantum numbers α, hence

$$\sum_{n=-\infty}^{\infty}\langle u_\alpha^{n+\ell}|u_\beta^{n+\ell'}\rangle=\delta_{\ell,\ell'}\delta_{\alpha\beta}\ . \tag{1.100}$$

Following Refs. [83, 87] we define the unitary transformation

$$(\boldsymbol{T})_\alpha^{nn'}=|u_\alpha^{n+n'}\rangle\ . \tag{1.101}$$

The components of the matrix $\boldsymbol{T}$ are still ket-states. The reason is that the Green's functions are still operators, as is $\boldsymbol{T}$. However, using Eqs. (1.99) and (1.100), it can be shown that $\boldsymbol{T}$ diagonalizes the Green's function

$$\left(\boldsymbol{T}^\dagger\frac{1}{\frac{1}{\hbar}\varepsilon-\frac{1}{\hbar}\mathbf{H}_F\pm i0^+}\boldsymbol{T}\right)_{\alpha\beta}^{nn'}=\frac{\delta_{\alpha\beta}\delta_{nn'}}{\frac{1}{\hbar}\varepsilon-\frac{1}{\hbar}\varepsilon_\alpha-n\Omega\pm i0^+}\ . \tag{1.102}$$

At this point we recall that the Floquet functions form an orthonormal basis only at equal times [20]

$$\sum_\alpha|u_\alpha(t)\rangle\langle u_\alpha(t)|=\mathbb{1}\ . \tag{1.103}$$

This relation can be generalized to different times by inserting a Dirac comb, cf. Eq. (1.78),

$$\sum_\alpha |u_\alpha(t_1')\rangle\langle u_\alpha(t_2')| \sum_{\ell=-\infty}^{\infty} \delta(t_1' - t_2' + \ell T) = \mathbb{1} \sum_{\ell=-\infty}^{\infty} \delta(t_1' - t_2' + \ell T) \ . \tag{1.104}$$

This relation gives particular insight regarding the question of whether the Green's function of Eq. (1.79) is in Lehmann representation. The Floquet functions in the numerator of $\mathcal{G}_0^{r,a}(\varepsilon, t_1', t_2')$ depend on different times, such that they are, in general, not eigenstates of the same Hamiltonian

$$H_F(t)|u_\alpha(t)\rangle = \varepsilon_\alpha |u_\alpha(t)\rangle \tag{1.105}$$
$$H_F(t)|u_\alpha(t')\rangle \neq \varepsilon_\alpha |u_\alpha(t')\rangle \ . \tag{1.106}$$

However, this is cured by the generalized completeness relation of the Floquet function derived in Eq. (1.104), such that

$$\mathcal{G}_0^{r,a}(\varepsilon, t_1', t_2') = \frac{\mathbb{1} \sum_{\ell=-\infty}^{\infty} \delta(t_1' - t_2' + \ell T)}{\frac{1}{\hbar}\varepsilon - \frac{1}{\hbar} H_F(t_1')} \tag{1.107}$$

where the Floquet Hamiltonian can either depend on t_1' or t_2'. Eq. (1.107) can also be derived by Fourier transforming the difference of times $(t_1 - t_2)$ in Eq. (1.77) onto an energy ε. After the analysis of the properties of the t-t'-Green's function, the focus is in the following section again on the conductivity.

1.4.3 Conductivity in terms of Green's functions

In Sec. 1.3 an expression for the conductivity of a clean system without impurities was found. The aim of the following is to successively include disorder in the clean system, where the impurities will be treated perturbatively using a Dyson series. In order to do so, the conductivity must be expressed in terms of Green's functions, the result of this section. With the use of the Dirac identity, the difference of a retarded and an advanced Green's function is

$$\Big(\mathcal{G}_0^r(\varepsilon, t_1', t_2') - \mathcal{G}_0^a(\varepsilon, t_1', t_2')\Big) = -i\frac{2\pi\hbar}{T} \sum_\alpha |u_\alpha(t_1')\rangle \, \langle u_\alpha(t_2')| \, \delta\big(\varepsilon - \varepsilon_\alpha\big) \tag{1.108}$$

where it was used that $|\varepsilon - \varepsilon_\alpha| \leqslant \hbar\Omega$. From this, a relation between the t-t'-Green's functions and Eq. (1.48)

$$\begin{aligned}\sigma(\varepsilon) = -\frac{1}{(2\pi\hbar)^2} \int_0^T dt_1' \int_0^T dt_2' \ \mathrm{tr}\Big[& p^x \Big(\mathcal{G}_0^r(\varepsilon, t_1', t_2') - \mathcal{G}_0^a(\varepsilon, t_1', t_2')\Big) \\ & \times p^x \Big(\mathcal{G}_0^r(\varepsilon, t_2', t_1') - \mathcal{G}_0^a(\varepsilon, t_2', t_1')\Big)\Big]\end{aligned} \tag{1.109}$$

is found, which can be proven immediately by inserting Eq. (1.108), using the Fourier expansion of the Floquet function (1.7), and performing the time integrations. Eq. (1.109) allows one to express the conductivity of the clean system (1.47)

in terms of the Green's functions found in Sec. 1.4

$$\lim_{\omega\to 0}\operatorname{Re}\sigma^{xx}(0,\omega)=\frac{-1}{4\pi\hbar V}\Big(\frac{e}{m}\Big)^2\int_{\lambda-\hbar\Omega/2}^{\lambda+\hbar\Omega/2}d\varepsilon\left(-\frac{\partial f}{\partial\varepsilon}\right)\int_0^T dt_1'\int_0^T dt_2' \\ \times\operatorname{tr}\Big[p^x\Big(\mathcal{G}_0^r(\varepsilon,t_1',t_2')-\mathcal{G}_0^a(\varepsilon,t_1',t_2')\Big)p^x\Big(\mathcal{G}_0^r(\varepsilon,t_2',t_1')-\mathcal{G}_0^a(\varepsilon,t_2',t_1')\Big)\Big]\ . \tag{1.110}$$

In the following, the Green's functions are kept in the form of Eq. (1.79) to show the coupling of the Fourier modes. The conductivity does not depend on t_1', t_2', which suggests later the use of the Green's function in the form given in Eq. (1.89). The ordering of the primed times creates a simple matrix product between the Green's function matrices spanned by the Fourier coefficients of Eq. (1.89). This is further discussed later.
The calculations in Sec. 1.3 are valid for any parabolic spectrum, which is the focus in the first part of this work. Nevertheless, models beyond the effective parabolic approximation might have time-dependent current operators. The power of the t-t'-formalism is that even in that case, the previously introduced four times Green's functions are still sufficient for the calculation of the conductivity. In Sec. 1.3 the current operator is of the form

$$\mathbf{J}(\mathbf{r})=-\frac{e}{2m}\sum_i\big(\mathbf{p}_i\delta(\mathbf{r}-\mathbf{r}_i)+\delta(\mathbf{r}-\mathbf{r}_i)\mathbf{p}_i\big)\ . \tag{1.111}$$

If the driving mechanism is also implemented by an electromagnetic vector potential, the momentum operator of the above current operator should be replaced according to

$$\mathbf{p}_i\mapsto\mathbf{p}_i+e\mathbf{A}(\mathbf{r}_i,t) \tag{1.112}$$

such that

$$\mathbf{J}(\mathbf{r})\mapsto\mathbf{J}(\mathbf{r})-\frac{e^2}{m}\mathbf{A}(\mathbf{r},t)\rho(\mathbf{r}) \tag{1.113}$$

with the particle density operator $\rho(\mathbf{r})=\sum_i\delta(\mathbf{r}-\mathbf{r}_i)$. However, for a spatially constant driving field $\mathbf{A}(\mathbf{r},t)=\mathbf{A}(t)$ in a system of spatially homogeneous density, the additional term in the foregoing equation does not contribute to the expectation values of the commutators in Eq. (1.23), and only leads to a further diamagnetic contribution of the form $-(e^2/m)\mathbf{A}(t)n$ [88]. The current operator for an arbitrary driven system is, in general, time-dependent. Assuming that the current operator has the same temporal periodicity as the Hamiltonian allows for the discrete Fourier expansion $\mathbf{J}^\ell(\mathbf{q},t)=\sum_{n=-\infty}^{\infty}\mathbf{J}_n^\ell(\mathbf{q})e^{-in\Omega t}$. Following the analogue steps as in Sec. 1.3 one ends up with the conductivity of

$$\lim_{\omega\to 0}\operatorname{Re}\sigma^{xx}(0,\omega)=\frac{\pi\hbar}{V}\int_{-\hbar\Omega/2}^{\hbar\Omega/2}d\varepsilon\left(-\frac{\partial f}{\partial\varepsilon}\right)\sigma(\varepsilon) \tag{1.114}$$

with

$$\sigma(\varepsilon)=\sum_{ss'nn'=-\infty}^{\infty}\sum_{\alpha\beta}\langle u_\alpha^{n+s}|\,\mathbf{j}_s^x\,|u_\beta^n\rangle\,\langle u_\beta^{n'+s'}|\,\mathbf{j}_{s'}^x\,|u_\alpha^{n'}\rangle\ \delta\big(\varepsilon-\varepsilon_\alpha\big)\delta\big(\varepsilon-\varepsilon_\beta\big)\ . \tag{1.115}$$

In case of time-dependent current operators, the four-time Green's functions, found in Sec. 1.4.1, can still be used to express the result for the conductivity, derived from the Kubo formula, in terms of Green's functions. Eq. (1.115) expressed with Green's functions is

$$\sigma(\varepsilon) = -\frac{1}{(2\pi\hbar)^2}\int_0^T dt_1' \int_0^T dt_2' \ \mathrm{tr}\Big[\mathbf{j}^x(t_1')\Big(\mathcal{G}_0^r(\varepsilon,t_1',t_2') - \mathcal{G}_0^a(\varepsilon,t_1',t_2')\Big) \times \mathbf{j}^x(t_2')\Big(\mathcal{G}_0^r(\varepsilon,t_2',t_1') - \mathcal{G}_0^a(\varepsilon,t_2',t_1')\Big)\Big] \ . \tag{1.116}$$

From this, the conductivity for time-dependent current operators is

$$\lim_{\omega\to 0}\mathrm{Re}\,\sigma^{xx}(0,\omega) = \frac{-1}{4\pi\hbar V}\int_{\lambda-\hbar\Omega/2}^{\lambda+\hbar\Omega/2} d\varepsilon\left(-\frac{\partial f}{\partial\varepsilon}\right)\int_0^T dt_1'\int_0^T dt_2' \times\mathrm{tr}\Big[\mathbf{j}^x(t_1')\Big(\mathcal{G}_0^r(\varepsilon,t_1',t_2') - \mathcal{G}_0^a(\varepsilon,t_1',t_2')\Big)\mathbf{j}^x(t_2')\Big(\mathcal{G}_0^r(\varepsilon,t_2',t_1') - \mathcal{G}_0^a(\varepsilon,t_2',t_1')\Big)\Big] \ . \tag{1.117}$$

This expression for the conductivity is valid for any Floquet system, since it even allows for time-dependent current operators. However, it describes the conductivity for a clean system without any disorder. The latter leads to a finite conductivity and is always present in realistic experiments. Thus, a rigorous scheme to include disorder is presented in the subsequent sections.

1.4.4 Justification of the *t*-*t*'-formalism

The aim of this section is to justify the *t*-*t*'-formalism introduced above. The necessity to use the *t*-*t*'-formalism is far from obvious, hence, the focus is again on the Green's function of the time dependent Schrödinger equation given in Eq. (1.91). It is desirable to express the result from the Kubo formula as trace over the difference of retarded and advanced Green's functions

$$\tilde{\sigma} \equiv \mathrm{tr}\Big[p^x\big(G^r(\cdot) - G^a(\cdot)\big)p^x\big(G^r(\cdot) - G^a(\cdot)\big)\Big] \ . \tag{1.118}$$

The time dependencies of the Green's functions $G^{r,a}(\cdot)$ are intentionally left blank, since the above expression should only show the desired structure. If $\tilde{\sigma}$ is assumed to have the above structure, there are only few possible time dependencies of the Green's functions. Using the Green's functions of the time-dependent Schrödinger equation, some attempts that fail to reproduce the result from the Kubo formula are presented in the following. Utilizing the two-time Green's function together with the same time ordering as in Eq. (1.110) yields the expression

$$\sigma(t_1,t_2) = \mathrm{tr}\Big[p^x\big(G_0^r(t_1,t_2) - G_0^a(t_1,t_2)\big)p^x\big(G_0^r(t_2,t_1) - G_0^a(t_2,t_1)\big)\Big] \ . \tag{1.119}$$

Introducing Wigner coordinates according to Eqs. (1.92), where the relative time is Fourier transformed into energy space and the mean time is averaged over one driving cycle, leads to

$$\sigma(\varepsilon) = \sum_{\alpha\beta}\sum_{nn'=-\infty}^{\infty}\langle u_\alpha^n|\,p^x\,|u_\beta^n\rangle\,\langle u_\beta^{n'}|\,p^x\,|u_\alpha^{n'}\rangle\,\delta\big(\varepsilon+\varepsilon_\alpha-\varepsilon_\beta\big) \ . \tag{1.120}$$

While the ordering of the Floquet indices is correct, the above quantity is proportional to a single delta distribution and thus not equal to Eq. (1.48). Any different time ordering in Eq. (1.119) leads to an incorrect ordering of the Floquet indices. Next, the attempt is analyzed, where the Green's functions depend on different relative times and the common mean time is averaged

$$\sigma(t,t') = \frac{1}{T}\int_0^T dT\ \mathrm{tr}\Big[p^x\big(G_0^r(t,T) - G_0^a(t,T)\big)p^x\big(G_0^r(t',T) - G_0^a(t',T)\big)\Big]\,. \quad (1.121)$$

Now, a Fourier transformation of both relative times is performed onto the same energy

$$\sigma(\varepsilon) = \int_{-\infty}^{\infty} dt \int_{-\infty}^{\infty} dt'\ e^{\frac{i}{\hbar}\varepsilon(t+t')}\sigma(t,t')\,, \quad (1.122)$$

which leads to the correct result for the conductivity if, and only if, the distribution function in Eq. (1.51) fulfills

$$\frac{\partial f}{\partial\big(\varepsilon + (n+n')\frac{\Omega}{2}\big)} = \frac{\partial f}{\partial \varepsilon} \quad \forall\, n, n' \in \mathbb{Z}\,. \quad (1.123)$$

The last equation requires a half integer periodicity of the derivative of the distribution function, which is likely not to be fulfilled by an actual distribution function. Rather curiously, defining a function by neglecting the summation over the Floquet indices in Eq. (1.79), namely

$$\tilde{G}^{r,a}(\varepsilon, t_1', t_2') = \frac{1}{T}\sum_\alpha \frac{|u_\alpha(t_1')\rangle\,\langle u_\alpha(t_2')|}{\frac{1}{\hbar}\varepsilon - \frac{1}{\hbar}\varepsilon_\alpha \pm i0^+}\,, \quad (1.124)$$

allows one to reproduce the result form the Kubo formula

$$\begin{aligned}\sigma(\varepsilon) = \int_0^T dt_1' \int_0^T dt_2'\ \mathrm{tr}\Big[&p^x\Big(\tilde{G}^r(\varepsilon, t_1', t_2') - \tilde{G}^a(\varepsilon, t_1', t_2')\Big)\\ &\times p^x\Big(\tilde{G}^r(\varepsilon, t_2', t_1') - \tilde{G}^a(\varepsilon, t_2', t_1')\Big)\Big]\,.\end{aligned} \quad (1.125)$$

However, the function given in Eq. (1.124) is neither a Green's function of the Schrödinger equation nor of the t-t'-Schrödinger equation. The results presented in this section are not intended to prove that it is not possible to express Eq. (1.48) in terms of the Green's function of the time-dependent Schrödinger equation. There might be a very complicated expression that relates Eq. (1.48) with the Green's function presented in Eq. (1.91). Nevertheless, if the structure given in Eq. (1.118) is desired, one is encouraged to use the four-time Green's functions introduced in Sec. 1.4.

1.5 Dyson equation

The results of the last sections were derived for a clean system. However, the aim is to find an expression for the conductivity in a disordered system. Finding the conductivity for a specific impurity configuration is a rather formidable task

and is not desirable since it is unlikely to have exactly the calculated impurity configuration in an experiment. Hence, the interest is on the statistically averaged, over impurity configurations, conductivity. To calculate the latter, the problem of including impurities must be tackled in a systematic way. If the Green's function of the unperturbed system is known, it is possible to relate it recursively to the Green's function of a system with impurities, i.e. via a Dyson series. In the following, Dyson series for time-dependent and static perturbations are derived, where the latter is further considered in the subsequent sections where the disorder average and the self-energy are discussed.

1.5.1 General

The expression for the conductivity derived in Sec. 1.4.3 describes a clean system without any perturbing potential such as impurities. Nevertheless, the conductivity is already expressed in terms of Green's functions that allow for a perturbative inclusion of impurities. First, a recursive expression for the Green's function in case of a time-dependent perturbing potential is formulated. In the second part of this section the perturbation is assumed to be time-independent. The calculations in this chapter are based on Ref. [48]. The Green's functions were thus far operators. In the following, the notation

$$\langle \mathbf{x}| \, \mathcal{G}^{r,a}(t_1, t_2, t_1', t_2') \, |\mathbf{x}'\rangle \equiv \mathcal{G}^{r,a}(t_1, t_2, \mathbf{x}, \mathbf{x}', t_1', t_2') \,, \tag{1.126}$$

$$\langle \mathbf{x}| \, \mathcal{G}^{r,a}(\varepsilon, t_1', t_2') \, |\mathbf{x}'\rangle \equiv \mathcal{G}^{r,a}(\varepsilon, \mathbf{x}, \mathbf{x}', t_1', t_2') \,, \tag{1.127}$$

for the matrix elements of the Green's function in real space, is used. The subscript in Eq. (1.126) is dropped, which indicates that this Green's function is either the bare Green's function or the one for the system with perturbation. The explicit form of the bare Green's function is

$$\mathcal{G}_0^{r,a}(\varepsilon, \mathbf{x}_1, \mathbf{x}_2, t_1', t_2') = \frac{1}{T} \sum_{\ell=-\infty}^{\infty} \sum_{\alpha} \frac{u_\alpha(\mathbf{x}_1, t_1') \big(u_\alpha(\mathbf{x}_2, t_2')\big)^*}{\frac{1}{\hbar}\varepsilon - \frac{1}{\hbar}\varepsilon_\alpha - \ell\Omega \pm i0^+} \, e^{i\ell\Omega(t_1' - t_2')} \tag{1.128}$$

$$= \frac{1}{T} \sum_{n,n'=-\infty}^{\infty} \mathcal{G}_0^{r,a}(\varepsilon, \mathbf{x}_1, \mathbf{x}_2, n, n') e^{-in\Omega t_1'} e^{in'\Omega t_2'} \tag{1.129}$$

together with the Fourier coefficients

$$\mathcal{G}_0^{r,a}(\varepsilon, \mathbf{x}_1, \mathbf{x}_2, n, n') = \sum_{\ell=-\infty}^{\infty} \sum_{\alpha} \frac{u_\alpha^{n+\ell}(\mathbf{x}_1) \big(u_\alpha^{n'+\ell}(\mathbf{x}_2)\big)^*}{\frac{1}{\hbar}\varepsilon - \frac{1}{\hbar}\varepsilon_\alpha - \ell\Omega \pm i0^+} \tag{1.130}$$

and the shortened notation

$$u_\alpha(\mathbf{x}_1, t_1') \equiv \big\langle \mathbf{x}_1 | u_\alpha(t_1') \big\rangle \quad , \quad u_\alpha^n(\mathbf{x}_1) \equiv \big\langle \mathbf{x}_1 | u_\alpha^n \big\rangle \,. \tag{1.131}$$

As already shown in Eq. (1.77), the bare Green's function $\mathcal{G}_0^{r,a}$ fulfills

$$\Big(i\partial_{t_1} - \tfrac{1}{\hbar} H_F(\mathbf{x}_1, t_1')\Big) \mathcal{G}_0^{r,a}(t_1, t_2, \mathbf{x}_1, \mathbf{x}_2, t_1', t_2') = \delta(t_1 - t_2)\delta(\mathbf{x}_1 - \mathbf{x}_2) \times \sum_{s=-\infty}^{\infty} \delta(t_1' - t_2' + sT)\mathbb{1} \tag{1.132}$$

where $H_F(\mathbf{x}_1, t_1')$ denotes the Floquet Hamiltonian for the unperturbed system. The Hamiltonian for the system with additional potential V is assumed to be

$$\mathcal{H}_F(\mathbf{x}_1, t_1, t_1') = H_F(\mathbf{x}_1, t_1') + V(\mathbf{x}_1, t_1, t_1') \tag{1.133}$$

where it is stressed that the dependency on t_1 is fully kept by the potential V. Obviously, the bare Green's function $\mathcal{G}_0^{r,a}$ fulfills

$$\begin{aligned}\Big(i\partial_{t_1} - \tfrac{1}{\hbar}\mathcal{H}_F(\mathbf{x}_1, t_1, t_1') + \tfrac{1}{\hbar}V(\mathbf{x}_1, t_1, t_1')\Big)\mathcal{G}_0^{r,a}(t_1, t_2, \mathbf{x}_1, \mathbf{x}_2, t_1', t_2') = \\ \delta(t_1 - t_2)\delta(\mathbf{x}_1 - \mathbf{x}_2)\sum_{s=-\infty}^{\infty}\delta(t_1' - t_2' + sT)\mathbb{1}\,,\end{aligned} \tag{1.134}$$

but the aim of this section is the derivation of a recursive expression for the Green's function of the perturbed system $\mathcal{G}_\mathrm{p}^{r,a}$ being a solution of

$$\begin{aligned}\Big(i\partial_{t_1} - \tfrac{1}{\hbar}\mathcal{H}_F(\mathbf{x}_1, t_1, t_1')\Big)\mathcal{G}_\mathrm{p}^{r,a}(t_1, t_2, \mathbf{x}_1, \mathbf{x}_2, t_1', t_2') = \delta(t_1 - t_2)\delta(\mathbf{x}_1 - \mathbf{x}_2) \\ \times\sum_{s=-\infty}^{\infty}\delta(t_1' - t_2' + sT)\mathbb{1}\ .\end{aligned} \tag{1.135}$$

Following Ref. [48] and equating Eq. (1.134) with Eq. (1.135) yield

$$\begin{aligned}&\Big(i\partial_{t_1} - \tfrac{1}{\hbar}\mathcal{H}_F(\mathbf{x}_1, t_1, t_1')\Big)\mathcal{G}_\mathrm{p}^{r,a}(t_1, t_2, \mathbf{x}_1, \mathbf{x}_2, t_1', t_2') = \\ &\Big(i\partial_{t_1} - \tfrac{1}{\hbar}\mathcal{H}_F(\mathbf{x}_1, t_1, t_1')\Big)\mathcal{G}_0^{r,a}(t_1, t_2, \mathbf{x}_1, \mathbf{x}_2, t_1', t_2') \\ &+ \tfrac{1}{\hbar}V(\mathbf{x}_1, t_1, t_1')\mathcal{G}_0^{r,a}(t_1, t_2, \mathbf{x}_1, \mathbf{x}_2, t_1', t_2')\ .\end{aligned} \tag{1.136}$$

The bare Green's function $\mathcal{G}_0^{r,a}$ is periodic in the primed times t_1', t_2', cf. Eq. (1.83), and therefore, without loss of generality, the primed times can be restricted to fulfill

$$t_1', t_2' \in \big[-\tfrac{T}{2}, \tfrac{T}{2}\big)\ . \tag{1.137}$$

Making use of the periodicity of the Green's function and claiming that the potential is periodic in the second time argument

$$V(\mathbf{x}, t_1, t_1' + T) = V(\mathbf{x}, t_1, t_1')\,, \tag{1.138}$$

it can be shown that

$$\begin{aligned}&\int_{V_\mathbf{x}} d^dx \int_{-\infty}^{\infty} dt \int_{-T/2}^{T/2} dt'\ \delta(t_1 - t)\delta(\mathbf{x}_1 - \mathbf{x})\sum_{s=-\infty}^{\infty}\delta(t_1' - t' + sT) \\ &\times V(\mathbf{x}, t, t')\mathcal{G}_0^{r,a}(t, t_2, \mathbf{x}, \mathbf{x}_2, t', t_2') = V(\mathbf{x}_1, t_1, t_1')\mathcal{G}_0^{r,a}(t_1, t_2, \mathbf{x}_1, \mathbf{x}_2, t_1', t_2')\end{aligned} \tag{1.139}$$

where it was used that the Dirac comb can only have support if $s = 0$. When comparing this with Eq. (1.136) one finds a Dyson expansion for the Green's function of the perturbed system

$$\begin{aligned}\mathcal{G}_\mathrm{p}^{r,a}(t_1, t_2, \mathbf{x}_1, \mathbf{x}_2, t_1', t_2') = \mathcal{G}_0^{r,a}(t_1, t_2, \mathbf{x}_1, \mathbf{x}_2, t_1', t_2') \\ + \frac{1}{\hbar}\int_{V_\mathbf{x}} d^dx \int_{-\infty}^{\infty} dt \int_{-T/2}^{T/2} dt' \Big[\mathcal{G}_\mathrm{p}^{r,a}(t_1, t, \mathbf{x}_1, \mathbf{x}, t_1', t') \\ \times V(\mathbf{x}, t, t')\mathcal{G}_0^{r,a}(t, t_2, \mathbf{x}, \mathbf{x}_2, t', t_2')\Big]\ .\end{aligned} \tag{1.140}$$

This result is thus far exact as long as the potential V is periodic in the second time argument. However, the Dyson series in Eq. (1.140) can be reformulated in an energy domain using Eqs. (1.81), and (1.82). In energy space, $V(\mathbf{x}, t, t')$ is also a matrix leading to an impracticable expression for $\mathcal{G}^{r,a}_{\mathrm{p}}$, because the potential matrix is not diagonalized by the transformation $\boldsymbol{T}$ of Eq. (1.101). The scenario of a time-independent potential is analyzed in the following section.

1.5.2 Static Potential

In the defining equation for the four time Green's function, see Eq. (1.77), the time derivative and the Hamiltonian depend on different times. This is not the case when a Hamiltonian as in Eq. (1.133), where the potential V depends on both times, is considered. The separation of times is retrieved when a potential that depends only on the periodic time component is assumed:

$$V(\mathbf{x}, t, t') = V(\mathbf{x}, t') \quad \Leftrightarrow \quad H_F(\mathbf{x}, t, t') = H_F(\mathbf{x}, t') \,. \tag{1.141}$$

In this case the Green's function for the perturbed system is - in the unprimed times - only a function of the difference of times

$$\mathcal{G}^{r,a}_{\mathrm{p}}(t_1, t_2, \mathbf{x}_1, \mathbf{x}_2, t_1', t_2') = \mathcal{G}^{r,a}_{\mathrm{p}}(t_1 - t_2, \mathbf{x}_1, \mathbf{x}_2, t_1', t_2') \,. \tag{1.142}$$

Fourier transforming Eq. (1.140), under use of the convolution theorem for the Fourier transform, into energy space leads to

$$\begin{aligned} &\mathcal{G}^{r,a}_{\mathrm{p}}(\varepsilon, \mathbf{x}_1, \mathbf{x}_2, t_1', t_2') = \mathcal{G}^{r,a}_{0}(\varepsilon, \mathbf{x}_1, \mathbf{x}_2, t_1', t_2') \\ &+ \frac{1}{\hbar} \int_{V_{\mathbf{x}}} d^d x \int_{-T/2}^{T/2} dt' \mathcal{G}^{r,a}_{\mathrm{p}}(\varepsilon, \mathbf{x}_1, \mathbf{x}, t_1', t') V(\mathbf{x}, t') \mathcal{G}^{r,a}_{0}(\varepsilon, \mathbf{x}, \mathbf{x}_2, t', t_2') \,. \end{aligned} \tag{1.143}$$

The demanded periodicity of the potential allows for an expansion into a discrete Fourier series equivalent to Eqs. (1.7) and (1.8)

$$V(\mathbf{x}, t') = \sum_{n=-\infty}^{\infty} V_n(\mathbf{x}) e^{-in\Omega t'} \quad , \quad V_n(\mathbf{x}) = \frac{1}{T} \int_0^T dt' \, V(\mathbf{x}, t') e^{in\Omega t'} \,. \tag{1.144}$$

Expressing Eq. (1.143) in Fourier components and performing the remaining time integration result in

$$\begin{aligned} &\mathcal{G}^{r,a}_{\mathrm{p}}(\varepsilon, \mathbf{x}_1, \mathbf{x}_2, n, n') = \mathcal{G}^{r,a}_{0}(\varepsilon, \mathbf{x}_1, \mathbf{x}_2, n, n') + \\ &\frac{1}{\hbar} \int_{V_{\mathbf{x}}} d^d x \sum_{n_1, n_2 = -\infty}^{\infty} \mathcal{G}^{r,a}_{\mathrm{p}}(\varepsilon, \mathbf{x}_1, \mathbf{x}, n, n_1) V_{n_1 - n_2}(\mathbf{x}) \mathcal{G}^{r,a}_{0}(\varepsilon, \mathbf{x}, \mathbf{x}_2, n_2, n') \,. \end{aligned} \tag{1.145}$$

The most important case for the rest of this chapter is a fully static potential

$$V(\mathbf{x}, t, t') = V(\mathbf{x}) \,. \tag{1.146}$$

The derivation of the Dyson series for a fully static potential follows the same steps as in the time-dependent case, and Eq. (1.145) simplifies to

$$\begin{aligned} &\mathcal{G}^{r,a}_{\mathrm{p}}(\varepsilon, \mathbf{x}_1, \mathbf{x}_2, n, n') = \mathcal{G}^{r,a}_{0}(\varepsilon, \mathbf{x}_1, \mathbf{x}_2, n, n') + \\ &\frac{1}{\hbar} \int_{V_{\mathbf{x}}} d^d x \sum_{n_1 = -\infty}^{\infty} \mathcal{G}^{r,a}_{\mathrm{p}}(\varepsilon, \mathbf{x}_1, \mathbf{x}, n, n_1) V(\mathbf{x}) \mathcal{G}^{r,a}_{0}(\varepsilon, \mathbf{x}, \mathbf{x}_2, n_1, n') \,. \end{aligned} \tag{1.147}$$

In the space of Floquet indices, the potential $V(\mathbf{x})$ is proportional to the unit matrix. The recursive equation above can be related to a set of infinitely many diagrams, namely the Feynman diagrams. Assuming randomly distributed impurities and averaging over all impurity positions allow for the identification of the the leading class of diagrams. Feynman rules allow one to describe the latter systematically.

1.6 Random Impurities and self average

In the previous section a perturbative approach was formulated to relate the Green's function of the clean system to the Green's function of a system with perturbation. In the following, the perturbation is assumed to be formed by an ensemble of randomly distributed impurities. In this section only the most relevant steps are presented, since a rigorous introduction of random impurities and of the disorder averaging procedure are not the aims of this work and can be found in standard textbooks like Refs. [48, 89, 90]. Formulating the Dyson series in momentum space and averaging over all impurity positions allow one to formulate Feynman rules. It will be shown that all Feynman rules for the static system remain valid for the driven case. However, for time-independent impurities there are two more Feynman rules that account for the Floquet index at each vertex. Consider N_{imp} identical impurities situated at the randomly distributed but fixed positions $\mathbf{r}$ [48]. The elastic scattering potential $V(\mathbf{x})$ is then governed by the sum over uncorrelated single impurity potentials v

$$V(\mathbf{x}) = \sum_{\ell=1}^{N_{\mathrm{imp}}} v(\mathbf{x} - \mathbf{r}_\ell) \ . \tag{1.148}$$

It is reasonable to claim translational invariance for the unperturbed system, hence the bare Green's function fulfills

$$\mathcal{G}_0^{r,a}(\varepsilon, \mathbf{x}_1, \mathbf{x}_2, n, n') = \mathcal{G}_0^{r,a}(\varepsilon, \mathbf{x}_1 - \mathbf{x}_2, n, n') \ . \tag{1.149}$$

It is rather convenient to consider scattering in momentum space. To translate the Dyson series found in Eq. (1.147) into momentum space, the bare Green's function is expanded to

$$\mathcal{G}_0^{r,a}(\varepsilon, \mathbf{x}_1 - \mathbf{x}_2, n, n') = \frac{1}{V_{\mathbf{k}}} \sum_{\mathbf{k}} \mathcal{G}_0^{r,a}(\varepsilon, \mathbf{k}, n, n')\, e^{i\mathbf{k}\cdot(\mathbf{x}_1 - \mathbf{x}_2)} \tag{1.150}$$

where $\mathcal{G}_0^{r,a}(\varepsilon, \mathbf{k}, n, n')$ only depends on a single momentum that is a consequence of the translational invariance. The summation over all momenta is normalized by the volume of the system $V_{\mathbf{k}}$. The random potential is equivalently expanded to

$$v(\mathbf{x} - \mathbf{r}_\ell) = \frac{1}{V_{\mathbf{q}}} \sum_{\mathbf{q}} v(\mathbf{q}) e^{i\mathbf{q}\cdot(\mathbf{x} - \mathbf{r}_\ell)} \ . \tag{1.151}$$

Utilizing the momentum representations of the Green's function and of the disorder potential yield

$$\begin{aligned}\mathcal{G}_{\mathrm{p}}^{r,a}(\varepsilon,\mathbf{x}_1,\mathbf{x}_2,n,n') &= \frac{1}{V_{\mathbf{k}_1}V_{\mathbf{k_2}}}\sum_{\mathbf{k}_1\mathbf{k}_2}\mathcal{G}_0^{r,a}(\varepsilon,\mathbf{k}_1,\mathbf{k}_2,n,n')\delta_{\mathbf{k}_1,\mathbf{k}_2}e^{i\mathbf{k}_1\cdot\mathbf{x}_1}e^{-i\mathbf{k}_2\cdot\mathbf{x}_2}\\ &+\frac{1}{\hbar}\frac{1}{V_{\mathbf{k}_1}V_{\mathbf{k}}}\sum_{\mathbf{k}_1\mathbf{k}}\frac{1}{V_{\mathbf{q}}}\sum_{\mathbf{q}}\frac{1}{V_{\mathbf{k}'}V_{\mathbf{k}}}\sum_{\mathbf{k}'\mathbf{k}_2}\sum_{n_1=-\infty}^{\infty}\sum_{\ell=1}^{N_{\mathrm{imp}}}\Big[\mathcal{G}_{\mathrm{p}}^{r,a}(\varepsilon,\mathbf{k}_1,\mathbf{k},n,n_1)v(\mathbf{q})\\ &\times\mathcal{G}_0^{r,a}(\varepsilon,\mathbf{k}',\mathbf{k}_2,n_1,n')\int_{V_{\mathbf{x}}}d^dx\; e^{i\mathbf{k}_1\cdot\mathbf{x}_1}e^{-i(\mathbf{k}-\mathbf{q}-\mathbf{k}')\cdot\mathbf{x}}e^{-i\mathbf{k_2}\cdot\mathbf{x_2}}e^{-i\mathbf{q}\cdot\mathbf{r}_\ell}\delta_{\mathbf{k}',\mathbf{k}_2}\Big]\,.\end{aligned}\tag{1.152}$$

Due to translational invariance, the bare Green's function only depends on a single momentum, cf. (1.150). To lighten the notation in the following, the short form is used in the subsequent considerations

$$\mathcal{G}_0^{r,a}(\varepsilon,\mathbf{k},\mathbf{k}',n,n')\delta_{\mathbf{k},\mathbf{k}'}\equiv\mathcal{G}_0^{r,a}(\varepsilon,\mathbf{k},n,n')\;.\tag{1.153}$$

Making use of

$$\mathcal{G}_{\mathrm{p}}^{r,a}(\varepsilon,\mathbf{x}_1,\mathbf{x}_2,n,n') = \frac{1}{V_{\mathbf{k}_1}V_{\mathbf{k}_2}}\sum_{\mathbf{k}_1\mathbf{k}_2}\mathcal{G}_{\mathrm{p}}^{r,a}(\varepsilon,\mathbf{k}_1,\mathbf{k}_2,n,n')e^{i\mathbf{k}_1\cdot\mathbf{x}_1}e^{-i\mathbf{k}_2\cdot\mathbf{x}_2}\;,\tag{1.154}$$

performing the position integral and the momentum sums the Dyson series in momentum space

$$\begin{aligned}\mathcal{G}_{\mathrm{p}}^{r,a}(\varepsilon,\mathbf{k}_1,\mathbf{k}_2,n,n') =&\,\mathcal{G}_0^{r,a}(\varepsilon,\mathbf{k}_1,n,n')\delta_{\mathbf{k}_1,\mathbf{k}_2}+\\ &\frac{1}{\hbar V_{\mathbf{k}}}\sum_{\mathbf{k}}\sum_{n_1=-\infty}^{\infty}\sum_{\ell=1}^{N_{\mathrm{imp}}}\Big[\mathcal{G}_{\mathrm{p}}^{r,a}(\varepsilon,\mathbf{k}_1,\mathbf{k},n,n_1)v(\mathbf{k}-\mathbf{k}_2)\\ &\times\mathcal{G}_0^{r,a}(\varepsilon,\mathbf{k}_2,n_1,n')e^{-i(\mathbf{k}-\mathbf{k}_2)\cdot\mathbf{r}_\ell}\Big]\end{aligned}\tag{1.155}$$

is straightforwardly deduced. The last equation depends on the exact positions of the impurities. However, the Green's function for a specific configuration is not desirable, but it is rather the average over all possible impurity locations [48]. Nevertheless, Eq. (1.155) is the fundament of the disorder average. To proceed further, the terms of all orders generated by iterating Eq. (1.155) have to be analyzed. The z-th order term generated by Eq. (1.155) describes the propagation with z scattering events, which can happen on $p\in\{1,...,z\}$ scattering centers. Averaging over all impurity positions $\mathbf{r}_i$ by performing a normalized integration over $\mathbf{r}_i$, with the restriction that the integration must be performed after the iteration, restores translational invariance

$$\frac{1}{V}\big\langle\mathcal{G}_{\mathrm{p}}^{r,a}(\varepsilon,\mathbf{k}_1,\mathbf{k}_2,n,n')\big\rangle_{\mathrm{imp}}\equiv\mathcal{G}_{\mathrm{p}}^{r,a}(\varepsilon,\mathbf{k}_1,n,n')\delta_{\mathbf{k}_1,\mathbf{k}_2}\,.\tag{1.156}$$

As already stated, a rigorous treatment of impurities fills textbooks. However, it is important to summarize the main assumptions made deriving the Feynman rules, whereas the technical details are mainly skipped. Most importantly, the impurities should be a small perturbation compared to the clean system. This manifests in two restriction. First, the concentration of impurities must be much smaller than the

particle density [48] and second, the impurity strength must be weak. The latter requires that the spatial extent of the impurities is much smaller than the particle wavelength [89], and that the potential associated with the impurities is smaller than any level spacing of the particle system. Additionally, the coherence length of the particles must be smaller than the sample size, such that self-averaging is present [48]. For a more detailed derivation see Ref. [48]. The Feynman rules are

1. Let scattering lines - - - - - - - - denote the scattering amplitude $v(\mathbf{q})$
2. Let $\otimes$ denote a momentum-conserving scattering event, i.e. the sum of all momenta leaving an impurity is zero
3. Let fermion lines ⟶ denote unperturbed Green's function
4. Draw p impurity dots and distribute the z impurity lines over the impurities
5. Draw all topologically different diagrams containing an unbroken chain of $z+1$ fermion lines and connect the end points of the z first fermion lines to one of the z scattering lines
6. Let the first and last fermion line be $\mathcal{G}_0^{r,a}(...)$
7. Maintain momentum conservation at each vertex
8. Perform the sum $\frac{1}{V_{\mathbf{k}}}\sum_{\mathbf{k}}$ over all free internal momenta $\mathbf{k}$
9. Sum over all orders z of scattering and over p, with $p \in \{1, ..., z\}$

---

10. Maintain Floquet mode conservation at each vertex •
11. Sum over all internal Floquet modes $\sum_{n=-\infty}^{\infty}$

The above Feynman rules describe all possible diagrams corresponding to propagation with any number of scattering events. The first nine Feynman rules are the same as for the undriven system. The last two account for the Floquet index at each scattering event. The Floquet mode is only conserved at each vertex if the impurity potential is time-independent, as assumed in Sec. 1.5.2. The impurity averaged

Green's function can be diagrammatically depicted as

$\left\langle \mathcal{G}^r_{\mathrm{p}}(\varepsilon, \mathbf{k}, n, n') \right\rangle_{\mathrm{imp}} =$

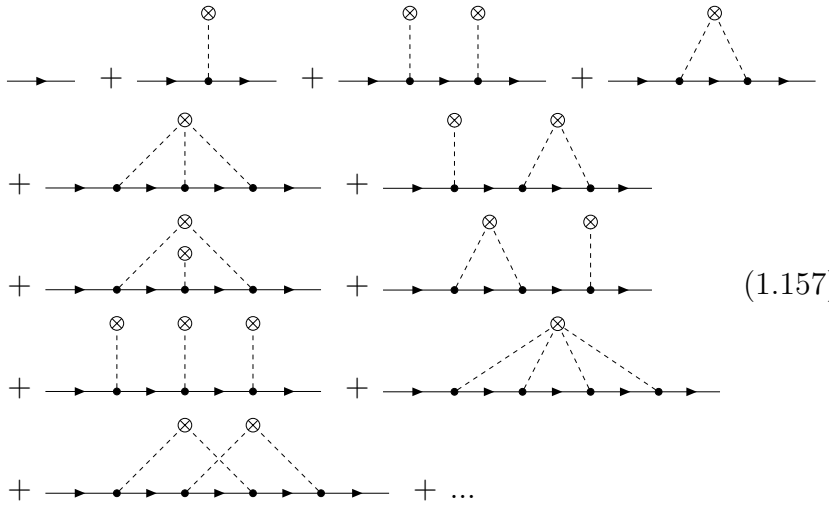

(1.157)

Remarkably, the diagrams for the driven system are the same as for the static one. This suggests using the same summation techniques known for the time-independent disorder problems. In the following, the scattering potential is further specified, which allows one to identify the leading contributions of the infinite number of diagrams.

1.7 Self-energy

In the previous section the Feynman rules for the impurity averaged Green's function in a driven system were found. Identifying the most relevant diagrams for Gaussian white noise is the aim of the first part of this section. This includes the definition of a Floquet self-energy being the sum over all one particle irreducible diagrams. Focusing on the leading order diagrams allows for the calculation of an analytically closed form for the Floquet self-energy. The latter can be shown to be equal to a scattering time derived from a generalized Floquet Fermi's golden rule, proving both consistency of the presented calculations and interpretability of the self-energy as scattering time. The generalized Floquet Fermi's golden rule accounts not only for intra- but as also for inter-Floquet zone scattering, like Floquet-Umklapp processes.

1.7.1 First order Born approximation

In the foregoing section, only mild assumptions were made about the explicit form of the impurity potential, namely that the impurity potential must be of short range nature compared to the wavelength of the particles carrying the current. Further specifying the impurity potential allows the identification of the dominating class of diagrams. These can be summed up, leading to the self-energy.
Now, assume that the perturbation V is a Gaussian random potential. The following holds for the disorder averaged impurity potential [89, 90]

$$\langle v(\mathbf{x}) \rangle_{\mathrm{imp}} = 0 \ , \tag{1.158}$$

$$\langle v(\mathbf{x}) v(\mathbf{x}') \rangle_{\mathrm{imp}} = \nu(\mathbf{x} - \mathbf{x}') \ . \tag{1.159}$$

For further information about the random potential at this point, see Refs. [48, 89, 90]. All diagrams with a dangling impurity line, like the second, third, or sixth diagram of Eq. (1.157), give a constant contribution upon averaging. Since the average impurity strength is set to zero, see Eq. (1.158), all diagrams with a dangling impurity line do not contribute to the averaged propagator [90]. In the language of Feynman diagrams, the impurity averaged Green's function becomes

$\left\langle \mathcal{G}^r_{\mathrm{p}}(\varepsilon, \mathbf{k}, n, n') \right\rangle_{\mathrm{imp}} =$ 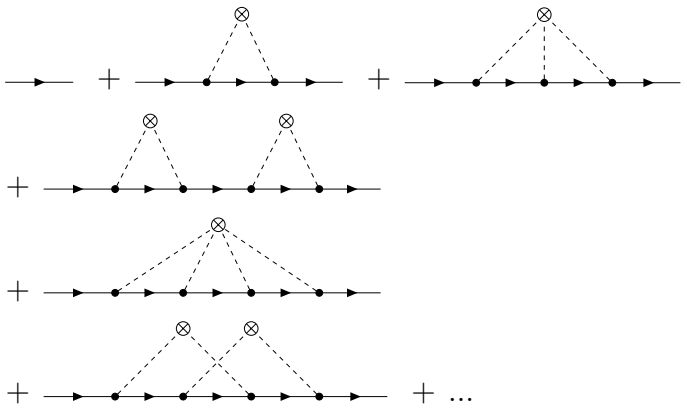 (1.160)

The diagrams, which cannot be divided into two diagrams by cutting a single impurity line, are called one-particle irreducible (1PI) diagrams [90], whereas the others are denoted as one-particle reducible diagrams (1PR). For example, the fourth diagram of Eq. (1.160) is a reducible diagram, whereas all the other depicted diagrams are irreducible. After averaging over disorder, the Dyson series for the perturbed Green's function is in time domain

$$\begin{aligned}\mathcal{G}^{r,a}(\varepsilon, \mathbf{k}, t_1', t_2') &= \mathcal{G}_0^{r,a}(\varepsilon, \mathbf{k}, t_1', t_2') \\ &+ \int_{-T/2}^{T/2} dt \int_{-T/2}^{T/2} dt' \left[\frac{1}{\hbar^2 V_{\mathbf{q}}} \sum_{\mathbf{q}} \nu(\mathbf{q}) \mathcal{G}_0^{r,a}(\varepsilon, \mathbf{k}, t_1', t) \right. \\ &\left. \times \; \mathcal{G}_0^{r,a}(\varepsilon, \mathbf{k} - \mathbf{q}, t, t') \mathcal{G}_0^{r,a}(\varepsilon, \mathbf{k}, t', t_2') \right] + \ldots \end{aligned} \tag{1.161}$$

$=$  . (1.162)

where the first two terms of Eq. (1.161) correspond to the first two diagrams in Eq. (1.160). The last equation is Fourier component-wise

$$\begin{aligned}\mathcal{G}^{r,a}(\varepsilon, \mathbf{k}, n, n') &= \mathcal{G}_0^{r,a}(\varepsilon, \mathbf{k}, n, n') \\ &+ \frac{1}{\hbar^2 V_{\mathbf{q}}} \sum_{\mathbf{q}} \sum_{n_1, n_2 = -\infty}^{\infty} \left[\nu(\mathbf{q}) \mathcal{G}_0^{r,a}(\varepsilon, \mathbf{k}, n, n_1) \right. \\ &\left. \times \; \mathcal{G}_0^{r,a}(\varepsilon, \mathbf{k} - \mathbf{q}, n_1, n_2) \mathcal{G}_0^{r,a}(\varepsilon, \mathbf{k}, n_2, n') \right] + \ldots \end{aligned} \tag{1.163}$$

$=$ 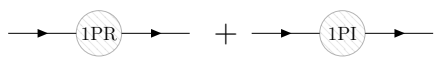 . (1.164)

The diagrams in Eqs. (1.162) and (1.164) that denote the sum over all reducible and irreducible diagrams. $\mathcal{G}^{r,a}(\varepsilon, \mathbf{k}, n, n')$ can be understood as entries of a matrix

$$\mathcal{G}^{r,a}_{(0)}(\varepsilon, \mathbf{k}, n, n') \equiv \left(\boldsymbol{G}^{r,a}_{(0)}(\varepsilon, \mathbf{k}) \right)_{nn'} . \tag{1.165}$$

Remembering the component-wise matrix-multiplication, one can imply that Eq. (1.163) becomes

$$\begin{aligned}\boldsymbol{G}^{r,a}(\varepsilon,\mathbf{k}) &= \boldsymbol{G}_0^{r,a}(\varepsilon,\mathbf{k}) \\ &\quad + \frac{1}{\hbar^2 V_{\mathbf{q}}}\sum_{\mathbf{q}} \nu(\mathbf{q})\boldsymbol{G}_0^{r,a}(\varepsilon,\mathbf{k})\boldsymbol{G}_0^{r,a}(\varepsilon,\mathbf{k}-\mathbf{q})\boldsymbol{G}_0^{r,a}(\varepsilon,\mathbf{k}) + \ldots \qquad (1.166)\end{aligned}$$

$$= \quad + \quad . \qquad (1.167)$$

All reducible diagrams can be expressed as powers of irreducible diagrams, leading to

$$\boldsymbol{G}^{r,a}(\varepsilon,\mathbf{k}) = \boldsymbol{G}_0^{r,a}(\varepsilon,\mathbf{k}) + \boldsymbol{G}_0^{r,a}(\varepsilon,\mathbf{k})\sum_{n=1}^{\infty}\left[\boldsymbol{\Sigma}^{r,a}(\varepsilon,\mathbf{k})\boldsymbol{G}_0^{r,a}(\varepsilon,\mathbf{k})\right]^n , \qquad (1.168)$$

where $\boldsymbol{\Sigma}^{r,a}$ is the sum over all irreducible diagrams, i.e. the Floquet self-energy

$$\boldsymbol{\Sigma}^{r,a}(\varepsilon,\mathbf{k}) = \quad . \qquad (1.169)$$

Even if the self-energy is truncated at finite order, the correction to $\boldsymbol{G}^{r,a}(\varepsilon,\mathbf{k})$ contains diagrams of all orders [48]. The lowest non-trivial order is called the "first order Born approximation" corresponding to the self-energy

$$\boldsymbol{\Sigma}^{r,a}_{\mathrm{1BA}}(\varepsilon,\mathbf{k}) = \quad = \frac{1}{\hbar^2 V_{\mathbf{q}}}\sum_{\mathbf{q}} \nu(\mathbf{k}+\mathbf{q})\boldsymbol{G}_0^{r,a}(\varepsilon,\mathbf{q})\,. \qquad (1.170)$$

If the potential decays on a length scale much shorter than the wavelength of the particles, it is reasonable to assume white noise characterized by

$$\langle v(\mathbf{x})v(\mathbf{x}')\rangle_{\mathrm{imp}} = \mathcal{V}_{\mathrm{imp}}\delta(\mathbf{x}-\mathbf{x}') \ . \qquad (1.171)$$

In this case, the self-energy becomes independent of the momentum because ν is constant in momentum space. The self-energy is the momentum sum over the bare Green's function multiplied with the impurity strength $\mathcal{V}_{\mathrm{imp}}$

$$\boldsymbol{\Sigma}^{r,a}_{\mathrm{1BA}}(\varepsilon) = \frac{\mathcal{V}_{\mathrm{imp}}}{\hbar^2 V_{\mathbf{k}}}\sum_{\mathbf{k}} \boldsymbol{G}_0^{r,a}(\varepsilon,\mathbf{k}) \ . \qquad (1.172)$$

In the following, the focus is on white noise. It can be shown that the self-energy in first order Born approximation for white noise is equal to a scattering time derived from a generalized Floquet Fermi's golden rule, which is proven in the following. The solution of the recursive equation (1.168) is

$$\boldsymbol{G}^{r,a}(\varepsilon,\mathbf{k}) = \left[\left(\boldsymbol{G}_0^{r,a}(\varepsilon,\mathbf{k})\right)^{-1} + \boldsymbol{\Sigma}^{r,a}(\varepsilon,\mathbf{k})\right]^{-1} . \qquad (1.173)$$

Applying the transformation $\boldsymbol{T}$ from Eq. (1.101) which diagonalizes the bare Green's function leads to

$$\boldsymbol{T}^{\dagger}(\mathbf{k})\boldsymbol{G}^{r,a}(\varepsilon,\mathbf{k})\boldsymbol{T}(\mathbf{k}) = \left[\boldsymbol{D}(\mathbf{k}) + \boldsymbol{T}^{\dagger}(\mathbf{k})\boldsymbol{\Sigma}^{r,a}(\varepsilon,\mathbf{k})\boldsymbol{T}(\mathbf{k})\right]^{-1} , \qquad (1.174)$$

together with the diagonal matrix containing the eigenvalues

$$\Big(\boldsymbol{D}(\mathbf{k})\Big)^{nn'}_{\alpha\beta} \equiv \Big(\boldsymbol{T}^{\dagger}(\mathbf{k})\boldsymbol{G}_0^{r,a}(\varepsilon,\mathbf{k})\boldsymbol{T}(\mathbf{k})\Big)^{nn'}_{\alpha\beta} \tag{1.175}$$

$$= \delta_{\alpha\beta}\delta_{nn'}\big(\tfrac{1}{\hbar}\varepsilon - \tfrac{1}{\hbar}\varepsilon_{\alpha} - n\Omega\big)\ . \tag{1.176}$$

However, the self-energy $\boldsymbol{\Sigma}$ is, in general, not diagonalized with the same transformation $\boldsymbol{T}$ from Eq. (1.101) as the bare Green's function. The transformed self-energy for white noise in first order Born approximation is governed by

$$\begin{aligned}\Big(\boldsymbol{T}^{\dagger}(\mathbf{k})\boldsymbol{\Sigma}_1^{r,a}(\varepsilon)\boldsymbol{T}(\mathbf{k})\Big)^{nn'}_{\alpha\beta} &= \frac{\mathcal{V}_{\mathrm{imp}}}{\hbar^2}\frac{1}{V_{\mathbf{k}'}}\sum_{\mathbf{k}'}\sum_{m,m'=-\infty}^{\infty}\\ \times\sum_{\ell=-\infty}^{\infty}\sum_{\gamma}&\frac{\big(u_{\alpha}^{m+n}(\mathbf{k})\big)^{*}u_{\gamma}^{m+\ell}(\mathbf{k}')\big(u_{\gamma}^{m'+\ell}(\mathbf{k}')\big)^{*}u_{\beta}^{m'+n'}(\mathbf{k})}{\frac{1}{\hbar}\varepsilon - \frac{1}{\hbar}\varepsilon_{\gamma}(\mathbf{k}') - \ell\Omega \pm i0^{+}}\ .\end{aligned} \tag{1.177}$$

Now, the focus is on the difference of the retarded and advanced self-energy

$$\begin{aligned}&\Big(\boldsymbol{T}^{\dagger}(\mathbf{k})\big(\boldsymbol{\Sigma}^{r}_{\mathrm{1BA}}(\varepsilon,\mathbf{k}) - \boldsymbol{\Sigma}^{a}_{\mathrm{1BA}}(\varepsilon,\mathbf{k})\big)\boldsymbol{T}(\mathbf{k})\Big)^{nn'}_{\alpha\beta} =\\ &-i\frac{2\pi\mathcal{V}_{\mathrm{imp}}}{\hbar}\frac{1}{V_{\mathbf{k}'}}\sum_{\mathbf{k}'}\sum_{\gamma}c^{n}_{\alpha\gamma}(\mathbf{k},\mathbf{k}')\big(c^{n'}_{\beta\gamma}(\mathbf{k},\mathbf{k}')\big)^{*}\,\delta\big(\varepsilon-\varepsilon_{\gamma}(\mathbf{k}')\big)\end{aligned} \tag{1.178}$$

with the abbreviation

$$c^{n}_{\alpha\beta}(\mathbf{k},\mathbf{k}') \equiv \sum_{m=-\infty}^{\infty}\big(u_{\alpha}^{m+n}(\mathbf{k})\big)^{*}u_{\beta}^{m}(\mathbf{k}')\ . \tag{1.179}$$

The difference of the retarded and advanced self-energy can be related to a scattering time derived within the framework of the Floquet Fermi Golden rule in Sec. 1.7.2. However, on the diagonal, the difference of the retarded and advanced Green's function is equal to the imaginary part of the retarded self-energy

$$\begin{aligned}&2i\mathrm{Im}\Big(\boldsymbol{T}^{\dagger}(\mathbf{k})\boldsymbol{\Sigma}^{r,a}_{\mathrm{1BA}}(\varepsilon,\mathbf{k})\boldsymbol{T}(\mathbf{k})\Big)^{nn}_{\alpha\alpha} =\\ &\Big(\boldsymbol{T}^{\dagger}(\mathbf{k})\big(\boldsymbol{\Sigma}^{r}_{\mathrm{1BA}}(\varepsilon,\mathbf{k}) - \boldsymbol{\Sigma}^{a}_{\mathrm{1BA}}(\varepsilon,\mathbf{k})\big)\boldsymbol{T}(\mathbf{k})\Big)^{nn}_{\alpha\alpha}.\end{aligned} \tag{1.180}$$

The explicit form of the imaginary part of the diagonal elements is

$$\begin{aligned}&-\mathrm{Im}\Big(\boldsymbol{T}^{\dagger}(\mathbf{k})\boldsymbol{\Sigma}^{r,a}_{\mathrm{1BA}}(\varepsilon,\mathbf{k})\boldsymbol{T}(\mathbf{k})\Big)^{nn}_{\alpha\alpha} =\\ &\frac{\pi\mathcal{V}_{\mathrm{imp}}}{\hbar}\frac{1}{V_{\mathbf{k}'}}\sum_{\mathbf{k}'}\sum_{m=-\infty}^{\infty}\sum_{\gamma}\big|u_{\alpha}^{m+n}(\mathbf{k})\big(u_{\gamma}^{m}(\mathbf{k}')\big)^{*}\big|^{2}\,\delta\big(\varepsilon-\varepsilon_{\gamma}(\mathbf{k}')\big)\end{aligned} \tag{1.181}$$

which will be of interest later on. As in the static case, the first order Born approximation for white noise yields the same scattering time as the Fermi's golden rule [89]. The corresponding holds for the driven system, which will be shown in the subsequent section.

1.7.2 Floquet Fermi's Golden Rule

The aim of this section is to relate the imaginary part of the self-energy in first order Born approximation, see Eq. (1.181), to a scattering time derived from Fermi's golden rule [7, 8, 89, 91, 92]. To show this relation, the Fermi's golden rule must be generalized to *t*-*t*'-Floquet states. First, a recall of Fermi's golden rule for Floquet states is presented to show that this is an approximation of the generalized Floquet Fermi's golden rule derived in the second part of this section. The latter accounts for both inter- as well intra-Floquet zone scattering. Remarkably, the generalized Floquet Fermi's golden rule is proven to yield the same result for the scattering time as the Floquet Dyson series.

Fermi's Golden Rule for Floquet States

For a time-independent perturbation V switched on at time $t = 0$, the transition rate between an initial and a final state is governed by

$$\Gamma_{\mathrm{if}} = \frac{2\pi}{\hbar} |\langle \psi_{\mathrm{f}} | V | \psi_{\mathrm{i}} \rangle|^2 \, \delta(E_f - E_i) \; . \tag{1.182}$$

For details or derivation of this formula, see Ref. [7, 8, 89–92]. Γ_{if} describes the long time limit of the transition probability of an initial state ψ_{i} into a final state ψ_{f} in the presence of a weak perturbation V. A generalization of Fermi's golden rule to time periodic Hamiltonians, i.e. the Floquet Fermi's golden rule

$$\Gamma_{\mathrm{if}} = \sum_{m=-\infty}^{\infty} |\langle \psi_{\mathrm{f}}^m(t) | V | \psi_{\mathrm{i}}^0(t) \rangle|^2 \delta(\varepsilon_{\mathrm{i}} - \varepsilon_{\mathrm{f}} - m\hbar\Omega) \tag{1.183}$$

together with

$$|\psi_{\mathrm{i,f}}^m(t)\rangle = \sum_{n=-\infty}^{\infty} e^{-in\Omega t} |u_{\mathrm{i,f}}^{n+m}\rangle \tag{1.184}$$

was already derived by Kitagawa *et al.* in Ref. [21]. A more detailed discussion of "Scattering theory for Floquet-Bloch states" is given in Ref. [93]. The Floquet Fermi's golden rule was used by Kibis in Ref. [28] to explain the suppression of backscattering of conduction electrons in the presence of a high-frequency electric field. In regard to the Fermi's golden rule for the *t*-*t*'-Floquet states, the derivation of the Floquet Fermi's golden rule is presented here in detail. It is assumed that the solution of the time-dependent Schrödinger equation

$$i\hbar \frac{\partial}{\partial t} |\psi_\alpha(t)\rangle = H(t) |\psi_\alpha(t)\rangle \tag{1.185}$$

and the corresponding time evolution operator $U_0(t, t_0)$, fulfilling the Schrödinger equation, are known. In the presence of a time-dependent perturbation $V(t)$, the Schrödinger equation becomes

$$i\hbar \frac{\partial}{\partial t} |\Psi_\alpha(t)\rangle = \big[H(t) + V(t)\big] |\Psi_\alpha(t)\rangle \; . \tag{1.186}$$

The potential $V(t)$ is switched on at a reference time t_0, such that the solutions of the Schrödinger equation coincide for times $t \leq t_0$

$$|\psi_\alpha(t)\rangle = |\Psi_\alpha(t)\rangle \quad \text{for} \quad t \leq t_0 \ . \tag{1.187}$$

At times $t \leq t_0$, the particle is in an eigenstate of the unperturbed Hamiltonian. According to Refs. [91–93], the interaction picture for the solution of the system with perturbation is

$$|\Psi_\alpha(t)\rangle_I = U_0^\dagger(t, t_0)|\Psi_\alpha(t)\rangle \ . \tag{1.188}$$

The operator $U(t, t_0)$ fulfills Eq. (1.185) and describes the time evolution of the system without perturbation. Inserting the wave function in the interaction picture (1.188) into the Schrödinger equation (1.186) leads to the Schrödinger equation in the interaction picture

$$i\hbar\frac{\partial}{\partial t}|\Psi_\alpha(t)\rangle_I = V_I(t)|\Psi_\alpha(t)\rangle_I \, , \tag{1.189}$$

where the role of the Hamiltonian is kept by the perturbation in the interaction picture

$$V_I(t) = U_0^\dagger(t, t_0)V(t)U_0(t, t_0) \ . \tag{1.190}$$

Following Ref. [91], the solution of the Schrödinger equation in the interaction picture (1.189) is a recursive integral series

$$|\Psi_\alpha(t)\rangle_I = |\Psi_\alpha(t_0)\rangle_I + \frac{1}{i\hbar}\int_{t_0}^{t} dt' \, V_I(t')|\Psi_\alpha(t')\rangle_I \tag{1.191}$$

which is thus far exact. At reference time t_0, Eq. (1.188) simplifies to

$$|\Psi_\alpha(t_0)\rangle_I = |\Psi_\alpha(t_0)\rangle \tag{1.192}$$

since $U(t_0, t_0) = \mathbb{1}$. Iterating Eq. (1.191) up to first order in the potential and using Eq. (1.187) yield the approximation

$$|\Psi_\alpha(t)\rangle_I \approx |\psi_\alpha(t_0)\rangle + \frac{1}{i\hbar}\int_{t_0}^{t} dt' \, V_I(t')|\psi_\alpha(t_0)\rangle \ . \tag{1.193}$$

Multiplying from the left with $\langle\psi_\beta(t_0)|$ leads to

$$\langle\psi_\beta(t_0)|\Psi_\alpha(t)\rangle_I = \langle\psi_\beta(t)|\Psi_\alpha(t)\rangle \tag{1.194}$$

$$= \delta_{\alpha\beta} + \frac{1}{i\hbar}\int_{t_0}^{t} dt' \, \langle\psi_\beta(t')|V(t')|\psi_\alpha(t')\rangle \tag{1.195}$$

describing up to first order in the potential the transition amplitude to find the particle in the state $|\Psi_\alpha(t)\rangle$. In the last step, the properties of the time-evolution operator were used, namely

$$\langle\psi_\beta(t_0)|U_0^\dagger(t, t_0) = \langle\psi_\beta(t)| \ , \tag{1.196}$$

$$U_0(t, t_0)|\psi_\alpha(t_0)\rangle = |\psi_\alpha(t)\rangle \ . \tag{1.197}$$

Without loss of generality t_0 can be set to zero, and for $\alpha \neq \beta$ the first nontrivial order of Eq. (1.194) is

$$a_{\alpha\beta}(t) = -\frac{i}{\hbar}\int_0^t dt' \, \langle \psi_\beta(t')|V(t')|\psi_\alpha(t')\rangle \ . \tag{1.198}$$

This formula, the Floquet Fermi's golden rule, is equal to Eq. (10) of Ref. [28]. The Floquet Fermi's golden rule will be used later in Sec. 1.9.3 to establish a link to the results for the scattering time derived using the Dyson series for the Floquet Green's function, see Sec. 1.7.1. To proceed further, scattering from a Floquet state into a state with constant quasienergy

$$|\psi_\alpha(\varepsilon, t)\rangle = e^{-\frac{i}{\hbar}\varepsilon t}|u_\alpha(t)\rangle \tag{1.199}$$

is considered. The quasienergy ε is independent of the quantum number. Hence, this state is not an eigenstate of the Hamiltonian. Nevertheless, it fulfills

$$\langle \psi_\alpha(t)|\psi_\beta(\varepsilon, t)\rangle = \delta_{\alpha\beta}\, e^{\frac{i}{\hbar}(\varepsilon_\alpha - \varepsilon)t} \ . \tag{1.200}$$

Consequently, Eq. (1.198) remains valid if the final state is $|\psi_\alpha(\varepsilon, t)\rangle$. Now consider a scattering event from a Floquet state into a state with constant energy

$$\psi_\alpha(\mathbf{k}', t) = e^{-\frac{i}{\hbar}\varepsilon_\alpha(\mathbf{k}')t} u_\alpha(\mathbf{k}', t) \mapsto e^{-\frac{i}{\hbar}\varepsilon t} u_\beta(\mathbf{k}, t) \ . \tag{1.201}$$

If the perturbation $V(t)$ is time-independent, Eq. (1.198) becomes

$$a_{\alpha\beta}(\mathbf{k}, \mathbf{k}', t) = -i\frac{V_{\mathbf{k}\mathbf{k}'}}{\hbar}\sum_{n,n'=-\infty}^{\infty}\int_0^t dt' \, e^{\frac{i}{\hbar}(\varepsilon - \varepsilon_\alpha(\mathbf{k}') - (n-n')\hbar\Omega)t'} \big(u_\beta^{n'}(\mathbf{k})\big)^* u_\alpha^n(\mathbf{k}') \, . \tag{1.202}$$

Considering the absolute squared of $a_{\alpha\beta}(\mathbf{k}, \mathbf{k}', t)$ and substituting in the time integral $t' = t'' - t/2$ yield

$$\begin{aligned} |a_{\alpha\beta}(\mathbf{k}, \mathbf{k}', t)|^2 = \frac{V_{\mathbf{k}\mathbf{k}'}^2}{\hbar^2}\Bigg| \sum_{nn'=-\infty}^{\infty} & e^{\frac{i}{2\hbar}(\varepsilon - \varepsilon_\alpha(\mathbf{k}') - (n-n')\hbar\Omega)t} \big(u_\beta^{n'}(\mathbf{k})\big)^* u_\alpha^n(\mathbf{k}') \\ & \times \int_{-t/2}^{t/2} dt' \, e^{\frac{i}{\hbar}(\varepsilon - \varepsilon_\alpha(\mathbf{k}') - (n-n')\hbar\Omega)t'}\Bigg|^2 \ . \end{aligned} \tag{1.203}$$

In the long time limit, the integral turns into a delta distribution

$$\delta(\varepsilon) = \frac{1}{2\pi\hbar}\lim_{t\to\infty}\int_{-t/2}^{t/2} dt' \, e^{\frac{i}{\hbar}\varepsilon t'} \tag{1.204}$$

and therefore

$$\begin{aligned} |a_{\alpha\beta}(\mathbf{k}, \mathbf{k}', t)|^2 = 4\pi^2 V_{\mathbf{k}\mathbf{k}'}^2\Bigg| \sum_{nn'=-\infty}^{\infty} & \big(u_\beta^{n'}(\mathbf{k})\big)^* u_\alpha^n(\mathbf{k}') \\ & \times \delta\big(\varepsilon - \varepsilon_\alpha(\mathbf{k}') - (n-n')\hbar\Omega\big)\Bigg|^2 \ . \end{aligned} \tag{1.205}$$

The quasienergies ε and ε_α are chosen to be in the central Floquet zone such that

$$|\varepsilon - \varepsilon_\alpha| \leq \hbar\Omega\,, \tag{1.206}$$

$$\delta(\varepsilon - \varepsilon_\alpha - n\hbar\Omega)\delta(\varepsilon - \varepsilon_\alpha - m\hbar\Omega) = \delta^2(\varepsilon - \varepsilon_\alpha - n\hbar\Omega)\delta_{nm}\ . \tag{1.207}$$

Hence, the absolute squared can be applied to each summand in Eq. (1.205) and with the definition given in Eq. (1.179):

$$\begin{aligned}|a_{\alpha\beta}(\mathbf{k},\mathbf{k}',t)|^2 = 4\pi^2 V_{\mathbf{k}\mathbf{k}'}^2 \sum_{n=-\infty}^{\infty} c_{\beta\alpha}^{-n}(\mathbf{k},\mathbf{k}')\big(c_{\beta\alpha}^{-n}(\mathbf{k},\mathbf{k}')\big)^* \\ \times\, \delta^2\big(\varepsilon - \varepsilon_\alpha(\mathbf{k}') - n\hbar\Omega\big)\ .\end{aligned} \tag{1.208}$$

The square of the delta distribution can be rewritten as [28]

$$\delta^2(\varepsilon) = \delta(\varepsilon)\delta(0) = \frac{\delta(\varepsilon)}{2\pi\hbar}\lim_{t\to\infty}\int_{-t/2}^{t/2} dt'\, e^{\frac{i}{\hbar}0t'} = \frac{\delta(\varepsilon)t}{2\pi\hbar}\ . \tag{1.209}$$

The transition probability is governed by the time derivative of Eq. (1.208):

$$\Gamma_{\alpha\beta}(\mathbf{k},\mathbf{k}') \equiv \frac{d|a_{\alpha\beta}(\mathbf{k},\mathbf{k}',t)|^2}{dt} \tag{1.210}$$

$$= \frac{2\pi}{\hbar}V_{\mathbf{k}\mathbf{k}'}^2 \sum_{n=-\infty}^{\infty} c_{\beta\alpha}^{-n}(\mathbf{k},\mathbf{k}')\big(c_{\beta\alpha}^{-n}(\mathbf{k},\mathbf{k}')\big)^*\,\delta\big(\varepsilon - \varepsilon_\alpha(\mathbf{k}') - n\hbar\Omega\big)\ . \tag{1.211}$$

The delta distribution can only have support if $n = 0$. Performing an impurity average according to Eq. (1.171) leads to $\langle V_{\mathbf{k}\mathbf{k}'}^2\rangle_{\text{imp}} = \mathcal{V}_{\text{imp}}$, such that

$$\langle\Gamma_{\alpha\beta}(\mathbf{k},\mathbf{k}')\rangle_{\text{imp}} = \langle\Gamma_{\alpha\beta}(\mathbf{k},\mathbf{k}')\rangle_{\text{imp}} \tag{1.212}$$

$$= \frac{2\pi}{\hbar}\mathcal{V}_{\text{imp}}|c_{\beta\alpha}^0(\mathbf{k},\mathbf{k}')|^2\delta\big(\varepsilon - \varepsilon_\alpha(\mathbf{k}')\big)\ . \tag{1.213}$$

The scattering time is governed by the sum over all initial states and momenta over the impurity averaged transition probability

$$\frac{1}{\tau_\beta(\varepsilon,\mathbf{k})} = \frac{1}{V_{\mathbf{k}'}}\sum_{\mathbf{k}'}\sum_{\alpha}\langle\Gamma_{\alpha\beta}(\mathbf{k},\mathbf{k}')\rangle_{\text{imp}} \tag{1.214}$$

$$= \frac{2\pi}{\hbar}\mathcal{V}_{\text{imp}}\frac{1}{V_{\mathbf{k}'}}\sum_{\mathbf{k}'}\sum_{\alpha}|c_{\beta\alpha}^0(\mathbf{k},\mathbf{k}')|^2\,\delta\big(\varepsilon - \varepsilon_\alpha(\mathbf{k}')\big)\,. \tag{1.215}$$

The last equation is the scattering time deduced from the Floquet Fermi's Golden rule. It is later shown that this scattering time is equal to the central entry of an infinite dimensional scattering time matrix derived from the generalized Floquet Fermi's Golden rule.

Fermi's Golden Rule for *t*-*t*'-Floquet States

In the following, the calculation steps are similar as in Refs. [28, 91]. The difference is in the use of the *t*-*t*'-Floquet states (cf. Eq. (1.60)) instead of Floquet states (cf. Eq. (1.3)). The *t*-*t*'-state of Eq. (1.60) fulfills the *t*-*t*'-Schrödinger equation (1.218)

$$i\hbar\frac{\partial}{\partial t}|\psi_\alpha^\ell(t,t')\rangle = H_F(t')|\psi_\alpha^\ell(t,t')\rangle\ . \tag{1.216}$$

There is a time-evolution operator fulfilling this Schrödinger equation, i.e.

$$U_0(t,t_0;t') = e^{-\frac{i}{\hbar}H_F(t')\cdot(t-t_0)} \ . \tag{1.217}$$

If a perturbation is switched on at time t_0, the Schrödinger equation becomes

$$i\hbar\frac{\partial}{\partial t}|\Psi_\alpha^\ell(t,t')\rangle = \big[H_F(t') + V(t,t')\big]|\Psi_\alpha^\ell(t,t')\rangle \tag{1.218}$$

together with the boundary condition that without perturbation, i.e. $t \leq t_0$, both solutions of the Schrödinger equation coincide [91]

$$|\psi_\alpha^\ell(t,t')\rangle = |\Psi_\alpha^\ell(t,t')\rangle \quad \text{for} \quad t \leq t_0 \ . \tag{1.219}$$

Now, the t-t'-state in the interaction picture

$$|\Psi_\alpha^\ell(t,t')\rangle_I = U_0^\dagger(t,t_0;t')|\Psi_\alpha^\ell(t,t')\rangle \tag{1.220}$$

and the perturbation in the interaction picture

$$V_I(t,t') = U_0^\dagger(t,t_0;t')V(t,t')U_0(t,t_0;t') \tag{1.221}$$

are defined. Inserting Eq. (1.220) into Eq. (1.218) leads to the t-t'-Schrödinger equation in the interaction picture

$$i\hbar\frac{\partial}{\partial t}|\Psi_\alpha^\ell(t,t')\rangle_I = V_I(t,t')|\Psi_\alpha^\ell(t,t')\rangle_I \tag{1.222}$$

with the solution

$$|\Psi_\alpha^\ell(t,t')\rangle_I = |\Psi_\alpha^\ell(t_0,t')\rangle_I + \frac{1}{i\hbar}\int_{t_0}^{t} dt_1\, V_I(t_1,t')|\Psi_\alpha^\ell(t_1,t')\rangle_I \ . \tag{1.223}$$

Iterating up to first order yields

$$|\Psi_\alpha^\ell(t,t')\rangle_I \approx |\psi_\alpha^\ell(t_0,t')\rangle + \frac{1}{i\hbar}\int_{t_0}^{t} dt_1\, V_I(t_1,t')|\psi_\alpha^\ell(t_0,t')\rangle \tag{1.224}$$

and multiplying from the left with $\langle\psi_\beta^{\ell'}(t_0,t'')|$ gives

$$\begin{aligned}\langle\psi_\beta^{\ell'}(t,t'')|\Psi_\alpha^\ell(t,t')\rangle = &\langle\psi_\beta^{\ell'}(t,t'')|\psi_\alpha^\ell(t,t')\rangle \\ &+ \frac{1}{i\hbar}\int_{t_0}^{t} dt_1\, \langle\psi_\beta^{\ell'}(t_1,t'')|V(t_1,t')|\psi_\alpha^\ell(t_1,t')\rangle \ .\end{aligned} \tag{1.225}$$

Now consider the matrix element

$$a_{\alpha\beta}^{\ell\ell'}(t,t') = \sum_{n=-\infty}^{\infty} a_{\alpha\beta}^{\ell\ell'}(t,n)\, e^{in\Omega t'} \tag{1.226}$$

$$= \langle\psi_\beta^\ell(t,t')|\Psi_\alpha^{\ell'}(t,t')\rangle \tag{1.227}$$

$$\approx \delta_{\alpha\beta}\, e^{i\Omega(\ell-\ell')(t'-t)} + \frac{1}{i\hbar}\int_{t_0}^{t} dt_1\, \langle\psi_\beta^\ell(t_1,t')|V(t_1,t')|\psi_\alpha^{\ell'}(t_1,t')\rangle \tag{1.228}$$

where the t-t'-Floquet states have the same time dependence but different Floquet indices. The Fourier coefficients for a, in the second time argument, time-independent perturbation $V(t)$ are governed by

$$a^{\ell\ell'}_{\alpha\beta}(t,n) = \frac{1}{T}\int_0^T dt'\, a^{\ell\ell'}_{\alpha\beta}(t,t')\, e^{in\Omega t'} \tag{1.229}$$

$$= \delta_{\alpha\beta}\delta_{n,\ell-\ell'}\, e^{-in\Omega t} + \frac{1}{i\hbar}\int_{t_0}^t dt_1\, e^{\frac{i}{\hbar}\left(\varepsilon_\alpha-\varepsilon_\beta+(\ell-\ell')\hbar\Omega\right)t_1} \sum_{m=-\infty}^{\infty} \langle u_\alpha^{m+\ell+n}|V(t_1)|u_\beta^{m+\ell'}\rangle \tag{1.230}$$

which is so far general. The transition amplitude is only a function of the difference of the Floquet indices

$$a^{\ell\ell'}_{\alpha\beta}(t,t') = a^{(\ell-\ell')}_{\alpha\beta}(t,t')\ . \tag{1.231}$$

Analogue to the last section, t_0 can be set to zero and for $\alpha \neq \beta$ the lowest order in V of Eq. (1.228) is

$$a^{\ell\ell'}_{\alpha\beta}(t,t') = -\frac{i}{\hbar}\int_0^t dt_1\, \langle \psi^\ell_\beta(t_1,t')|V(t_1,t')|\psi^{\ell'}_\alpha(t_1,t')\rangle\ . \tag{1.232}$$

Now, lets assume a scattering event from a t-t'-Floquet state into another t-t'-Floquet state with constant quasienergy

$$|\psi^\ell_\alpha(\varepsilon,t,t')\rangle \equiv e^{-\frac{i}{\hbar}(\varepsilon+\ell\hbar\Omega)t}|u_\alpha(t,t')\rangle e^{i\ell\Omega t'}\ . \tag{1.233}$$

The quasienergy ε is independent of the quantum number α. This state is not necessary an eigenstate of the Hamiltonian, but nevertheless it fulfills

$$\langle\psi^\ell_\alpha(t,t')|\psi^{\ell'}_\beta(\varepsilon,t,t')\rangle = \delta_{\alpha\beta}e^{-\frac{i}{\hbar}(\varepsilon-\varepsilon_\alpha+(\ell'-\ell)\hbar\Omega)t}\, e^{i\Omega(\ell'-\ell)t'}\ . \tag{1.234}$$

Hence, Eq. (1.232) remains valid if the final state is of the form as in Eq. (1.233). Now, consider a scattering event from a t-t'-Floquet state into a state with constant energy

$$\psi^\ell_\alpha(\mathbf{k}',t,t') = e^{-\frac{i}{\hbar}(\varepsilon_\alpha(\mathbf{k}')+\ell\hbar\Omega)t}u_\alpha(\mathbf{k}',t')\, e^{i\ell\Omega t'} \mapsto e^{-\frac{i}{\hbar}(\varepsilon+\ell'\hbar\Omega)t}u_\beta(\mathbf{k},t')\, e^{i\ell'\Omega t'}\ . \tag{1.235}$$

The Fourier coefficient of the matrix element for a scattering, as in Eq. (1.235), is for a time-independent perturbation

$$a^{\ell\ell'}_{\alpha\beta}(\mathbf{k},\mathbf{k}',t,n) = -i\frac{V_{\mathbf{k}\mathbf{k}'}}{\hbar}\int_0^t dt'\, e^{\frac{i}{\hbar}(\varepsilon-\varepsilon_\alpha(\mathbf{k}')-(\ell-\ell')\hbar\Omega)t'} \times \sum_{m=-\infty}^{\infty}\left(u_\beta^{m+\ell+n}(\mathbf{k})\right)^* u_\alpha^{m+\ell'}(\mathbf{k}') \tag{1.236}$$

$$= -i\frac{V_{\mathbf{k}\mathbf{k}'}}{\hbar}\int_0^t dt'\, e^{\frac{i}{\hbar}(\varepsilon-\varepsilon_\alpha(\mathbf{k}')-(\ell-\ell')\hbar\Omega)t'} c^{\ell-\ell'+n}_{\beta\alpha}(\mathbf{k},\mathbf{k}') \tag{1.237}$$

where in the last step the definition given in Eq. (1.179) was used. This allows for the definition of a transition probability matrix

$$\left(\mathbf{A}^{\ell\ell' jj'}_{\alpha\beta}(\mathbf{k},\mathbf{k}',t)\right)_{n,n'} \equiv \sum_\gamma a^{\ell\ell'}_{\gamma\alpha}(\mathbf{k},\mathbf{k}',t,n)\left(a^{jj'}_{\gamma\beta}(\mathbf{k},\mathbf{k}',t,n')\right)^*\ . \tag{1.238}$$

Equivalently to Eq. (1.203), the substitution $t' = t'' - t/2$ of the integral is performed, and in the long time limit, using Eq. (1.204), the transition probability matrix becomes

$$\begin{aligned}\left(\mathbf{A}_{\alpha\beta}^{\ell\ell' jj'}(\mathbf{k},\mathbf{k}',t)\right)_{n,n'} = 4\pi^2 V_{\mathbf{k}\mathbf{k}'}^2 \sum_{\gamma} c_{\alpha\gamma}^{\ell-\ell'+n}(\mathbf{k},\mathbf{k}')\,\delta\big(\varepsilon - \varepsilon_\gamma(\mathbf{k}') - (\ell-\ell')\hbar\Omega\big) \\ \times \left(c_{\beta\gamma}^{j-j'+n'}(\mathbf{k},\mathbf{k}')\right)^* \delta\big(\varepsilon - \varepsilon_\gamma(\mathbf{k}') - (j-j')\hbar\Omega\big)\ .\end{aligned} \tag{1.239}$$

The quasienergies are always in the central Floquet zone, c.f. Eq. (1.207), therefore

$$\left(\mathbf{A}_{\alpha\beta}^{\ell\ell' jj'}(\mathbf{k},\mathbf{k}',t)\right)_{n,n'} = 4\pi^2 V_{\mathbf{k}\mathbf{k}'}^2 \sum_{\gamma} c_{\alpha\gamma}^{n}(\mathbf{k},\mathbf{k}')\left(c_{\beta\gamma}^{n'}(\mathbf{k},\mathbf{k}')\right)^* \delta^2\big(\varepsilon - \varepsilon_\gamma(\mathbf{k}')\big)\ . \tag{1.240}$$

Using Eq. (1.209) and performing the time derivative of each matrix element yield the transition amplitude matrix

$$\Gamma_{\alpha\beta}^{nn'}(\mathbf{k},\mathbf{k}') \equiv \frac{d\left(\mathbf{A}_{\alpha\beta}^{\ell\ell' jj'}(\mathbf{k},\mathbf{k}',t)\right)_{n,n'}}{dt} \tag{1.241}$$

$$= \frac{2\pi}{\hbar} V_{\mathbf{k}\mathbf{k}'}^2 \sum_{\gamma} c_{\alpha\gamma}^{n}(\mathbf{k},\mathbf{k}')\left(c_{\beta\gamma}^{n'}(\mathbf{k},\mathbf{k}')\right)^* \delta\big(\varepsilon - \varepsilon_\gamma(\mathbf{k}')\big)\ . \tag{1.242}$$

Once again, an impurity average allows to identify $\langle V_{\mathbf{k}\mathbf{k}'}^2\rangle_{\text{imp}} = \mathcal{V}_{\text{imp}}$. The inverse scatting time matrix is the sum over all momenta over the transition probability matrix

$$\left(\frac{1}{\boldsymbol{\tau}(\varepsilon,\mathbf{k})}\right)_{\alpha\beta}^{nn'} \equiv \frac{1}{V_{\mathbf{k}'}} \sum_{\mathbf{k}'} \langle \Gamma_{\alpha\beta}^{nn'}(\mathbf{k},\mathbf{k}')\rangle_{\text{imp}} \tag{1.243}$$

$$= \frac{2\pi}{\hbar}\mathcal{V}_{\text{imp}} \frac{1}{V_{\mathbf{k}'}} \sum_{\mathbf{k}'}\sum_{\gamma} c_{\alpha\gamma}^{n}(\mathbf{k},\mathbf{k}')\left(c_{\beta\gamma}^{n'}(\mathbf{k},\mathbf{k}')\right)^* \delta\big(\varepsilon - \varepsilon_\gamma(\mathbf{k}')\big) \tag{1.244}$$

$$= i\Big(\boldsymbol{T}^\dagger(\mathbf{k})\big(\boldsymbol{\Sigma}_{\text{1BA}}^r(\varepsilon,\mathbf{k}) - \boldsymbol{\Sigma}_{\text{1BA}}^a(\varepsilon,\mathbf{k})\big)\boldsymbol{T}(\mathbf{k})\Big)_{\alpha\beta}^{nn'} \tag{1.245}$$

being equal to the result from the Dyson series for the Floquet Green's function (cf. Eq. (1.178)). Interpreting the (n,n')-th entry of the foregoing scattering time matrix as scattering from the n-th Floquet zone into the n'-th Floquet zone allows for disorder-mediated inter-Floquet mode scattering, like Floquet Umklapp processes. A comparison of the results of Refs. [21, 28, 93] and the central entry, i.e. the $(n,n') = (0,0)$-entry, shows that both coincide. In general, there is not only intra-Floquet zone scattering within the central Floquet mode, but rather within every Floquet zone and inter-Floquet zone scattering between every Floquet zone, see Fig. 1.2.

1.8 Floquet-Drude conductivity

In the previous sections, a successive scheme to include disorder in the conductivity was set up. Assuming a time-independent white noise disorder potential, a recursive expansion of the Green's function to all orders in the impurity potential was found, see Sec. 1.6. In this section, the focus is on the lowest non-trivial order approximation

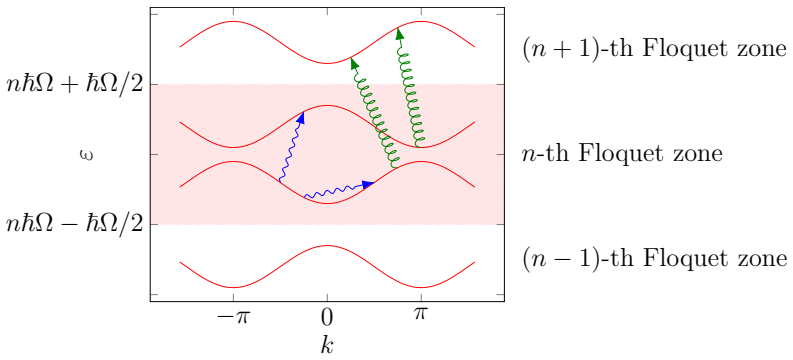

Figure 1.2: The red shaded area shows the n-th Floquet replica of some two band model. The blue wavy arrows label both intra-Floquet mode scattering, where the left one shows an inter-band and the right one an intra-band process. As opposed to them, the the green curly arrows show scattering between different Floquet zones.

of the Green's for the disordered system. Replacing the impurity average over the product of two Green's function by the average over each Green's function

$$\begin{aligned}&\left\langle \mathcal{G}^{r,a}(\varepsilon,\mathbf{k},t_1',t_2')\mathcal{G}^{r,a}(\varepsilon,\mathbf{k},t_2',t_1')\right\rangle_{\text{imp}} \approx \\ &\left\langle \mathcal{G}^{r,a}(\varepsilon,\mathbf{k},t_1',t_2')\right\rangle_{\text{imp}}\left\langle \mathcal{G}^{r,a}(\varepsilon,\mathbf{k},t_2',t_1')\right\rangle_{\text{imp}}\end{aligned} \tag{1.246}$$

is known as "Boltzmann approximation" [50, 89, 90]. In this approximation, all interference terms arising in the disorder average are neglected. These are further investigated in Sec. 1.10. In the Boltzmann approximation, Eq. (1.51) becomes

$$\begin{aligned}\lim_{\omega\to 0}\operatorname{Re}\left[\sigma^{xx}(0,\omega)\right] = \frac{-\hbar}{4\pi V}\left(\frac{e}{m}\right)^2 \int_{\lambda-\hbar\Omega/2}^{\lambda+\hbar\Omega/2} d\varepsilon \left(-\frac{\partial f}{\partial\varepsilon}\right)\int_0^T dt_1'\int_0^T dt_2' \\ \times \frac{1}{V_{\mathbf{k}}}\sum_{\mathbf{k}} k_x^2 \operatorname{tr}\Big[\Big(\mathcal{G}^r(\varepsilon,\mathbf{k},t_1',t_2') - \mathcal{G}^a(\varepsilon,\mathbf{k},t_1',t_2')\Big) \\ \Big(\mathcal{G}^r(\varepsilon,\mathbf{k},t_2',t_1') - \mathcal{G}^a(\varepsilon,\mathbf{k},t_2',t_1')\Big)\Big].\end{aligned} \tag{1.247}$$

Performing the time integrations over the primed times with the Fourier expansion of the Floquet functions (1.7) yields

$$\begin{aligned}\lim_{\omega\to 0}\operatorname{Re}\left[\sigma^{xx}(0,\omega)\right] = \frac{-\hbar}{4\pi V}\left(\frac{e}{m}\right)^2 \int_{\lambda-\hbar\Omega/2}^{\lambda+\hbar\Omega/2} d\varepsilon \left(-\frac{\partial f}{\partial\varepsilon}\right)\frac{1}{V_{\mathbf{k}}}\sum_{\mathbf{k}} k_x^2 \\ \times \operatorname{tr}\Big[\sum_{n,n'=-\infty}^{\infty}\Big(\mathcal{G}^r(\varepsilon,\mathbf{k},n,n') - \mathcal{G}^a(\varepsilon,\mathbf{k},n,n')\Big) \\ \Big(\mathcal{G}^r(\varepsilon,\mathbf{k},n',n) - \mathcal{G}^a(\varepsilon,\mathbf{k},n',n)\Big)\Big].\end{aligned} \tag{1.248}$$

Using again the matrix notation of the Green's function (1.165), the Floquet-Drude conductivity can be written in the compact form

$$\begin{aligned}\lim_{\omega\to 0}\operatorname{Re}\left[\sigma^{xx}(0,\omega)\right] = \frac{-\hbar}{4\pi V}\left(\frac{e}{m}\right)^2 \int_{\lambda-\hbar\Omega/2}^{\lambda+\hbar\Omega/2} d\varepsilon \left(-\frac{\partial f}{\partial\varepsilon}\right)\frac{1}{V_{\mathbf{k}}}\sum_{\mathbf{k}} k_x^2 \\ \times \operatorname{tr}\Big[\big(\boldsymbol{G}^r(\varepsilon,\mathbf{k}) - \boldsymbol{G}^a(\varepsilon,\mathbf{k})\big)\big(\boldsymbol{G}^r(\varepsilon,\mathbf{k}) - \boldsymbol{G}^a(\varepsilon,\mathbf{k})\big)\Big].\end{aligned} \tag{1.249}$$

The last equation is only valid for the parabolic dispersion. To obtain an expression for any other model, one must evaluate Eq. (1.117). As for the parabolic dispersion one is, for the general expression for the conductivity after disorder averaging, left with

$$\begin{aligned}\lim_{\omega\to 0}\mathrm{Re}\left[\sigma^{xx}(0,\omega)\right] = \frac{-1}{4\pi\hbar V}\int\limits_{\lambda-\frac{\hbar\Omega}{2}}^{\lambda+\frac{\hbar\Omega}{2}} d\varepsilon\left(-\frac{\partial f}{\partial\varepsilon}\right)\frac{1}{V_{\mathbf{k}}}\sum_{\mathbf{k}} \\ \times\ \mathrm{tr}\Bigg[\sum_{s,s',n,n'=-\infty}^{\infty}\Big(\mathbf{j}_s^x(\mathbf{k})\Big(\mathcal{G}^r(\varepsilon,\mathbf{k},n,n'+s')-\mathcal{G}^a(\varepsilon,\mathbf{k},n,n'+s')\Big) \\ \mathbf{j}_{s'}^x(\mathbf{k})\Big(\mathcal{G}^r(\varepsilon,\mathbf{k},n',n+s)-\mathcal{G}^a(\varepsilon,,\mathbf{k},n',n+s)\Big)\Big)\Bigg]\,.\end{aligned} \tag{1.250}$$

The shifted matrix product $\odot_s$ between two infinite dimensional matrices A and B is defined as

$$(A\odot_s B)_{ij} = \sum_{\ell=-\infty}^{\infty} a_{i,\ell+s}b_{\ell,j} \tag{1.251}$$

and the trace over the minor diagonal is defined as

$$\mathrm{tr}_s[A] = \sum_{\ell=-\infty}^{\infty} a_{\ell,\ell+s} \tag{1.252}$$

such that the conductivity becomes

$$\begin{aligned}\lim_{\omega\to 0}\mathrm{Re}\left[\sigma^{xx}(0,\omega)\right] = \frac{-1}{4\pi\hbar V}\int\limits_{\lambda-\frac{\hbar\Omega}{2}}^{\lambda+\frac{\hbar\Omega}{2}} d\varepsilon\left(-\frac{\partial f}{\partial\varepsilon}\right)\frac{1}{V_{\mathbf{k}}}\sum_{\mathbf{k}} \\ \times\sum_{s,s'=-\infty}^{\infty}\mathbf{j}_s^x(\mathbf{k})\,\mathbf{j}_{s'}^x(\mathbf{k})\,\mathrm{tr}_s\Big[\left(\boldsymbol{G}^r(\varepsilon,\mathbf{k})-\boldsymbol{G}^a(\varepsilon,\mathbf{k})\right)\odot_{s'}\left(\boldsymbol{G}^r(\varepsilon,\mathbf{k})-\boldsymbol{G}^a(\varepsilon,\mathbf{k})\right)\Big]\,.\end{aligned} \tag{1.253}$$

The evaluation of Eqs. (1.253) and (1.249) is the aim of the following. The focus will be on two different single band models for a 2DEG. One is an effective model, i.e. the parabolic dispersion, which allows analytical progress, and the other one is the square lattice. The latter is investigated rather numerically.

1.9 Application of the theory

Until now everything presented has been rather general. The first nontrivial application of the derived theory, investigated in the following, is a two dimensional electron gas (2DEG). First, the focus is on an effective model with different driving mechanisms, where the peculiarity of a Fermi energy in an unbounded single band Floquet system is discussed. Second, different driving regimes, i.e. resonant and off-resonant drivings, are analyzed. The latter allows for analytical progress and to

formulate an analytically closed form for the conductivity of a 2DEG described by an effective model under circular driving. These results as well the predictions for other polarizations are compared with results already known in literature. Next, a tight-binding model is used as toy model for the 2DEG. The conductivity of the tight-binding model yields an entirely different driving dependency, even in the low energy limit, than the effective model. This observation is mainly caused by the different eigenstates, rather than the similar Floquet spectra.

1.9.1 2DEG with circular driving

The system of interest is a 2DEG at the Γ-point of a direct semiconductor under illumination with circularly polarized light. The effective model for the lowest s-type conduction band near the Γ-point of the Brillouin zone is

$$H = \frac{\mathbf{p}^2}{2m} \tag{1.254}$$

where m is understood as effective mass. The parabolic dispersion is a rather simple model, but it covers a large number of materials, such as GaAs [94]. Additionally, it gives a deeper insight in the renormalization of conductivity caused by the driving, particularly when the results of this section are compared with the findings from a more general model as, done in Sec. 1.9.4. The focus is on circular driving in order to embed this work into the results already known in literature for the driven 2DEG [4]. The appropriate vector potential is

$$\mathbf{A}(t) = \mathcal{A}\sin(\Omega t)\hat{\mathbf{e}}_x + \mathcal{A}\cos(\Omega t)\hat{\mathbf{e}}_y\,, \tag{1.255}$$

where $\hat{\mathbf{e}}_\mathbf{i}$ is the unit vector showing into the subscript direction and $\mathcal{A}\Omega$ is the field strength of the electric field. Minimal coupling leads in the basis of plane waves $e^{i\mathbf{k}\cdot\mathbf{x}}$ to the time-dependent Hamiltonian

$$H(t) = \frac{\hbar^2}{2m}\Big[\mathbf{k}^2 + \gamma^2 + 2\gamma\big(k_x\sin(\Omega t) + k_y\cos(\Omega t)\big)\Big] \tag{1.256}$$

with $\gamma = e\mathcal{A}/\hbar$. The solution of the time-dependent Schrödinger equation [4]

$$i\hbar\frac{\partial}{\partial t}\Psi(\mathbf{k},t) = H(\mathbf{k},t)\Psi(\mathbf{k},t) \tag{1.257}$$

is

$$\Psi(\mathbf{k},t) = e^{-\frac{i}{\hbar}\epsilon_\mathbf{k} t}\, e^{i\left(\frac{\hbar^2\gamma k}{m}/\hbar\Omega\right)\cos(\Omega t+\phi)}, \tag{1.258}$$

where, in comparison to Eq. (1.3), the index α is missing, since the Hamiltonian is an effective single band model. The quasienergy and Fourier components of the Floquet function are

$$\epsilon_\mathbf{k} = \frac{\hbar^2}{2m}\big[\mathbf{k}^2 + \gamma^2\big] \quad , \quad u_n(\mathbf{k}) = J_n\left(\frac{\hbar^2\gamma k}{m}\Big/\hbar\Omega\right)e^{in(\phi+\pi/2)}\,. \tag{1.259}$$

The momentum above is given in polar coordinates

$$\mathbf{k} = \begin{pmatrix} k_x = k\cos(\phi) \\ k_y = k\sin(\phi)\end{pmatrix}\,. \tag{1.260}$$

The circular driving induces a shift, quadratic in γ, of the band structure, which can be compensated by an appropriate choice of the Floquet zone. A suitable choice of the Floquet zone in Eq. (1.249) is $\lambda = \epsilon_{\mathbf{k}}$ to assure

$$|\varepsilon - \epsilon_{\mathbf{k}}| \leq \hbar\Omega \ . \tag{1.261}$$

It was shown in Sec. 1.7.1 that, on the diagonal, the difference of the retarded and advanced self-energy is equal to the imaginary part of the self-energy. The reason why the focus is on the diagonal will be clarified later. The imaginary part of the self-energy on the diagonal is governed by

$$\begin{aligned}
-\mathrm{Im}\big(\boldsymbol{T}^\dagger(\mathbf{k})\boldsymbol{\Sigma}^r_{\mathrm{1BA}}(\varepsilon,\mathbf{k})\boldsymbol{T}(\mathbf{k})\big)_{nn} &= \frac{2\pi\mathcal{V}_{\mathrm{imp}}}{\hbar}\frac{1}{V_{\mathbf{k}'}}\sum_{\mathbf{k}'}\big|c^n(\mathbf{k},\mathbf{k}')\big|^2\delta(\varepsilon-\epsilon_{\mathbf{k}'}) && (1.262)\\
&= \frac{\mathcal{V}_{\mathrm{imp}}m}{2\pi\hbar^3}\int_0^{2\pi}d\phi'\sum_{m,m'=-\infty}^{\infty}J_{m+n}(z_k)J_m(z_\varepsilon) && (1.263)\\
&\quad\times J_{m'+n}(z_k)J_{m'}(z_\varepsilon)\,e^{i\phi(m-m')}\,e^{i\phi'(m'-m)} \\
&= \frac{\mathcal{V}_{\mathrm{imp}}m}{\hbar^3}\sum_{m=-\infty}^{\infty}J^2_{m+n}(z_k)J^2_m(z_\varepsilon) && (1.264)\\
&= \left(\frac{1}{\boldsymbol{\tau}(\varepsilon,\mathbf{k})}\right)_{nn} && (1.265)
\end{aligned}$$

together with

$$z_k \equiv \frac{\hbar^2\gamma k}{m}\Big/\hbar\Omega \quad , \quad z_\varepsilon \equiv \frac{\hbar^2\gamma\sqrt{2m\varepsilon/\hbar^2}}{m}\Big/\hbar\Omega \ . \tag{1.266}$$

Remarkably, the scattering time given in Eq. (1.265) is independent of the angle of the momentum $\mathbf{k}$. Fig.1.3 shows the central entry of the scattering time, normalized on the bare scattering time for some experimentally relevant parameters. Keeping only the diagonal of the imaginary part of the self-energy in the expression for the conductivity leads to

$$\begin{aligned}
\lim_{\omega\to0}\mathrm{Re}\,\sigma^{xx}(0,\omega) = \frac{\hbar}{4\pi V}\left(\frac{e}{m}\right)^2\int_{-\hbar\Omega/2}^{\hbar\Omega/2}d\varepsilon\left(-\frac{\partial f}{\partial\varepsilon}\right)\frac{1}{V_{\mathbf{k}}}\sum_{\mathbf{k}}k_x^2 \\
\times\sum_{n=-\infty}^{\infty}\left(\frac{1}{\boldsymbol{\tau}(\varepsilon,\mathbf{k})}\right)^2_{nn}\left[\left(\tfrac{1}{\hbar}\varepsilon-\tfrac{\hbar\mathbf{k}^2}{2m}-n\Omega\right)^2+\left(\frac{1}{2\boldsymbol{\tau}(\varepsilon,\mathbf{k})}\right)^2_{nn}\right]^{-2} .
\end{aligned} \tag{1.267}$$

The disorder is not supposed to change the eigenenergies of the bare system, hence all off-diagonal elements of the self-energy were dropped. To evaluate the expression for the conductivity, one must specify the distribution function further. In the off resonant regime, absorption of photons is suppressed, hence a Fermi distribution can be assumed. However, it is not obvious how to set the Fermi energy for the driven parabolic spectrum. In the following, three possible choices and the arising difficulties are discussed. The first possibility is to set a constant Fermi energy through all Floquet zones, as schematically depicted in Fig. 1.4. The first problem that arises with this choice of the quasi-Fermi energy is that it violates the fundament of the derivation of the expression for the conductivity found in Eq. (1.49), namely

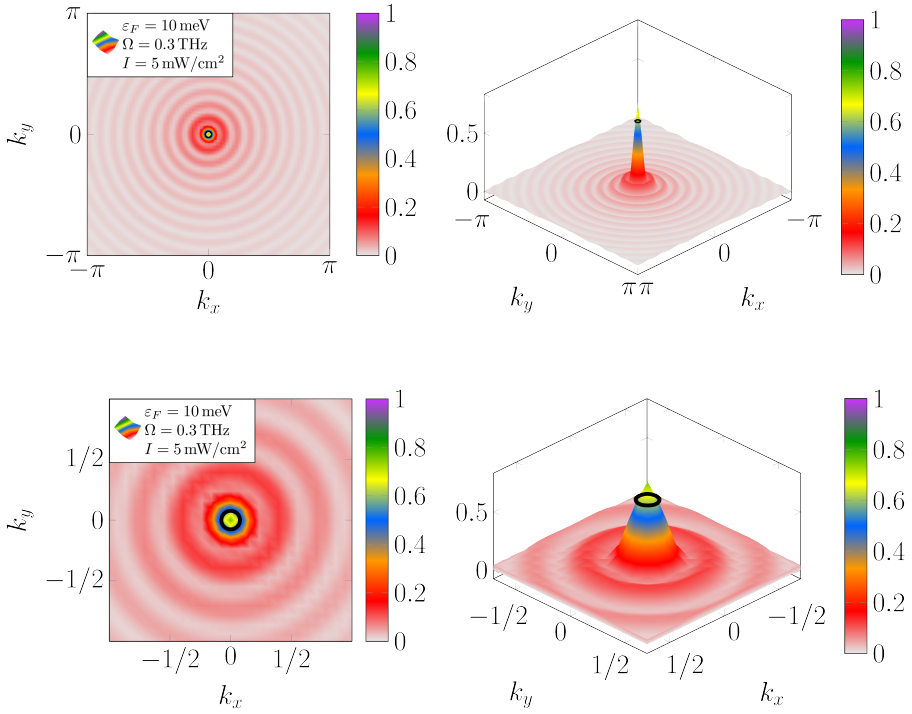

Figure 1.3: The figure shows the ratio between the central entry of the dressed inverse scattering time with the bare scattering time $(1/\boldsymbol{\tau}_{00}(\mathbf{k}))/(1/\boldsymbol{\tau}_{00}(\mathbf{k})|_{\gamma=0})$ for the parabolic dispersion. The Fermi energy was set to 10 meV, the driving frequency to 0.3 THz and the intensity to 5 mW/cm^2. The Fermi energy is shown as a black contour. (Reprinted figure with permission from [36]. Copyright (2020) by the American Physical Society.)

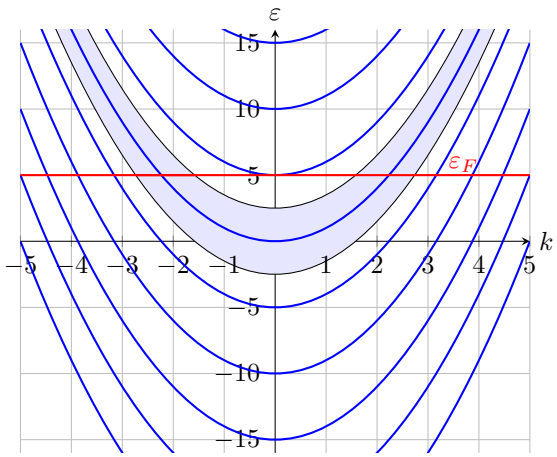

Figure 1.4: The Floquet zones are chosen to wrap around the parabolas. The quasi-Fermi energy, the red curve, is constant and defined in all Floquet zones. (Reprinted figure with permission from [36]. Copyright (2020) by the American Physical Society.)

that all quasienergies are in the central Floquet zone. Moreover, an infinite number of bands are crossing the quasi-Fermi energy, leading to a divergent conductivity, even in the disordered system. Another choice for the quasi-Fermi energy is shown

in Fig. 1.5. If the quasi-Fermi energy has the contour seen in Fig. 1.5, it obviously

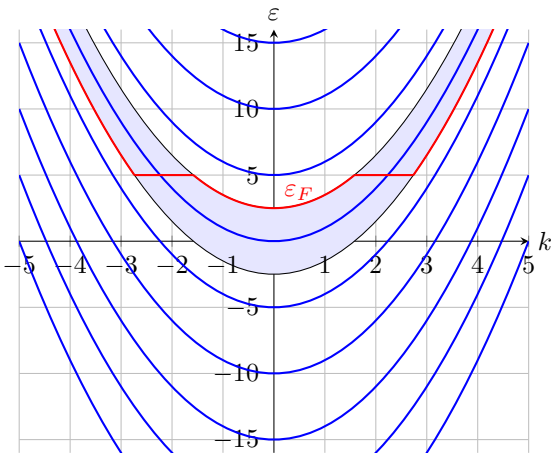

Figure 1.5: The Floquet zones are chosen to wrap around the parabolas. The quasi-Fermi energy follows the Floquet zone edge, apart from a certain momentum range where it passes from the lower to the upper Floquet zone edge.

fulfills Eq. (1.49). However, this choice once again leads to a divergent conductivity, which is only confirmed numerically. The reason for the diverging conductivity is that the energetic distance between the quasienergy and the quasi-Fermi energy is constant for all momenta, apart from the momenta where it passes from the lower to the upper Floquet zone edge. Due to the energy-denominator, the contribution of the Green's function to the conductivity is not suppressed, since the quasienergetic distance is constant for almost all momenta. Thus, one is left with the truncation of the momentum range where the quasi-Fermi energy is defined, as in Fig. 1.6, giving a physically consistent result. This limits the validity of the calculation to the high

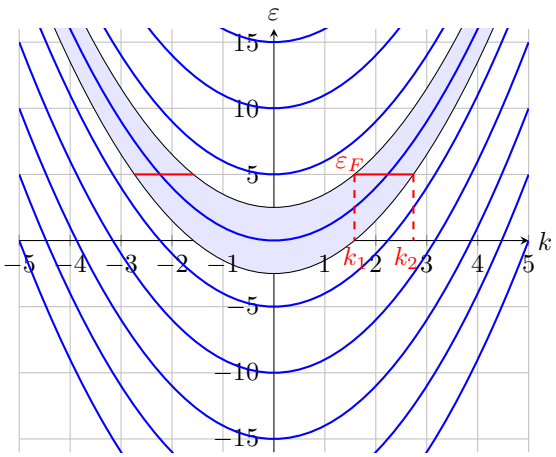

Figure 1.6: The Floquet zones are chosen to wrap around the parabolas. The quasi-Fermi energy is only defined in a certain momentum range, i.e., $k \in [k_1, k_2)$, in the central Floquet zone. (Reprinted figure with permission from [36]. Copyright (2020) by the American Physical Society.)

frequency regime. In Fig. 1.6 k_1 and k_2 are functions of the driving frequency Ω. For decreasing Ω, the momenta k_1 and k_2 move closer together. If the momentum range $k \in [k_1, k_2)$ is of the order of the broadening of the Green's function, the

truncation leads to an incorrect result for the conductivity. This is rather an issue of the parabolic spectrum than of the theory for the conductivity of a driven system. If $\Omega\tau_0 \gg 1$, τ_0 being the scattering time of the undriven system, the broadening of the nonzero Floquet modes is small enough such that the leaking into the central Floquet zone is negligibly small, see Fig. 1.7.

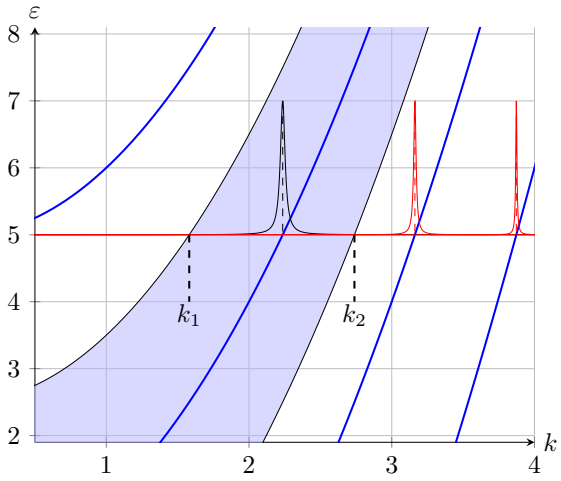

Figure 1.7: The peaks show the broadening of the Floquet bands caused by the scattering time. The blue shaded area is the central Floquet zone. If $\Omega\tau_0 \gg 1$, the leaking of the nonzero Floquet modes (red curves) into the central Floquet zone is negligibly small. (Reprinted figure with permission from [36]. Copyright (2020) by the American Physical Society.)

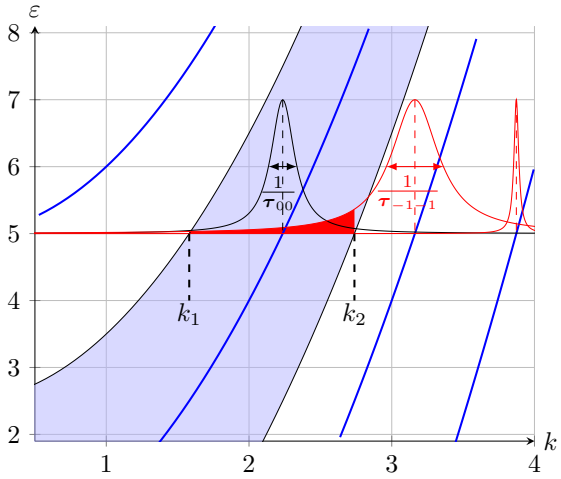

Figure 1.8: The peaks show the broadening of the Floquet bands caused by the scattering time. The blue shaded area is the central Floquet zone. If $\Omega\tau_0 \simeq 1$, the nonzero Floquet modes are leaking into the central Floquet zone. The red shaded area marks the contribution of the minus one Floquet band to the conductivity. (Reprinted figure with permission from [36]. Copyright (2020) by the American Physical Society.)

If $\Omega\tau_0 \simeq 1$, the nonzero modes give a significant contribution to the conductivity, as depicted in Fig. 1.8. In the following, the focus will be on the off resonant

regime $\Omega\tau_0 \gg 1$. Furthermore, assuming that the distribution function is the Fermi function and its derivative is sharply peaked around the Fermi energy leads, for the conductivity, to

$$\begin{aligned}\lim_{\omega\to 0} \operatorname{Re}\sigma^{xx}(0,\omega) = \frac{\hbar}{4\pi V}\left(\frac{e}{m}\right)^2 \frac{1}{V_{\mathbf{k}}} \sum_{\mathbf{k}} k_x^2 \Big[2\boldsymbol{G}^r(\varepsilon_F,\mathbf{k})\boldsymbol{G}^a(\varepsilon_F,\mathbf{k}) \\ - \boldsymbol{G}^r(\varepsilon_F,\mathbf{k})\boldsymbol{G}^r(\varepsilon_F,\mathbf{k}) - \boldsymbol{G}^a(\varepsilon_F,\mathbf{k})\boldsymbol{G}^a(\varepsilon_F,\mathbf{k})\Big]_{00} \,.\end{aligned} \tag{1.268}$$

Now, all pairings of only retarded or advanced Green's functions are neglected. The central entry of the product of the retarded with an advanced Green's function is

$$\begin{aligned}\big[\boldsymbol{G}^r(\varepsilon_F,\mathbf{k})\boldsymbol{G}^a(\varepsilon_F,\mathbf{k})\big]_{00} &= \frac{1}{\left(\frac{1}{\hbar}\varepsilon_F - \frac{1}{\hbar}\epsilon_{\mathbf{k}}\right)^2 + \left(\frac{1}{2\boldsymbol{\tau}(\varepsilon_F,\mathbf{k})}\right)^2_{00}} && (1.269)\\ &\approx 2\pi\hbar\big[\boldsymbol{\tau}(\varepsilon_F,\mathbf{k})\big]_{00}\delta(\varepsilon_F - \epsilon_{\mathbf{k}}) \,. && (1.270)\end{aligned}$$

Dropping the retarded and advanced Green's function pairs, the conductivity of the last equation becomes

$$\begin{aligned}\lim_{\omega\to 0} \operatorname{Re}\sigma^{xx}(0,\omega) &= \frac{\hbar^2}{V(2\pi)^2}\left(\frac{e}{m}\right)^2 \int_{V_{\mathbf{k}}} d^2k\, k_x^2 \big[\boldsymbol{\tau}(\varepsilon_F,\mathbf{k})\big]_{00}\delta(\varepsilon_F - \epsilon_{\mathbf{k}}) && (1.271)\\ &= \frac{1}{V4\pi}\left(\frac{e^2}{m}\right) k_F^2 \big[\boldsymbol{\tau}(\varepsilon_F,\mathbf{k}_F)\big]_{00}\Big|_{k_F=\frac{\sqrt{2m\varepsilon_F}}{\hbar}} && (1.272)\end{aligned}$$

with the scattering time evaluated at the Fermi energy and Fermi wave vector

$$\big(\boldsymbol{\tau}(\varepsilon_F,\sqrt{2m\varepsilon_F}/\hbar)\big)_{00} = \left(\frac{\mathcal{V}_{\mathrm{imp}} m}{\hbar^3}\sum_{m=-\infty}^{\infty} J_m^4(z_{\varepsilon_F})\right)^{-1} \,. \tag{1.273}$$

Hence, the ratio between conductivity without driving and dressed conductivity is

$$\frac{\lim_{\omega\to 0}\operatorname{Re}\sigma^{xx}(0,\omega)}{\lim_{\omega\to 0}\operatorname{Re}\sigma^{xx}(0,\omega)\big|_{\gamma=0}} = \frac{1}{\sum_{m=-\infty}^{\infty} J_m^4(z_{\varepsilon_F})} \,. \tag{1.274}$$

In Fig. 1.9 the results from the following section are anticipated. The figure shows the normalized conductivity for a 2DEG described by an effective model in the presence of circularly and linearly polarized light. Since the comparison of these results with the findings from a tight-binding model is essential, the discussion of experimentally relevant quantities will be presented later on.

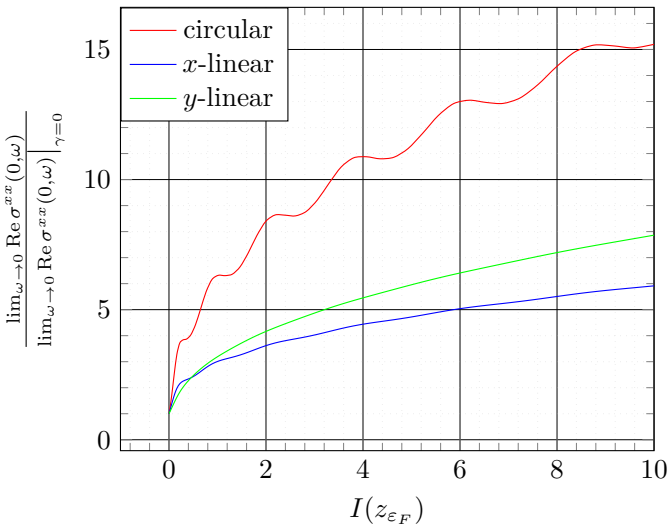

Figure 1.9: The ratio of bare conductivity and light dressed conductivity as a function of intensity: The three curves show the longitudinal conductivity in the presence of circularly, in x-, and y-direction linearly polarized light.

1.9.2 2DEG with linear driving

In this section the focus is on linear driving. The calculations are similar to Sec. 1.9.1 and are thus presented in condensed manner. The vector potential corresponding to an in x-direction oscillating electric field is governed by

$$\mathbf{A}(t) = \mathcal{A}\cos(\Omega t)\hat{\mathbf{e}}_x \ . \tag{1.275}$$

The vector potential $\mathbf{A}(t)$ is coupled to the momentum $\mathbf{p}$ again via minimal coupling. In the basis of plane waves $e^{i\mathbf{k}\cdot\mathbf{x}}$ the Hamiltonian (1.254) becomes time-independent in the presence of the driving and reads

$$H(\mathbf{k},t) = \frac{\hbar^2}{2m}\Big[\mathbf{k}^2 + 2k_x\gamma\cos(\Omega t) + \frac{\gamma^2}{2}\Big(1+\cos(2\Omega t)\Big)\Big] \tag{1.276}$$

with γ defined as in Sec. 1.9.1. To calculate the Floquet-Drude conductivity, the solution of the time-dependent Schrödinger equation, i.e. the Floquet state, is needed. The Schrödinger equation (1.257), along with the Hamiltonian of Eq. (1.276), was already solved by O. V. Kibis in Ref. [28]. Adopting the result from Ref. [28], the wave function is given by

$$\Psi(\mathbf{k},t) = e^{-\frac{i}{\hbar}\frac{\hbar^2}{2m}\left(\mathbf{k}^2+\frac{\gamma^2}{2}\right)t}\, e^{-if(\gamma^2/4)\sin(2\Omega t)}\, e^{-if(2\gamma k_x)\sin(\Omega t)} \tag{1.277}$$

with the the function

$$f(x) \equiv \frac{\hbar^2 x}{2m}\Big/\hbar\Omega \ . \tag{1.278}$$

Using the Jacobi-Anger expansion (1.435), one can write the wave function as

$$\Psi(\mathbf{k},t) = e^{-\frac{i}{\hbar}\epsilon_{\mathbf{k}}t}\sum_{n=-\infty}^{\infty} u_n(\mathbf{k})e^{-in\Omega t} \tag{1.279}$$

with the quasienergy $\epsilon_{\mathbf{k}}$ and the Fourier components u_n:

$$\epsilon_{\mathbf{k}} = \frac{\hbar^2}{2m}\left(\mathbf{k}^2 + \frac{\gamma^2}{2}\right) \quad , \quad u_n(\mathbf{k}) = J_n\big(f(2\gamma k_x), f(\gamma^2/4)\big) \; . \tag{1.280}$$

The function $J_n(\cdot,\cdot)$ is a generalized Bessel function [95]

$$J_n(x,y) = \sum_{m=-\infty}^{\infty} J_{n-2m}(x) J_m(y) \tag{1.281}$$

where $J_n(\cdot)$ is the ordinary Bessel function of the first kind [96]. Properties of the generalized Bessel function are analyzed in Ref. [95]. A particularly useful relation is

$$\sum_{m=-\infty}^{\infty} J_m(x',y') J_{n\mp m}(x,y) = J_n(x \pm x', y \pm y') \, . \tag{1.282}$$

The Floquet zone is chosen equivalently to Eq. (1.261) to compensate for the shift of the band structure caused by the linear drive. With the knowledge of the eigenstates of the Floquet Hamiltonian, i.e. the u_n, it is possible to calculate the self-energy. With the help of Eq. (1.179), using the identity for the generalized Bessel function (1.282) yields

$$\begin{aligned} c^n(\mathbf{k},\mathbf{k}') &= \sum_{m=-\infty}^{\infty} u^{m+n}(\mathbf{k}) u^m(\mathbf{k}') && (1.283)\\ &= J_n\big(f\big[2\gamma(k_x - k_x')\big], 0\big) && (1.284)\\ &= J_n\big(f\big[2\gamma(k_x - k_x')\big]\big) \; . && (1.285) \end{aligned}$$

The imaginary part of the self-energy, using the Dirac identity (1.433), becomes

$$\begin{aligned} &-\operatorname{Im}\Big(\boldsymbol{T}^\dagger(\mathbf{k})\boldsymbol{\Sigma}^r_{\mathrm{1BA}}(\varepsilon,\mathbf{k})\boldsymbol{T}(\mathbf{k})\Big)_{nn'} = \\ &\frac{2\pi\mathcal{V}_{\mathrm{imp}}}{\hbar}\frac{1}{V_{\mathbf{k}'}}\sum_{\mathbf{k}'} c^n(\mathbf{k},\mathbf{k}')c^{n'}(\mathbf{k},\mathbf{k}')\delta(\varepsilon_F - \epsilon_{\mathbf{k}'}) \, . \end{aligned} \tag{1.286}$$

The central entry, i.e. $n = n' = 0$, is equal to Eq. (3) of Ref. [4]. Replacing the summation over momenta with an integral in polar coordinates yields

$$-\operatorname{Im}\Big(\boldsymbol{T}^\dagger(\mathbf{k})\boldsymbol{\Sigma}^r_{\mathrm{1BA}}(\varepsilon,\mathbf{k})\boldsymbol{T}(\mathbf{k})\Big)_{nn'} = \frac{\mathcal{V}_{\mathrm{imp}} m}{2\pi\hbar^3}\int_0^{2\pi} d\phi \, J_n(z_\phi) J_{n'}(z_\phi) \tag{1.287}$$

with

$$z_\phi \equiv \frac{\hbar^2 2\gamma}{2m\hbar\Omega}\big[k_x - k'\cos(\phi)\big]\Big|_{k'=\frac{\sqrt{2m\varepsilon_F}}{\hbar}} \; . \tag{1.288}$$

Finally, the conductivity for in x-direction linearly polarized driving is

$$\lim_{\omega\to 0}\operatorname{Re}\sigma^{xx}(0,\omega) = \frac{1}{V(2\pi)^2}\left(\frac{e^2}{m}\right)k_F^2\int_0^{2\pi} d\phi \, \cos^2(\phi)\big[\boldsymbol{\tau}(\varepsilon_F,\mathbf{k})\big]_{00}\Big|_{k=\frac{\sqrt{2m\varepsilon_F}}{\hbar}} \tag{1.289}$$

and equivalently for y-polarization

$$\lim_{\omega\to 0}\operatorname{Re}\sigma^{xx}(0,\omega) = \frac{1}{V(2\pi)^2}\left(\frac{e^2}{m}\right)k^2\int_0^{2\pi} d\phi \, \sin^2(\phi)\big[\boldsymbol{\tau}(\varepsilon_F,\mathbf{k})\big]_{00}\Big|_{k=\frac{\sqrt{2m\varepsilon_F}}{\hbar}} \; . \tag{1.290}$$

The Eqs. (1.289) and (1.290) are evaluated numerically. The results are shown in Fig. 1.9.

1.9.3 Comparison to other works

The aim of this section is to compare the results of the foregoing sections with the results already known in literature. In Ref. [4], Morina *et al.* investigate the same setup as in Sec. 1.9.1 and 1.9.2, i.e. the transport properties of a two dimensional electron gas dressed by light. The calculations in Refs. [4, 25, 35] are limited by two conditions that must be fulfilled by the driving frequency. Due to consistency, the driving frequency is denoted as Ω in this work, whereas in Ref. [4] the authors use ω. The first requirement is that the driving frequency should not meet any electronic transitions. Additionally, the driving frequency is supposed to be much larger than the inverse scattering time of the undriven system

$$\Omega\tau_0 \gg 1 \ . \tag{1.291}$$

The authors of Refs. [4, 25, 35] consider Fermions, hence the equilibrium distribution function is the Fermi-distribution function. This is reasonable, since absorption is negligibly small in the off resonant driving regime. However, the mean free time at the Fermi energy used in Refs. [4, 25, 35] is [97]

$$\frac{1}{\tau_F} = \sum_{\mathbf{k}'_F} w_{\mathbf{k}_F\mathbf{k}'_F} \tag{1.292}$$

along with the scattering probability $w_{\mathbf{k}'\mathbf{k}}$, calculated in Ref. [28] within the framework of the Floquet-Fermi golden rule [21, 93]

$$w_{\mathbf{k}'\mathbf{k}} = \frac{2\pi}{\hbar} J_0^2(f_{\mathbf{k}\mathbf{k}'})|U_{\mathbf{k}'\mathbf{k}}|^2\delta(\epsilon_{\mathbf{k}'} - \epsilon_{\mathbf{k}}) \ . \tag{1.293}$$

The result above coincides with the central entry of the scattering time matrix derived in this work, see Eq. (1.262). For linearly polarized light, the argument of the Bessel function is

$$f_{\mathbf{k}\mathbf{k}'} = \frac{\hbar\gamma(k_x - k'_x)}{m\Omega} \tag{1.294}$$

and for circular polarized light, it is

$$f_{\mathbf{k}\mathbf{k}'} = \frac{2\hbar\gamma k}{m\Omega} \sin\left(\frac{\phi - \phi'}{2}\right) \ . \tag{1.295}$$

γ and the quasienergy $\epsilon_{\mathbf{k}}$ are adopted from the previous two sections. In the previous equation, it was already used that later only the case $|\mathbf{k}| = |\mathbf{k}'|$ contributes to the conductivity. The angles ϕ and ϕ' correspond to the momenta $\mathbf{k}$ and $\mathbf{k}'$. This scattering probability was calculated for transitions of an electron from

$$\frac{1}{\sqrt{V}} e^{i\mathbf{k}\cdot\mathbf{r}}\Psi(\mathbf{k}, t) = \psi_{\mathbf{k}}(\mathbf{r}, t) \mapsto \psi_{\mathbf{k}'}(\mathbf{r}, t) \tag{1.296}$$

where $\Psi(\mathbf{k}, t)$ is adopted from Eq. (1.277) and V denotes the Volume of the system. The authors of Ref. [4] claim that the current density for a periodically driven 2DEG is

$$\mathbf{j} = \frac{e^2}{2\pi^2} \int_{V_{\mathbf{k}}} d^2k \, \mathbf{E}\cdot\mathbf{v}(\mathbf{k})\tau(\mathbf{k})\mathbf{v}(\mathbf{k})\delta(\varepsilon_F - \epsilon_{\mathbf{k}}) \tag{1.297}$$

where $\mathbf{E}$ is a stationary electric field and $\mathbf{v}(\mathbf{k}) = (1/\hbar)\nabla_{\mathbf{k}}\epsilon_{\mathbf{k}}$ is the electron velocity. This formula is derived without driving in Ref. [98]. The conductivity can be determined by [98]

$$j_\ell = \sum_i \sigma_{\ell i} E_i \ , \tag{1.298}$$

$$\sigma_{\ell i} = \frac{e^2}{2\pi^2} \int_{V_{\mathbf{k}}} d^2k \, \tau(\mathbf{k}) \delta(\varepsilon_F - \varepsilon_{\mathbf{k}}) v_\ell(\mathbf{k}) v_i(\mathbf{k}) \ . \tag{1.299}$$

With that, an expression for the conductivity in the presence of a circular driving was derived in Ref. [4]

$$\frac{\lim_{\omega\to 0} \operatorname{Re}\sigma^{xx}(0,\omega)}{\lim_{\omega\to 0} \operatorname{Re}\sigma^{xx}(0,\omega)\big|_{\gamma=0}} = 2\pi \left[\int_0^{2\pi} d\theta \, (1-\cos\theta) J_0^2\left[2 z_{\varepsilon_F} \sin(\theta/2)\right] \right]^{-1} \tag{1.300}$$

where z_ε is defined in Eq. (1.266). In Eq. (1.300), the angle $\theta = \phi - \phi'$ denotes the angle between the wave vectors $\mathbf{k}$ and $\mathbf{k}'$ [4]. Curiously, Eq. (1.300) depends on the angle ϕ'. This dependency should not arise due to the momentum summation over $\mathbf{k}'_F$ in Eq. (1.292). This explains the difference between the results of Ref. [4] and the results derived in this work. A direct comparison is shown in Fig. 1.10. Properly evaluating Eq. (1.292) together with Eq. (1.293) for circular polarized light lead to the same result as in Eq. (1.265), where the scattering time is independent of the angle ϕ'. Hence, the ansatz used by the authors of Ref. [4] leads to the same result for the ratio between light dressed conductivity and bare conductivity as in Sec. 1.9.1

$$\frac{\lim_{\omega\to 0} \operatorname{Re}\sigma^{xx}(0,\omega)}{\lim_{\omega\to 0} \operatorname{Re}\sigma^{xx}(0,\omega)\big|_{\gamma=0}} = \frac{1}{\sum_{m=-\infty}^{\infty} J_m^4(z_{\varepsilon_F})} \ . \tag{1.301}$$

In conclusion, the formalism presented in this work proves on the one hand the expression used by the authors of Ref. [4]. On the other hand, it corrects the final results for the conductivity in presence of circular polarized light. So far, an effective model under driving has been analyzed. In the following, a lattice model is used two describe a 2DEG. The square lattice is still far from a realistic model, but it provides a deep insight into the comparability of different Floquet models describing the same system.

1.9.4 Square lattice

In the following, a periodically driven square lattice as model for a 2DEG is investigated. The Schrödinger equation is solved to obtain quasienergy and Floquet function. The two lattice vectors of the square lattice are

$$\mathbf{a}_1 = a \begin{pmatrix} 1 \\ 0 \end{pmatrix} \quad , \quad \mathbf{a}_2 = a \begin{pmatrix} 0 \\ 1 \end{pmatrix} \tag{1.302}$$

with a being the lattice constant. To find the solution of the Schrödinger equation for linear, circular and elliptic polarization, the vector potential is

$$\mathbf{A}(t) = \begin{pmatrix} \mathcal{A}_x \sin(\Omega t) \\ \mathcal{A}_y \cos(\Omega t) \end{pmatrix} \ , \tag{1.303}$$

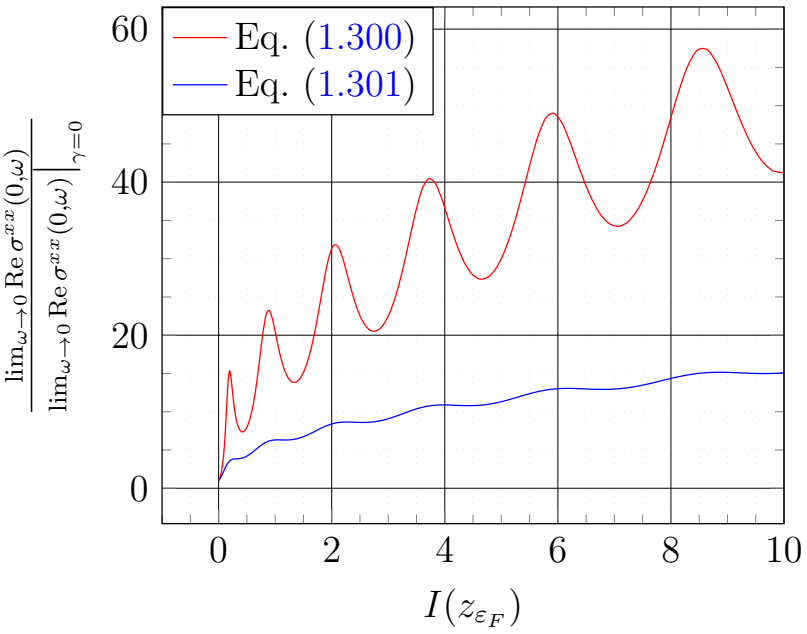

Figure 1.10: Both curves show the ratio between bare longitudinal conductivity and dressed longitudinal conductivity. The red curve, which overestimates the effect of the circular driving, shows the result derived in Ref. [4]. The blue curve shows the result derived in this work.

which allows one to tune between the polarizations by choosing the amplitudes appropriately. In the presence of a vector potential, the hopping parameter g acquires a Peierls phase

$$g_{\mathbf{a}_j} \mapsto g e^{i\phi_j(t)} \quad \text{with} \quad \phi_j = \frac{e}{\hbar}\int_{\mathbf{R}}^{\mathbf{R}+\mathbf{a}_j} \mathbf{A}(t)\cdot d\mathbf{r}\,. \tag{1.304}$$

In the case of a time-independent vector potential, the Peierls phase is the scalar product of vector potential and nearest neighbor vector. Thus, the time-dependent tight-binding Hamiltonian for the square lattice is

$$H(\mathbf{k},t) = -g\Big[e^{i\mathbf{k}\cdot\mathbf{a}_1}\, e^{i\frac{e}{\hbar}\mathbf{A}(t)\cdot\mathbf{a}_1} + e^{i\mathbf{k}\cdot\mathbf{a}_2}\, e^{i\frac{e}{\hbar}\mathbf{A}(t)\cdot\mathbf{a}_2} + h.c.\Big]\,. \tag{1.305}$$

To solve the Schrödinger equation, the following identities based on the Jacobi-Anger expansion (1.435) will be used:

$$\int dt\, e^{i\gamma\sin(\omega t)} = \sum_{n=-\infty}^{\infty} J_n(\gamma)\int dt\, e^{in\omega t} = \sum_{n\neq 0}\frac{J_n(\gamma)}{in\omega}e^{in\omega t} + J_0(\gamma)t\,, \tag{1.306}$$

$$\int dt\, e^{i\gamma\cos(\omega t)} = 2\sum_{n=1}^{\infty}\frac{i^n J_n(\gamma)}{n\omega}\sin(n\omega t) + J_0(\gamma)t\,. \tag{1.307}$$

The time-dependent Schrödinger equation can be solved by the ansatz [28]

$$\psi(\mathbf{k},t) = e^{\frac{i}{\hbar}F(\mathbf{k},t)}\,, \tag{1.308}$$

where the exponent is the time integral over the Hamiltonian

$$F(\mathbf{k},t) = \int dt\, H(\mathbf{k},t)\,. \tag{1.309}$$

Integrating the Hamiltonian of Eq. (1.305) over time yields

$$\begin{aligned} F(\mathbf{k},t) = & -2g\big[J_0(\gamma_x)\cos(k_x a) + J_0(\gamma_y)\cos(k_y a)\big]t \\ & - ge^{ik_x a}\sum_{n\neq 0}\frac{J_n(\gamma_x)}{in\omega}e^{in\omega t} - ge^{-ik_x a}\sum_{n\neq 0}\frac{J_n(\gamma_x)}{-in\omega}e^{-in\omega t} \\ & - 2ge^{ik_y a}\sum_{n=1}^{\infty}\frac{i^n J_n(\gamma_y)}{n\omega}\sin(n\omega t) - 2ge^{-ik_y a}\sum_{n=1}^{\infty}\frac{(-i)^n J_n(\gamma_y)}{n\omega}\sin(n\omega t) \end{aligned} \tag{1.310}$$

with the light parameter

$$\gamma_{x,y} = \frac{ea\mathcal{A}_{x,y}}{\hbar}\ . \tag{1.311}$$

The quasienergy is the non-oscillatory part of $F(\mathbf{k},t)$

$$\epsilon_{\mathbf{k}} = -2g\big[J_0(\gamma_x)\cos(k_x a) + J_0(\gamma_y)\cos(k_y a)\big] \tag{1.312}$$

and the corresponding Floquet function is

$$\begin{aligned} u(t,\gamma_x,\gamma_y) = \prod_{n\neq 0}\exp\Bigg[& -i\frac{2g}{\hbar}\frac{J_n(\gamma_y)}{n\omega}\sin(k_y a + n\omega t) \\ & - i\frac{2g}{\hbar}\frac{(-1)^n J_n(\gamma_x)}{n\omega}\sin(k_x a + n\omega t - \tfrac{n\pi}{4})\Bigg]\ . \end{aligned} \tag{1.313}$$

Interestingly, the quasiband structure of a periodically driven square lattice can be completely flattened if the light parameters meet the zeros of the zeroth Bessel function $J_0(\cdot)$. According to M. Genske [65], the current density $\mathbf{j}$ is given by the continuity equation

$$\frac{\partial\rho(\mathbf{r},t)}{\partial t} = -\nabla\cdot\mathbf{j}(\mathbf{r},t)\,, \tag{1.314}$$

where ρ describes the charge density. Introducing the polarization operator $\mathbf{P}(t) = \int d^3r\,\mathbf{r}\rho(\mathbf{r},t)$, it can be shown that

$$\frac{\partial\mathbf{P}(t)}{\partial t} = \int d^3r\,\mathbf{r}\frac{\partial\rho(\mathbf{r},t)}{\partial t} = -\int d^3r\,\mathbf{r}\nabla\cdot\mathbf{j}(\mathbf{r},t) = \int d^3r\,\mathbf{j}(\mathbf{r},t)\ . \tag{1.315}$$

Now, assume a hopping Hamiltonian in second quantization. The polarization operator is the product of position operator $\mathbf{r}_{m,n}$ and particle number operator $n_{n,m} = c^\dagger_{n,m}c_{n,m}$

$$\mathbf{P} = e\sum_{m,n}\mathbf{r}_{n,m}n_{n,m}\,. \tag{1.316}$$

With the help of the Heisenberg equation of motion, the current operator is

$$\mathbf{J}(t) = \frac{\partial\mathbf{P}}{\partial t} = \frac{i}{\hbar}[H(t),\mathbf{P}] = i\frac{e}{\hbar}\sum_{n,m,n',m'}\big(\mathbf{r}_{n,m} - \mathbf{r}_{n',m'}\big)g_{n,m,n',m'}(t)c^\dagger_{n,m}c_{m',n'}\,. \tag{1.317}$$

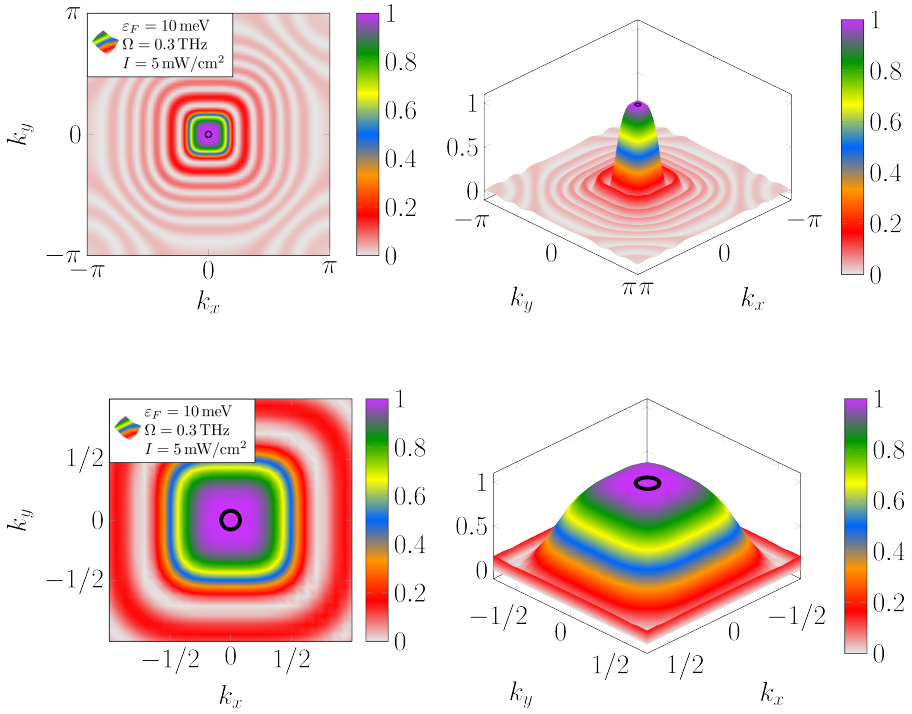

Figure 1.11: The figure shows the ratio between the central entry of the dressed inverse scattering time with the bare scattering time $(1/\boldsymbol{\tau}_{00}(\mathbf{k}))/(1/\boldsymbol{\tau}_{00}(\mathbf{k})|_{\gamma=0})$ for the tight-binding model. The Fermi energy was set to 10 meV; the driving frequency was set to 0.3 THz and the intensity to 5 $\mathrm{mW/cm^2}$. The Fermi energy is shown as a black contour. (Reprinted figure with permission from [36]. Copyright (2020) by the American Physical Society.)

Assuming that only hopping to nearest neighbors is present and denoting the nearest neighbor vectors as $\mathbf{a}$, lead, for the current operator, to

$$\mathbf{J}(t) = i\frac{e}{\hbar}\sum_{n,m,j}\mathbf{a}_j g_{\mathbf{a}_j}(t) c^\dagger_{n,m} c_{(n,m)+\mathbf{a}_j}\,. \tag{1.318}$$

In the last step, it was assumed that the hopping amplitude is only a function of the difference of the positions. Expanding the creation and annihilation operators in momentum space

$$c^{(\dagger)}_{n,m} = \sum_{\mathbf{k}} e^{(-)i\mathbf{k}\cdot\mathbf{r}_{n,m}} c^{(\dagger)}_{\mathbf{k}} \tag{1.319}$$

and performing the sum over all positions yield, for the current operator,

$$\mathbf{J}(t) = i\frac{eg}{\hbar}\sum_{j,\mathbf{k}}\mathbf{a}_j e^{i\frac{e}{\hbar}\mathbf{A}(t)\cdot\mathbf{a}_j}\, e^{i\mathbf{k}\cdot\mathbf{a}_j} c^\dagger_{\mathbf{k}} c_{\mathbf{k}} \tag{1.320}$$

$$\equiv \sum_{\mathbf{k}} \mathbf{J}(\mathbf{k},t)\, c^\dagger_{\mathbf{k}} c_{\mathbf{k}}\,. \tag{1.321}$$

Now, the square lattice with nearest neighbor vectors given in Eq. (1.302) and circularly polarized driving $\mathbf{A}(t) = \mathcal{A}\big(\sin(\Omega t), \cos(\Omega t)\big)^{\mathrm{T}}$ is considered. The current

coefficient becomes

$$\mathbf{J}(\mathbf{k},t) = i\frac{ega}{\hbar}\begin{pmatrix} e^{i\mathbf{k}\cdot\mathbf{a}_1}\, e^{i\frac{e}{\hbar}\mathbf{A}(t)\cdot\mathbf{a}_1} - e^{-i\mathbf{k}\cdot\mathbf{a}_1}\, e^{-i\frac{e}{\hbar}\mathbf{A}(t)\cdot\mathbf{a}_1} \\ e^{i\mathbf{k}\cdot\mathbf{a}_2}\, e^{i\frac{e}{\hbar}\mathbf{A}(t)\cdot\mathbf{a}_2} - e^{-i\mathbf{k}\cdot\mathbf{a}_2}\, e^{-i\frac{e}{\hbar}\mathbf{A}(t)\cdot\mathbf{a}_2} \end{pmatrix} \tag{1.322}$$

$$= i\frac{ega}{\hbar}\sum_{n=-\infty}^{\infty}\begin{pmatrix} e^{i\mathbf{k}\cdot\mathbf{a}_1}\, J_n(\gamma)e^{in\Omega t} - e^{-i\mathbf{k}\cdot\mathbf{a}_1}\, J_n(\gamma)e^{-in\Omega t} \\ e^{i\mathbf{k}\cdot\mathbf{a}_2}\, i^n J_n(\gamma)e^{in\Omega t} - e^{-i\mathbf{k}\cdot\mathbf{a}_2}\, (-i)^n J_n(\gamma)e^{-in\Omega t} \end{pmatrix} . \tag{1.323}$$

Focusing on the $n = 0$ component, i.e. average over one driving period, leads to

$$\bar{\mathbf{J}}(\mathbf{k}) \equiv \frac{1}{T}\int_0^T dt\, \mathbf{J}(\mathbf{k},t) \tag{1.324}$$

$$= i\frac{ega}{\hbar}J_0(\gamma)\begin{pmatrix} e^{i\mathbf{k}\cdot\mathbf{a}_1} - e^{-i\mathbf{k}\cdot\mathbf{a}_1} \\ e^{i\mathbf{k}\cdot\mathbf{a}_2} - e^{-i\mathbf{k}\cdot\mathbf{a}_2} \end{pmatrix} \tag{1.325}$$

$$= -2\frac{ega}{\hbar}J_0(\gamma)\begin{pmatrix} \sin(k_x a) \\ \sin(k_y a) \end{pmatrix} . \tag{1.326}$$

A comparison with the quasienergy of the circularly driven square lattice $\epsilon(\mathbf{k}) = -2gJ_0(\gamma)[\cos(k_x a) + \cos(k_y a)]$ yields

$$\bar{\mathbf{J}}(\mathbf{k}) = -\frac{e}{\hbar}\nabla_{\mathbf{k}}\epsilon_{\mathbf{k}} . \tag{1.327}$$

Focusing on the one-cycle averaged current allows for the evaluation of Eq. (1.253). Despite the solution of the Schrödinger equation being known, an analytic progress towards a closed form for the conductivity of the driven square lattice is a rather formidable task. This manifests itself in the complexity of the Floquet function. The latter, given in Eq. (1.313), can be expressed as

$$u(t,\gamma_x,\gamma_y) = \prod_{n\neq 0}\sum_{\ell,\ell'=-\infty}^{\infty} c_{n,\ell,\ell'}e^{i(\ell+\ell')n\Omega t} \tag{1.328}$$

$$= \sum_{n=-\infty}^{\infty} u_n^s(\gamma_x,\gamma_y)e^{in\Omega t} \tag{1.329}$$

together with

$$\begin{aligned} c_{n,\ell,\ell'} \equiv & J_\ell\left(-\frac{2g}{\hbar}\frac{J_n(\gamma_y)}{n\Omega}\right) J_{\ell'}\left(-\frac{2g}{\hbar}\frac{(-1)^n J_n(\gamma_x)}{n\Omega}\right) \\ & \times e^{i\ell k_y a}e^{i\ell'\left(k_x a - \frac{n\pi}{4}\right)} . \end{aligned} \tag{1.330}$$

However, focusing on the $n = n' = 0$ contribution to the conductivity yields

$$\lim_{\omega\to 0}\operatorname{Re}\sigma^{xx}(0,\omega) = \frac{e^2}{V(2\pi\hbar)^2}\int_{\mathrm{BZ}} d^2k[\nabla_{\mathbf{k}}\epsilon_{\mathbf{k}}]_x^2\left[\boldsymbol{\tau}(\varepsilon_F,\mathbf{k})\right]_{00}\delta(\varepsilon_F - \epsilon_{\mathbf{k}}) . \tag{1.331}$$

This expression can be numerically evaluated with high precision by applying the triangle method [99–101]. What one would expect is that the results for the square lattice and parabolic dispersion coincide in the low intensity regime. The spectra of the two models almost coincide for low Fermi energies, where "low" means at the lower end of the bandwidth of the square lattice. However, as depicted in Fig. 1.12, the conductivities as functions of the intensity show a strikingly different behavior, even for low intensities. This rather surprising result needs further analysis to deepen the understanding of the reason for this discrepancy. In the following section, the results for the conductivity from the effective model and the predictions from the tight-binding approach are compared.

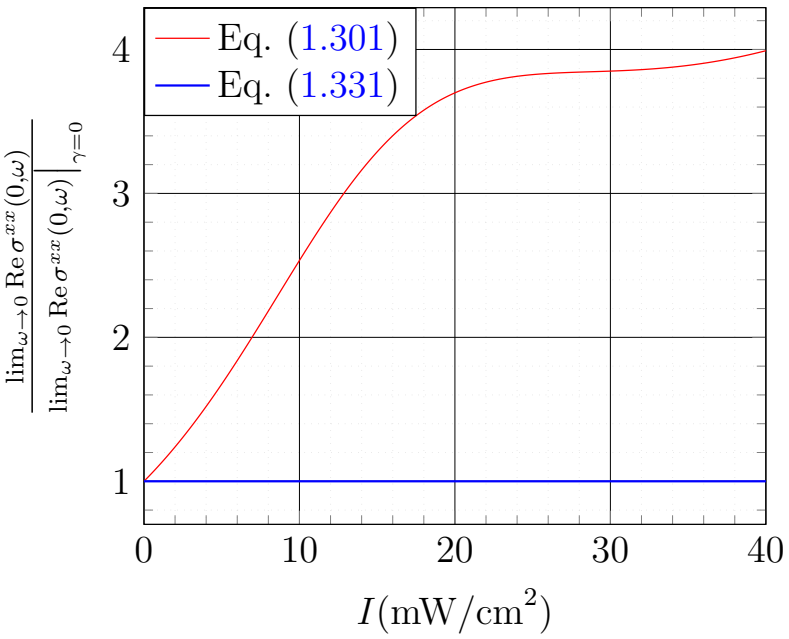

Figure 1.12: The red curve shows the result for the longitudinal conductivity for the parabolic model discussed in Sec. 1.9.1. The blue curve shows the pendant for the tight-binding model, i.e. the result of Eq. (1.331). The Fermi energy ε_F was set to 10 meV and the driving frequency Ω was set to 0.3 THz.

1.9.5 Comparison of parabolic dispersion with the square lattice

In this section, all derivations and calculations presented so far are used to underline the main finding of the first part of this work. The focus for both models, parabolic dispersion and square lattice, for the 2DEG is on circularly polarized light. The electric field corresponding to the vector potential used in Secs. 1.9.1 and 1.9.4 is governed by

$$\mathbf{E}(t) = -\frac{\partial \mathbf{A}(t)}{\partial t} = \mathcal{A}\Omega \begin{pmatrix} \cos(\Omega t) \\ -\sin(\Omega t) \end{pmatrix} . \tag{1.332}$$

The speed of light will be labeled as c in the following, the refractive index with n, the dielectric constant with ε_0, and $\langle\cdot\rangle_T$ denotes the average over one period. With these definitions, the intensity is

$$I = cn\varepsilon_0 \left\langle \mathbf{E}(t)^2 \right\rangle_T \tag{1.333}$$

$$= \frac{cn\varepsilon_0}{2} (\mathcal{A}\Omega)^2 . \tag{1.334}$$

The intensity and frequency regime for the parabolic dispersion must be found where the conductivity is significantly altered. From Eq. (1.274), it is obviously deduced that the conductivity is renormalized if the argument of the Bessel functions is of the order of one

$$z_\varepsilon = \frac{\hbar^2 \gamma_\mathrm{p} \sqrt{2m\varepsilon_F/\hbar^2}}{m} \Big/ \hbar\Omega \propto 1 \quad \text{with} \quad \gamma_\mathrm{p} \equiv \frac{e\mathcal{A}}{\hbar} . \tag{1.335}$$

In what follows, the representative parameters of an effective mass of $m = 0.071\, m_e$ corresponding to a tight-binding model on the square lattice with lattice constant of $a = 5.6\,\text{Å}$ and hopping energy of $g = 1.7$ eV are used. These exemplary parameters for GaAs are taken from Ref. [94]. Nevertheless, the subsequent discussion remains valid for a broad class of other materials with comparable parameters. Furthermore, the driving frequency is assumed to be in the Terahertz (THz) regime, the Fermi energy to be in the range of eV, and the intensity should be of the order of mW/cm^2. This suggests the introduction of the dimensionless quantities

$$\begin{aligned} \tilde{\Omega} &\equiv \Omega/[\text{THz}] \\ \tilde{\varepsilon}_F &\equiv \varepsilon_F/[\text{eV}] \\ \tilde{I} &\equiv I/[\text{mW/cm}^2] \\ \tilde{a} &\equiv a/[\text{Å}]\,. \end{aligned} \tag{1.336}$$

Together with these quantities, the aforementioned argument of the Bessel function becomes

$$z_\varepsilon = 0.29 \frac{\sqrt{\tilde{\varepsilon}_F}\sqrt{\tilde{I}}}{\tilde{\Omega}^2}\,. \tag{1.337}$$

A Fermi energy of 10 meV seems to be reasonable for an experimental realization. In the following discussion, the driving frequency is fixed at 0.3 THz, such that

$$z_\varepsilon = 0.33\sqrt{\tilde{I}}\,. \tag{1.338}$$

In doing so, one can then expect a conductivity change in the mW/cm^2 regime. The frequency range of the external driving is rather limited for intensities in the mW/cm^2 regime. A driving frequency of the order of tens or hundreds of THz would require an enormous Fermi energy, which is far beyond the parabolic approximation. However, if the Fermi energy is set on the meV scale, a driving frequency of hundreds of THz only leads to a significant renormalization of the conductivity if the intensity reaches GW/cm^2. Once again, this is far beyond experimental realizability. Now, the driven square lattice is investigated. The zeroth Fourier component of the Floquet function might be used as rough estimate for the regime, where a change of the conductivity could be expected. If the intensity is increased, the absolute squared of the zeroth Fourier component should start to deviate from 1 at some intensity. This would then be the first estimate for the appropriate intensity regime. However, expanding the Floquet function of the square lattice given in Eq. (1.313) analytically into a Fourier series is rather challenging. The Fourier components of the Floquet function of the square lattice, see Eq. (1.313), are denoted with u_n^{sl}, and the corresponding ones of the parabolic dispersion given in Eq. (1.280) with u_n^{p}. Firstly, the overlap of the Fourier components as a function of the momentum

$$o(\mathbf{k}) = \sum_{n=-\infty}^{\infty} \left|[u_n^{\text{sl}}(\mathbf{k})]^*[u_n^{\text{p}}(\mathbf{k})]\right|^2 \tag{1.339}$$

is considered. The results for some representative parameters are plotted in Fig. 1.13. Despite the fact that the intensity chosen is very low, it can be seen that the maximal overlap is less than 30 %. Along the Fermi contour corresponding to 10 meV, shown

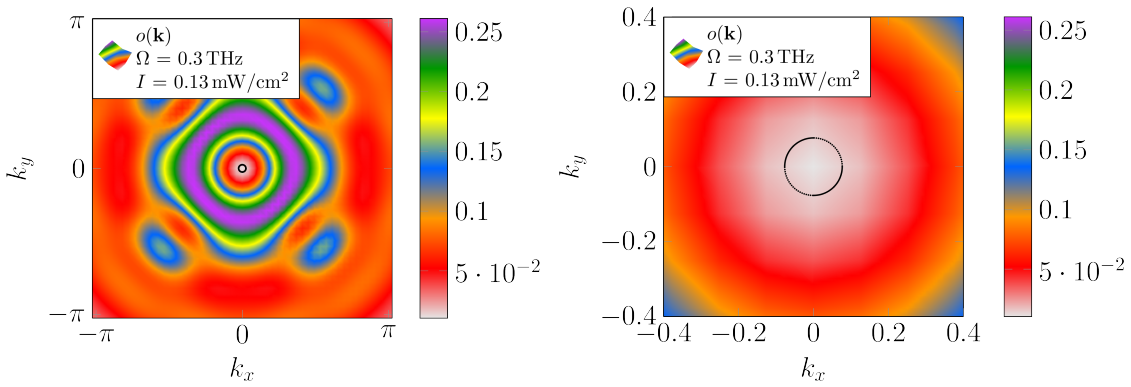

Figure 1.13: The overlap of the Fourier components of the Floquet function for the square lattice and parabolic dispersion: The maximal overlap is below 30 %, despite that the intensity chosen is very low. The black ring in the center shows the Fermi contour corresponding to $\varepsilon_F = 10$ meV.

as black ring in Fig. 1.13, the overlap is of the order of 1 %. To give an estimate of how the overlap behaves as a function of intensity, the averaged overlap is defined as

$$O = \frac{1}{V_{\mathrm{BZ}}} \int_{V_{\mathrm{BZ}}} d^2k \, o(\mathbf{k}) \,. \tag{1.340}$$

Figure 1.14 shows that the averaged overlap O for $\Omega = 0.3$ THz is rapidly decaying as the intensity is increased. Nevertheless, to fully quantify the reason for the differences of the conductivity of the driven square lattice and parabolic dispersion, it is mandatory to investigate the quasienergy spectra as well. The intensity as a

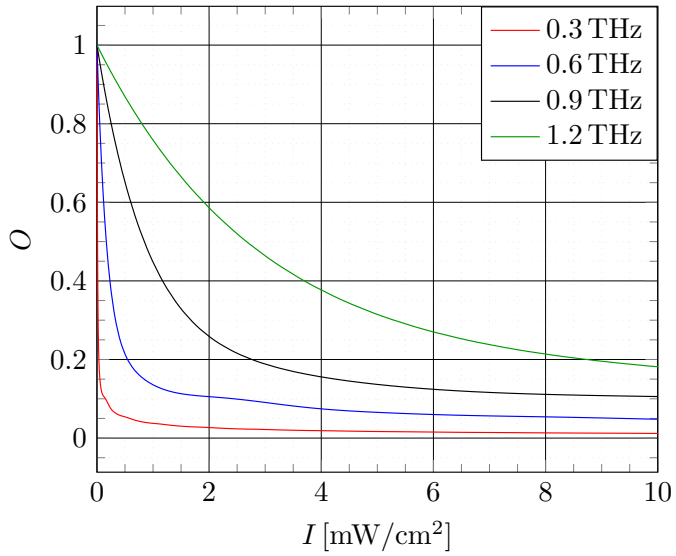

Figure 1.14: The averaged overlap of the eigenstates of driven square lattice and parabolic dispersion: The overlap is rapidly decaying as a function of intensity.

function of the dimensionless quantities introduced in Eqs. (1.336) is

$$I = 5.57 \cdot 10^9 \left(\frac{\tilde{\Omega}\gamma_{\mathrm{sl}}}{\tilde{a}} \right)^2 \frac{\mathrm{mW}}{\mathrm{cm}^2} \quad \text{with} \quad \gamma_{\mathrm{sl}} = \frac{e\mathcal{A}a}{\hbar} \tag{1.341}$$

such that for $\Omega = 0.3$ THz and $a = 5.6$ Å

$$I = 1.60 \cdot 10^7 \gamma_{\mathrm{sl}}^2 \frac{\mathrm{mW}}{\mathrm{cm}^2} \,. \tag{1.342}$$

Hence, to obtain an intensity of the order of $\mathrm{mW/cm^2}$, a $\gamma_{\mathrm{sl}} \propto 10^{-4}$ must be chosen. The quasienergy spectrum for the square lattice is known, see Eq. (1.312). Because $\gamma_{\mathrm{sl}} \ll 1$, an expansion in γ_{sl} and $\mathbf{k}$ using

$$J_0(x) \approx 1 - \frac{x^2}{4} + O(x^4) \,, \tag{1.343}$$

$$\cos(x) \approx 1 - \frac{x^2}{2} + O(x^4) \tag{1.344}$$

leads to

$$\epsilon_{\mathrm{sl}}(\mathbf{k}) \approx -4g + ga^2\mathbf{k}^2 + O(\gamma_{\mathrm{sl}}^2) \tag{1.345}$$

$$= -4g + \frac{\hbar^2\mathbf{k}^2}{2m} + O(\gamma_{\mathrm{sl}}^2) \,. \tag{1.346}$$

A comparison with the quasienergy spectrum for the parabolic case

$$\epsilon_{\mathrm{p}}(\mathbf{k}) = \frac{\hbar^2\mathbf{k}^2}{2m} \tag{1.347}$$

shows that both perfectly coincide since the corrections in Eq. (1.346), due to the driving, are negligibly small for the present choice of $\gamma_{\mathrm{sl}} \propto 10^{-4}$. In conclusion, the striking difference in the conductivities observed above is dominantly caused by the eigenstates rather than the similar quasienergy spectra. An analysis of the overlap of the wave functions of the continuum and tight-binding model shows that the overlap is rapidly decaying as a function of intensity. This statement is even true at very low intensities, suggesting that there is no intermediate intensity regime where the conductivities smoothly start to deviate from each other. Proving that the quasienergies almost coincide allows for the conclusion that the eigenstates dominate the behavior of the conductivity as the intensity is changed. Both the parabolic dispersion and the square lattice are rather simple models for a realistic material. Nevertheless, even the results from these simplified models strongly deviate from each other, underlining the importance to start with a realistic model. Both models used in this work are single band models. The impact of higher or lower lying bands might be important as well. However, a deeper analysis of multiband models is left for future work. The findings for the square lattice and parabolic dispersion might also be true for other materials, e.g. graphene [35]. As a consequence, previous works using effective models should be revised.

1.10 Weak localization

1.10.1 Diffuson

This section summarizes the most important thoughts and prerequisites for the weak localization effect. There are numerous textbooks explaining and deriving the *Diffuson* and the *Cooperon*. For further details see Refs. [10, 48, 89, 90, 102–104]. Thus far, multiple scattering, leading to interference effects, has been neglected in this work. The following considerations are valid for the weak disorder regime, where the mean free path ℓ_0 is much greater than the Fermi wave length λ. Interference effects can only occur if the phase coherence length ℓ_ϕ is larger than the mean free path of the electrons ℓ_0. The sample size L must be much larger than the phase coherence length. If both are of the same scale, numerous coherence effects occur, leading to universal conductance fluctuations [89]. However, the weak localization survives the self averaging due to the large sample size. Weak localization is mostly pronounced if

$$\lambda \ll \ell_0 \ll \ell_\phi \ll L \ . \tag{1.348}$$

If the dephasing length is of the order of the system size, geometric effects of the sample become important [105]. For short range disorder, see Eq. (1.171), and in the weak disorder limit, the collisions are independent. Focusing only on paths with an equal number of scattering events is called *Diffuson approximation* [89]. The contribution to the conductivity of the diagrams with equal number of scattering events is dominated by those diagrams where the two trajectories pass through the same scattering centers [89], i.e. the Diffuson diagrams. The disorder averaged Green's function, given in Eq. (1.160) will from now on be depicted as

$$\langle \mathcal{G}^r_{\mathrm{p}}(\varepsilon, \mathbf{k}, n, n') \rangle_{\mathrm{imp}} = \quad \underset{(\mathbf{k}, n, n')}{\longrightarrow} \tag{1.349}$$

where the dependence on ε is suppressed. The Diffuson diagrams can be summed up recursively, due to the iterative structure of the Dyson series. The sum over all Diffuson diagrams is called *Diffuson*

$\mathbf{\Gamma}_D(\mathbf{q}) =$ 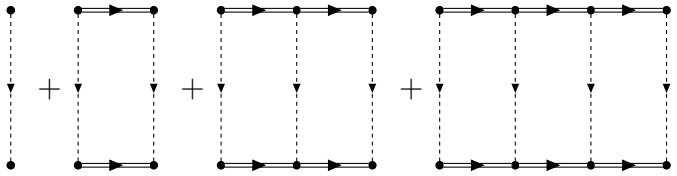 $+ \ \ldots$ (1.350)

If the system is time-reversal invariant, the reciprocity theorem [106] allows one to time reverse the lower path in order to get the Cooperon. In the present work, the conductivity correction only depends on the Floquet Hamiltonian. Hence, if the Floquet Hamiltonian has time-reversal symmetry, the Cooperon can be derived as in the undriven case.

1.10.2 Cooperon

The aim of this section is to derive the quantum correction to the conductivity by the Cooperon diagrams. In the foregoing sections, it was already mentioned that

the reciprocity theorem allows one to time-reverse the lower paths of the Diffuson diagrams depicted in Eq. (1.350). These diagrams are called Cooperon

$\mathbf{\Gamma}(\mathbf{q}) =$ 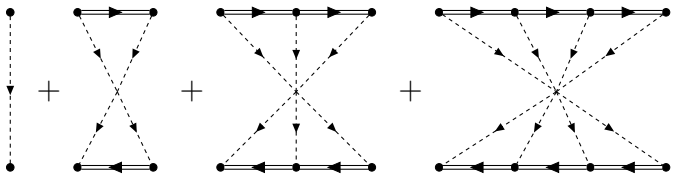 $+ \ ...$ (1.351)

These diagrams can be summed up, due to the large number of impurities, using the geometric series, such that the Cooperon

$$\mathbf{\Gamma}(\mathbf{q}) = \frac{\mathcal{V}_{\text{imp}}}{\mathbb{1} \otimes \mathbb{1} - \mathcal{V}_{\text{imp}} \mathbf{\Pi}(\mathbf{q})} \tag{1.352}$$

together with the correlation matrix, spanned by the sum over momenta over the Kronecker product $\otimes$ of a retarded and an advanced Green's function

$$\mathbf{\Pi}(\mathbf{q}) \equiv \frac{1}{\hbar^2 V_{\mathbf{k}}} \sum_{\mathbf{k}} \boldsymbol{G}^r(\mathbf{k}) \otimes \boldsymbol{G}^a(\mathbf{q} - \mathbf{k}) \,. \tag{1.353}$$

For example the fourth order diagram of the above series is

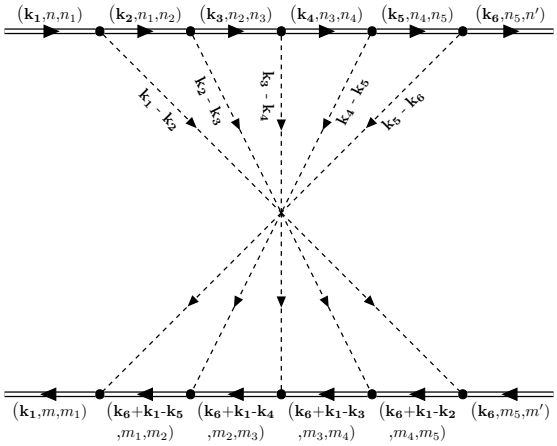

$$\begin{aligned} = \frac{1}{V_{\mathbf{k}_6} V_{\mathbf{k}_1}} \sum_{\mathbf{k}_6 \mathbf{k}_1} \Big[\boldsymbol{G}^r(\mathbf{k_1}) \otimes \boldsymbol{G}^a(\mathbf{k_1}) \Big] \Big[\frac{\mathcal{V}_{\text{imp}}}{\hbar^2 V_{\mathbf{k}}} \sum_{\mathbf{k}} \boldsymbol{G}^r(\mathbf{k}) \otimes \boldsymbol{G}^a(\mathbf{k_1} + \mathbf{k_6} - \mathbf{k}) \Big]^4 \\ \times \Big[\boldsymbol{G}^r(\mathbf{k_6}) \otimes \boldsymbol{G}^a(\mathbf{k_6}) \Big] \end{aligned} \tag{1.354}$$

where it was used that for matrices A, B, C, D holds

$$AC \otimes BD = \big(A \otimes B\big)\big(C \otimes D\big) \ . \tag{1.355}$$

The conductivity caused by coherent propagation, i.e. the Cooperon, is

$$\begin{aligned} \sigma_C = \frac{\hbar}{2\pi V} \left(\frac{e}{m}\right)^2 \int_{\lambda - \hbar\Omega/2}^{\lambda + \hbar\Omega/2} d\varepsilon \left(-\frac{\partial f}{\partial \varepsilon}\right) \frac{1}{V_{\mathbf{k}} V_{\mathbf{k}'}} \sum_{\mathbf{k}\mathbf{k}'} k_x k'_x \\ \times \ \text{tr} \Big[\Big[\boldsymbol{G}^r(\mathbf{k}) \otimes \boldsymbol{G}^a(\mathbf{k}) \Big] \mathbf{\Gamma}(\mathbf{k} + \mathbf{k}') \Big[\boldsymbol{G}^r(\mathbf{k}') \otimes \boldsymbol{G}^a(\mathbf{k}') \Big] \Big] \,. \end{aligned} \tag{1.356}$$

Assuming that the dominant contribution to the Cooperon comes in a driven system still from $\mathbf{k}+\mathbf{k}' \approx 0$, and claiming that $\boldsymbol{G}^{r,a}(-\mathbf{k}) = \boldsymbol{G}^{r,a}(\mathbf{k})$, one obtains for the Cooperon conductivity

$$\begin{aligned}\sigma_C = \frac{\hbar}{2\pi V}\left(\frac{e}{m}\right)^2 \int_{\lambda-\hbar\Omega/2}^{\lambda+\frac{\hbar\Omega}{2}} d\varepsilon \left(\frac{\partial f}{\partial \varepsilon}\right) \frac{1}{V_{\mathbf{k}} V_{\mathbf{q}}} \sum_{\mathbf{kq}} k_x^2 \\ \times \ \mathrm{tr}\Big[\Big[\boldsymbol{G}^r(\mathbf{k}) \otimes \boldsymbol{G}^a(\mathbf{k})\Big]\boldsymbol{\Gamma}(\mathbf{q})\Big[\boldsymbol{G}^r(\mathbf{k}) \otimes \boldsymbol{G}^a(\mathbf{k})\Big]\Big] .\end{aligned} \tag{1.357}$$

The transformation diagonalizing the bare Green's function, cf. Eq. (1.174), obviously fulfills

$$\Big(\boldsymbol{T}^\dagger(\mathbf{k}) \otimes \boldsymbol{T}^\dagger(\mathbf{k})\Big)\Big(\boldsymbol{T}(\mathbf{k}) \otimes \boldsymbol{T}(\mathbf{k})\Big) = \mathbb{1} \otimes \mathbb{1} . \tag{1.358}$$

Now, the transformed structure factor

$$\boldsymbol{\Gamma}_{\boldsymbol{T}}(\mathbf{q},\mathbf{k}) = \frac{\mathcal{V}_{\mathrm{imp}}}{\mathbb{1} \otimes \mathbb{1} - \mathcal{V}_{\mathrm{imp}}\big(\boldsymbol{T}^\dagger(\mathbf{k}) \otimes \boldsymbol{T}^\dagger(\mathbf{k})\big)\boldsymbol{\Pi}(\mathbf{q})\big(\boldsymbol{T}(\mathbf{k}) \otimes \boldsymbol{T}(\mathbf{k})\big)} \tag{1.359}$$

and the transformed Green's function

$$\boldsymbol{D}^{r,a}_{\boldsymbol{T}}(\mathbf{k}) = \boldsymbol{T}^\dagger(\mathbf{k})\boldsymbol{G}^{r,a}(\mathbf{k})\boldsymbol{T}(\mathbf{k}) \tag{1.360}$$

are introduced. Assuming that the disorder does not change the eigenenergies of the system allow one to drop all off-diagonal elements of the self energy. Hence, the Green's function in Eq. (1.360) is diagonal within this approximation. With this assumption, the weak localization correction becomes

$$\begin{aligned}\sigma_C = \frac{\hbar}{2\pi V}\left(\frac{e}{m}\right)^2 \int_{\lambda-\hbar\Omega/2}^{\lambda+\frac{\hbar\Omega}{2}} d\varepsilon \left(\frac{\partial f}{\partial \varepsilon}\right) \frac{1}{V_{\mathbf{k}} V_{\mathbf{q}}} \sum_{\mathbf{kq}} k_x^2 \\ \times \ \mathrm{tr}\Big[\Big[\boldsymbol{D}^r_{\boldsymbol{T}}(\mathbf{k}) \otimes \boldsymbol{D}^a_{\boldsymbol{T}}(\mathbf{k})\Big]^2 \boldsymbol{\Gamma}_{\boldsymbol{T}}(\mathbf{q},\mathbf{k})\Big] .\end{aligned} \tag{1.361}$$

It might give some deeper insight to compare the above equation with the static case and weak spin-orbit coupling. Despite there being structural similarities, there is one striking difference. For weak spin-orbit coupling, the Drude part, i.e. the integral over the product of $\boldsymbol{G}^{r,a}$, is assumed to be negligibly altered by the spin-orbit coupling [18, 19]. Hence, the additional transformation applied in Eq. (1.360) is not necessary in this case. The present case of a driven system is rather comparable to a multiband system with strong spin-orbit coupling, where the analogue to the multiple bands are the Floquet replica and the analogue to the strong spin-orbit coupling is the coupling of the different Floquet modes induced by the external driving. The structure factor given in Eq. (1.359) has a pole if

$$\mathcal{V}_{\mathrm{imp}}\boldsymbol{\Pi}(\mathbf{q}) \approx \mathbb{1} \otimes \mathbb{1} . \tag{1.362}$$

In the following, the structure factor $\boldsymbol{\Gamma}_{\boldsymbol{T}}(\mathbf{q},\mathbf{k})$ and additionally the correlation function $\boldsymbol{\Pi}(\mathbf{q})$ are further analyzed. Following the procedure suggested in Refs. [18, 19]

and inserting an identity matrix in the correlation matrix lead to

$$\begin{aligned}\mathbf{\Pi}(\mathbf{q}) = \frac{1}{\hbar^2 V_{\mathbf{k}}} \sum_{\mathbf{k}} & \boldsymbol{G}^r(\mathbf{k}) \otimes \boldsymbol{G}^a(\mathbf{q}-\mathbf{k}) \\ & \times \left(\boldsymbol{G}^r(\mathbf{k})^{-1} \otimes \mathbb{1} - \mathbb{1} \otimes \boldsymbol{G}^a(\mathbf{q}-\mathbf{k})^{-1} \right) \\ & \times \left(\boldsymbol{G}^r(\mathbf{k})^{-1} \otimes \mathbb{1} - \mathbb{1} \otimes \boldsymbol{G}^a(\mathbf{q}-\mathbf{k})^{-1} \right)^{-1} .\end{aligned} \tag{1.363}$$

Using the identity for the Kronecker product defined in Eq. (1.355) and the Floquet matrix representation of the Green's function of Eq. (1.89), one can show that the correlation matrix becomes

$$\begin{aligned}\mathbf{\Pi}(\mathbf{q}) = \frac{1}{\hbar^2 V_{\mathbf{k}}} \sum_{\mathbf{k}} & \underbrace{\left(\mathbb{1} \otimes \boldsymbol{G}^a(\mathbf{q}-\mathbf{k}) - \boldsymbol{G}^r(\mathbf{k}) \otimes \mathbb{1} \right)}_{\equiv \mathbf{\Delta_G}} \\ & \times \underbrace{\frac{1}{-\frac{1}{\hbar}\mathbf{H}_F(\mathbf{k}) \otimes \mathbb{1} + \frac{1}{\hbar}\mathbb{1} \otimes \mathbf{H}_F(\mathbf{q}-\mathbf{k}) + i\frac{1}{2\boldsymbol{\tau}_{\mathbf{k}}} \otimes \mathbb{1} + i\mathbb{1} \otimes \frac{1}{2\boldsymbol{\tau}_{\mathbf{q}-\mathbf{k}}}}}_{\equiv \mathbf{\Delta_E}}\end{aligned} \tag{1.364}$$

where the two factors commute. Again, a comparison of the last equation with the scenario of weak spin-orbit coupling underlines the peculiarity of weak localization in a driven system. For the spin-orbit coupling case, $\mathbf{\Delta_G}$ can be assumed to be diagonal, and the spin-orbit coupling is only kept in $\mathbf{\Delta_E}$. This assumption is not applicable in strongly driven systems. Hence, evaluating Eq. (1.361) analytically in full glory is similar to the calculation of the weak localization effect in a multiband system with strong spin-orbit coupling. There is a long standing paradigm that weak localization will not survive in a driven system, due to heating and destruction of phase coherence [107]. However, the argumentation thus far has been based on rather heuristic arguments. Now, a deeper investigation is possible with the presented formalism, which might give further insight into the mechanisms leading to the suppression of localization effects.

1.11 Homogenous electric field: A Floquet approach

The investigation of the interaction of condensed matter systems with a constant electric field finds its origin in the early stage of the 19th century, with the seminal works of Voigt [108] and Stark [109]. Zak showed in Ref. [110] that the derivations of the Stark ladder by Wannier [111, 112] and Callaway [113] had flaws. Shortly afterwards, Fukuyama *et al.* proved the existence of a Stark ladder in a linear chain, using a tight-binding approach. The aim of this section is to recall the results of Ref. [114], and shine new light on the stark ladder in the linear chain in the context of Floquet physics. The spatial periodicity of the linear chain allows for a Floquet approach, tackling the constant electric field. Despite the original Hamiltonian being time-independent, it can be mapped on a time-dependent Hamiltonian periodic in time. This justifies the use of Floquet theory. First, some rather general considerations are presented. It is proven that the linear chain with a constant electric field

can be unitarily mapped onto a linear chain with Peierls phase. The discussion also includes finite systems and models with more than one band. Then, the mapping of the system investigated in Ref. [114] onto a Floquet system is constructed. It will be shown that the constant electric field can be mapped onto the time-derivative in Floquet space. Furthermore, the presented scheme allows for the treatment of the next-nearest neighbor hoppings in a straightforward manner, since they correspond to higher harmonic terms in the Floquet Hamiltonian. In the last section, the momentum dependency of the Stark ladder in two dimensions is investigated.

1.11.1 General

A time-independent constant electric field can be described by either the gradient of a scalar potential ϕ or by the time-derivative of a vector potential $\mathbf{A}$

$$\mathbf{E} = -\nabla\phi - \frac{\partial \mathbf{A}}{\partial t}\,. \tag{1.365}$$

In this section, it will be shown that, if the constant electric field is introduced via the second term of the last equation, depending on the representation, some Hamiltonians are time-periodic, despite the electric field obviously being time-independent. Consider a generic tight-binding model [114]

$$H = -g\sum_{n=-\infty}^{\infty}\left(c_n^\dagger c_{n+1} + c_{n+1}^\dagger c_n\right) - qEa\sum_{n=-\infty}^{\infty} n c_n^\dagger c_n \tag{1.366}$$

where the first term is the kinetic part with hopping energy g and the second term accounts for the constant electric field. The creation and annihilation operators are either fermionic or bosonic. The time-dependent Schrödinger equation, together with the Hamiltonian above, are, in what follows, transformed with the time-dependent gauge transformation

$$U = e^{i\frac{q}{\hbar}\Lambda} \quad , \quad \Lambda = -Eat\sum_{n=-\infty}^{\infty} n c_n^\dagger c_n\,. \tag{1.367}$$

Defining the transformed eigenstate

$$|\psi'(t)\rangle = U|\psi(t)\rangle \tag{1.368}$$

and applying the unitary transformation given in Eq. (1.367) lead to the Schrödinger equation for $|\psi'(t)\rangle$

$$i\hbar\frac{\partial}{\partial t}|\psi'(t)\rangle = \underbrace{\left(UHU^\dagger + i\hbar\left(\frac{\partial U}{\partial t}\right)U^\dagger\right)}_{\equiv H'(t)}|\psi'(t)\rangle\,. \tag{1.369}$$

A particularly useful commutation relation is

$$\left[\sum_{n=-\infty}^{\infty} n c_n^\dagger c_n\,,\,\sum_{n'=-\infty}^{\infty} c_{n'}^\dagger c_{n'+1}\right] = -\sum_{n=-\infty}^{\infty} c_n^\dagger c_{n+1} \tag{1.370}$$

allowing the straightforward proof of

$$U \sum_{n=-\infty}^{\infty} c_n^\dagger c_{n+1} = \left(\sum_{n=-\infty}^{\infty} c_n^\dagger c_{n+1} \right) e^{\frac{i}{\hbar} qEat} U \tag{1.371}$$

from which the explicit form of the transformed Hamiltonian is readily deduced

$$H'(t) = -g \sum_{n=-\infty}^{\infty} \left(c_n^\dagger c_{n+1} e^{\frac{i}{\hbar} qEat} + c_{n+1}^\dagger c_n e^{-\frac{i}{\hbar} qEat} \right) . \tag{1.372}$$

This Hamiltonian is time-periodic, with period $T = 2\pi\hbar/(qEa)$. In higher dimensions, this holds only if the components of the electric field are commensurate. $H'(t)$ is also translationally invariant. This is analogous to the continuum case, where

$$H(t) = \frac{(\mathbf{p} - q\mathbf{A})^2}{2m} \quad , \quad \mathbf{A} = -\mathbf{E}t \, . \tag{1.373}$$

The transformed Hamiltonian given in Eq. (1.372) also makes sense for finite systems, i.e. for periodic boundary conditions. The Hamiltonian corresponding to a finite system with N sites is

$$H(t) = -g \sum_{n=0}^{N-1} \left(c_n^\dagger c_{n+1} e^{\frac{i}{\hbar} qEat} + c_{n+1}^\dagger c_n e^{-\frac{i}{\hbar} qEat} \right) \tag{1.374}$$

$$= -g \sum_{\bar{k}} \left[2 \cos \left(\bar{k}a + \frac{qEat}{\hbar} \right) c_{\bar{k}}^\dagger c_{\bar{k}} \right] \tag{1.375}$$

together with the creation and annihilation operators

$$c_{n+N}^{(\dagger)} = c_n^{(\dagger)} = \frac{1}{\sqrt{N}} \sum_{\bar{k}} e^{(-)i\bar{k}na} c_{\bar{k}}^{(\dagger)} \quad , \quad \bar{k} = \frac{2\pi}{Na} m \ , \ m \in \{0, ..., N-1\} \, . \tag{1.376}$$

The quantity $\bar{k}$ labeling the states

$$|\bar{k}\rangle = c_{\bar{k}}^\dagger |0\rangle = \frac{1}{\sqrt{N}} \sum_{n=0}^{N-1} e^{i\bar{k}na} c_n^\dagger |0\rangle \tag{1.377}$$

corresponds to a canonical momentum and not the kinematic one. Applying the inverse of the gauge transformation defined in Eq. (1.367) yields

$$|k\rangle = U^\dagger |\bar{k}\rangle = \frac{1}{\sqrt{N}} \sum_{n=0}^{N-1} e^{i\left(\bar{k} + \frac{qE}{\hbar} t\right) na} c_n^\dagger |0\rangle \tag{1.378}$$

leading to the lattice analog of the kinematic momentum

$$k = \bar{k} + \frac{qE}{\hbar} t \, . \tag{1.379}$$

Now, consider a more general scenario. The instantaneous eigenstates of a Hamiltonian

$$H = \sum_{\mathbf{k}} \varepsilon_{\mathbf{k}}(t) c_{\mathbf{k}}^\dagger c_{\mathbf{k}} \tag{1.380}$$

are just given by $|\mathbf{k}\rangle = c_{\mathbf{k}}^{\dagger}|0\rangle$, and are therefore independent of time. A solution of the time-dependent Schrödinger equation is then

$$|\psi_{\mathbf{k}}(t)\rangle = e^{-\frac{i}{\hbar}\int_{t_0}^{t} dt' \, \varepsilon_{\mathbf{k}}(t')}|\mathbf{k}\rangle \, . \tag{1.381}$$

The situation becomes more complicated if the momentary eigenstates are time-dependent. This will generally be the case for lattice bases with more than one element, or in the presence of spin-orbit coupling. This scenario is analyzed in the following. Consider a more general Hamiltonian

$$\mathcal{H} = \sum_{\substack{\alpha,\beta,j \\ n=-\infty}}^{\infty} \left[h_{\alpha\beta,j} c_{\alpha,n}^{\dagger} c_{\beta,n+j} + \text{h.c.} \right] - qEa \sum_{\alpha,n=-\infty}^{\infty} n \mathbb{1}_{\alpha\alpha} c_{\alpha,n}^{\dagger} c_{\alpha,n} \tag{1.382}$$

where α and β label discrete sets of quantum numbers, e.g. spin or sublattice degrees, j is a finite number of neighbors, and n is the position coordinate. Analogue to Eq. (1.367), the unitary transformation

$$\mathcal{U} = e^{i\frac{q}{\hbar}\Upsilon} \quad , \quad \Upsilon = -Eat \sum_{\alpha,n=-\infty}^{\infty} n \mathbb{1}_{\alpha\alpha} c_{\alpha,n}^{\dagger} c_{\alpha,n} \tag{1.383}$$

is defined and the commutator

$$\left[\sum_{\alpha,n=-\infty}^{\infty} n \mathbb{1}_{\alpha\alpha} c_{\alpha,n}^{\dagger} c_{\alpha,n}, \sum_{\substack{\alpha,\beta,j \\ n=-\infty}}^{\infty} h_{\alpha\beta,j} c_{\alpha,n}^{\dagger} c_{\beta,n+j} \right] = - \sum_{\substack{\alpha,\beta,j \\ n=-\infty}}^{\infty} h_{\alpha\beta,j} c_{\alpha,n}^{\dagger} c_{\beta,n+j} \tag{1.384}$$

leads to the transformed Hamiltonian

$$\mathcal{H}' = \left(\mathcal{U}\mathcal{H}\mathcal{U}^{\dagger} + i\hbar \left(\frac{\partial \mathcal{U}}{\partial t} \right) \mathcal{U}^{\dagger} \right) \tag{1.385}$$

$$= \sum_{\substack{\alpha,\beta,j \\ n=-\infty}}^{\infty} \left[h_{\alpha\beta,j} c_{\alpha,n}^{\dagger} c_{\beta,n+j} e^{\frac{i}{\hbar} qEat} + \text{h.c.} \right] . \tag{1.386}$$

Expanding the creation (annihilation) operators as Fourier series

$$c_{\alpha,n}^{(\dagger)} = \frac{1}{V} \sum_{\mathbf{k}} c_{\alpha,\mathbf{k}}^{\dagger} e^{(-)i\mathbf{k}\cdot\mathbf{r}_n} \tag{1.387}$$

yields

$$\mathcal{H}' = \sum_{\substack{\alpha,\beta,j \\ \mathbf{k}}} h_{\alpha\beta,j} e^{i\mathbf{k}\cdot\mathbf{r}_j + \frac{i}{\hbar} qEat} c_{\alpha,\mathbf{k}}^{\dagger} c_{\beta,\mathbf{k}} + \text{h.c.} \tag{1.388}$$

which is always periodic in time, since the electric field in Eq. (1.382) was set parallel to the symmetry axis of the system. The Hamiltonian above is equivalently obtained by a Peierls substitution in the gauge $\mathbf{E} = -\partial\mathbf{A}/(\partial t)$. The investigation of the general validity of the Peierls phase for a constant electric field is left as part of future work. This will cover a detailed analysis of commensurate directions of the electric field.

1.11.2 Square lattice in real space

In this section the focus is on the real space representation of a linear chain with a constant electric field. Hence, direct contact to existing literature can be made, i.e. Refs. [110, 114]. As already mentioned, it is possible to map the setup discussed in Ref. [114] onto a simple time-periodic model, which allows for the application of Floquet theory. First, the frequency

$$\Omega = -\frac{eAa}{\hbar} \tag{1.389}$$

is introduced, leading for the Hamiltonian given in Eq. (1.366) to

$$H = -g \sum_{n=-\infty}^{\infty} \left(c_n^\dagger c_{n+1} + c_{n+1}^\dagger c_n \right) - \hbar\Omega \sum_{n=-\infty}^{\infty} n c_n^\dagger c_n \,. \tag{1.390}$$

Using the representation

$$c_n^\dagger |0\rangle \equiv |u_n\rangle \tag{1.391}$$

yields for the time-independent Schrödinger equation

$$-g\big(|u_{n-1}\rangle + |u_{n+1}\rangle\big) - \hbar\Omega n |u_n\rangle = \varepsilon |u_n\rangle \,. \tag{1.392}$$

In anticipation of the use of the Floquet formalism, the Fourier coefficients

$$H_n = \begin{cases} -g & \text{for} \quad n = \pm 1 \,, \\ 0 & \text{else} \end{cases} \tag{1.393}$$

are defined. They allow one to rewrite Eq. (1.392) in the following form

$$\sum_{m=-\infty}^{\infty} \big(H_{n-m} - n\hbar\Omega\delta_{nm} \big) |u_m\rangle = \varepsilon |u_n\rangle \tag{1.394}$$

which is equal to Eq. (1.11). Hence, using the Fourier series of a time-dependent Hamiltonian as in Eq. (1.8) leads - together with the Fourier coefficient of Eq. (1.393) - to the time-dependent Hamiltonian

$$H(t) = -2g\cos(\Omega t) \,. \tag{1.395}$$

Whereas the multiple of the photon energy on the diagonal in Eq. (1.392) has its origin in the constant electric field of the Hamiltonian given in Eq. (1.390), it has its origin in the Fourier representation of the Schrödinger equation given in Eq. (1.11) in the time-derivative of the time-dependent Schrödinger equation. This leads to the conclusion that the constant electric field can be mapped onto the time-derivative occurring in the Schrödinger equation. Furthermore, only nearest neighbor hopping is considered in Eq. (1.390). Consequently, the time-dependent Hamiltonian has only ± 1 Fourier components. Next-nearest neighbor hopping causes higher harmonics in the time-dependent Hamiltonian. The time-dependent Schrödinger equation, together with the Hamiltonian of Eq. (1.395), is solved by the exponential of the time integrated Hamiltonian

$$\psi(t) = e^{-\frac{i}{\hbar}\int dt\, H(t)} = e^{i\frac{2g}{\hbar\Omega}\sin(\Omega t)} = \sum_{n=-\infty}^{\infty} J_n\left(\frac{2g}{\hbar\Omega}\right) e^{in\Omega t} \,. \tag{1.396}$$

A time-ordering is not needed here, since the Hamiltonian for this single band model commutes at all times. Expanding the wave function into a Fourier series

$$\psi(t) = \sum_{n=-\infty}^{\infty} u_n e^{in\Omega t} \quad \text{with} \quad u_n = J_n\left(\frac{2g}{\hbar\Omega}\right) \tag{1.397}$$

yields the same solution u_n as provided by the authors of Ref. [114]. From Eq. (1.397), it can obviously be deduced that the quasienergy is zero. Hence, the stark ladder predicted by Fukuyama *et al.* are just the Floquet replica of a trivial quasienergy.

1.11.3 Square lattice in momentum space

Now, consider a tight-binding model on the square lattice, together with a constant electric Field in x-direction. Only nearest neighbor hopping is taken into account with nearest neighbor vectors

$$\mathbf{a}_1 = a\begin{pmatrix}1\\0\end{pmatrix} \quad , \quad \mathbf{a}_2 = a\begin{pmatrix}0\\1\end{pmatrix} . \tag{1.398}$$

The electric field is supposed to show in x-direction

$$\mathbf{A}(t) = \begin{pmatrix}-Et\\0\end{pmatrix} \quad \Leftrightarrow \quad \mathbf{E} = -\frac{\partial \mathbf{A}(t)}{\partial t} . \tag{1.399}$$

The time-dependent tight-binding Hamiltonian for the square lattice is

$$H(t) = -g\left[e^{i\mathbf{k}\cdot\mathbf{a}_1}e^{i\frac{e}{\hbar}\mathbf{A}(t)\cdot\mathbf{a}_1} + e^{i\mathbf{k}\cdot\mathbf{a}_2}e^{i\frac{e}{\hbar}\mathbf{A}(t)\cdot\mathbf{a}_2} + h.c.\right] \tag{1.400}$$

$$= -2g\left[\cos(k_x a - \Omega t) + \cos(k_y a)\right] \tag{1.401}$$

together with the frequency

$$\Omega \equiv \frac{eEa}{\hbar}. \tag{1.402}$$

To solve the time-dependent Schrödinger equation, the same ansatz as in Eq. (1.308) can be chosen, leading to

$$\psi(\mathbf{k},t) = e^{-\frac{i}{\hbar}2g\left(-\sin(k_x a-\Omega t)/\Omega+\cos(k_y a)t\right)} \tag{1.403}$$

$$= e^{-\frac{i}{\hbar}2g\cos(k_y a)t}e^{-iz_{\mathbf{k}}\sin(\Omega t)+iw_{\mathbf{k}}\cos(\Omega t)} \tag{1.404}$$

where in the last equation the definitions

$$z_{\mathbf{k}} \equiv \frac{2g}{\hbar\Omega}\cos(k_x a) \quad , \quad w_{\mathbf{k}} \equiv \frac{2g}{\hbar\Omega}\sin(k_x a) \tag{1.405}$$

were used. The quasienergy and Fourier components of the Floquet function are readily calculated using the Jacobi-Anger expansion, see Eqs. (1.435),

$$\epsilon_{\mathbf{k}} = -2g\cos(k_y a) \quad , \quad u_n(\mathbf{k}) = \sum_{m=-\infty}^{\infty} J_{m+n}(z_{\mathbf{k}})J_m(w_{\mathbf{k}})e^{im\frac{\pi}{2}} . \tag{1.406}$$

Remarkably, the quasienergy in k_x-direction is completely flat, however, the eigenstates depend on k_x non-trivially. The Fourier components of the Floquet functions can be further simplified using the Graf and Gegenbauer theorem [115]

$$J_n(\alpha)\,\mathrm{trig}(n\chi) = \sum_{m=-\infty}^{\infty} J_{m+n}(z)J_m(w)\,\mathrm{trig}(m\phi)\,, \tag{1.407}$$

$$\mathrm{trig} \in \{\sin, \cos\}\,, \tag{1.408}$$

$$\alpha = \sqrt{z^2 + w^2 - 2zw\cos(\phi)}\,, \tag{1.409}$$

$$\chi = \arcsin\left(\frac{w}{\alpha}\sin(\phi)\right)\,. \tag{1.410}$$

For the present case of u_n, identifying the parameters

$$\phi = \frac{\pi}{2} \quad \Rightarrow \quad \alpha = \frac{2g}{\hbar\Omega} \quad \Rightarrow \quad \chi = k_x a \tag{1.411}$$

allows for the application of the Graf and Gegenbauer theorem and simplify the Floquet function to

$$u_n(\mathbf{k}) = J_n(\tilde{g})e^{ink_x a} \quad , \quad \tilde{g} = \frac{2g}{\hbar\Omega}\,. \tag{1.412}$$

The scattering time is needed for the calculation of the conductivity. For this reason, Eq. (1.179) is again investigated

$$c^n(\mathbf{k},\mathbf{k}') = \sum_{m=-\infty}^{\infty} J_{n+m}(\tilde{g})J_m(\tilde{g})e^{-ink_x a}e^{im(k'_x-k_x)a}\,. \tag{1.413}$$

The last equation can be further simplified by again using the Graf and Gegenbauer theorem with

$$\phi = (k'_x - k_x)a \;\Rightarrow\; \alpha = 2\tilde{g}|\sin(\phi/2)| \;\Rightarrow\; \chi = \arcsin\left(\frac{\sin(\phi)}{2|\sin(\frac{\phi}{2})|}\right) \tag{1.414}$$

such that

$$c^n(\mathbf{k},\mathbf{k}') = e^{-ink_x a}J_n\big[2\tilde{g}|\sin(\Delta_k)|\big]e^{in\arcsin\left[\sin(\Delta_k)/(2|\sin(\Delta_k/2)|)\right]}, \tag{1.415}$$

$$\Delta_k \equiv (k'_x - k_x)a\,. \tag{1.416}$$

The absolute squared of the above quantity simplifies to

$$|c^n(\mathbf{k},\mathbf{k}')|^2 = J_n^2\big[2\tilde{g}\sin(\Delta_k/2)\big] \tag{1.417}$$

where the absolute of the argument of the Bessel function was dropped, since the Bessel function is squared. Using the quantity above, one can imply that the inverse scattering time is

$$\left(\frac{1}{\boldsymbol{\tau}(\varepsilon,\mathbf{k})}\right)_{nn} = \frac{\mathcal{V}_{\mathrm{imp}}}{2\pi\hbar}\int_{-\pi/a}^{\pi/a}dk'_x\int_{-\pi/a}^{\pi/a}dk'_y|c^n(\mathbf{k},\mathbf{k}')|^2\delta\big(\varepsilon + 2g\cos(k'_y a)\big)\,. \tag{1.418}$$

First, the k'_y-integral is evaluated. The integration interval is split into a negative and positive integration variable region

$$I_{k'_y}(\varepsilon) \equiv \int_{-\pi/a}^{\pi/a} dk'_y\, \delta\big(\varepsilon + 2g\cos(k'_y a)\big) \tag{1.419}$$

$$= \int_{-\pi/a}^{0} dk'_y\, \delta\big(\varepsilon + 2g\cos(k'_y a)\big) + \int_{0}^{\pi/a} dk'_y\, \delta\big(\varepsilon + 2g\cos(k'_y a)\big) \tag{1.420}$$

$$\begin{aligned} &= \int_{-\pi/a}^{0} dk'_y\, \frac{\delta\big(k'_y - \arccos[-\varepsilon/(2g)]/a\big)}{2ga\sin(k'_y a)} \\ &\quad + \int_{0}^{\pi/a} dk'_y\, \frac{\delta\big(k'_y - \arccos[-\varepsilon/(2g)]/a\big)}{2ga\sin(k'_y a)} \end{aligned} \tag{1.421}$$

$$= \frac{1}{ga\sqrt{1-(\frac{\varepsilon}{2g})}}\,. \tag{1.422}$$

The remaining task is to evaluate the k'_x integral

$$I^n_{k'_x}(\varepsilon, \mathbf{k}) \equiv \int_{-\pi/a}^{\pi/a} dk'_x\, J_n^2\left(2\tilde{g}\sin\left(\frac{a(k'_x - k_x)}{2}\right)\right) \tag{1.423}$$

$$= \frac{2}{a}\int_{-\pi/2}^{\pi/2} dk'_x\, J_n^2\Big(2\tilde{g}\sin(k'_x - \tilde{k})\Big) \quad \text{with} \quad \tilde{k} = \frac{ak_x}{2} \tag{1.424}$$

$$= \frac{2}{a}\int_{0}^{\pi} dk'_x\, J_n^2\Big(2\tilde{g}\cos(k'_x - \tilde{k})\Big) \tag{1.425}$$

$$= \frac{2\pi}{a}\sum_{m=-\infty}^{\infty} J^2_{m+n}(\tilde{g})J^2_m(\tilde{g})\,. \tag{1.426}$$

In the last step, the integral formula derived in App. 1.13.5 was used. Collecting the results from Eqs. (1.426) and (1.422) yields the scattering time

$$\left(\frac{1}{\boldsymbol{\tau}(\varepsilon,\mathbf{k})}\right)_{nn} = \frac{\mathcal{V}_{\text{imp}}}{\hbar g a^2\sqrt{1-(\frac{\varepsilon}{2g})}}\sum_{m=-\infty}^{\infty} J^2_{m+n}(\tilde{g})J^2_m(\tilde{g}) \tag{1.427}$$

which is rather surprisingly momentum independent. Analogue steps, as in Sec. 1.9.4, lead for the current operator to

$$\mathbf{J}(\mathbf{k},t) = -2\frac{ega}{\hbar}\begin{pmatrix}\sin(k_x a - \Omega t)\\ \sin(k_y a)\end{pmatrix} \tag{1.428}$$

and a comparison with the quasienergy provides an exact expression for the y-component of the current

$$\mathbf{J}_y(\mathbf{k},t) = -\frac{e}{\hbar}\big[\nabla_{\mathbf{k}}\epsilon_{\mathbf{k}}\big]_y\,. \tag{1.429}$$

Concentrating on the contribution of the central Floquet zone to the conductivity yields

$$\lim_{\omega\to 0} \mathrm{Re}\ \sigma^{yy}(0,\omega) = \frac{e^2}{V(2\pi\hbar)^2}\int_{\mathrm{BZ}} d^2k\,[\nabla_{\mathbf{k}}\epsilon_{\mathbf{k}}]_y^2[\boldsymbol{\tau}(\varepsilon_F,\mathbf{k})]_{00}\delta(\varepsilon_F-\epsilon_{\mathbf{k}}) \tag{1.430}$$

$$\begin{aligned} &= \frac{e^2[\boldsymbol{\tau}(\varepsilon_F,\mathbf{k})]_{00}}{V(2\pi\hbar)^2}(2ga)^2 \\ &\quad\times\int_{\mathrm{BZ}} d^2k\ \sin^2(k_y a)\delta\big[\varepsilon_F+2g\cos(k_y a)\big] \end{aligned} \tag{1.431}$$

$$= \frac{2e^2}{V\pi\hbar^2}g[\boldsymbol{\tau}(\varepsilon_F,\mathbf{k})]_{00}\sqrt{1-\left(\frac{\varepsilon_F}{2g}\right)}\,. \tag{1.432}$$

Remarkably, an increase of the electric field strength in x-direction leads to a decrease of the conductivity in y-direction. One should note that the limit of vanishing electric field is not properly described by the expression above, since during the derivation it was used that the driving frequency - and thus the electric field strength - is much larger than the broadening of the Floquet bands caused by the disorder.

1.12 Summary and Outlook

In recent years there has been a growing interest in the field of non-perturbatively driven systems, which were already studied intensively in the last century. The growing activity is mainly connected with the idea of having access to the topological properties of the system under consideration. That, until now, a formalism which allows for a rigorous derivation of the conductivity from an appropriate Dyson series by means of the Floquet formalism has been missing is rather surprising. This work presents a new type of four-times Green's functions, which not only facilitates a closed analytical expression of the Floquet-Drude conductivity, but also gives a missing direct connection to scattering theory for Floquet states. The formalism is derived in a general manner. Hence, the resulting physics is independent of the type of material, and addresses a broad audience on both the theoretical as well as the experimental side. Following the formalism presented in this manuscript, a generalized Floquet Fermi's golden rule is derived which also comprises inter-Floquet-zone-scattering, like the Floquet-Umklapp scattering. Treating conductivity in this non-perturbative manner, for instance, shows that previous results have been overestimating the effect of external driving on the Drude conductivity. Concerning the scattering theory under driving, it could be shown that present theories are an approximation of the analytical result gained from the formalism presented in this work. Realistic solids are described by their atomic lattice structure, and effective-mass approximations are a rather simplistic approach. Indeed, drastic deviations of the Drude conductivity from effective-mass predictions are found. These findings point out the necessity of a revision of previous studies on conductivity in driven systems using effective models. Independent of the type of material, the findings in this work give a new fundamental insight into the field of transport under driving. This work can be expanded in various directions due to its generality. The contributions from neighboring Floquet modes to the conductivity are relevant, if the

broadening caused by the drive is comparable to the photon energy. A proper description of this regime has not been available thus far. It is well known that the first order Born approximation is valid in the weak disorder limit for static systems [90], namely if $k_F \ell_e \gg 1$. However, the calculation of higher order contributions, like the self-consistent Born approximation, might give further insight into scattering theory for Floquet states. Interference effects play a minor role in this work. Nevertheless, the formalism for weak localization in a driven systems is formulated. As already mentioned in Sec. 1.10, the investigation of the mechanisms that might lead to a suppression of localization effects is now possible. Time-dependencies of distribution function, impurities, and current operators offer further directions for extensions and might unravel new, interesting physics. The driving itself needs further considerations; some instances would be that the magnetic field was mainly neglected in this work or multiple driving frequencies.

1.13 Appendix

1.13.1 Mathematical definitions

This section contains commonly occurring mathematical definitions. The first identity used is the Dirac-identity [96]

$$\frac{1}{x \pm i0^+} = P\left(\frac{1}{x}\right) \mp i\pi\delta(x) \tag{1.433}$$

splitting a divergent fraction in a regular part, i.e. the principal value $P(\cdot)$, and a divergent part proportional to the delta-distribution $\delta(\cdot)$. During this work the 0^+-notation is used as an alternative for

$$\frac{1}{x \pm i0^+} \equiv \lim_{\epsilon \to 0^+} \frac{1}{x \pm i\epsilon}\,. \tag{1.434}$$

A particularly useful relation for the investigation of driven system is the Jacobi-Anger expansion for both sine and cosine exponent [96]

$$e^{iz\sin(\Omega t)} = \sum_{n=-\infty}^{\infty} J_n(z)e^{in\Omega t} \quad , \quad e^{iz\cos(\Omega t)} = \sum_{n=-\infty}^{\infty} i^n J_n(z)e^{in\Omega t}\,. \tag{1.435}$$

In the last equation, $J_n(\cdot)$ labels the n-th order Bessel function of the first kind. The Heaviside or step function is of particular interest for section 1.4 about Green's functions. The integral representation of the step function is

$$\Theta(t) = \lim_{\epsilon \to 0^+} \frac{i}{2\pi} \int_{-\infty}^{\infty} d\omega\, \frac{e^{-i\omega t}}{\omega + i\epsilon}\,. \tag{1.436}$$

The (inverse-) Fourier transformation has the following normalizations

$$f(\omega) = \int_{-\infty}^{\infty} dt\, f(t)e^{i\omega t}\,, \tag{1.437}$$

$$f(t) = \frac{1}{2\pi} \int_{-\infty}^{\infty} d\omega\, f(\omega)e^{-i\omega t}\,. \tag{1.438}$$

1.13.2 Drude conductivity

This section aims in a rigorous calculation of the Drude conductivity for a parabolic dispersion without any driving mechanism. First, the conductivity is calculated, taking into account all pairing of retarded and advanced Green's functions. After that, the focus is on pairings of retarded and advanced Green's functions only, leading to a divergent result. However, making further approximations regularizes the integral leading, to the correct result. This peculiarity is analyzed in detail in the following, since a rigorous discussion seems to be missing in literature thus far. The retarded and advanced Green's function of the time-independent Schrödinger equation for the parabolic dispersion are

$$G^{r,a}(E, \mathbf{k}) = \frac{1}{E - \frac{\hbar^2\mathbf{k}^2}{2m} \pm i\frac{\hbar}{2\tau}}\,. \tag{1.439}$$

The derivation of the Drude conductivity in d-dimensions

$$\sigma_0^{xx} = \frac{-\hbar^3}{2\pi d}\left(\frac{e}{m}\right)^2 \frac{1}{(2\pi)^d}\int_{V_{\mathbf{k}}} d^dk \Big[\big(G^r(E,\mathbf{k}) - G^a(E,\mathbf{k})\big)k_x \times \big(G^r(E,\mathbf{k}) - G^a(E,\mathbf{k})\big)k_x\Big] \tag{1.440}$$

can be found in standard textbooks, like Refs. [48, 49, 89, 90] and therefore omitted here. Introducing polar coordinates in the momentum space $\mathbf{k} = k(\cos(\phi), \sin(\phi))^T$ and performing the angular integration yield

$$\sigma_0^{xx} = \frac{\hbar^3}{2\pi d}\left(\frac{e}{m}\right)^2 \frac{4\Omega_d}{(2\pi)^d}\left(\frac{\hbar}{2\tau}\right)^2 \int_0^\infty dk \, \frac{k^{d+1}}{\left(\left(E - \frac{\hbar^2k^2}{2m}\right)^2 + \left(\frac{\hbar}{2\tau}\right)^2\right)^2} \tag{1.441}$$

with Ω_d being the result of the angular integration in d-dimensions. Now, the substitution

$$x = \frac{\hbar^2k^2}{2m} \quad \Leftrightarrow \quad \frac{m}{\hbar^2}dx = kdk \tag{1.442}$$

is performed such that the conductivity becomes

$$\sigma_0^{xx} = \frac{\hbar^3}{2\pi d}\left(\frac{e}{m}\right)^2 \frac{2\Omega_d}{(2\pi)^d}\left(\frac{\hbar}{2\tau}\right)^2 \left(\frac{2m}{\hbar^2}\right)^{\frac{d}{2}+1} \int_0^\infty dx \, \frac{x^{\frac{d}{2}}}{\left((x-E)^2 + \left(\frac{\hbar}{2\tau}\right)^2\right)^2} \tag{1.443}$$

$$= \frac{\hbar^3}{2\pi d}\left(\frac{e}{m}\right)^2 \frac{2\Omega_d}{(2\pi)^d}\left(\frac{\hbar}{2\tau}\right)^2 \left(\frac{2m}{\hbar^2}\right)^{\frac{d}{2}+1} E^{\frac{d}{2}-3} \underbrace{\int_0^\infty dx \, \frac{x^{\frac{d}{2}}}{\left((x-1)^2+u\right)^2}}_{=I_d(u)} \tag{1.444}$$

where the abbreviation $u = \left(\frac{\hbar}{2\tau E}\right)^2$ was used. To calculate $I_d(u)$ in either one, two or three dimensions residue analysis [116] can be performed by using

$$\int_0^\infty dx \, x^\alpha R(x) = \frac{2\pi i}{1 - e^{i2\pi\alpha}} \sum_{z\neq 0} \mathrm{res}_z\big(\zeta^\alpha R(\zeta)\big) \quad \text{for } d \in \{1,3\}\,, \tag{1.445}$$

$$\int_0^\infty dx \, R(x) = -\sum_{z\neq 0} \mathrm{res}_z\big(R(\zeta)\ln(\zeta)\big) \quad \text{for } d = 2\,. \tag{1.446}$$

The main interest is in the two dimensional case. Hence, only $I_2(u)$ is analyzed in the following. $I_2(u)$ has two double poles at

$$z_\pm = 1 \pm i\sqrt{u} \tag{1.447}$$

and the corresponding residues are governed by

$$\begin{aligned}
\mathrm{res}_z\big(R(\zeta)\ln(\zeta)\big) &= \lim_{z\to z_\pm}\frac{\partial}{\partial z}(z-z_\pm)^2\frac{z\ln(z)}{(z-z_+)^2(z-z_-)^2} && (1.448)\\
&= \lim_{z\to z_\pm}\frac{\partial}{\partial z}\frac{z\ln(z)}{(z-z_\mp)^2} && (1.449)\\
&= \frac{\ln(z_\pm)+1}{(z_\pm-z_\mp)^2}-\frac{2z_\pm\ln(z_\pm)}{(z_\pm-z_\mp)^3} && (1.450)\\
&= \frac{(z_\pm-z_\mp)\ln(z_\pm)+(z_\pm-z_\mp)-2z_\pm\ln(z_\pm)}{(z_\pm-z_\mp)^3} && (1.451)\\
&= \frac{-(z_\pm+z_\mp)\ln(z_\pm)+(z_\pm-z_\mp)}{(z_\pm-z_\mp)^3}\,. && (1.452)
\end{aligned}$$

Since the branch cut is set along the positive real axis, the integral I_2 becomes

$$\begin{aligned}
I_2(u) &= \frac{2\ln(z_+)}{-8iu\sqrt{u}}-\frac{1}{-4u}+\frac{2\ln(z_-)}{8iu\sqrt{u}}-\frac{1}{-4u} && (1.453)\\
&= \frac{1}{2u}+\frac{\ln(z_-)-\ln(z_+)}{4iu\sqrt{u}} && (1.454)\\
&= \frac{\pi+2\arctan\left(\frac{1}{\sqrt{u}}\right)+2\sqrt{u}}{4u\sqrt{u}} && (1.455)\\
&\approx \frac{\pi}{2u\sqrt{u}} && (1.456)
\end{aligned}$$

where, in the last step the weak disorder limit was used, namely that $E\tau \gg \hbar$. Hence, the leading contribution to the Drude conductivity is

$$\sigma_0^{xx} = \frac{e^2}{2\pi\hbar}\frac{E\tau}{\hbar}\,. \tag{1.457}$$

In the last equation, $\Omega_2 = \pi$ was used. The particle density is the energy integral over density of states and distribution function. The density of states in two dimensions is given by

$$D = \frac{1}{(2\pi)^2}\int_{V_{\mathbf{k}}} d^2k\,\delta\left(E-\frac{\hbar^2\mathbf{k}^2}{2m}\right) = \frac{m}{2\pi\hbar^2}\,. \tag{1.458}$$

The current carriers are electrons such that the particle density at zero temperature, together with the above result for the density of states, becomes

$$n = \frac{mE}{2\pi\hbar^2}\,. \tag{1.459}$$

Finally, inserting the last equation into Eq. (1.457) yields the well known Drude conductivity

$$\sigma_0^{xx} = \frac{e^2\tau n}{m}\,. \tag{1.460}$$

Now, the focus is on pairings of a retarded and an advanced Green's function only, whereas the other pairings are neglected, such that the conductivity becomes

$$\sigma_0^{xx} = \frac{\hbar^3}{4\pi}\left(\frac{e}{m}\right)^2 \frac{2}{(2\pi)^2}\int_{V_\mathbf{k}} d^2k\, k_x^2 G^r(E,\mathbf{k})G^a(E,\mathbf{k})\,. \tag{1.461}$$

Performing the substitution given in Eq. (1.442) yields, for the conductivity,

$$\sigma_0^{xx} = \frac{\hbar e^2}{(2\pi)^2 E}\int_0^\infty dx\, \frac{x}{(x-1)^2+u}\,. \tag{1.462}$$

The integral in the last equation is logarithmically divergent. This suggests that neglecting the pairings of retarded and advanced Green's function is not possible. However, reformulating the product of retarded and advanced Green's function as Dirac series regularizes the divergent integral. The limit of a Lorentz curve is the delta distribution

$$\lim_{\varepsilon\to 0}\frac{\varepsilon}{x^2+\varepsilon^2} = \pi\delta(x)\,. \tag{1.463}$$

Using the above, it can be shown that for the product of Green's functions holds that

$$G^r(E,\mathbf{k})G^a(E,\mathbf{k}) = \frac{1}{\left(E-\frac{\hbar^2\mathbf{k}^2}{2m}\right)^2+\left(\frac{\hbar}{2\tau}\right)^2} \tag{1.464}$$

$$\approx \left(\frac{2\tau}{\hbar}\right)\lim_{\tau\to\infty}\frac{\left(\frac{\hbar}{2\tau}\right)}{\left(E-\frac{\hbar^2\mathbf{k}^2}{2m}\right)^2+\left(\frac{\hbar}{2\tau}\right)^2} \tag{1.465}$$

$$= \pi\left(\frac{2\tau}{\hbar}\right)\delta\left(E-\frac{\hbar^2\mathbf{k}^2}{2m}\right)\,. \tag{1.466}$$

Performing the momentum integration in Eq. (1.461) yields

$$\sigma_0^{xx} = \frac{e^2}{2\pi\hbar}\frac{E\tau}{\hbar} \tag{1.467}$$

which is equivalent to the result obtained in Eq. (1.457).

1.13.3 Cooperon divergence at $q = 0$

The aim is to prove that the Cooperon has a divergence at $\mathbf{q} = 0$ and that there is no divergence stemming from a Cooperon build from pairing only retarded or advanced Green's functions. In two dimensions, the weak localization correction to the conductivity is governed by [48, 89, 90]

$$\sigma_{\mathrm{wl}} = \frac{\hbar^3}{2\pi V}\left(\frac{e}{m}\right)^2\frac{1}{(2\pi)^4}\int_{V_\mathbf{k}}\int_{V_\mathbf{q}} d^2k\, d^2q\, k_x^2 \tag{1.468}$$

$$\times\Big[G^r(E,\mathbf{k})G^a(E,\mathbf{k})\Big]\mathcal{C}(E,\mathbf{q})\Big[G^r(E,\mathbf{k})G^a(E,\mathbf{k})\Big] \tag{1.469}$$

together with the Cooperon

$$\mathcal{C}(E,\mathbf{q}) = \mathcal{V}_{\mathrm{imp}}\left[1-\mathcal{V}_{\mathrm{imp}}\frac{1}{(2\pi)^2}\int_{V_\mathbf{k}} d^2k\, G^r(E,\mathbf{k}-\mathbf{q})G^a(E,\mathbf{k})\right]^{-1}\,. \tag{1.470}$$

To prove the existence of the divergence of the weak localization correction to the conductivity, it must be shown that the denominator of the Cooperon $\mathcal{C}$ vanishes with $\mathbf{q} \to 0$. First, the correlation function Π is defined

$$\Pi^{r,a}(\mathbf{q}) \equiv \mathcal{V}_{\text{imp}} \frac{1}{(2\pi)^2} \int_{V_{\mathbf{k}}} d^2k \, G^r(E, \mathbf{k}-\mathbf{q}) G^a(E, \mathbf{k}) \,. \tag{1.471}$$

To confirm the statement about the divergence above, it must be verified that

$$\Pi^{r,a}(0) = \mathcal{V}_{\text{imp}} \frac{1}{(2\pi)^2} \int d^2k \frac{1}{E - \frac{\hbar^2\mathbf{k}^2}{2m} + i\frac{\hbar}{2\tau}} \frac{1}{E - \frac{\hbar^2\mathbf{k}^2}{2m} - i\frac{\hbar}{2\tau}} \tag{1.472}$$

$$\stackrel{!}{=} 1 \,. \tag{1.473}$$

For the correlation function, the same substitution as in Eqs. (1.442) yields

$$\Pi^{r,a}(0) = \mathcal{V}_{\text{imp}} \frac{m}{2\pi\hbar^2} \int_0^\infty dx \frac{1}{x - (E + i\frac{\hbar}{2\tau})} \frac{1}{x - (E - i\frac{\hbar}{2\tau})} \,. \tag{1.474}$$

The latter has two first order poles at $z_\pm = E \pm i\frac{\hbar}{2\tau}$. To use Eq. (1.446), the residuum

$$\lim_{z \to z_\pm} (z - z_\pm) \frac{\ln(z)}{(z - z_+)(z - z_-)} = \frac{\ln(z_\pm)}{(z_\pm - z_\mp)} \tag{1.475}$$

is needed. This allows one to calculate the integral for the correlation function in the last equation. Hence, Eq. (1.474) becomes

$$\Pi^{r,a}(0) = \mathcal{V}_{\text{imp}} \frac{m}{2\pi\hbar^2} \left(\frac{\ln(z_-) - \ln(z_+)}{z_+ - z_-} \right) \tag{1.476}$$

$$= \mathcal{V}_{\text{imp}} \frac{m}{2\pi\hbar^2} \left(\frac{\pi + 2\arctan\left(\frac{2\tau E}{\hbar}\right)}{\frac{\hbar}{\tau}} \right) \,. \tag{1.477}$$

Taking the limit of weak disorder, $E\tau \gg \hbar$ finally proves the $\mathbf{q} = 0$ divergence of the Cooperon

$$\lim_{E\tau \to \infty} \Pi^{r,a}(0) = \frac{2\pi \mathcal{V}_{\text{imp}} D\tau}{\hbar} = 1 \,. \tag{1.478}$$

In the last step, it was used that the scattering time in first order Born approximation is given by $\hbar/\tau = 2\pi\mathcal{V}_{\text{imp}} D$. Besides, the density of states D given in Eq. (1.458) was inserted. Next, it is shown that the weak localization correction stemming from pairs of two retarded or advanced Green's functions does not have a pole at $\mathbf{q} = 0$. The calculations are only presented for the retarded case, since the other follows from analogue steps. The correlation function for the retarded Green's functions is

$$\Pi^{r,r}(0) = \mathcal{V}_{\text{imp}} \frac{1}{(2\pi)^2} \int d^2k \frac{1}{E - \frac{\hbar^2k^2}{2m} + i\frac{\hbar}{2\tau}} \frac{1}{E - \frac{\hbar^2k^2}{2m} + i\frac{\hbar}{2\tau}} \tag{1.479}$$

having one second order pole at $z_0 = E + i\frac{\hbar}{2\tau}$. Again, the residuum must be calculated

$$\lim_{z \to z_0} \frac{\partial}{\partial z} (z - z_0) \frac{\ln(z)}{(z - z_0)^2} = \frac{1}{z_0} \tag{1.480}$$

to use Eq. (1.446). A substitution as in Eqs. (1.442) yields

$$\Pi^{r,r}(0) = \mathcal{V}_{\text{imp}} \frac{m}{2\pi\hbar^2} \int_0^\infty dx \frac{1}{\left[x - (E + i\frac{\hbar}{2\tau})\right]^2} \tag{1.481}$$

$$= \mathcal{V}_{\text{imp}} \frac{m}{2\pi\hbar^2} \frac{1}{E + i\frac{\hbar}{2\tau}} \tag{1.482}$$

and, in the weak disorder limit,

$$\lim_{E\tau\to\infty} \Pi^{r,r}(0) = \lim_{E\tau\to\infty} \frac{1}{\pi} \frac{\hbar}{2E\tau + i\hbar} = 0\,. \tag{1.483}$$

Hence, there is no divergent contribution to the conductivity stemming from a Cooperon of only retarded or advanced Green's functions. The Drude part of the weak localization has already been calculated in this section, since it differs from the integrand of the Drude conductivity by just a constant

$$\left[G^r(E,\mathbf{k}) - G^a(E,\mathbf{k})\right]^2 = -\left(\frac{\hbar}{\tau}\right)^2 \left[G^r(E,\mathbf{k})G^a(E,\mathbf{k})\right]^2. \tag{1.484}$$

Finally, another integral approximation is proven to complete the analysis of the weak localization. Ref. [89] provides the integral approximation

$$f^{m,n} \equiv \mathcal{V}_{\text{imp}} \frac{1}{(2\pi)^2} \int_{V_{\mathbf{k}}} d^2k \left[G^r(E,\mathbf{k})\right]^m \left[G^a(E,\mathbf{k})\right]^n \tag{1.485}$$

$$= \left(\frac{\tau}{\hbar}\right)^{m+n-2} i^{n-m} \frac{(m+n-2)!}{(m-1)!(n-1)!}\,. \tag{1.486}$$

The focus is only on the case $m = n = 2$. The substitution given in Eq. (1.442) transforms Eq. (1.485) into

$$f^{2,2} = \mathcal{V}_{\text{imp}} \frac{m}{2\pi\hbar^2} \int_0^\infty dx \left[\frac{1}{x - (E + i\frac{\hbar}{2\tau})} \cdot \frac{1}{x - (E - i\frac{\hbar}{2\tau})}\right]^2 \tag{1.487}$$

having two second order poles at $z_\pm = E \pm i\frac{\hbar}{2\tau}$ and residues

$$\lim_{z\to z_\pm} \frac{\partial}{\partial z}(z - z_\pm)^2 \frac{\ln(z)}{(z - z_+)^2(z - z_-)^2} = \lim_{z\to z_\pm} \frac{\partial}{\partial z} \frac{\ln(z)}{(z - z_\mp)^2} \tag{1.488}$$

$$= \frac{1}{z_\pm(z_\pm - z_\mp)^2} - \frac{2\ln(z_\pm)}{(z_\pm - z_\mp)^3}\,. \tag{1.489}$$

This finally yields

$$\lim_{E\tau\to\infty} f^{2,2} = \lim_{E\tau\to\infty} \frac{\hbar}{2\pi\tau} \left(\frac{-2E}{\left(E^2 + \left(\frac{\hbar}{2\tau}\right)^2\right)\left(\frac{\hbar}{\tau}\right)^2} + \frac{2\pi + 4\arctan\left(\frac{2\tau E}{\hbar}\right)}{\left(\frac{\hbar}{\tau}\right)^3}\right) \tag{1.490}$$

$$= 2\left(\frac{\tau}{\hbar}\right)^2. \tag{1.491}$$

The last equation justifies Eq. (1.486) for $m = n = 2$ in the weak disorder limit.

1.13.4 Graphene with linearly polarized light

The following is based on Ref. [117]. The notation is widely adopted from this article. In this section, an attempt is made to solve the time-dependent Schrödinger equation for graphene in Dirac approximation, in the presence of linearly polarized light propagating in y-direction

$$H(t) = v_F \begin{pmatrix} 0 & \pi_x - i\pi_y \\ \pi_x + i\pi_y & 0 \end{pmatrix} \tag{1.492}$$

together with

$$\boldsymbol{\pi} = \mathbf{p} - e\mathbf{A}(t) \quad , \quad \mathbf{A}(t) = \begin{pmatrix} \frac{E_0}{\omega}\cos(ky - \omega t) \\ 0 \end{pmatrix} . \tag{1.493}$$

The solution of the time-dependent Schrödinger equation

$$i\hbar\frac{\partial}{\partial t}\boldsymbol{\psi} = H(t)\boldsymbol{\psi} \tag{1.494}$$

is a two component spinor

$$\boldsymbol{\psi} = \begin{pmatrix} \psi_A \\ \psi_B \end{pmatrix} . \tag{1.495}$$

Inserting into the Schrödinger equation and multiplying with $i\hbar\frac{\partial}{\partial t}$ from the left yield the two coupled equations

$$i\hbar\frac{\partial}{\partial t} v_F\big(\pi_x - i\pi_y\big)\psi_B = -\hbar^2\frac{\partial^2}{\partial t^2}\psi_A \tag{1.496}$$

$$i\hbar\frac{\partial}{\partial t} v_F\big(\pi_x + i\pi_y\big)\psi_A = -\hbar^2\frac{\partial^2}{\partial t^2}\psi_B \, . \tag{1.497}$$

Performing the time derivative and inserting again the Schrödinger equation, it is obtained that

$$-i\hbar e E_0 v_F \sin(ky - \omega t)\psi_B + v_F^2(\pi_x - i\pi_y)(\pi_x + i\pi_y)\psi_A = -\hbar^2\frac{\partial}{\partial t^2}\psi_A \tag{1.498}$$

$$-i\hbar e E_0 v_F \sin(ky - \omega t)\psi_A + v_F^2(\pi_x + i\pi_y)(\pi_x - i\pi_y)\psi_B = -\hbar^2\frac{\partial}{\partial t^2}\psi_B \, . \tag{1.499}$$

In the following the expression

$$(\pi_x \mp i\pi_y)(\pi_x \pm i\pi_y) = \pi_x^2 + \pi_y^2 \mp i\pi_y\pi_x \pm i\pi_x\pi_y \tag{1.500}$$

$$\begin{aligned} &= -\hbar^2\frac{\partial^2}{\partial x^2} + i\hbar e\frac{\partial}{\partial x}A_x + i\hbar e A_x\frac{\partial}{\partial x} + e^2A_x^2 \\ &\quad - \hbar^2\frac{\partial^2}{\partial y^2} + i\hbar e\frac{\partial}{\partial y}A_y + i\hbar e A_y\frac{\partial}{\partial y} + e^2A_y^2 \\ &\quad \mp \hbar e\left[\frac{\partial}{\partial x}A_y - \frac{\partial}{\partial y}A_x + A_x\frac{\partial}{\partial y} - A_y\frac{\partial}{\partial x}\right] \end{aligned} \tag{1.501}$$

$$= -\hbar^2\frac{\partial^2}{\partial x^2} + 2i\hbar e A_x\frac{\partial}{\partial x} + e^2A_x^2 - \hbar^2\frac{\partial^2}{\partial y^2} \pm \hbar e\Big(\frac{\partial A_x}{\partial y}\Big) \tag{1.502}$$

is needed where in the last step $A_y = 0$ was used. Introducing the same abbreviations as in Ref. [117]

$$\xi \equiv \frac{eE_0 v_F}{\omega} \quad , \quad \phi \equiv ky - \omega t \tag{1.503}$$

the equation (7) from Ref. [117] is obtained

$$\begin{aligned} -\hbar^2 \left[v_F^2 \left(\frac{\partial^2 \boldsymbol{\psi}}{\partial x^2} + \frac{\partial^2 \boldsymbol{\psi}}{\partial y^2} \right) - \frac{\partial^2 \boldsymbol{\psi}}{\partial t^2} \right] + 2i\hbar\xi v_F \cos(\phi) \frac{\partial \boldsymbol{\psi}}{\partial x} \\ + \Big[\xi^2 \cos^2(\phi) - \xi v_F \hbar \sigma^z k \sin(\phi) - i\hbar\omega\xi\sigma^x \sin(\phi) \Big] \boldsymbol{\psi} = 0 \,. \end{aligned} \tag{1.504}$$

The authors of Ref. [117] suggest the ansatz

$$\boldsymbol{\psi} = e^{i\frac{p_x x}{\hbar} + i\frac{p_y y}{\hbar} - i\frac{\varepsilon t}{\hbar}} \boldsymbol{F}(\phi) \tag{1.505}$$

to solve the Eq. (1.504), where ε is a parameter that one is free to choose. The second derivatives of the wave function $\boldsymbol{\psi}$, with respect to position coordinates and time, are needed: first, the second derivative with respect to y

$$-\hbar^2 \frac{\partial^2 \boldsymbol{\psi}}{\partial y^2} = p_y^2 \boldsymbol{\psi} - 2i\hbar k p_y e^{i\frac{p_x x}{\hbar} + i\frac{p_y y}{\hbar} - i\frac{\varepsilon t}{\hbar}} \frac{\partial \boldsymbol{F}(\phi)}{\partial \phi} - \hbar^2 k^2 e^{i\frac{p_x x}{\hbar} + i\frac{p_y y}{\hbar} - i\frac{\varepsilon t}{\hbar}} \frac{\partial^2 \boldsymbol{F}(\phi)}{\partial \phi^2} \tag{1.506}$$

with respect to time

$$-\hbar^2 \frac{\partial^2 \boldsymbol{\psi}}{\partial t^2} = \varepsilon^2 \boldsymbol{\psi} - 2i\hbar\varepsilon\omega e^{i\frac{p_x x}{\hbar} + i\frac{p_y y}{\hbar} - i\frac{\varepsilon t}{\hbar}} \frac{\partial \boldsymbol{F}(\phi)}{\partial \phi} - \hbar^2 \omega^2 e^{i\frac{p_x x}{\hbar} + i\frac{p_y y}{\hbar} - i\frac{\varepsilon t}{\hbar}} \frac{\partial^2 \boldsymbol{F}(\phi)}{\partial \phi^2} \tag{1.507}$$

and finally, the derivative with respect to x

$$-\hbar^2 \frac{\partial^2 \boldsymbol{\psi}}{\partial x^2} = p_x^2 \boldsymbol{\psi} \,. \tag{1.508}$$

The parameter ε is chosen such that it cancels the contributions from the position and time derivatives

$$\varepsilon^2 \equiv v_F^2 \big(p_x^2 + p_y^2 \big) \quad , \quad \eta \equiv \varepsilon\omega - v_F^2 k p_y \,. \tag{1.509}$$

Collecting the previous results, one obtains equation (9) from Ref. [118]

$$\begin{aligned} -\hbar^2 \big(v_F^2 k^2 - \omega^2 \big) \frac{\partial^2 \boldsymbol{F}(\phi)}{\partial \phi^2} + 2i\hbar\eta \frac{\partial \boldsymbol{F}(\phi)}{\partial \phi} + \big[-2\xi v_F p_x \cos(\phi) \\ - \xi v_F \hbar \sigma^z k \sin(\phi) + \xi^2 \cos^2(\phi) - i\hbar\omega\xi\sigma^x \sin(\phi) \big] \boldsymbol{F}(\phi) = 0 \,. \end{aligned} \tag{1.510}$$

Solving the differential equation above is a rather formidable task. However, the authors of Ref. [118] claim that the results of Ref. [117] are still valid in the long-wavelength limit. The intention of this limit seems to aim in neglecting the second derivative of the function $\boldsymbol{F}$. Assuming that such a limit exists, the resulting differential equation, Eq. (9) of Ref. [117], is solved in Ref. [117] by the ansatz

$$\boldsymbol{F}(\phi) = e^{G(\phi)} \boldsymbol{u} \,, \tag{1.511}$$

where $\boldsymbol{u}$ is the solution of the free Dirac equation

$$\boldsymbol{u} = \frac{1}{\sqrt{2}} \begin{pmatrix} e^{-i\frac{\varphi}{2}} \\ e^{i\frac{\varphi}{2}} \end{pmatrix} \quad , \quad \varphi = \tan\left(\frac{p_y}{p_x}\right) . \tag{1.512}$$

Furthermore, the exponent in the ansatz in Eq. (1.511) is calculated as

$$\begin{aligned} 2i\hbar\eta\, G(\phi) = \int \Big[& 2\xi v_F p_x \cos(\phi) + \xi v_F \hbar \sigma^z k \sin(\phi) && (1.513) \\ & - \xi^2 \cos^2(\phi) + i\hbar\omega\xi\sigma^x \sin(\phi) \Big] d\phi && (1.514) \end{aligned}$$

leading to

$$\begin{aligned} G(\phi) = & -i\frac{\xi v_F p_x}{\hbar\eta} \sin(\phi) + i\frac{\xi v_F k}{2\eta}\sigma^z \cos(\phi) + i\frac{\xi^2}{4\hbar\eta}\phi \\ & + i\frac{\xi^2}{8\hbar\eta} \sin(2\phi) - \frac{\omega\xi}{2\eta}\sigma^x \cos(\phi) . \end{aligned} \tag{1.515}$$

This is equal to equation (11) from Ref. [117], except for the sign of the second term proportional to σ^z. However, the derivative of G does not commute with G

$$\left[\frac{\partial G(\phi)}{\partial\phi}, G(\phi)\right] \neq 0 , \tag{1.516}$$

leading to an uncontrolled approximation of the solution of the differential equation (1.510) .

1.13.5 Proof of integral formula for square of Bessel function

The aim is to prove the integral identity for the square of Bessel function with cosine argument

$$I_n(x) \equiv \int_0^\pi d\theta\, J_m^2(2x\cos(\theta - \vartheta)) = \pi \sum_{n=-\infty}^{\infty} J_{n+m}^2(x) J_n^2(x) . \tag{1.517}$$

First, the functions

$$u(t, x, \phi) = \sum_{n=-\infty}^{\infty} u_n(x, \phi) e^{-in\Omega t} = e^{-ix\cos(\phi+\Omega t)}, \tag{1.518}$$

$$u_n(x, \phi) = J_n(x) e^{-in(\phi+\pi/2)}, \tag{1.519}$$

are defined, which are used subsequently. The right hand side of Eq. (1.517) can be expanded to

$$\begin{aligned} I_n(x) = & \frac{1}{2}\int_0^{2\pi} d\theta \sum_{m,m'=-\infty}^{\infty} J_{m+n}(x) J_m(x) J_{m'+n}(x) J_{m'}(x) \\ & \times e^{i\theta(m'-m)} e^{i\vartheta(m-m')} \end{aligned} \tag{1.520}$$

where one summation is canceled by the Kronecker delta that arises when the integral is performed. Now, the Fourier component

$$c^n(x,\theta,\vartheta) = \sum_{m=-\infty}^{\infty} \left[u_{n+m}(x,\theta)\right]^* u_m(x,\vartheta) \tag{1.521}$$

are defined, where summation over the Fourier series yields

$$\begin{aligned} c(t,x,\theta,\vartheta) &= \sum_{n=-\infty}^{\infty} c^n(x,\theta,\vartheta) e^{in\Omega t} && (1.522)\\ &= \sum_{n,m=-\infty}^{\infty} \left[u_{n+m}(x,\theta)\right]^* u_m(x,\vartheta) e^{in\Omega t} && (1.523)\\ &= \sum_{n,m=-\infty}^{\infty} \left[u_n(x,\theta)\right]^* u_m(x,\vartheta) e^{i(n-m)\Omega t} && (1.524)\\ &= \left[u(t,x,\theta)\right]^* u(t,x,\vartheta) && (1.525) \end{aligned}$$

which is correct for any choice of $u_n(x,\theta)$ and not only for the present one. Nevertheless, for the present case, using an addition theorem for trigonometric functions, one obtains

$$\begin{aligned} \left[u(t,x,\theta)\right]^* u(t,x,\vartheta) &= e^{-i2x\sin\left(\Omega t+\frac{\theta+\vartheta}{2}\right)\sin\left(\frac{\theta-\vartheta}{2}\right)} && (1.526)\\ &= \sum_{n=-\infty}^{\infty} J_n\left(2x\sin\left(\frac{\theta-\vartheta}{2}\right)\right) e^{-in\left(\frac{\theta+\vartheta}{2}\right)} e^{-in\Omega t} && (1.527) \end{aligned}$$

where, in the last step, the Jacobi-Anger expansion was used. A comparison with Eq. (1.522) allows one to identify

$$c^n(x,\theta,\vartheta) = J_n\left(2x\sin\left(\frac{\theta-\vartheta}{2}\right)\right) e^{in\left(\frac{\theta+\vartheta}{2}+\pi\right)} \tag{1.528}$$

where $J_{-n}(x) = (-1)^n J_n(x)$ was used. Finally, integrating the absolute squared of the quantity above as well as substitution provide the desired integral formula

$$\begin{aligned} I_n(x) &= \frac{1}{2}\int_0^{2\pi} d\theta\, |c^n(x,\theta,\vartheta)|^2 && (1.529)\\ &= \frac{1}{2}\int_0^{2\pi} d\theta\, J_n^2\left(2x\sin\left(\frac{\theta-\vartheta}{2}\right)\right) && (1.530)\\ &= \int_0^{\pi} d\theta\, J_n^2\left(2x\sin\left(\theta-\vartheta\right)\right)\,. && (1.531) \end{aligned}$$

Remarkably, the integral is independent of the shift ϑ.

Chapter 2

Topology in driven systems

2.1 Introduction

The integer quantum Hall effect [119, 120] marks, in hindsight, the inception of the field of topological insulators [121, 122]. This discovery was preceded a few years by Hofstadter's seminal work on hopping models on a two-dimensional square lattice in a perpendicular magnetic field [123]. The celebrated Hofstadter butterfly contains the Landau level structure, underlying the quantum Hall effect in the limit of small fluxes per unit cell. The relation of the band structure to the Hall conductance at general flux was clarified [124] in terms of Chern numbers [125] shortly afterwards. Moreover, an important recent direction of work in the area of topological insulators are systems under external driving, mainly by electromagnetic radiation, and the formation of nontrivial topological phases dubbed Floquet topological insulators [1–3, 23, 126–130]. In fact, the study of light-matter interaction is one of the fastest growing research areas in physics. Here, two-dimensional systems with underlying honeycomb lattice structure have attracted particular interest, including graphene [2, 22, 23, 55, 131–136], silicene [43, 45], germanene [45, 137], and transition metal dichalcogenides [138]. To access e.g. the feasibility of ac-driven fields to generate a finite spin polarization of carriers in graphene, the effect of periodically driven spin-orbit coupling was studied in Refs. [139, 140].

Furthermore, as seen from the quantum Hall effect [120], the topological properties of two-dimensional systems are also drastically altered by applying a perpendicular magnetic field, also leading to fractal structures as the Hofstadter butterfly [123, 141–149]. The question arises in which way an external periodic driving can modify or destroy the fractal structure. Moreover, following the seminal paper by Rudner *et al.*, Ref. [129], it becomes clear that the topology analysis of driven systems needs a different approach compared to the static case, which goes beyond the Chern number calculation.

The pioneering work of measuring the Hofstadter butterfly in móire superlattices [150], which shows the possibility of measuring the Hofstadter butterfly on a hexagonal lattice structure as well, underlines the experimental realizability of the theory developed in this work. Utilizing superlattice structures, one can lower the necessary magnetic field to easily accessible field strengths of about tens of Tesla. Furthermore, the formation of Floquet bands does not only exist on paper. Using ARPES methods, the periodic band structure was resolved in momentum space, and even the gap opening of driven topological insulators was realized and measured [151]. Thus,

the path to experimental accessibility has already been paved by modern techniques and, the study presented in this work aims to give a better understanding of the fundamental building blocks by focusing on a single graphene sheet, subjected to a strong perpendicular magnetic field and externally driven by polarized light.
First, the Hofstadter butterfly problem [123] on the honeycomb lattice [141, 142, 145, 152] is treated in a rigorous manner, where the periodicity of the Hofstadter spectrum of the hexagonal lattice is explicitly proven. Section 2.9.3 aims to generalize the Hofstadter problem for the case with periodic driving and focus on circularly polarized light. The topological properties of the Floquet-Hofstadter problem are characterized with Chern numbers and W_3-invariants. This invariant is thereby compared with the often used summation over Chern numbers in the truncated Floquet space for different frequencies and intensities. (Reprinted text with permission from [153]. Copyright (2019) by the American Physical Society.)

2.2 The time evolution operator

This section gives a brief overview of time evolution operators. They are a major ingredient for the topological analysis of driven systems, and will be used in the following. For time-independent systems described by a Hamiltonian H, the time evolution operator is governed by the exponential of the Hamiltonian multiplied with time

$$U(t,t') = e^{-\frac{i}{\hbar}H\cdot(t-t')} \ , \tag{2.1}$$

whereas, for a general time-dependent system described by $H(t)$ the construction of the time evolution operator is, in general, delicate. However, the evolution in time is formally governed by

$$U(t,t') = \mathcal{T}\exp\left[-\frac{i}{\hbar}\int_t^{t'} d\tau H(\tau)\right] \tag{2.2}$$

where the difficulty is in the time ordering operator $\mathcal{T}$. The latter is necessary if the Hamiltonian $H(t)$ does not commute with itself at different times, $[H(t), H(t')] \neq 0$. Nevertheless, the time evolution operator always fulfills the time-dependent Schrödinger equation (1.2)

$$i\hbar\frac{\partial}{\partial t}U(t,t') = H(t)U(t,t') \tag{2.3}$$

and can be constructed as

$$U(t,t') = \sum_\alpha |\psi_\alpha(t)\rangle \langle\psi_\alpha(t')| \tag{2.4}$$

if the solutions of the time-dependent Schrödinger equation $|\psi_\alpha(t)\rangle$ are known. In the case of a time-periodic Hamiltonian [20], $H(t) = H(t+T)$, the wave functions are Floquet states (1.3) and

$$U(t,0) = \sum_\alpha e^{-\frac{i}{\hbar}\varepsilon_\alpha t} |u_\alpha(t)\rangle \langle u_\alpha(0)| \tag{2.5}$$

where, without loss of generality, $t' = 0$. Even if the Hamiltonian is periodic in time, this does in general not hold for the corresponding time evolution operator. As a consequence, the topological properties cannot be directly calculated from the time evolution operator, as discussed further in Sec. 2.7.

2.3 Chern number

First, elementary principles and results of Chern numbers are recalled, since they are an indispensable part of the topological study in the following sections. This section follows the historical growth of topology, rather than trying to give an introduction to topology with full mathematical rigor. M. V. Berry found that the wave function of an adiabatically evolving system can be written as [154]

$$|\psi(t)\rangle = \exp\left[-\frac{i}{\hbar}\int_0^t dt' E_n\big(\mathbf{R}(t')\big)\right]\exp\Big[i\gamma_n(t)\Big]\big|n\big(\mathbf{R}(t)\big)\big\rangle \tag{2.6}$$

where the first factor is a dynamical phase factor and

$$H(\mathbf{R})\,|n(\mathbf{R})\rangle = E_n(\mathbf{R})\,|n(\mathbf{R})\rangle \ . \tag{2.7}$$

$\mathbf{R}$ labels the parameter space. The geometrical phase is given by the circuit integral along a path C in the parameter space

$$\gamma_n(C) = i\oint_{C=\partial S}\mathbf{A}_n(\mathbf{R})\cdot d\mathbf{R} = \int_S \mathbf{F}_n(\mathbf{R})\cdot d\mathbf{S} \tag{2.8}$$

where, in the last step, Stoke's theorem was applied, and, with the Berry connection $\mathbf{A}_n$ and the Berry curvature $\mathbf{F}_n$,

$$\mathbf{A}_n(\mathbf{R}) = \langle n(\mathbf{R})|\,\nabla_{\mathbf{R}}\,|n(\mathbf{R})\rangle \tag{2.9}$$

$$\mathbf{F}_n(\mathbf{R}) = i\big\langle\nabla_{\mathbf{R}}n(\mathbf{R})\big|\times\big|\nabla_{\mathbf{R}}n(\mathbf{R})\big\rangle \tag{2.10}$$

were used. Identifying the parameter space $\mathbf{R}$ as a two-dimensional Brillouin zone leads to the Chern number [155] of the n-th band

$$C_n = \frac{1}{2\pi i}\int_{BZ} d^2k\, F_n(\mathbf{k}) \tag{2.11}$$

with the Berry connection [125]

$$F_n(\mathbf{k}) = \partial_{k_x}A_n^y(\mathbf{k}) - \partial_{k_y}A_n^x(\mathbf{k}) \quad \text{and} \quad A_n^i(\mathbf{k}) = \big\langle n(\mathbf{k})\big|\partial_{k_i}\big|n(\mathbf{k})\big\rangle \ . \tag{2.12}$$

The Chern number was later used to explain the quantized Hall conductance [124]

$$\sigma_H = \frac{e^2}{h}\sum_n^{\text{occupied}} C_n \tag{2.13}$$

with the sum over all occupied bands. Some years later, Haldane proposed a model exhibiting a quantum Hall effect without Landau levels [156]. The existence of such a state of matter is related to the nonzero Chern number.

2.4 Topology in odd dimension

There is a topological invariant in one dimension for operators that map the Brillouin zone, i.e. a circle, onto the space of unitary $m\times m$ matrices. This invariant is defined by

$$W_1[U_k] = \frac{1}{2\pi}\int_{BZ} dk\,\mathrm{tr}\big[U_k^{-1}(T)i\partial_k U_k(T)\big] \ . \tag{2.14}$$

Kitagawa *et al.* [126] showed that, in the basis of Floquet states, the invariant is

$$W_1[U_k] = \sum_\alpha \frac{T}{2\pi} \int_{BZ} dk \, \frac{d\varepsilon_\alpha(k)}{dk} \tag{2.15}$$

and can be interpreted as averaged group velocity of a Floquet band. This invariant can be related to quantization of pumped charge [157]. Let $\{U_\mathbf{k}\}$ be the set of maps from the ℓ-dimensional torus T_ℓ to the space of $m \times m$ unitary matrices $\mathrm{U}(m)$. There is a nontrivial topological invariant associated with the homotopy group of $\mathrm{U}(m)$ in every odd dimension [158]. Especially in three dimensions, $\mathbf{k} \in \mathbb{R}^3$, the topological invariant reads [21, 129]

$$W_3[U_\mathbf{k}] = \frac{1}{24\pi^2} \int_{\mathrm{BZ}} d^3k \, \varepsilon_{\alpha\beta\gamma} \mathrm{tr}\big[(U_\mathbf{k}^{-1}\partial_{\mathbf{k}_\alpha} U_\mathbf{k})(U_\mathbf{k}^{-1}\partial_{\mathbf{k}_\beta} U_\mathbf{k})(U_\mathbf{k}^{-1}\partial_{\mathbf{k}_\gamma} U_\mathbf{k})\big] \tag{2.16}$$

where $\varepsilon_{\alpha\beta\gamma}$ is the antisymmetric tensor and $\mathbf{k}$ is integrated over the first Brillouin zone, given that $U_\mathbf{k}$ is periodic in all three dimensions [159]

$$\begin{aligned} U_\mathbf{k} = U(k_x, k_y, k_z) &= U(k_x + 1, k_y, k_z) && (2.17)\\ &= U(k_x, k_y + 1, k_z) && (2.18)\\ &= U(k_x, k_y, k_z + 1) \; . && (2.19) \end{aligned}$$

Without loss of generality, the periodicity in every argument is one. Following Höckendorf *et al.* [159, 160], the unitary matrix $U_\mathbf{k}$ can be decomposed in a diagonal matrix $D_\mathbf{k}$ and a unitary matrix $S_\mathbf{k}$

$$U_\mathbf{k} = S_\mathbf{k} D_\mathbf{k} S_\mathbf{k}^\dagger \; . \tag{2.20}$$

Introducing the definitions

$$X_\alpha \equiv S_\mathbf{k}^\dagger \partial_{\mathbf{k}_\alpha} S_\mathbf{k} \quad , \quad Y_\alpha \equiv D_\mathbf{k}^\dagger \partial_{\mathbf{k}_\alpha} D_\mathbf{k} \tag{2.21}$$

and the Berry curvature matrix

$$F_\alpha = \frac{1}{2\pi i} \varepsilon_{\alpha\beta\gamma} \big(\partial_{\mathbf{k}_\beta} X_\alpha\big) \tag{2.22}$$

as in Ref. [159], one follows from Eq. (2.16) that

$$W_3[U_\mathbf{k}] = \frac{1}{2\pi i} \int_{\mathrm{BZ}} d^3k \, \mathrm{tr}\big[F_\alpha Y_\alpha\big] \; . \tag{2.23}$$

The above defined quantities Y_α and F_α also allow for the calculation of the W_1 and Chern invariant. With the bands $\phi_\mathbf{k}$ defined by

$$D_\mathbf{k} = \exp\big[i\phi_\mathbf{k}\big] \tag{2.24}$$

the W_3-invariant given in Eq. (2.23) can be expressed as

$$\begin{aligned} W_3[U_\mathbf{k}] = \frac{1}{2\pi}\Bigg(&- \int_{[0,1)^3} \mathrm{tr}\Big[(\partial_{\mathbf{k}_\alpha} F_\alpha)\Big] d^3k \\ &+ \sum_{\alpha=1\neq\beta\neq\gamma}^{3} \int_0^1 \int_0^1 \mathrm{tr}\big[F_\alpha \phi_\mathbf{k}\big]\Big|_{k_\alpha=0}^{k_\alpha=1} dk_\beta dk_\gamma \Bigg) \; . \end{aligned} \tag{2.25}$$

This equation is the basis for the numerical algorithm presented in the following section [159].

2.5 Construction of the numerical algorithm for W_3

This section aims to present the algorithm proposed by Höckendorf *et al.* in Ref. [159]. Notation and nomenclature are widely adopted from Ref. [159]. Eq. (2.25) is the basis for the numerical algorithm for the W_3-invariant. From the eigenvectors of $U_{\mathbf{k}}$, i.e. the matrix $S_{\mathbf{k}}$, one can derive the U(1) link variable [125] for the band ν

$$\mathcal{U}^{\nu}(\mathbf{k}_i, \mathbf{k}_j) = \frac{\langle s^{\nu}_{\mathbf{k}_i}, s^{\nu}_{\mathbf{k}_j} \rangle}{|\langle s^{\nu}_{\mathbf{k}_i}, s^{\nu}_{\mathbf{k}_j} \rangle|} \tag{2.26}$$

where $\langle \cdot, \cdot \rangle$ denotes the complex Euclidean scalar product. One can assign a field strength $\hat{F}^{\nu}_{\mathbf{k},\alpha} \in \mathbb{R}$ of

$$\hat{F}^{\nu}_{\mathbf{k},\alpha} = \frac{1}{2\pi i} \log \left[\mathcal{U}^{\nu}(\mathbf{k}_1, \mathbf{k}_2) \mathcal{U}^{\nu}(\mathbf{k}_2, \mathbf{k}_3) \mathcal{U}^{\nu}(\mathbf{k}_3, \mathbf{k}_4) \mathcal{U}^{\nu}(\mathbf{k}_4, \mathbf{k}_1) \right] \tag{2.27}$$

to every face, where the vertices of the Field strength follow from the table:

	$\mathbf{k}_1$	$\mathbf{k}_2$	$\mathbf{k}_3$	$\mathbf{k}_4$
$\hat{F}_{\mathbf{k},1}$:	$\mathbf{k}$	$\mathbf{k}+\boldsymbol{\delta}_2$	$\mathbf{k}+\boldsymbol{\delta}_2+\boldsymbol{\delta}_3$	$\mathbf{k}+\boldsymbol{\delta}_3$
$\hat{F}_{\mathbf{k},2}$:	$\mathbf{k}$	$\mathbf{k}+\boldsymbol{\delta}_3$	$\mathbf{k}+\boldsymbol{\delta}_1+\boldsymbol{\delta}_3$	$\mathbf{k}+\boldsymbol{\delta}_1$
$\hat{F}_{\mathbf{k},3}$:	$\mathbf{k}$	$\mathbf{k}+\boldsymbol{\delta}_1$	$\mathbf{k}+\boldsymbol{\delta}_1+\boldsymbol{\delta}_2$	$\mathbf{k}+\boldsymbol{\delta}_2$

Every point $\mathbf{k}$ corresponds a cube

$$\hat{C}^{\nu}_{\mathbf{k}} = \sum_{\alpha=1}^{3} \left[\hat{F}^{\nu}_{\mathbf{k}+\boldsymbol{\delta}_\alpha,\alpha} - \hat{F}^{\nu}_{\mathbf{k},\alpha} \right] \tag{2.28}$$

which gives the Chern number of the band ν on an infinitesimal surface at $\mathbf{k}$. $\hat{C}^{\nu}_{\mathbf{k}}$ can only be nonzero if it contains a degeneracy point, where two eigenvalues of a band ν and ν' coincide. In that case, $\hat{C}^{\nu}_{\mathbf{k}} = -\hat{C}^{\nu'}_{\mathbf{k}}$. The phases $\phi^{\nu}_{\mathbf{k}}$ of the complex eigenvalues $d^{\nu}_{\mathbf{k}}$ of $U_{\mathbf{k}}$ are

$$\phi^{\nu}_{\mathbf{k}} = -i \log \left(d^{\nu}_{\mathbf{k}} \right) . \tag{2.29}$$

The face numbers $m^{\nu}_{\mathbf{k},\alpha}$ and cube numbers $M^{\nu}_{\mathbf{k}}$ are determined such that

$$|\phi^{\nu}_{\mathbf{k}} - \phi^{\nu}_{\mathbf{k}-\boldsymbol{\delta}_\alpha} + 2\pi m^{\nu}_{\mathbf{k},\alpha}| < \pi \quad \text{and} \quad |\phi^{\nu}_{\mathbf{k}} - \phi^{\nu'}_{\mathbf{k}} + 2\pi M^{\nu}_{\mathbf{k}}| < \pi \, . \tag{2.30}$$

The above equations are equivalent to the following functions

$$m^{\nu}_{\mathbf{k},\alpha} = \left[\frac{\phi^{\nu}_{\mathbf{k}-\boldsymbol{\delta}_\alpha} - \phi^{\nu}_{\mathbf{k}}}{2\pi} \right] \quad \text{and} \quad M^{\nu}_{\mathbf{k}} = \left[\frac{\phi^{\nu'}_{\mathbf{k}} - \phi^{\nu}_{\mathbf{k}}}{2\pi} \right] \tag{2.31}$$

where $[\cdot]$ denotes rounding to the closest integer. The discretized version of Eq. (2.25) is

$$W_3[U_{\mathbf{k}}] \approx \hat{W}_3 = \sum_{i_1,i_2,i_3=1}^{N} \sum_{\nu=1}^{n} \left(\hat{C}^{\nu}_{\mathbf{k}} M^{\nu}_{\mathbf{k}} + \sum_{\alpha=1}^{3} \hat{F}^{\nu}_{\mathbf{k},\alpha} m^{\nu}_{\mathbf{k},\alpha} \right) . \tag{2.32}$$

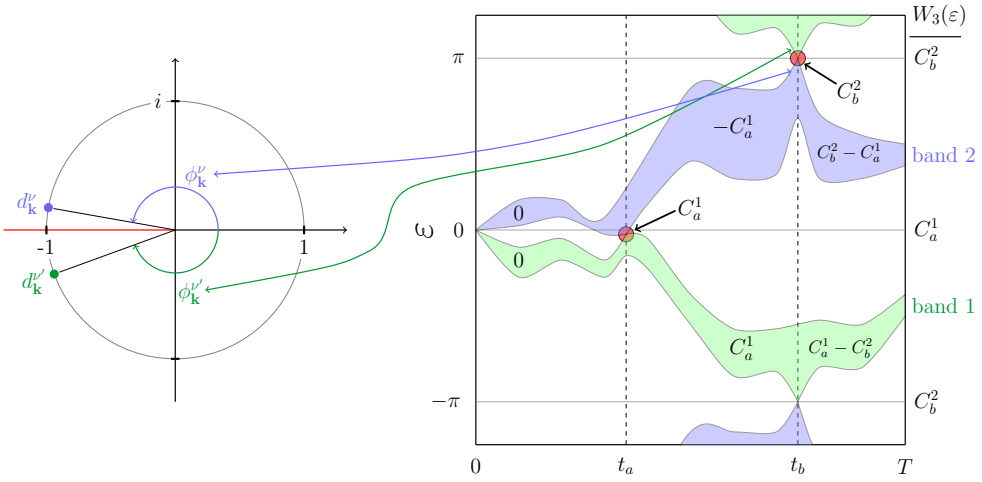

Figure 2.1: The branch cut of the complex logarithm was chosen to be along the negative real axis, indicated as red line in the left plot. The left plot shows exemplary phases of the eigenvalues of the cube $\hat{C}^{\nu}_{\mathbf{k}}$, containing the degeneracy point with charge C_b^2 in the right plot. The degeneracy point in the right panel with charge C_b^2 lies exactly on the zone edge, i.e. on the branch cut of the logarithm.

Let, for example, the branch cut of the complex logarithm be along the negative real axis. Then, the phases $\phi^{\nu}_{\mathbf{k}}$ are in the interval $[-\pi, \pi)$. The term $\hat{C}^{\nu}_{\mathbf{k}} M^{\nu}_{\mathbf{k}}$ of Eq. (2.32) is only nonzero if the cube $\hat{C}^{\nu}_{\mathbf{k}}$ contains a degeneracy point and the phases of the eigenvalues differ by more than π. This implies that the degeneracy point, in order to contribute to W_3, must always be exactly on the branch cut of the logarithm, see Fig. 2.1. Consider the case where the touching is not on the branch cut, as depicted in Fig. 2.2. Here, the branch cut was chosen such that the degeneracy point C_b^2 of the right panel is not on the branch cut anymore. Hence, it does not contribute to W_3. Nevertheless, the contribution is then carried by a surface in the k_x-k_y-t space, where the phases $\phi^{\nu}_{\mathbf{k}}$ of the eigenvalues jump by 2π from one discretization point to another, i.e. $m^{\nu}_{\mathbf{k},\alpha} \neq 0$. This follows from the invariance of Eq. (2.32) against shifts of the form $\phi_{\mathbf{k}} \mapsto \phi^{\nu}_{\mathbf{k}} + 2\pi M$, compare Sec. 4.5. of Ref. [159]. This statement can be traced back to the fact that the phases $\phi^{\nu}_{\mathbf{k}}$ of two eigenvalues can only differ by 2π when the branch cut of the logarithm is changed

$$\log_{\phi_1}(z) - \log_{\phi_2}(z) \in \{0, \pm 2\pi i\} \tag{2.33}$$

together with the logarithm with rotated branch cut

$$\log_{\varphi}(z) = \log(|z|) + i\big(\arg\left(ze^{i\varphi}\right) - \varphi\big) \ . \tag{2.34}$$

2.6 W_3-invariant for flat band Hamiltonians

The authors of Ref. [159] provide two examples of spin-1/2 rotations in their work. Both have the remarkable property that the quasienergy bands of these models are flat and the Chern numbers differ from the W_3-invariant. These are, in hindsight of the scheme proposed by Rudner *et al.* [129], discussed in detail.

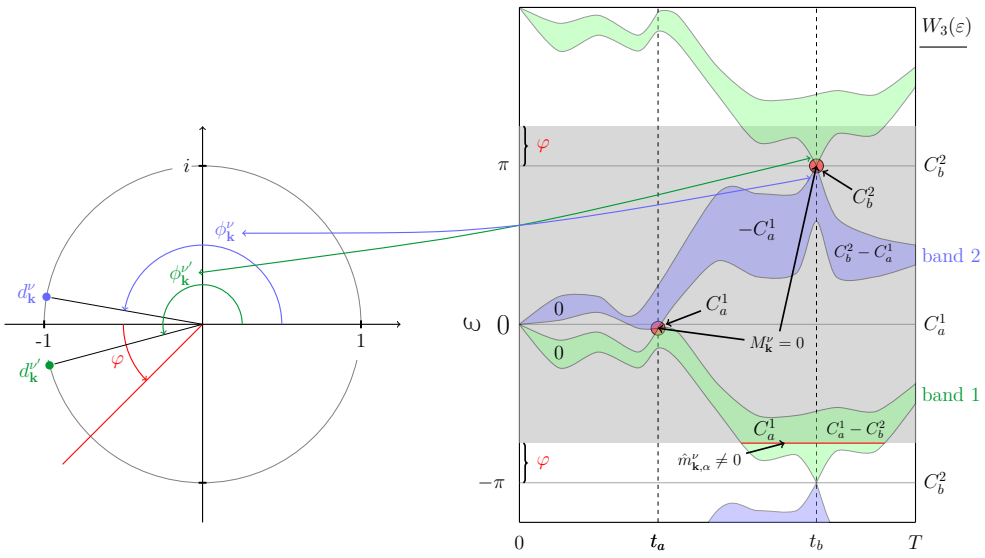

Figure 2.2: With the present choice of the branch cut of the logarithm, the phases of the eigenvalues of $U_{\mathbf{k}}$ lie in the gray shaded zone. The degeneracy point with charge C_b^2 does not lie on the zone edge. The phases of the bands 1 and 2 differ by less than π at that point. Consequently, this point does not contribute to W_3.

2.6.1 Time-independent flat band Hamiltonian

The first example is described by the time independent Hamiltonian

$$H(x, y) = 2\pi w\, \mathbf{f}(x, y) \cdot \boldsymbol{\sigma}\,. \tag{2.35}$$

In the following, $x, y \in [0, 1]$ are referred to as position coordinates and $w \in \mathbb{Z}$. The function $\mathbf{f}(\cdot)$ is a map from the square $[0, 1]^2$, depicted in Fig. 2.3, to the unit sphere $\mathbb{S}^2 \in \mathbb{R}^3$, and $\boldsymbol{\sigma}$ is a vector containing the Pauli matrices. For the construction of $\mathbf{f}(\cdot)$

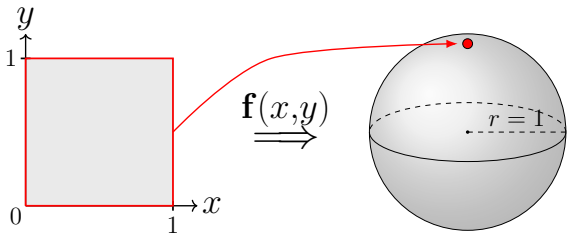

Figure 2.3: The function $\mathbf{f}$ maps the inside of the square onto the surface of the sphere, and the boundary onto the north pole of the sphere.

three different mappings are needed. The first one shifts and stretches the square

$$\mathbf{s}(\mathbf{r}) : [0, 1]^2 \to [-1, 1]^2 \quad , \quad \mathbf{s}(\mathbf{r}) : \begin{pmatrix} x \\ y \end{pmatrix} \to \begin{pmatrix} 2x - 1 \\ 2y - 1 \end{pmatrix}\,. \tag{2.36}$$

The second one is mapping the square to the circle

$$\begin{aligned} &\mathbf{c}(\mathbf{r}) : [-1, 1]^2 \to \{|\mathbf{r}| \leq 1 : \mathbf{r} \in \mathbb{R}^2\} \\ &\mathbf{c}(\mathbf{r}) : \begin{pmatrix} x \\ y \end{pmatrix} \to \begin{pmatrix} x\sqrt{1 - \frac{y^2}{2}} \\ y\sqrt{1 - \frac{x^2}{2}} \end{pmatrix} \end{aligned} \tag{2.37}$$

and the third one is the mapping from the circle to the sphere

$$\begin{aligned}\mathbf{b}(\mathbf{r}) &: \{|\mathbf{r}| \leq 1 : \mathbf{r} \in \mathbb{R}^2\} \to \{|\mathbf{r}| = 1 : \mathbf{r} \in \mathbb{R}^3\} \\ \mathbf{b}(\mathbf{r}) &: \begin{pmatrix} x \\ y \end{pmatrix} \to \begin{pmatrix} \frac{x}{n}\sin(\pi n) \\ \frac{y}{n}\sin(\pi n) \\ \cos(\pi n) \end{pmatrix}\end{aligned} \tag{2.38}$$

with $n \equiv \sqrt{x^2+y^2}$. Finally, the mapping above from the square to the sphere is governed by

$$\mathbf{f}(x,y) = \mathbf{b}\big(\mathbf{c}\big(\mathbf{s}(\mathbf{r})\big)\big) \quad \text{with} \quad \mathbf{r} = \begin{pmatrix} x \\ y \end{pmatrix} . \tag{2.39}$$

The operator $\mathbf{f}(x,y)\cdot\boldsymbol{\sigma}$ can be diagonalized by a transformation Λ

$$\Lambda \mathbf{f}(x,y)\cdot\boldsymbol{\sigma}\Lambda^\dagger = \sigma^z \tag{2.40}$$

where Λ depends on the choice of the map from the unit square to the unit sphere. However, the topological properties are, of course, independent of the details of the mapping [159]. The eigenvalues are independent of the position coordinates. Λ is constructed from the two eigenvectors of H

$$\psi_1(x,y) = \begin{pmatrix} \frac{\sin\left(\frac{\pi}{2}g_2(x,y)\right)}{\sqrt{2}g_2(x,y)}\big(2ig_1(x)y - ig_1(x) + g_1(y) - 2xg_1(y)\big) \\ \cos\left(\frac{\pi}{2}g_2(x,y)\right) \end{pmatrix} \tag{2.41}$$

$$\psi_2(x,y) = \begin{pmatrix} -\frac{\cos\left(\frac{\pi}{2}g_2(x,y)\right)}{\sqrt{2}g_2(x,y)}\big(2ig_1(x)y - ig_1(x) + g_1(y) - 2xg_1(y)\big) \\ \cos\left(\frac{\pi}{2}g_2(x,y)\right) \end{pmatrix} \tag{2.42}$$

with $g_1(x) = \sqrt{1+4(1-x)x}$ and $g_2(x,y) = \sqrt{1-16xy(1-x)(1-y)}$. The time evolution operator corresponding to the Hamiltonian (2.35) is

$$U(\mathbf{r},t) = e^{-iH(x,y)t} \tag{2.43}$$

with $t \in [0,1]$. Evaluating either Eq. (2.16) or Eq. (2.23) yields

$$W_3[U] = 2w\int_{[0,1)^2} dxdy\, \frac{g_1(x)+g_1(y)-2}{g_1(x)g_1(y)g_2(x,y)}\sin\big(\pi g_2(x,y)\big) \tag{2.44}$$

$$= 2w \tag{2.45}$$

whereas the Chern numbers are $C_\pm = \pm 1$. These results will be pursued in Sec. 2.6.3

2.6.2 Time-dependent flat band Hamiltonian

The second example discussed by Höckendorf in Ref. [159] is a spin-1/2 rotation once more. The z-component of the position vector is in the following identified with time. The time evolution operator is given via

$$U(\mathbf{r}) = e^{-i2\pi w\mathbf{g}(\mathbf{r})\cdot\boldsymbol{\sigma}} \tag{2.46}$$

where $\mathbf{g}(\cdot)$ is a bijective map from the cube $[0,1]^3$ to the unit ball $|\mathbf{r}| \leq 1$ that maps the surface (center) of the cube to the surface (center) of the unit ball. This mapping

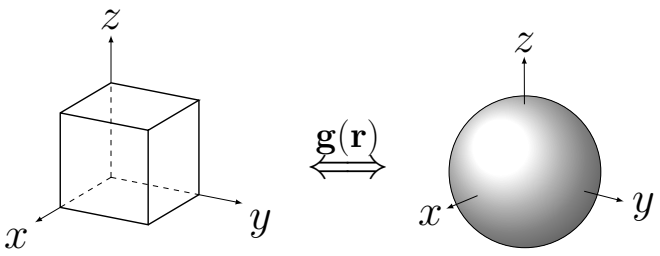

Figure 2.4: The function $\mathbf{g}$ maps the unit cube bijectively onto the unit ball.

is schematically depicted in Fig. 2.4. To construct $\mathbf{g}(\cdot)$, two maps are needed. The first one shifts the unit cube and stretches it

$$\mathbf{s}(\mathbf{r}) : [0,1]^3 \to [-1,1]^3 \quad \text{with} \quad \mathbf{s}(\mathbf{r}) : \begin{pmatrix} x \\ y \\ z \end{pmatrix} \to \begin{pmatrix} 2x-1 \\ 2y-1 \\ 2z-1 \end{pmatrix} \tag{2.47}$$

and the second one is the map to the unit ball

$$\mathbf{c}(\mathbf{r}) : [-1,1]^3 \to \{|\mathbf{r}| \leq 1 : \mathbf{r} \in \mathbb{R}^3\} \quad \text{with} \tag{2.48}$$

$$\mathbf{c}(\mathbf{r}) : \begin{pmatrix} x \\ y \\ z \end{pmatrix} \to \begin{pmatrix} x\sqrt{1-\frac{y^2}{2}-z^2\left(\frac{1}{2}-\frac{y^2}{3}\right)} \\ y\sqrt{1-\frac{z^2}{2}-x^2\left(\frac{1}{2}-\frac{z^2}{3}\right)} \\ z\sqrt{1-\frac{x^2}{2}-y^2\left(\frac{1}{2}-\frac{x^2}{3}\right)} \end{pmatrix} . \tag{2.49}$$

The described mapping above can be constructed as

$$\mathbf{g}(\mathbf{r}) = \mathbf{c}\big(\mathbf{s}(\mathbf{r})\big) \quad \text{with} \quad \mathbf{r} = \begin{pmatrix} x \\ y \\ z \end{pmatrix} . \tag{2.50}$$

The eigenvalues of the operator $\mathbf{g}(\mathbf{r}) \cdot \boldsymbol{\sigma}$ are

$$\lambda_\pm = \pm\sqrt{1 + 64xyz(x-1)(y-1)(z-1)}\,. \tag{2.51}$$

By computing the W_3-invariant, one obtains

$$W_3 = 2w \tag{2.52}$$

whereas the Chern numbers of the two bands are $C_\pm = \pm 1$.

2.6.3 W_3-invariant and truncated Floquet-Hamiltonian

It is possible to construct the time-dependent Hamiltonian from the time evolution operators given in Eq. (2.43) and Eq. (2.46) via

$$H(\mathbf{r},t) = i\big(\partial_t U(\mathbf{r},t)\big)U^\dagger(\mathbf{r},t)\,. \tag{2.53}$$

With the knowledge of the time-dependent Hamiltonian, one can construct the Floquet Hamiltonian (1.6) with time-independent eigenenergies, the quasienergies. It

is well known that the spectra of $U(\mathbf{r}, t = T)$, T being the period, and of the Floquet Hamiltonian coincide. For the cases given in Eq. (2.43) and Eq. (2.46), the quasienergies are

$$\varepsilon_{\pm} = 0\,. \tag{2.54}$$

Both quasienergy bands are degenerate everywhere. Consequently, there is only one gap in the Floquet zone [161]. Now, the discrepancies between the W_3-invariant and the calculation scheme suggested by Rudner [129] in frequency space for W_3 are discussed. Rudner *et al.* suggested truncating the Floquet Hamiltonian in frequency domain at a sufficiently large number of modes. To calculate the generalized topological invariant for driven systems, one must compute the Chern number of all bands of the truncated Floquet Hamiltonian below the investigated gap. The generalized invariant is then given by the sum of all Chern numbers below this gap. Applying this scheme to the above models for $w = 1$ yields, in both cases, $W_3 = 0$ for every gap. The Chern numbers do not need to be known, since the bands are degenerate everywhere and the corresponding Chern numbers fulfill $C_+ = -C_-$. This result is in striking contrast to the analytical $W_3 = 2$. Despite the two examples above proving that the summation scheme suggested by the authors of Ref. [129] is not valid for all models, it will later be shown that the summation scheme and the W_3-invariant for graphene show a perfect agreement.

2.6.4 Time-independent flat band projector Hamiltonians

Rudner *et al.*, Appendix C in Ref. [129], made an attempt to map all time-independent flat band Hamiltonians onto

$$H_P(\mathbf{r}) = \frac{2\pi}{T} P(\mathbf{r}) \tag{2.55}$$

with $P(\mathbf{r})$ being a projection operator and T the period. They were able to show that, for this class of Hamiltonians, the W_3-invariant is equal to the Chern number. One should note that the quasienergies of a Hamiltonian of the form given in Eq. (2.55) suggested by Rudner [129] would be degenerate everywhere, whereas the Chern numbers are defined. In the following, it will be shown that there is a class of flat band Hamiltonians that cannot be written in the form as found in Eq. (2.55), for example, the Hamiltonian given in Eq. (2.35). First, a "period" T must be defined. The period T is understood as the smallest time, greater than a reference time t_0, such that the time evolution operators at times T and t_0 coincide. Without loss of generality, t_0 can be set to zero. The period is then defined as

$$T = \min\{T \in \mathbb{R}_+ | U(t + T, 0) = U(t, 0)\}\,. \tag{2.56}$$

For the time evolution operator of Eq. (2.43) to achieve being periodic on $[0, 1]^3$, one must set $w = 1$ and consequently $T = 1$. As shown in Sec. 2.6.1, the operator from Eq. (2.40)

$$\Lambda \mathbf{f}(x, y) \cdot \boldsymbol{\sigma} \Lambda^{\dagger} = \sigma^z \tag{2.57}$$

is not a projection operator. To construct a projection operator, the eigenvalues must be shifted and rescaled

$$\frac{2\pi}{T} \Lambda^{\dagger} \underbrace{\left(\frac{1}{2}\sigma^z + \frac{1}{2}\mathbb{1} \right)}_{P} \Lambda = \frac{\pi}{T} \mathbf{f}(x, y) \cdot \boldsymbol{\sigma} + \frac{\pi}{T}\mathbb{1}\,. \tag{2.58}$$

This operator has a period of $T = 1$ as well, which assures that the difference in the W_3-invariant does not arise from a different choice of periods. The W_3-invariant of the time evolution operators of this operator is equal to the Chern number ± 1, as shown in Ref. [129]. Nevertheless, the W_3-invariant is not necessarily equal to the Chern number for all time-independent flat band Hamiltonians, as shown is Sec. 2.6.1.

2.7 Non-periodic time evolution operators

If the Hamiltonian is periodic in momentum and time, the corresponding time evolution operator in Eq. (2.5) is, in general, not periodic in time, impeding a direct computation of W_3 from Eq. (2.16). However, the time evolution operator for a Floquet system, see Eq. (2.5), fulfills $U(\mathbf{k}, t = 0) = \mathbb{1}$. If there is a mapping from $U(t = T)$ to $\mathbb{1}$ that maintains all gaps of $U(\mathbf{k}, t = T)$, one is able to compute W_3, since the resulting time evolution operator $\tilde{U}_\varepsilon(\mathbf{k}, t)$ is periodic in time and topologically equivalent to $U(\mathbf{k}, t)$. Such a mapping can be constructed as

$$\tilde{U}_\varepsilon(\mathbf{k}, t) = \begin{cases} U(\mathbf{k}, 2t) & \text{if} \quad 0 \leq t \leq T/2 \\ V_\varepsilon(\mathbf{k}, 2T - 2t) & \text{if} \quad T/2 \leq t \leq T \end{cases} \tag{2.59}$$

with the return map [129]

$$V_\varepsilon(\mathbf{k}, t) = e^{-iH_{\text{eff}}t} \quad \text{with} \quad H_{\text{eff}}(\mathbf{k}) = \frac{i}{T} \log_\varepsilon \Big(U(\mathbf{k}, T) \Big) . \tag{2.60}$$

The eigenvalues $d^\nu_{\mathbf{k}} = e^{i\phi^\nu_{\mathbf{k}}}$ with $0 \leq \phi^\nu_{\mathbf{k}} < \varepsilon \leq 2\pi$ are rotated clockwise to one, and the eigenvalues with $0 \leq \varepsilon < \phi^\nu_{\mathbf{k}} \leq 2\pi$ are rotated counterclockwise to one, compare Fig. 2.5.

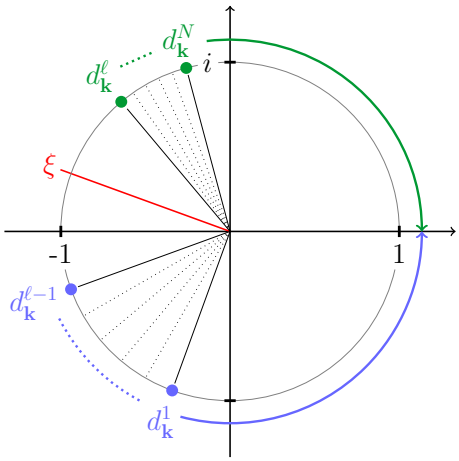

Figure 2.5: The action of the map V_ξ onto the eigenvalues $d^\nu_{\mathbf{k}}$ of $U(\mathbf{k}, t)$: The eigenvalues with phases smaller than $\xi = e^{i\varepsilon}$ are rotated counterclockwise to one, the eigenvalues with larger phase are rotated clockwise to one.

The topological invariant associated with the map given in Eq. (2.59) is related to the one in Eq. (2.25), but with an additional term accounting for V_ε

$$W_3[\tilde{U}_\varepsilon] = W_3[U] - \frac{1}{2\pi i} \int_0^1 d^2k \, \text{tr} \big[F_3(\mathbf{k}, t) \log_\varepsilon [D(\mathbf{k}, t)] \big]_{t=1} . \tag{2.61}$$

It has already been pointed out in Ref. [129] and Ref. [159] that the Chern numbers of the Floquet bands and the W_3-invariant are related via

$$W_3[U_{\varepsilon_a}] = W_3[U_{\varepsilon_b}] - \sum_{\nu=1}^{\nu_K} C_3^{\nu}\big|_{t=1} \,. \tag{2.62}$$

The W_3-invariants for gaps ε_a and ε_b differ by the sum of the Chern numbers of the bands that lie in between ε_a and ε_b. Of course, this leads to modifications of the numerical algorithm. The ε-dependent term in Eq. (2.61) leads to a correction of Eq. (2.32). The integer

$$K_{i_1,i_2}^{\nu} = \left[\frac{-i \log_{\varepsilon} \left(d_{\mathbf{k}}^{\nu} \right) - \phi_{\mathbf{k}}^{\nu}}{2\pi} \right] \tag{2.63}$$

is 1 if the Floquet band $\phi_{\mathbf{k}}^{\nu}$ is below a gap ε, and zero if it is above ε. The W_3-invariant for the periodic unitary map $\tilde{U}(\mathbf{k}, t)$ is then governed by the equation [159]

$$W_3[\tilde{U}_{\varepsilon}] \approx \hat{W}_3 + \sum_{i_1,i_2=1}^{N} \sum_{\nu=1}^{n} K_{i_1,i_2}^{\nu} \hat{F}_{\mathbf{k},3}^{\nu}\big|_{i_3=1} \,. \tag{2.64}$$

A slightly different algorithm is presented in Ref. [160].

2.8 W_3-invariant and the truncated Floquet Hamiltonian

The calculation scheme in frequency space, which was suggested by Rudner *et al.* in Ref. [129], is described in the following. To calculate the generalized topological invariant for driven systems, one first computes the Chern numbers of all bands below the investigated gap of a truncated Floquet matrix. The generalized invariant is then given by the sum over all Chern numbers below this gap. In Fig. 2.6, the

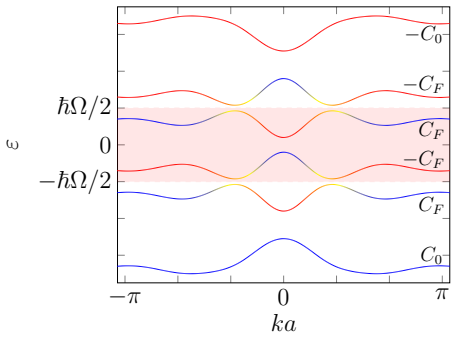

Figure 2.6: The lowest and highest band have different Chern numbers than the inner Floquet bands. This is caused by the finite truncation of the a priori infinite dimensional Floquet matrix.

lowest band of the truncated Floquet matrix has Chern number C_0 different from C_F [129]. The reason why that Chern number is not C_F is due to the truncation. As already shown by Shirley [162, 163], from the Fourier expansion in Eq. (1.7)

it follows that the eigenvector, corresponding to a quasienergy ε_α, differs from the eigenvector of the quasienergy $\varepsilon_\alpha + \hbar\Omega$ only by an index shift of the entries and a phase ϑ, which one is free to choose [162]

$$\varepsilon_\alpha \leftrightarrow \begin{pmatrix} \vdots \\ u_\alpha^{-2} \\ u_\alpha^{-1} \\ u_\alpha^{0} \\ u_\alpha^{1} \\ u_\alpha^{2} \\ \vdots \end{pmatrix} \Longleftrightarrow \varepsilon_\alpha + \hbar\Omega \leftrightarrow e^{i\vartheta} \begin{pmatrix} \vdots \\ u_\alpha^{-3} \\ u_\alpha^{-2} \\ u_\alpha^{-1} \\ u_\alpha^{0} \\ u_\alpha^{1} \\ \vdots \end{pmatrix} . \tag{2.65}$$

α labels a discrete set of quantum numbers, e.g. spin or sublattice degrees. This holds equivalently for arbitrary shifts $n\hbar\Omega$ with $n \in \mathbb{Z}$ of the quasienergy. This shows that the Chern number C_{ε_α} of a band described by ε_α must be equal to the Chern number of the shifted band

$$C_{\varepsilon_\alpha} = C_{\varepsilon_\alpha + n\hbar\Omega} \, . \tag{2.66}$$

For the numerics, this means that if only a finite number of eigenvector entries are different from zero, one must choose the truncation of the Floquet modes large enough to achieve convergence of these. One can assume that m Floquet replica are enough to achieve convergence of the central quasienergy and the corresponding eigenvector. However, the eigenvector corresponding to $\varepsilon_\alpha \pm m\hbar\Omega$ is, in general, not converged, which leads to different results in the quasienergy spectrum as well as Chern numbers. To sum up these non converged Chern numbers might lead to an incorrect topological characterization.

2.9 W_3-invariant for graphene

The Hofstadter problem on the hexagonal lattice is derived in a rigorous manner in this section. First, an explicit proof of the periodicity of the Hofstadter spectrum is presented. After a generalization of the Hofstadter Butterfly to the Floquet-Hofstadter Butterfly, the topological properties are investigated: first without magnetic field and then for a flux per unit cell of $p/q = 1/3$. In light of the peculiarity regarding the proper calculation of the topological invariant for driven systems, the two computation schemes presented above are applied and the results compared in the following.

2.9.1 The Hofstadter Butterfly for the hexagonal lattice

Consider a tight-binding model in the hexagonal lattice, where only nearest neighbor hopping can take place. The underlying lattice vectors are chosen to be

$$\mathbf{b}_1 = a \begin{pmatrix} 0 \\ \sqrt{3} \end{pmatrix} \quad , \quad \mathbf{b}_2 = a \begin{pmatrix} \frac{3}{2} \\ \frac{\sqrt{3}}{2} \end{pmatrix} \tag{2.67}$$

with a being the lattice constant. The nearest neighbor vectors are

$$\mathbf{a}_1 = a \begin{pmatrix} 1 \\ 0 \end{pmatrix} \, , \, \mathbf{a}_2 = \frac{a}{2} \begin{pmatrix} -1 \\ \sqrt{3} \end{pmatrix} \, , \, \mathbf{a}_3 = \frac{a}{2} \begin{pmatrix} -1 \\ -\sqrt{3} \end{pmatrix} \tag{2.68}$$

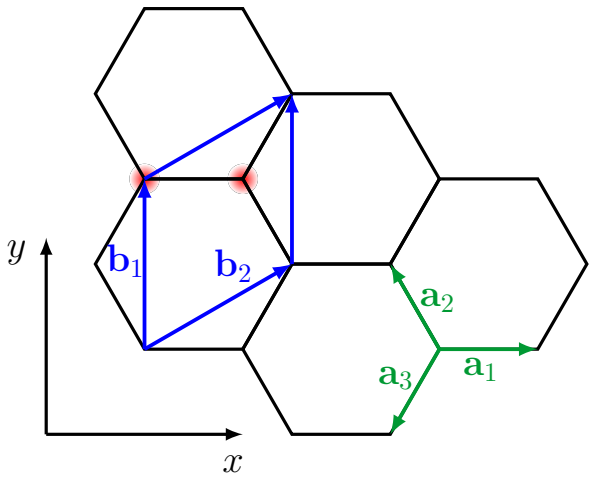

Figure 2.7: Coordinate geometry used on the honeycomb lattice: The green arrows represent the different nearest neighbor vectors and the blue ones the lattice vectors. (Reprinted figure with permission from [153]. Copyright (2019) by the American Physical Society.)

as depicted in Fig. 2.7. The position of an arbitrary unit cell is

$$\mathbf{R}(m,n) = m\mathbf{b}_1 + n\mathbf{b}_2, \quad m,n \in \mathbb{Z}\,. \tag{2.69}$$

In the presence of a vector potential, the hopping parameter g becomes modified by the Peierls phase,

$$g \mapsto g_{m,n} e^{i\phi_{m,n}}\,, \tag{2.70}$$

where the phase is the integral over the vector potential along the hopping path

$$\phi_{m,n} = \frac{e}{\hbar} \int_{\mathbf{R}(m,n)}^{\mathbf{R}(m,n)+\mathbf{a}_i} \mathbf{A}(\mathbf{r}) \cdot d\mathbf{r} \quad , \quad i = 1,2,3\,. \tag{2.71}$$

For Landau gauge $\mathbf{A}(\mathbf{r}) = (0, Bx, 0)$, the Peierls phase becomes independent of the index m

$$\int_{\mathbf{R}(m,n)}^{\mathbf{R}(m,n)+\mathbf{a}_{2,3}} \mathbf{A}(\mathbf{r}) \cdot d\mathbf{r} = \pm\frac{3\sqrt{3}}{4} Ba^2\big(n - \tfrac{1}{6}\big) \tag{2.72}$$

and zero for the hopping in $\mathbf{a}_1$ direction. B is the magnetic field strength. Note that the prefactor in the expression above is related to the area of the elementary unit cell A_{cell} by $3\sqrt{3}a^2/4 = A_{\text{cell}}/2$. As usual, the flux per unit cell in units of the elementary charge over Planck's constant is restricted to a rational value

$$\phi \equiv \frac{e}{h} BA_{\text{cell}} = \frac{p}{q}\,. \tag{2.73}$$

Thus, the Peierls phase can be written as

$$\frac{e}{\hbar}\frac{3\sqrt{3}}{4} Ba^2\big(n - \tfrac{1}{6}\big) = \pi\phi\big(n - \tfrac{1}{6}\big) \tag{2.74}$$

which then leads then to the explicit form of the Hamiltonian

$$H = -g \sum_{mn} \Big[a^\dagger_{m,n} \big(b_{m,n} + e^{i\pi\phi(n-\frac{1}{6})} b_{m+1,n-1} + e^{-i\pi\phi(n-\frac{1}{6})} b_{m,n-1} \big) + h.c. \Big], \tag{2.75}$$

where the sum is over all unit cell positions. The solutions of the stationary Schrödinger equation are plane-wave type states of the general form

$$|\mathbf{k}\rangle = \sum_{mn} e^{i\mathbf{k}\cdot\mathbf{R}(m,n)} \big(\zeta_n a^\dagger_{m,n} + \mu_n b^\dagger_{m,n} \big) |0\rangle \tag{2.76}$$

where the creation operators $a^\dagger_{m,n}, b^\dagger_{m,n}$ for the different sublattice sites are acting on the fermionic vacuum $|0\rangle$. ζ_n, μ_n are complex amplitudes depending only on n, since the Peierls phase does so, see Eq. (2.74). Making a projection on a state $\langle 0|a_{m',n'}$ or $\langle 0|b_{m',n'}$ leads to a system of coupled equations for the amplitudes

$$-\frac{\varepsilon}{g}\zeta_n = \mu_n + z_n(\mathbf{k})\mu_{n-1} \tag{2.77}$$

$$-\frac{\varepsilon}{g}\mu_n = \zeta_n + z^*_{n+1}(\mathbf{k})\zeta_{n+1} \tag{2.78}$$

with

$$z_n(\mathbf{k}) = e^{-i\pi\phi(n-\frac{1}{6}) - i\mathbf{k}\cdot\mathbf{b_2}} + e^{i\pi\phi(n-\frac{1}{6})} e^{i\mathbf{k}\cdot(\mathbf{b}_1 - \mathbf{b}_2)} \ . \tag{2.79}$$

The spectrum as a function of the flux per unit cell is depicted in Fig. 2.8. The

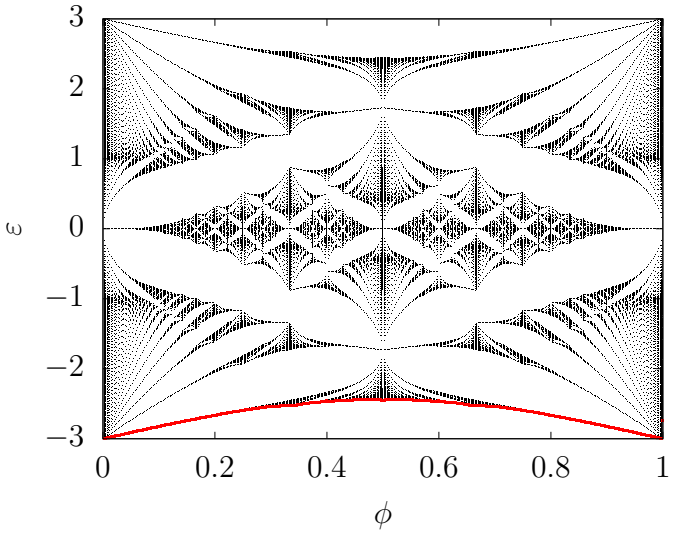

Figure 2.8: Hofstadter butterfly for the honeycomb lattice: The energy is given in units of the hopping parameter t. The ground state of the Hofstadter spectrum is defined as the state with lowest energy represented by the red line. (Reprinted figure with permission from [153]. Copyright (2019) by the American Physical Society.)

red curve marks the state of lowest energy, which is of particular interest in what follows.

2.9.2 Periodicity of the Hofstadter Problem

Eqs. (2.77), (2.78) define a prima vista infinite system of linear equation, which, however, closes to a finite one due to periodicity properties of the amplitudes involved. The periodicity is explicitly proven in the following. First, the operators

$$T_r \begin{pmatrix} a_{m,n} \\ b_{m,n} \end{pmatrix} T_r^\dagger = \begin{pmatrix} a_{m,n+r} \\ b_{m,n+r} \end{pmatrix} \tag{2.80}$$

$$u \begin{pmatrix} a_{m,n} \\ b_{m,n} \end{pmatrix} u^\dagger = (-1)^n \begin{pmatrix} a_{m,n} \\ b_{m,n} \end{pmatrix} \tag{2.81}$$

are defined such that for

$$p \text{ even:} \quad T_q H T_q^\dagger = H \,, \tag{2.82}$$

$$p \text{ odd :} \quad u T_q H T_q^\dagger u^\dagger = H \,. \tag{2.83}$$

For even p, the translation operator T_q acts on the state ansatz as

$$|\mathbf{k}\rangle = e^{i\mathbf{k}\cdot\mathbf{b}_2 q}\, T_q \,|\mathbf{k}\rangle \tag{2.84}$$

and, consequently, the amplitudes have the periodicity

$$\zeta_{n+q} = \zeta_n \quad , \quad \mu_{n+q} = \mu_n \,. \tag{2.85}$$

In the other case where p is odd

$$|\mathbf{k}\rangle = e^{i\mathbf{k}\cdot\mathbf{b}_2 q}\, u T_q \,|\mathbf{k}\rangle \,, \tag{2.86}$$

the amplitudes must fulfill

$$\zeta_{n+q} = (-1)^{n+q}\zeta_n \quad , \quad \mu_{n+q} = (-1)^{n+q}\mu_n \,. \tag{2.87}$$

The relations (2.85) and (2.87) can be summarized as

$$\zeta_q = (-1)^{pq}\zeta_0 \quad , \quad \mu_q = (-1)^{pq}\mu_0 \,. \tag{2.88}$$

Thus, Eqs. (2.77) and (2.78) define a finite linear system of equations for, say, $\zeta_0 \dots \zeta_{q-1}$ and $\mu_0 \dots \mu_{q-1}$, and if both p and q are odd, the relation between the missing amplitudes ζ_q, μ_q and ζ_0, μ_0 contains an additional minus sign. This sign can be compensated by shifting the wave vectors by half a reciprocal lattice vector such as $k_x \to k_x + \frac{2\pi}{3q}$, leading to

$$\zeta_{n+q} = (-1)^{n+1+q}\zeta_n \,, \tag{2.89}$$

$$\mu_{n+q} = (-1)^{n+1+q}\mu_n \,. \tag{2.90}$$

This allows one to use Eq. (2.85) for all flux values for the calculation of the Hofstadter spectrum and Chern numbers. But, one should keep in mind that one gets a shifted band structure for odd flux values according to Eqs. (2.86)-(2.90). As a result, a $2q \times 2q$ matrix is sufficient to obtain the full Hofstadter spectrum.

2.9.3 Floquet-Hofstadter spectrum

The following vector potential represents in-plane, circularly polarized light and a perpendicular magnetic field

$$\mathbf{A}(\mathbf{r},t) = \begin{pmatrix} A\sin(\Omega t) \\ A\cos(\Omega t) + Bx \end{pmatrix} . \tag{2.91}$$

The vector potential is included in the Hamiltonian via Peierls substitution. In what follows, $\mathbf{A}$ only represents the time-dependent part of Eq. (2.91), such that the Hamiltonian reads

$$\begin{aligned} H = -g\sum_{mn}\Big[a^\dagger_{m,n}\big(\, & e^{i\frac{e}{\hbar}\mathbf{A}\cdot\mathbf{a}_1}b_{m,n} + e^{i\pi\phi(n-\frac{1}{6})+i\frac{e}{\hbar}\mathbf{A}\cdot\mathbf{a}_2}b_{m+1,n-1} \\ & + e^{-i\pi\phi(n-\frac{1}{6})+i\frac{e}{\hbar}\mathbf{A}\cdot\mathbf{a}_3}b_{m,n-1}\big) + h.c.\Big] . \end{aligned} \tag{2.92}$$

According to Eq. (2.76), the general solution of the Floquet Hamiltonian H_F can be written in the form

$$|\mathbf{k},t\rangle = \sum_{mn} e^{i\mathbf{k}\cdot\mathbf{R}(m,n)}\Big(\zeta_n(t)a^\dagger_{m,n} + \mu_n(t)b^\dagger_{m,n}\Big)|0\rangle . \tag{2.93}$$

Due to the periodicity of $|\mathbf{k},t\rangle$, one can expand the terms $\zeta_n(t), \mu_n(t)$ using the Fourier series (1.7)

$$\zeta_n(t) = \sum_{l=-\infty}^{\infty}\zeta_{n,l}e^{-il\Omega t} \quad \text{and} \quad \mu_n(t) = \sum_{l=-\infty}^{\infty}\mu_{n,l}e^{-il\Omega t} , \tag{2.94}$$

where the index l is the quantum number of the Floquet mode. Additionally, using the Jacobi-Anger expansion [136] leads to

$$e^{iz\cos(\Omega t)} = \sum_{n=-\infty}^{\infty} J_n(z)e^{in\left(\Omega t+\frac{\pi}{2}\right)} , \tag{2.95}$$

where J_n denotes the n-th order Bessel function of the first kind. The Floquet equation (1.6) leads to the following coupled expressions for the amplitudes

$$l\hbar\Omega\zeta_{n,l} - g\sum_{l'}J_{l'}(\gamma)\Big[\mu_{n,l-l'} + f_{n,l'}(\mathbf{k})\mu_{n-1,l-l'}\Big] = \varepsilon\zeta_{n,l} \tag{2.96}$$

$$l\hbar\Omega\mu_{n,l} - g\sum_{l'}J_{l'}(\gamma)\Big[\zeta_{n,l+l'} + f^*_{n+1,l'}(\mathbf{k})\zeta_{n+1,l+l'}\Big] = \varepsilon\mu_{n,l} \tag{2.97}$$

with

$$f_{n,l'}(\mathbf{k}) = e^{i\pi\phi(n-\frac{1}{6})-il'\frac{4\pi}{3}}e^{i\mathbf{k}\cdot(\mathbf{b}_1-\mathbf{b}_2)} + e^{-i\pi\phi(n-\frac{1}{6})-il'\frac{2\pi}{3}}e^{-i\mathbf{k}\cdot\mathbf{b}_2} \tag{2.98}$$

where $\gamma \equiv eAa/\hbar$. Exemplary numerical results can be seen in Fig. 2.9 and 2.10. The bending direction represented by the green dashed line depends on the sign of the driving frequency Ω.

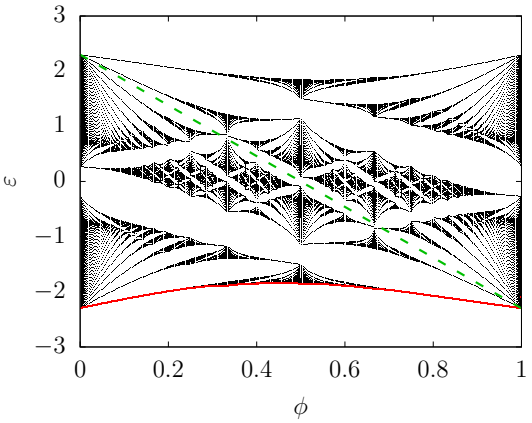

Figure 2.9: The Hofstadter butterfly becomes deformed in presence of circularly polarized light. The frequency of the periodic driving was set to $6.0\,g/\hbar$ and the intensity to $1.0\,eAa/\hbar$. With the present choice of frequency, the different butterflies of the different Floquet modes do not overlap. The red line shows the state of the central Floquet mode with lowest quasienergy. (Reprinted figure with permission from [153]. Copyright (2019) by the American Physical Society.)

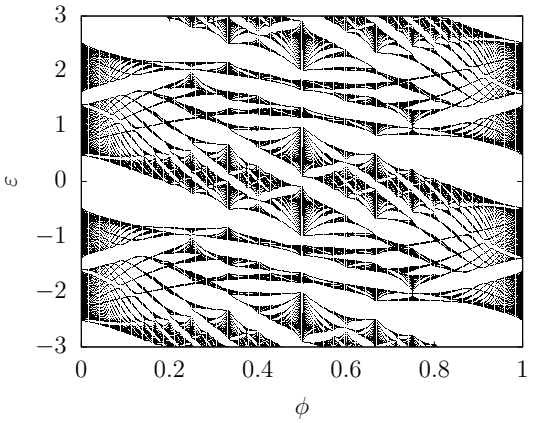

Figure 2.10: The frequency of the circularly polarized radiation was set to $3.0\,g/\hbar$ and the intensity to $1.0\,eAa/\hbar$: With the present choice of parameters, the spectra of the different Floquet modes overlap. (Reprinted figure with permission from [153]. Copyright (2019) by the American Physical Society.)

2.9.4 Graphene without magnetic field

Although there are examples where the summation over the Chern numbers of the truncated Floquet Hamiltonian fails to give the correct topological invariant, as for instance shown by two examples in Ref. [159], the procedure gives the correct results for several models, including circularly polarized driven graphene. In the seminal work on Floquet topological insulators by Mikami *et al.* [3], the authors were able to relate topological phase transitions to effective hopping amplitudes. Moreover, the topological phase diagram of graphene with circularly polarized driving has been investigated. To make direct contact with the work by Mikami *et al.* [3], the discretization of the time-momentum Brillouin zone is set to $200 \times 200 \times 200$ and the number of Floquet replicas to 50. Although the lowest and topmost eigenvalues and eigenvectors of the truncated Floquet Hamiltonian are not converged, i.e. they are different from the index shifted eigenvectors with eigenvectors taken from the central Floquet zone, compare Eq. (2.65), they remain relevant for the topological classification of driven graphene. In the converged Floquet zones, the sum over all bands inside one specific Floquet zone must be zero [159]. For the lowest and highest Floquet zones, this is not necessarily the case. The deviation from the converged Chern numbers contains the information about the difference of Chern numbers and the W_3-invariants, such that the summation indeed gives the correct topological invariant. This can be seen when one compares the sum over all Chern numbers of the truncated Floquet Hamiltonian depicted in Fig. 2.11 with the W_3-invariant shown in Fig. 2.12. The difference between the two values is plotted in Fig. 2.17.

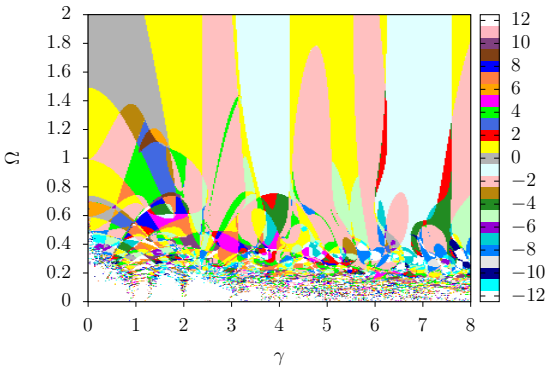

Figure 2.11: The sum over all Chern numbers of the truncated Floquet Hamiltonian below $\varepsilon = 0$ for graphene with circular driving and without magnetic field: The results almost perfectly reproduce the findings from Ref. [3]. (Reprinted figure with permission from [153]. Copyright (2019) by the American Physical Society.)

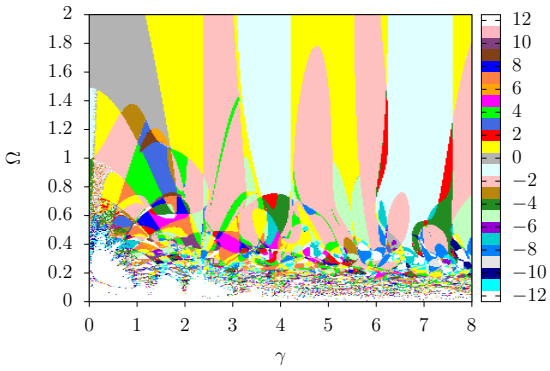

Figure 2.12: The W_3-invariant coincides with the sum over Chern numbers in reliable regions. Except for numerical unstable regions, the Chern number sum and the W_3-invariant show a striking agreement. (Reprinted figure with permission from [153]. Copyright (2019) by the American Physical Society.)

In the region of small intensities γ and $\hbar\Omega < 1.5g$, they do not agree. However, this is due to numerical instabilities of the algorithm for the W_3-invariant. To show that there is indeed no difference between the sum over Chern numbers and W_3, the sizes of the gaps at zero quasienergy and $-\Omega/2$ are analyzed.

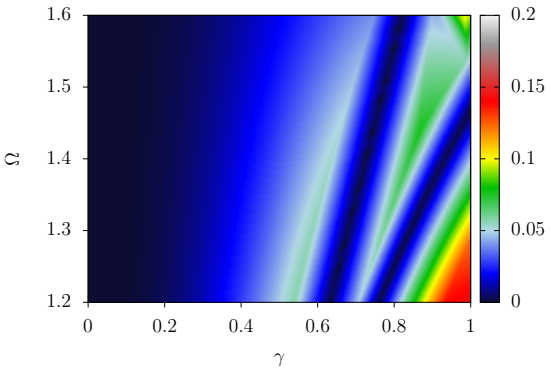

Figure 2.13: The size of the zone edge gap in dependence of intensity γ and driving frequency Ω: The data were calculated as distance between the minimum of the lower band of the central Floquet zone and $-\Omega/2$. The zero lines in the right half of the plot are also visible as topological phase transition in Fig. 2.18. (Reprinted figure with permission from [153]. Copyright (2019) by the American Physical Society.)

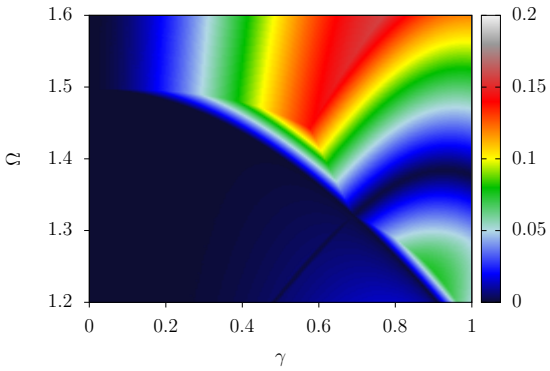

Figure 2.14: The minimum of the upper band of the central Floquet zone in dependence of intensity γ and driving frequency Ω is plotted. The zeros, as well as the band touchings, can be directly mapped to a change of the sum over Chern numbers, compare Fig. 2.11. (Reprinted figure with permission from [153]. Copyright (2019) by the American Physical Society.)

Fig. 2.13 shows the difference between $-\Omega/2$ and the minimum of the lower band of the central Floquet zone. Comparing the regions where the $-\Omega/2$-gap is closed with the corresponding regions where the Chern number changes, Fig. 2.18, one can see that the zeros of the $-\Omega/2$-gap are responsible for a change of Chern numbers. The arc in Fig. 2.14 starting from $(\gamma, \Omega) = (0.5\, eAa/\hbar, 1.2\, g/\hbar)$ to $(\gamma, \Omega) = (1.0\, eAa/\hbar, 1.36\, g/\hbar)$, where the zero gap is closed, can be seen in Fig. 2.12 as well as in Fig. 2.18. In the following, it is clarified whether there is a difference

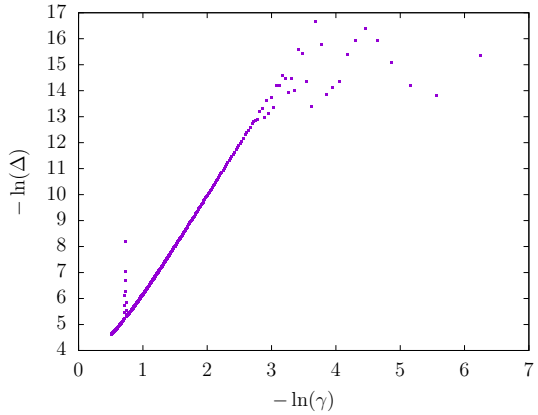

Figure 2.15: Δ is the minimum of the upper band of the central Floquet zone. The plot shows the gap size, i.e. the difference between the minimum of the upper band and zero, for $\gamma = 1/520$ to $\gamma = 3/5$ at fixed $\Omega = 1.2g/\hbar$. The peak at $-\ln(\gamma) \approx 0.7$ is evidence of a gap closing at $\gamma = 0.5$. However, for $-\ln(0.2) \approx 1.6$, no peak is visible, which implies that there is no topological phase transition at $\gamma = 0.2$. (Reprinted figure with permission from [153]. Copyright (2019) by the American Physical Society.)

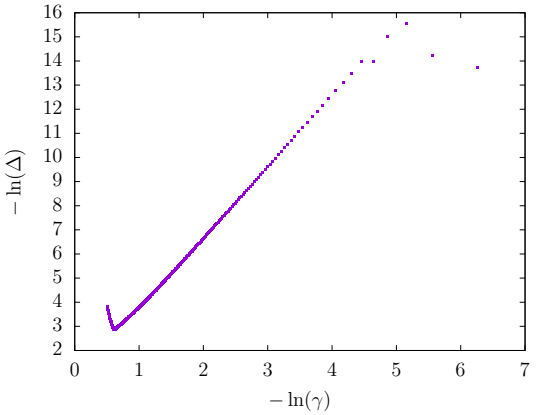

Figure 2.16: Δ is the distance between the minimum of the lower band of the central Floquet zone and $-\Omega/2$, and, as in Fig. 2.15, no peak is visible in this plot, where γ and Ω are in the same parameter range as in Fig. 2.15. (Reprinted figure with permission from [153]. Copyright (2019) by the American Physical Society.)

between the sum over Chern number of the truncated Floquet Hamiltonian and the W_3-invariant. For this reason, the gap sizes in the interval $\gamma \in [0.0, 0.6]\, eAa/\hbar$ for $\Omega = 1.2\, g/\hbar$ are calculated. The Brillouin zone is discretized by using 3500×3500 points. If there was a gap closing, e.g. at $(\gamma, \Omega) = (0.2\, eAa/\hbar, 1.2\, g/\hbar)$ in Fig. 2.12, one should see a signature of a gap closing either in Fig. 2.15 or in Fig. 2.16. The figures 2.15 and Fig. 2.16 show the gap sizes in a double logarithmic plot for the zero and the $-\Omega/2$ gap. If there was a gap closing, there should be a signature at -ln(γ) $\approx$ 1.6. This, however, is not the case, which also shows that the deviations between Chern number summation and W_3 can be traced back to numerical instabilities. Indeed, one can achieve agreement between the results of the summation over Chern numbers and the W_3-invariant by increasing the discretization of the time-momentum Brillouin zone. This was done for some representative points. As an example, $(\gamma, \Omega) = (0.1\, eAa/\hbar, 1.4\, g/\hbar)$ was investigated: An increase of the number of discretization points to $800 \times 800 \times 800$ is necessary to achieve convergence of the W_3-algorithm and with that agreement with the summation over Chern numbers.

Besides, from numerical demanding regions, both topological characterizations show a striking agreement which is colored in gray in Fig. 2.17. Apart from the observation that the sum over the Chern numbers of the truncated Floquet Hamiltonian and the W_3-invariant seem to coincide for circularly driven graphene, a proof seems to be missing thus far. Remarkably, even in the cases where both the Chern number

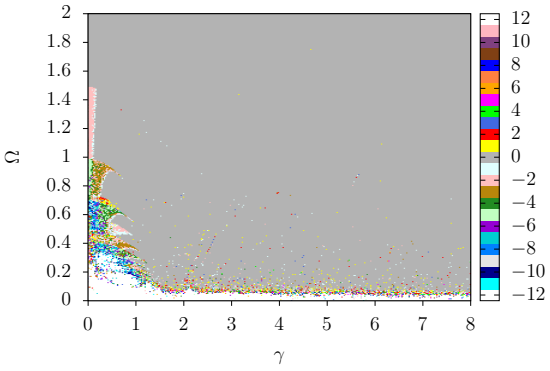

Figure 2.17: The difference between the W_3-invariant and the sum over Chern numbers of the truncated Floquet Hamiltonian: The parameter spaces where W_3- invariant and the sum over Chern numbers agree are shaded in grey. (Reprinted figure with permission from [153]. Copyright (2019) by the American Physical Society.)

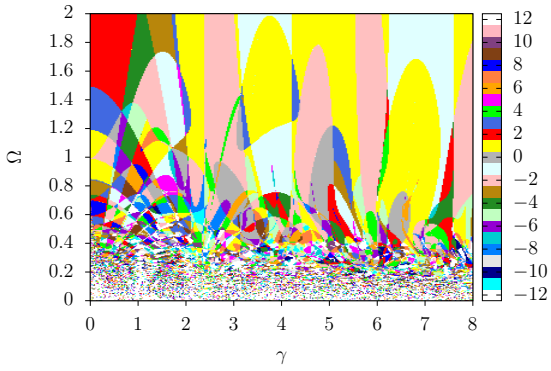

Figure 2.18: The Chern number of the lower band of graphene of the central Floquet zone: The driving is once more circularly polarized. One can see the difference to the W_3-invariant in Fig. 2.12. (Reprinted figure with permission from [153]. Copyright (2019) by the American Physical Society.)

and the W_3-invariant coincide, e.g. compare $(\gamma, \Omega) = (4.0\, eAa/\hbar, 2.0\, g/\hbar)$ Fig. 2.18 and Fig. 2.12, not all Floquet zones of the truncated Floquet Hamiltonian have the same Chern numbers as the central Floquet zone, as depicted in Fig. 2.19. This holds even for the off resonant regime. Fig. 2.20 extends Fig. 2.19 to higher driving frequencies. This feature survives for even higher driving frequencies $\Omega \propto 10^6\, g/\hbar$. Again, this can be understood by having a closer look at the quasienergy band structure. In the far off resonant regime, the gap between the two bands of graphene is very small. Hence, even when the Floquet zones are far away from each other, a small coupling is enough to close and reopen the small gap of some Floquet zones.

2.9.5 Graphene with magnetic field

To assure the correctness of the topological invariant, the algorithm proposed by Höckendorf *et al.*, Ref. [159], to compute numerically the W_3-invariant for the Floquet-Hofstadter spectrum at $p/q = 1/3$, was applied. The result is plotted in Fig. 2.24. To compare to the static topological invariants, first the Chern number of the state with lowest energy of the central Floquet zone for a flux per unit cell of $p/q = 1/3$ and circular driving are computed. The three dimensional momentum-time Brillouin zone is discretized by 200×200×200 points together with 30 Floquet replicas. The resulting Chern numbers are plotted in Fig. 2.21 for different amplitudes γ and frequencies Ω of the driving field. In the left lower region of Fig. 2.21, inside the arc from $(\gamma, \Omega) = (0.0\, eAa/\hbar, 5.1\, g/\hbar)$ to $(\gamma, \Omega) = (1.9\, eAa/\hbar, 2.0\, g/\hbar)$,

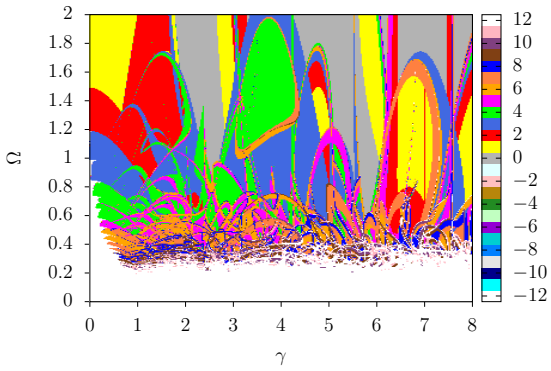

Figure 2.19: The innermost Floquet zone has other Chern numbers than the central Floquet zone. The counting of the Floquet zones starts here with the lowest mode, e.g. for $(\gamma, \Omega) = (4.0\, eAa/\hbar, 1.6\, g/\hbar)$, the (-50+4)'th Floquet zone has other Chern numbers than the central Floquet zone. (Reprinted figure with permission from [153]. Copyright (2019) by the American Physical Society.)

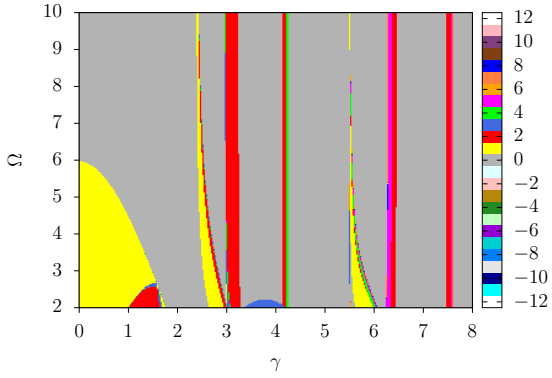

Figure 2.20: Even in the far off resonant regime, not all Chern numbers of the Floquet zones of the truncated Floquet Hamiltonian agree with the Chern numbers of the central Floquet zone. (Reprinted figure with permission from [153]. Copyright (2019) by the American Physical Society.)

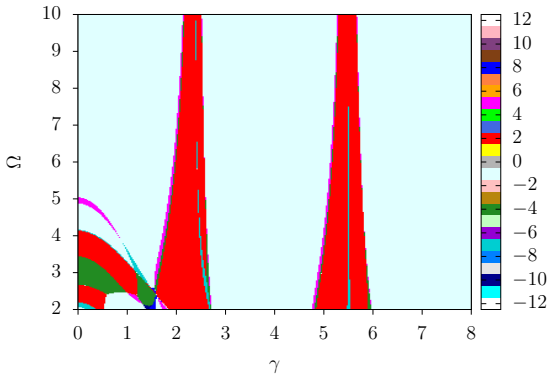

Figure 2.21: The Chern number of the state with lowest energy of the central Floquet zone for a flux per unit cell of $p/q = 1/3$ and circular driving. (Reprinted figure with permission from [153]. Copyright (2019) by the American Physical Society.)

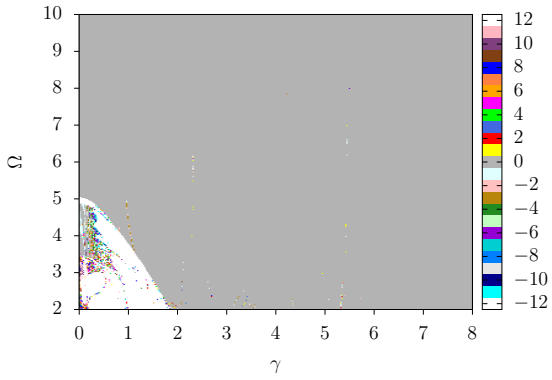

Figure 2.22: The difference between the sum over Chern numbers and the W_3-invariant: Grey regions show parameter configurations (γ, Ω) where the Chern number sum and the W_3-invariant coincide. (Reprinted figure with permission from [153]. Copyright (2019) by the American Physical Society.)

the numerical values cannot be trusted. The reason can be understood when investigating the band structure. In the parameter space where $\hbar\Omega < 6.0g$, the bands of the Floquet-Hofstadter spectrum overlap and the Chern numbers are not computable numerically [125]. With rising intensity, the degeneracies are lifted and anti-crossings occur. Moreover, there are (γ, Ω) regions where no gap between the lowest and the second lowest band exists but the bands are nowhere degenerate, see

Fig. 2.25.
In the last step, the W_3 calculation scheme following Ref. [129] is applied. The flux and polarization are the same as that depicted in Fig. 2.21. The result is plotted in Fig. 2.23. In the following, the results of both W_3 calculations are compared and contrasted against the corresponding Chern numbers.
The difference between both results for the W_3-invariant is depicted in Fig. 2.22. The comparison shows that, apart from zones close to topological phase transitions, the results coincide. Interestingly, the Chern number itself also shows a great agreement

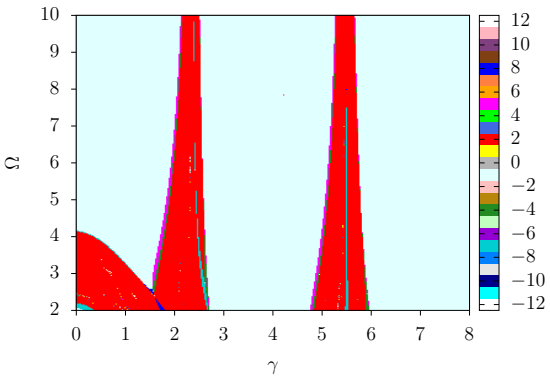

Figure 2.23: The sum over all Chern numbers below $\varepsilon = 0$ computed from the truncated Floquet Hamiltonian with the same flux and polarization as in Fig. 2.21 and Fig. 2.24. (Reprinted figure with permission from [153]. Copyright (2019) by the American Physical Society.)

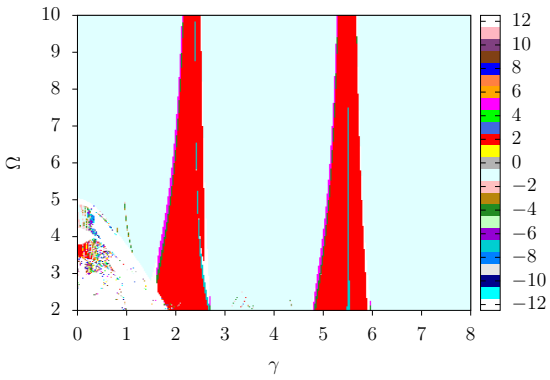

Figure 2.24: The W_3-invariant computed with the algorithm of Höckendorf [159] for the Floquet-Hofstadter spectrum at $p/q = 1/3$: The driving was circularly polarized. (Reprinted figure with permission from [153]. Copyright (2019) by the American Physical Society.)

with both the sum over the Chern numbers and W_3. Using the connection between edge modes and the W_3-invariant which has been proven in Ref. [129], one can conclude that the results allow for the prediction of the number of edge modes in this driven system.
There is a global gap between two bands if the minimum of the upper band is always greater than the maximum of the lower band. Consider the case of two bands without a global energy gap. It does not imply that there is a degeneracy of the two bands. This scenario occurs for specific (γ, Ω) configurations of the Floquet Hofstadter spectrum between the lowest and second lowest band, marked as black stripes in Fig. 2.26. An exemplary quasienergy band structure is shown in Fig. 2.25. There is no gap between the lowest two non-degenerate bands.

2.10 Summary and Outlook

In this work, an explicit and rigorous treatment of the Hofstadter problem on the hexagonal lattice is presented. One important result is the explicit proof of the periodicity of the Hofstadter butterfly: Depending on whether the numerator of the flux per unit cell is even or odd, the periodicity of the fractal spectrum is different. Yet, the appropriate topological invariant to look at in case of a periodically driven system is the W_3-invariant. There are two different computation schemes in

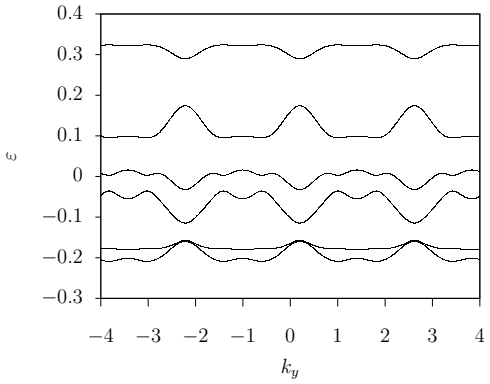

Figure 2.25: The quasienergy band structure for $p/q = 1/3$, $(\gamma, \Omega) = (2.65\, eAa/\hbar, 3.0\, g/\hbar)$ and $k_x = 0$: The lowest two bands are not degenerate but they do not have a gap in the sense that the minimum of the second lowest band is always greater than the maximum of the lowest band. (Reprinted figure with permission from [153]. Copyright (2019) by the American Physical Society.)

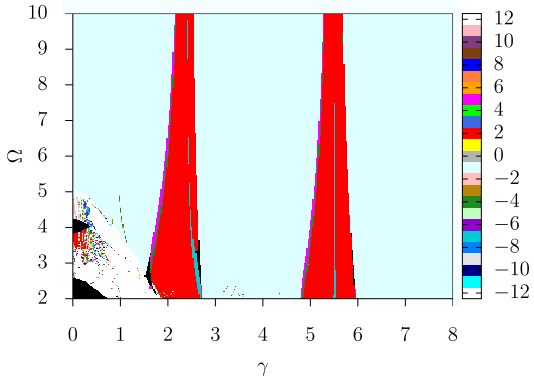

Figure 2.26: The W_3-invariant computed with the algorithm of Höckendorf [159] for the Floquet-Hofstadter spectrum at $p/q = 1/3$: The driving was circularly polarized. Parameter spaces (γ, Ω) without a gap are marked black. (Reprinted figure with permission from [153]. Copyright (2019) by the American Physical Society.)

literature. One is based on Chern numbers of the truncated Floquet Hamiltonian and the other is evaluated in time-domain. By presenting two examples, it could be shown that in general, both calculation schemes do not provide the same topological results, although they are supposed to give the same invariant. A deeper justification of the Chern number summation of the truncated Floquet Hamiltonian seems to be missing in literature. Nevertheless, this scheme is widely accepted and used in literature. To assure that the topological characterization of the Floquet-Hofstadter butterfly is correct, both computational schemes are applied.

To understand how illumination of graphene with circularly polarized light in the presence of a magnetic field will effect the fractal spectrum, the Hofstadter butterfly was unified with Floquet theory. To assure the correctness of the topological analysis, the Chern numbers, the sum over all Chern numbers of the truncated Floquet Hamiltonian, and the W_3-invariant were computed. In the high-frequency limit, all three topological characterizations coincide, yielding the correct number of edge modes appearing in a system of finite size. The low frequency limit, compared to the bandwidth of the hexagonal lattice, was only analyzed without a magnetic field. Remarkably, the sum over Chern numbers of the Floquet Hamiltonian and the W_3-invariant show a striking agreement. This justifies the results of various formed works [3, 136, 164, 165] numerically, whereby an analytical connection is still missing.

The topological characterization of driven systems is still in its infancy, which manifests in the fact that there are still many open questions. First, the interpretation of the non-zero W_3-invariant discussed in Sec. 2.6.1 needs further analysis. Despite the system being time-independent, the topology deduced from the time evolution

differs from the Chern number. Whereas the latter is related to edge states in a finite system, a physical interpretation or experimental access of the W_3-invariant seems to be missing.
Furthermore, it is unclear where the difference between the sum over Chern numbers of the truncated Floquet Hamiltonian and W_3 in the examples mentioned earlier comes from. It seems that there are models where both show a striking agreement. This covers, for example, circularly driven graphene, and some where both disagree, like the examples discussed above. To find a classification of whether the summation over Chern number is justified or not is of ultimate interest.
More thought must be put into the interpretation of the Chern number as function of time. Whether this is a mathematical auxiliary quantity is still an open question. Besides, there has been no answer thus far to whether there is an experimental access to a time-varying Chern number. (Reprinted text with permission from [153]. Copyright (2019) by the American Physical Society.)

Bibliography

[1] M. Holthaus, "Floquet engineering with quasienergy bands of periodically driven optical lattices", J. Phys. B: Atm. Mol. Opt. **49**, 013001 (2016).

[2] Z. Gu, H. A. Fertig, D. P. Arovas, and A. Auerbach, "Floquet spectrum and transport through an irradiated graphene ribbon", Phys. Rev. Lett. **107**, 216601 (2011).

[3] T. Mikami, S. Kitamura, K. Yasuda, N. Tsuji, T. Oka, and H. Aoki, "Brillouin-wigner theory for high-frequency expansion in periodically driven systems: application to floquet topological insulators", Phys. Rev. B **93**, 144307 (2016).

[4] S. Morina, O. V. Kibis, A. A. Pervishko, and I. A. Shelykh, "Transport properties of a two-dimensional electron gas dressed by light", Phys. Rev. B **91**, 155312 (2015).

[5] P. Drude, "Zur Elektronentheorie der Metalle", Annalen der Physik **306**, 566 (1900).

[6] P. Drude, "Zur Ionentheorie der Metalle", Physikalische Zeitschrift **14**, 161 (1900).

[7] P. A. M. Dirac and N. H. D. Bohr, "The quantum theory of the emission and absorption of radiation", Proceedings of the Royal Society of London. Series A, Containing Papers of a Mathematical and Physical Character **114**, 243 (1927).

[8] J. Orear, E. Fermi, A. Rosenfeld, and R. Schluter, *Nuclear physics: a course given by enrico fermi at the university of chicago*, Midway reprint (University of Chicago Press, 1950), ISBN: 9780226243658.

[9] B. L. Al'tshuler, A. G. Aronov, A. I. Larkin, and D. E. Khmel'nitskii, "The anomalous magnetoresistance in semiconductors", Sov. Phys. JETP **54**, 0411 (1981).

[10] S. Hikami, A. I. Larkin, and Y. Nagaoka, "Spin-Orbit Interaction and Magnetoresistance in the Two Dimensional Random System", Progress of Theoretical Physics **63**, 707 (1980).

[11] S. Chakravarty and A. Schmid, "Weak localization: The quasiclassical theory of electrons in a random potential", Physics Reports **140**, 193 (1986).

[12] C. W. J. Beenakker and H. van Houten, "Boundary scattering and weak localization of electrons in a magnetic field", Physical Review B **38**, 3232 (1988).

[13] S. V. Iordanskii, Y. B. Lyandageller, and G. E. Pikus, "Weak-localization in quantum-wells with spin-orbit interaction", Jetp Letters **60**, 206 (1994).

[14] D. H. Berman, M. Khodas, and M. E. Flatté, "Spin polarization oscillations without spin precession: spin-orbit entangled resonances in quasi-one-dimensional spin transport", Phys. Rev. X **4**, 011048 (2014).

[15] W. Knap, C. Skierbiszewski, A. Zduniak, E. Litwin-Staszewska, D. Bertho, F. Kobbi, J. L. Robert, G. E. Pikus, F. G. Pikus, S. V. Iordanskii, V. Mosser, K. Zekentes, and Y. B. Lyanda-Geller, "Weak antilocalization and spin precession in quantum wells", Phys. Rev. B **53**, 3912 (1996).

[16] J. S. Meyer, V. I. Fal'ko, and B. L. Altshuler, *Quantum in-plane magnetoresistance in 2d electron systems* (Springer Netherlands, 2002), pp. 117–164, ISBN: 978-94-010-0530-2.

[17] P. Wenk and S. Kettemann, "Dimensional dependence of weak localization corrections and spin relaxation in quantum wires with rashba spin-orbit coupling", Phys. Rev. B **81**, 125309 (2010).

[18] M. Kammermeier, P. Wenk, J. Schliemann, S. Heedt, and T. Schäpers, "Weak (anti)localization in tubular semiconductor nanowires with spin-orbit coupling", Phys. Rev. B **93**, 205306 (2016).

[19] S. Kettemann, "Dimensional control of antilocalization and spin relaxation in quantum wires", Phys. Rev. Lett. **98**, 176808 (2007).

[20] M. Grifoni and P. Hänggi, "Driven quantum tunneling", Physics Reports **304**, 229 (1998).

[21] T. Kitagawa, T. Oka, A. Brataas, L. Fu, and E. Demler, "Transport properties of nonequilibrium systems under the application of light: photoinduced quantum hall insulators without landau levels", Phys. Rev. B **84**, 235108 (2011).

[22] Y. Zhou and M. W. Wu, "Optical response of graphene under intense terahertz fields", Phys. Rev. B **83**, 245436 (2011).

[23] T. Oka and H. Aoki, "Photovoltaic hall effect in graphene", Phys. Rev. B **79**, 081406 (2009).

[24] M. A. Skvortsov, "Weak antilocalization in a 2D electron gas with chiral splitting of the spectrum", Journal of Experimental and Theoretical Physics Letters **67**, 133 (1998).

[25] A. A. Pervishko, O. V. Kibis, S. Morina, and I. A. Shelykh, "Control of spin dynamics in a two-dimensional electron gas by electromagnetic dressing", Phys. Rev. B **92**, 205403 (2015).

[26] J. Shi and X. C. Xie, "Radiation-induced "zero-resistance state" and the photon-assisted transport", Phys. Rev. Lett. **91**, 086801 (2003).

[27] H. Dehghani, T. Oka, and A. Mitra, "Out-of-equilibrium electrons and the hall conductance of a floquet topological insulator", Phys. Rev. B **91**, 155422 (2015).

[28] O. V. Kibis, "How to suppress the backscattering of conduction electrons?", EPL (Europhysics Letters) **107**, 57003 (2014).

[29] T. Herrmann, Z. D. Kvon, I. A. Dmitriev, D. A. Kozlov, B. Jentzsch, M. Schneider, L. Schell, V. V. Bel'kov, A. Bayer, D. Schuh, D. Bougeard, T. Kuczmik, M. Oltscher, D. Weiss, and S. D. Ganichev, "Magnetoresistance oscillations induced by high-intensity terahertz radiation", Phys. Rev. B **96**, 115449 (2017).

[30] M. Genske and A. Rosch, "Floquet-boltzmann equation for periodically driven fermi systems", Phys. Rev. A **92**, 062108 (2015).

[31] I. Esin, M. S. Rudner, G. Refael, and N. H. Lindner, "Quantized transport and steady states of floquet topological insulators", Physical Review B **97**, 245401 (2018).

[32] P. Titum, N. H. Lindner, M. C. Rechtsman, and G. Refael, "Disorder-induced floquet topological insulators", Phys. Rev. Lett. **114**, 056801 (2015).

[33] P. Titum, N. H. Lindner, and G. Refael, "Disorder-induced transitions in resonantly driven floquet topological insulators", Phys. Rev. B **96**, 054207 (2017).

[34] T. Paraj, "Disorder driven transitions in non-equilibrium quantum systems", PhD thesis (California Institute of Technology, 2016).

[35] K. Kristinsson, O. V. Kibis, S. Morina, and I. A. Shelykh, "Control of electronic transport in graphene by electromagnetic dressing", Scientific Reports **6**, Article, 20082 EP (2016).

[36] M. Wackerl, P. Wenk, and J. Schliemann, "Floquet-Drude conductivity", Phys. Rev. B **101**, 184204 (2020).

[37] F. Bloch, "Über die Quantenmechanik der Elektronen in Kristallgittern", Zeitschrift für Physik **52**, 555 (1929).

[38] G. Floquet, "Sur les équations différentielles linéaires à coefficients périodiques", fr, Annales scientifiques de l'École Normale Supérieure **2e série, 12**, 47 (1883).

[39] E. Ince, *Ordinary differential equations*, Dover Books on Mathematics (Dover Publications, 1956), ISBN: 9780486603490.

[40] Y. B. Zel'dovich, "The quasienergy of a quantum-mechanical system subjected to a periodic action", Journal of Experimental and Theoretical Physics **24**, 1492 (1966).

[41] J. Schliemann, "On time-dependent quantum systems", (unpublished notes).

[42] E. M. Landau and L. D. Lifshitz, *Lehrbuch der Theoretischen Physik, vol. III, Quantenmechanik* (Akademie-Verlag, Berlin, 1988), ISBN: 978-0-08-017801-1.

[43] A. López, A. Scholz, B. Santos, and J. Schliemann, "Photoinduced pseudospin effects in silicene beyond the off-resonant condition", Phys. Rev. B **91**, 125105 (2015).

[44] A. G. Grushin, A. Gómez-León, and T. Neupert, "Floquet fractional chern insulators", Phys. Rev. Lett. **112**, 156801 (2014).

[45] P. Mohan, R. Saxena, A. Kundu, and S. Rao, "Brillouin-wigner theory for floquet topological phase transitions in spin-orbit-coupled materials", Phys. Rev. B **94**, 235419 (2016).

[46] R. Kubo, "Statistical-Mechanical Theory of Irreversible Processes. I. General Theory and Simple Applications to Magnetic and Conduction Problems", Journal of the Physical Society of Japan **12**, 570 (1957).

[47] R. Kubo, H. Hasegawa, and N. Hashitsume, "Quantum Theory of Galvanomagnetic Effect. I. Basic Considerations", Journal of the Physical Society of Japan **14**, 56 (1959).

[48] H. Bruus and K. Flensberg, *Many-body quantum theory in condensed matter physics - an introduction* (Oxford University Press, United States, 2004), ISBN: 9780198566335.

[49] G. Mahan, *Many-particle physics*, Physics of Solids and Liquids (Springer US, 2000), ISBN: 9780306463389.

[50] W. Nolting, *Grundkurs Theoretische Physik 7: Viel-Teilchen-Theorie*, Springer-Lehrbuch (Springer Berlin Heidelberg, 2014), ISBN: 9783642258084.

[51] A. M. Glass, D. von der Linde, and T. J. Negran, "High-voltage bulk photovoltaic effect and the photorefractive process in LiNbO3", Applied Physics Letters **25**, 233 (1974).

[52] W. Koch, R. Munser, W. Ruppel, and P. Wü"rfel, "Bulk photovoltaic effect in BaTiO3", Solid State Communications **17**, 847 (1975).

[53] A. K. Gupta, O. E. Alon, and N. Moiseyev, "Generation and control of high-order harmonics by the interaction of an infrared laser with a thin graphite layer", Phys. Rev. B **68**, 205101 (2003).

[54] H. Hsu and L. E. Reichl, "Floquet-bloch states, quasienergy bands, and high-order harmonic generation for single-walled carbon nanotubes under intense laser fields", Phys. Rev. B **74**, 115406 (2006).

[55] A. Scholz, A. López, and J. Schliemann, "Interplay between spin-orbit interactions and a time-dependent electromagnetic field in monolayer graphene", Phys. Rev. B **88**, 045118 (2013).

[56] T. Shirai, T. Mori, and S. Miyashita, "Condition for emergence of the floquet-gibbs state in periodically driven open systems", Phys. Rev. E **91**, 030101 (2015).

[57] T. Shirai, J. Thingna, T. Mori, S. Denisov, P. Hänggi, and S. Miyashita, "Effective floquet–gibbs states for dissipative quantum systems", New Journal of Physics **18**, 053008 (2016).

[58] F. Schwabl, R. Hilton, and A. Lahee, *Advanced quantum mechanics*, Advanced texts in physics (Springer, 2005), ISBN: 9783540259015.

[59] K. I. Seetharam, C.-E. Bardyn, N. H. Lindner, M. S. Rudner, and G. Refael, "Controlled population of floquet-bloch states via coupling to bose and fermi baths", Phys. Rev. X **5**, 041050 (2015).

[60] H. Dehghani, T. Oka, and A. Mitra, "Dissipative floquet topological systems", Phys. Rev. B **90**, 195429 (2014).

[61] K. Drese and M. Holthaus, "Floquet theory for short laser pulses", The European Physical Journal D - Atomic, Molecular, Optical and Plasma Physics **5**, 119 (1999).

[62] M. S. Rudner and N. H. Lindner, "Band structure engineering and non-equilibrium dynamics in floquet topological insulators", Nature Reviews Physics **2**, 229 (2020).

[63] S. A. Weidinger and M. Knap, "Floquet prethermalization and regimes of heating in a periodically driven, interacting quantum system", Scientific Reports **7**, 45382 (2017).

[64] K. I. Seetharam, C.-E. Bardyn, N. H. Lindner, M. S. Rudner, and G. Refael, "Steady states of interacting floquet insulators", Phys. Rev. B **99**, 014307 (2019).

[65] M. Genske, "Periodically driven many-body quantum systems : quantum ratchets, topological states and the floquet-boltzmann equation", PhD thesis (Universität zu Köln, 2017).

[66] Q. Chen, L. Du, and G. A. Fiete, "Floquet band structure of a semi-dirac system", Phys. Rev. B **97**, 035422 (2018).

[67] K. I. Seetharam, "Thermalization in periodically-driven interacting quantum systems", PhD thesis (California Institute of Technology, May 2018).

[68] M. S. Rudner and N. H. Lindner, *Floquet topological insulators: from band structure engineering to novel non-equilibrium quantum phenomena*, 2019, arXiv:1909.02008 [cond-mat.mes-hall].

[69] L. D'Alessio and M. Rigol, "Long-time behavior of isolated periodically driven interacting lattice systems", Phys. Rev. X **4**, 041048 (2014).

[70] D. Yudin and I. A. Shelykh, "Two-dimensional electron gas in the regime of strong light-matter coupling: dynamical conductivity and all-optical measurements of rashba and dresselhaus coupling", Phys. Rev. B **94**, 161404 (2016).

[71] M. Bukov, M. Heyl, D. A. Huse, and A. Polkovnikov, "Heating and many-body resonances in a periodically driven two-band system", Phys. Rev. B **93**, 155132 (2016).

[72] D. A. Abanin, W. De Roeck, and F. Huveneers, "Exponentially slow heating in periodically driven many-body systems", Phys. Rev. Lett. **115**, 256803 (2015).

[73] D. A. Abanin, W. De Roeck, W. W. Ho, and F. Huveneers, "Effective hamiltonians, prethermalization, and slow energy absorption in periodically driven many-body systems", Phys. Rev. B **95**, 014112 (2017).

[74] U. Peskin and N. Moiseyev, "The solution of the time-dependent schrödinger equation by the (t,t') method: theory, computational algorithm and applications", The Journal of Chemical Physics **99**, 4590 (1993).

[75] J. Schliemann, "On *t-t'*-formalism", (unpublished).

[76] H. Sambe, "Steady states and quasienergies of a quantum-mechanical system in an oscillating field", Phys. Rev. A **7**, 2203 (1973).

[77] D. F. Martinez, "Floquet-green function formalism for harmonically driven hamiltonians", Journal of Physics A: Mathematical and General **36**, 9827 (2003).

[78] D. F. Martinez, "High-order harmonic generation and dynamic localization in a driven two-level system, a non-perturbative solution using the floquet–green formalism", Journal of Physics A: Mathematical and General **38**, 9979 (2005).

[79] D. F. Martinez and R. A. Molina, "Localization properties of driven disordered one-dimensional systems", The European Physical Journal B - Condensed Matter and Complex Systems **52**, 281 (2006).

[80] A. K. Eissing, V. Meden, and D. M. Kennes, "Renormalization in periodically driven quantum dots", Phys. Rev. Lett. **116**, 026801 (2016).

[81] A. K. Eissing, V. Meden, and D. M. Kennes, "Functional renormalization group in floquet space", Phys. Rev. B **94**, 245116 (2016).

[82] C. O. Taberner, "Periodically driven s-qd-s junctions", MA thesis (University of Copenhagen, 2017).

[83] H. Aoki, N. Tsuji, M. Eckstein, M. Kollar, T. Oka, and P. Werner, "Nonequilibrium dynamical mean-field theory and its applications", Rev. Mod. Phys. **86**, 779 (2014).

[84] J. F. Rentrop, S. G. Jakobs, and V. Meden, "Nonequilibrium transport through a josephson quantum dot", Phys. Rev. B **89**, 235110 (2014).

[85] B. H. Wu and J. C. Cao, "A floquet–green's function approach to mesoscopic transport under ac bias", Journal of Physics: Condensed Matter **20**, 085224 (2008).

[86] T. Brandes, "Truncation method for green's functions in time-dependent fields", Phys. Rev. B **56**, 1213 (1997).

[87] N. Tsuji, T. Oka, and H. Aoki, "Correlated electron systems periodically driven out of equilibrium: floquet+dmft formalism", Phys. Rev. B **78**, 235124 (2008).

[88] J. Schliemann, "Conductivity in periodically driven systems", (unpublished notes).

[89] E. Akkermans and G. Montambaux, *Mesoscopic physics of electrons and photons* (Cambridge University Press, 2007), ISBN: 9780521349475.

[90] J. Rammer, *Quantum transport theory*, Frontiers in Physics (Avalon Publishing, 2004), ISBN: 9780813346229.

[91] F. Schwabl, *Quantenmechanik (QM I)*, Springer-Lehrbuch (Springer, 2002), ISBN: 9783540431060.

[92] J. Sakurai and J. Napolitano, *Modern quantum mechanics*, (Addison-Wesley, 2011), ISBN: 9780805382914.

[93] T. Bilitewski and N. R. Cooper, "Scattering theory for floquet-bloch states", Phys. Rev. A **91**, 033601 (2015).

[94] R. Winkler, *Spin-orbit coupling effects in two-dimensional electron and hole systems*, Springer tracts in modern physics (Springer, Berlin, 2003), ISBN: 9783662146002.

[95] H. R. Reiss, "Effect of an intense electromagnetic field on a weakly bound system", Phys. Rev. A **22**, 1786 (1980).

[96] M. Abramowitz and I. Stegun, *Handbook of mathematical functions: with formulas, graphs, and mathematical tables*, Applied mathematics series (Dover Publications, 1965), ISBN: 9780486612720.

[97] R. S. Sorbello, "On the anisotropic relaxation time", Journal of Physics F: Metal Physics **4**, 503 (1974).

[98] A. I. Anselm, *Introduction to semiconductor theory*, English, Translation of: Vvedenie v teoriiu poluprovodnikov (Moscow : Mir ; Englewood Cilffs, N.J. : Prenctice-Hall, 1981), ISBN: 0134960343 (Prentice-Hall).

[99] R. Winkler, "A note on analytic quadratic brillouin zone integration", Journal of Physics: Condensed Matter **5**, 2321 (1993).

[100] M. H. Boon, M. S. Methfessel, and F. M. Mueller, "Singular integrals over the brillouin zone: the analytic-quadratic method for the density of states", Journal of Physics C: Solid State Physics **19**, 5337 (1986).

[101] G. Wiesenekker and E. J. Baerends, "Quadratic integration over the three-dimensional brillouin zone", Journal of Physics: Condensed Matter **3**, 6721 (1991).

[102] S. Doniach and E. Sondheimer, *Green's functions for solid state physicists*, Frontiers in physics (W. A. Benjamin, 1974), ISBN: 9780805323948.

[103] D. Vollhardt, ed., *Der metall-isolator übergang in ungeordneten systemen*, Max-Planck-Institut für Physik und Astrophysik, Werner-Heisenberg-Institut für Physik (Unordnungsphänomene in Festkörpern, 1985).

[104] B. L. Altshuler, D. Khmel'nitzkii, A. I. Larkin, and P. A. Lee, "Magnetoresistance and hall effect in a disordered two-dimensional electron gas", Phys. Rev. B **22**, 5142 (1980).

[105] P. T. Wenk, "Itinerant spin dynamics in structures of reduced dimensionality", PhD thesis (Jacobs Universität, 2012).

[106] D. E. Bilhorn, L. L. Foldy, R. M. Thaler, W. Tobocman, and V. A. Madsen, "Remarks Concerning Reciprocity in Quantum Mechanics", Journal of Mathematical Physics **5**, 435 (1964).

[107] B. Altshuller, A. Aronov, and D. Khmelnitsky, "Suppression of localization effects by the high frequency field and the nyquist noise", Solid State Communications **39**, 619 (1981).

[108] W. Voigt, "Über das elektrische Analogon des Zeemaneffectes", Annalen der Physik **309**, 197 (1901), eprint:

[109] J. Stark, "Beobachtungen über den Effekt des elektrischen Feldes auf Spektrallinien. I. Quereffekt", Annalen der Physik **348**, 965 (1914).

[110] J. Zak, "Stark ladder in solids?", Phys. Rev. Lett. **20**, 1477 (1968).

[111] G. H. Wannier, "Dynamics of band electrons in electric and magnetic fields", Rev. Mod. Phys. **34**, 645 (1962).

[112] G. H. Wannier, "Wave functions and effective hamiltonian for bloch electrons in an electric field", Phys. Rev. **117**, 432 (1960).

[113] J. Callaway, "Optical absorption in an electric field", Phys. Rev. **130**, 549 (1963).

[114] H. Fukuyama, R. A. Bari, and H. C. Fogedby, "Tightly bound electrons in a uniform electric field", Phys. Rev. B **8**, 5579 (1973).

[115] F. W. Olver, D. W. Lozier, R. F. Boisvert, and C. W. Clark, *Nist handbook of mathematical functions*, 1st (Cambridge University Press, USA, 2010), ISBN: 0521140633.

[116] W. Fischer and I. Lieb, *Funktionentheorie* (Vieweg+Teubner Verlag, 1994), ISBN: 9783322969736.

[117] F. J. López-Rodríguez and G. G. Naumis, "Analytic solution for electrons and holes in graphene under electromagnetic waves: gap appearance and nonlinear effects", Phys. Rev. B **78**, 201406 (2008).

[118] F. J. López-Rodríguez and G. G. Naumis, "Erratum: analytic solution for electrons and holes in graphene under electromagnetic waves: gap appearance and nonlinear effects [phys. rev. b 78, 201406 (2008)]", Phys. Rev. B **79**, 049901 (2009).

[119] K. v. Klitzing, G. Dorda, and M. Pepper, "New method for high-accuracy determination of the fine-structure constant based on quantized hall resistance", Phys. Rev. Lett. **45**, 494 (1980).

[120] K. von Klitzing, "The quantized hall effect", Rev. Mod. Phys. **58**, 519 (1986).

[121] M. Z. Hasan and C. L. Kane, "*Colloquium* : topological insulators", Rev. Mod. Phys. **82**, 3045 (2010).

[122] X.-L. Qi and S.-C. Zhang, "Topological insulators and superconductors", Rev. Mod. Phys. **83**, 1057 (2011).

[123] D. R. Hofstadter, "Energy levels and wave functions of bloch electrons in rational and irrational magnetic fields", Phys. Rev. B **14**, 2239 (1976).

[124] D. J. Thouless, M. Kohmoto, M. P. Nightingale, and M. den Nijs, "Quantized hall conductance in a two-dimensional periodic potential", Phys. Rev. Lett. **49**, 405 (1982).

[125] T. Fukui, Y. Hatsugai, and H. Suzuki, "Chern numbers in discretized brillouin zone: efficient method of computing (spin) hall conductances", J. Phys. Soc. Jpn. **74**, 1674 (2005).

[126] T. Kitagawa, E. Berg, M. Rudner, and E. Demler, "Topological characterization of periodically driven quantum systems", Phys. Rev. B **82**, 235114 (2010).

[127] N. H. Lindner, G. Refael, and V. Galitski, "Floquet topological insulator in semiconductor quantum wells", Nat. Phys. **7**, 490 (2011).

[128] J. Cayssol, B. Dóra, F. Simon, and R. Moessner, "Floquet topological insulators", phys. stat. sol. (RRL) **7**, 101 (2013).

[129] M. S. Rudner, N. H. Lindner, E. Berg, and M. Levin, "Anomalous edge states and the bulk-edge correspondence for periodically driven two-dimensional systems", Phys. Rev. X **3**, 031005 (2013).

[130] J. Klinovaja, P. Stano, and D. Loss, "Topological floquet phases in driven coupled rashba nanowires", Phys. Rev. Lett. **116**, 176401 (2016).

[131] J. Karch, P. Olbrich, M. Schmalzbauer, C. Zoth, C. Brinsteiner, M. Fehrenbacher, U. Wurstbauer, M. M. Glazov, S. A. Tarasenko, E. L. Ivchenko, D. Weiss, J. Eroms, R. Yakimova, S. Lara-Avila, S. Kubatkin, and S. D. Ganichev, "Dynamic hall effect driven by circularly polarized light in a graphene layer", Phys. Rev. Lett. **105**, 227402 (2010).

[132] H. L. Calvo, H. M. Pastawski, S. Roche, and L. E.F. F. Torres, "Tuning laser-induced band gaps in graphene", Appl. Phys. Lett. **98**, 232103 (2011).

[133] G. Usaj, P. M. Perez-Piskunow, L. E. F. Foa Torres, and C. A. Balseiro, "Irradiated graphene as a tunable floquet topological insulator", Phys. Rev. B **90**, 115423 (2014).

[134] M. A. Sentef, M. Claassen, A. F. Kemper, B. Moritz, T. Oka, J. K. Freericks, and T. P. Devereaux, "Theory of Floquet band formation and local pseudospin textures in pump-probe photoemission of graphene", Nat. Comm. **6**, 7047 (2015).

[135] A. López, A. Di Teodoro, J. Schliemann, B. Berche, and B. Santos, "Laser-induced modulation of the landau level structure in single-layer graphene", Phys. Rev. B **92**, 235411 (2015).

[136] Y.-X. Wang and F. Li, "Edge states and phase diagram for graphene under polarized light", Physica B: Condensed Matter **492**, 1 (2016).

[137] M. Tahir, Q. Y. Zhang, and U. Schwingenschlögl, "Floquet edge states in germanene nanoribbons", Sci. Rep. **6**, 31821 (2016).

[138] M. Claassen, C. Jia, B. Moritz, and T. P. Devereaux, "All-optical materials design of chiral edge modes in transition-metal dichalcogenides", Nat. Comm. **7**, 13074 (2016).

[139] A. López, Z. Z. Sun, and J. Schliemann, "Floquet spin states in graphene under ac-driven spin-orbit interaction", Phys. Rev. B **85**, 205428 (2012).

[140] A. López, A. Scholz, Z. Z. Sun, and J. Schliemann, "Graphene with time-dependent spin-orbit coupling: truncated Magnus expansion approach", Eur. Phys. J. B **86**, 366 (2013).

[141] R. Rammal, "Landau level spectrum of bloch electrons in a honeycomb lattice", J. Phys. France **46**, 1345 (1985).

[142] Y. Hasegawa and M. Kohmoto, "Quantum hall effect and the topological number in graphene", Phys. Rev. B **74**, 155415 (2006).

[143] J. Wang and J. Gong, "Butterfly floquet spectrum in driven SU(2) systems", Phys. Rev. Lett. **102**, 244102 (2009).

[144] J.-W. Rhim and K. Park, "Self-similar occurrence of massless dirac particles in graphene under a magnetic field", Phys. Rev. B **86**, 235411 (2012).

[145] F. Yilmaz, F. N. Ünal, and M. O. Oktel, "Evolution of the hofstadter butterfly in a tunable optical lattice", Phys. Rev. A **91**, 063628 (2015).

[146] F. Yilmaz and M. O. Oktel, "Hofstadter butterfly evolution in the space of two-dimensional bravais lattices", Phys. Rev. A **95**, 063628 (2017).

[147] J. K. Asbóth and A. Alberti, "Spectral flow and global topology of the hofstadter butterfly", Phys. Rev. Lett. **118**, 216801 (2017).

[148] S. H. Kooi, A. Quelle, W. Beugeling, and C. Morais Smith, "Genesis of the floquet hofstadter butterfly", Phys. Rev. B **98**, 115124 (2018).

[149] L. Du, Q. Chen, A. D. Barr, A. R. Barr, and G. A. Fiete, "Floquet hofstadter butterfly on the kagome and triangular lattices", Phys. Rev. B **98**, 245145 (2018).

[150] Dean C. R., Wang L., Maher P., Forsythe C., Ghahari F., Gao Y., Katoch J., Ishigami M., Moon P., Koshino M., Taniguchi T., Watanabe K., Shepard K. L., Hone J., and Kim P., "Hofstadter's butterfly and the fractal quantum Hall effect in moiré superlattices", Nature **497**, 598 (2013).

[151] Y. H. Wang, H. Steinberg, P. Jarillo-Herrero, and N. Gedik, "Observation of floquet-bloch states on the surface of a topological insulator", Science **342**, 453 (2013).

[152] S. Owerre, "Magnonic floquet hofstadter butterfly", Annals of Physics **399**, 93 (2018).

[153] M. Wackerl, P. Wenk, and J. Schliemann, "Driven hofstadter butterflies and related topological invariants", Phys. Rev. B **100**, 165411 (2019).

[154] M. V. Berry, "Quantal phase factors accompanying adiabatic changes", Proceedings of the Royal Society of London. A. Mathematical and Physical Sciences **392**, 45 (1984).

[155] B. Simon, "Holonomy, the Quantum Adiabatic Theorem, and Berry's Phase", Phys. Rev. Lett. **51**, 2167 (1983).

[156] F. D. M. Haldane, "Model for a quantum hall effect without landau levels: condensed-matter realization of the "parity anomaly"", Phys. Rev. Lett. **61**, 2015 (1988).

[157] D. J. Thouless, "Quantization of particle transport", Phys. Rev. B **27**, 6083 (1983).

[158] M. Nakahara and M. Delbrück, *Differentialgeometrie, topologie und physik* (Springer Berlin Heidelberg, 2015), ISBN: 9783662452998.

[159] B. Höckendorf, A. Alvermann, and H. Fehske, "Efficient computation of the W3 topological invariant and application to floquet–bloch systems", J. Phys. A: Math. Theor. **50**, 295301 (2017).

[160] B. Höckendorf, A. Alvermann, and H. Fehske, "Topological invariants for floquet-bloch systems with chiral, time-reversal, or particle-hole symmetry", Phys. Rev. B **97**, 045140 (2018).

[161] F. Nathan and M. S. Rudner, "Topological singularities and the general classification of floquet–bloch systems", New Journal of Physics **17**, 125014 (2015).

[162] J. H. Shirley, "Interaction of a quantum system with a strong oscillating field", PhD thesis (California Institute of Technology, 1963).

[163] J. H. Shirley, "Solution of the schrödinger equation with a hamiltonian periodic in time", Phys. Rev. **138**, B979 (1965).

[164] A. Gómez-León, P. Delplace, and G. Platero, "Engineering anomalous quantum hall plateaus and antichiral states with ac fields", Phys. Rev. B **89**, 205408 (2014).

[165] P. M. Perez-Piskunow, L. E. F. Foa Torres, and G. Usaj, "Hierarchy of floquet gaps and edge states for driven honeycomb lattices", Phys. Rev. A **91**, 043625 (2015).

Acknowledgement

There are some people which I want to particularly mention in this work. These were my personal external driving during my work as PhD-student in Regensburg. My supervisor Prof. Dr. John Schliemann offered me the opportunity to do my PhD. He guided me threw this work with various ideas and scientific expertise.
Without the fruits from the uncountable number of discussions with Dr. Paul Wenk this work would certainly not be of the same value.
I certainly do not want to miss the time with my office colleague Patrick Grössing. Through him I got insight to various other topics of the field of condensed matter physics.
I gratefully acknowledge the language checking by Haley Culpepper and Christian Maag.

Eidesstattliche Erklärung zur Prüfungsleistung

Hiermit versichere ich, dass ich die vorliegende Arbeit selbstständig verfasst und keine anderen Hilfsmittel als die angegebenen verwendet habe. Die Stellen, die anderen Werken (gilt ebenso für Werke aus elektronischen Datenbanken oder aus dem Internet) wörtlich oder sinngemäß entnommen sind, habe ich unter Angabe der Quelle und Einhaltung der Regeln wissenschaftlichen Zitierens kenntlich gemacht. Diese Versicherung umfasst auch in der Arbeit verwendete bildliche Darstellungen, Tabellen, Kartenskizzen und gelieferte Zeichnungen. Mir ist bewusst, dass Täuschungen nach der für mich gültigen Studien- und Prüfungsordnung geahndet werden.

Ort, Datum

Unterschrift des Verfassers

Publications

- M. Wackerl, P. Wenk, and J. Schliemann,
  Driven Hofstadter butterflies and related topological invariants,
  Phys. Rev. B **100**, 165411 (2019)
- M. Wackerl, P. Wenk, and J. Schliemann,
  Floquet-Drude conductivity,
  Phys. Rev. B **101**, 184204 (2020)